Structural and functional regulation of Vps4 by ESCRT proteins

by

Cody J. Vild

A dissertation submitted in partial fulfillment
of the requirements for the degree of
Doctor of Philosophy
(Biological Chemistry)
in the University of Michigan
2014

Doctoral Committee:

Associate Professor Zhaohui Xu, Chair
Professor Robert S. Fuller
Professor Stephen W. Ragsdale
Professor Janet Smith
Professor Lois Weisman

Dedication

This thesis work is dedicated to my parents, Elaine Bratko and Gary Vild. They gave me the drive to try to push myself in all matters, whether it is academic or otherwise. From them, I have gained the inspiration to pursue work that will always be intellectually and emotionally satisfying. Without their unconditional support, this dissertation would not be possible.

Acknowledgements

I am greatly appreciative of all the support I have received throughout my graduate school studies, in particular my mentor Dr. Zhaohui Xu. When joining Zhaohui's lab, I knew he was an incredibly brilliant man and excellent teacher, but what I did not fully appreciate at the time was how much effort he was going to put into me, to allow me to become a successful researcher. Many will wax on about how special their mentor was, but I truly feel distinguished from others in this regard. Through his patience, he was able to hone my skills as a critical thinker, and through his trust, he has given me confidence in my abilities to take on any future challenge. I also owe a great deal of gratitude to my thesis committee members: Drs. Robert Fuller, Stephen Ragsdale, Janet Smith, and Lois Weisman. From their wonderful insights and to their dedication to challenge me on my scientific endeavors, I am forever grateful, as your guidance along the way will prove invaluable to me for the rest of my career.

I would also like to thank my fellow lab members, both past and present, for an extremely enjoyable work environment, engaging scientific conversation and friendship. To the many undergraduates and junior graduate students I have tutored along the way, I thank you for helping me learn how to be a mentor and making me a better researcher. In particular, I thank Melvin Chan for the comradery in the early days in the lab, Mia Miller for her youthful exuberance,

and Daniel Gawron for his assistance in many experiments. I thank Ulla Lilienthal and her family, for their wonderful support over the years. To Emily Guo and Yan Li, the two amazing post-docs in the lab, I thank you as well. You make lab a place I look forward to coming to everyday and for fruitful scientific debates.

I thank all of my friends that I have made over the years here at Michigan. You have definitely relieved much of the drudgery and doldrums that may be associated with graduate school. Furthermore, I thank you for your support because my success was ultimately predicated on it. I also thank my parents – to whom this work is dedicated - and the rest of my family, whose love and support I do not take for granted and has been instrumental in all of my pursuits.

Finally, I would like to thank my beautiful, charming and gifted girlfriend, Jennifer Rauch. Personally, I believe there is a direct correlation between my scientific successes to the time we have been together. Finding such an incredible intellect within a person that is so funny and so radiant is truly a blessing. No amount of words can truly capsulate all you have done for me; hopefully with time I can repay some of this debt I owe to you.

“In Northeast Ohio, nothing is given. Everything is earned. You work for what you have.” ~LeBron James

Preface

This thesis is comprised of two related manuscripts plus unpublished material that make up Chapters 2-4. Chapter 2 contains unpublished data and some data used in a yet to be published manuscript. Chapter 3 is made of work that as has been submitted to a peer reviewed journal in conjunction with some data from Chapter 2. Chapter 4 represents work published in Journal of Biological Chemistry, 2014, 289(15):10378-86. Chapter 1 gives background information and details our current understanding of various processes within the field. Chapter 5 summarizes the work from this thesis and proposes future directions the field may take. The appendix contains work that I contributed to and is significantly relevant to other work in this thesis. It was published in the Journal of Biological Chemistry, 2012, 287(52):43899-908.

Table of Contents

List of Figures

List of Tables

Abstract

The Endosomal Sorting Complexes Required for Transport (ESCRT) machinery controls key cellular processes, including multivesicular body (MVB) biogenesis, retroviral release, division between daughter cells, and closure of small plasma membrane wounds, all of which require the budding of membrane away from the cytosol. The ESCRT proteins function by binding membrane, generating curvature, and through the enzymatic activity of an AAA-ATPase Vps4, executing membrane scission. Both the localization and oligomerization state of Vps4 are important mechanisms that control Vps4 activity. The ESCRT-III proteins are themselves substrates of Vps4 activity but also participate in regulating Vps4 function. These proteins are structurally related, and contain a unique protein-interaction motif known as the MIT-interacting motif (MIM) that engages the Vps4 microtubule-interacting and trafficking (MIT) domain. Through this MIT-MIM interaction, the ESCRT-III proteins are thought to drive oligomerization and recruit Vps4 to the site of action.

Vps4 regulation is further expanded by its co-factor Vta1, which itself contains two tandem MIT domains that bind to the ESCRT-III proteins. Two yeast ESCRT-III proteins, Did2 and Vps60, were initially found to bind the second Vta1 MIT domain that stimulates Vps4 via Vta1 binding. Biochemical analysis showed that Did2 does not bind to the second MIT domain as previously thought, but in fact binds to the first MIT domain. The crystal structure of the LIP5-

CHMP1B complex (human orthologs of Vta1 and Did2) showed that this mode of interaction is conserved. Interestingly, the binding interface of Vps60 to Vta1 has diverged in higher species. It appears that LIP5 has evolved different structural requirements for VPS4 stimulation as well, and that CHMP5 (human ortholog of Vps60) has also gained an inhibitory function for LIP5 stimulation, which is in contrast to yeast Vps60. Another interesting difference between the human and yeast systems is that yeast harbor a novel ESCRT-III protein Vfa1. Vfa1 regulates Vps4 through a high-affinity MIT-MIM interaction that can greatly stimulate Vps4 ATPase activity. Taken together, these results suggest that while the basic mechanism of ESCRT function is conserved, there is a significant divergence in the regulatory mechanism of ESCRT action, with Vps4 as a prime example.

Chapter 1 Introduction

Maintenance of cellular membrane is one of the most important aspects of cell viability. Not only do biological membranes define “self” from “not self”, but also are key for the homeostasis of a variety of cellular processes. Twenty years ago, the mechanism of how membrane buds away from the cytosol was essentially unknown. Then emerged the endosomal sorting complexes required for transport (ESCRT) proteins, a series of complexes that function to carry out this unique topological event (Figure 1.1). Classically discovered from yeast genetics, they were found to be essential in the endolysosomal trafficking pathway. The ESCRT machinery directs cell-surface receptors into multi-vesicular bodies (MVBs), which fuse with the lysosome to degrade these receptors. The ESCRT proteins are also responsible for the membrane-restructuring event that generates MVBs. As a result, defects in the ESCRT machinery have serious implications for development of cancer and other pathological states through the deregulation of its client proteins. It was also observed that many enveloped viruses hijack the host ESCRT proteins to help them egress from infected cells, a process topologically similar to MVB biogenesis. Another critical cellular role for the ESCRT proteins is to complete abscission between daughter cells during cytokinesis, with failure to do so having direct ties to cancer progression. While most of our understanding of ESCRT function comes from studying their roles in processes described above, it does

not diminish the fact that the ESCRT proteins have also been implicated in: plasma membrane repair, autophagosome maturation, exosome biogenesis, and the shedding of microvesicles. Due to the complex role of the ESCRT machinery in cell viability and prevention of pathogenic states, there has been an extensive effort to understand how the ESCRT proteins work.

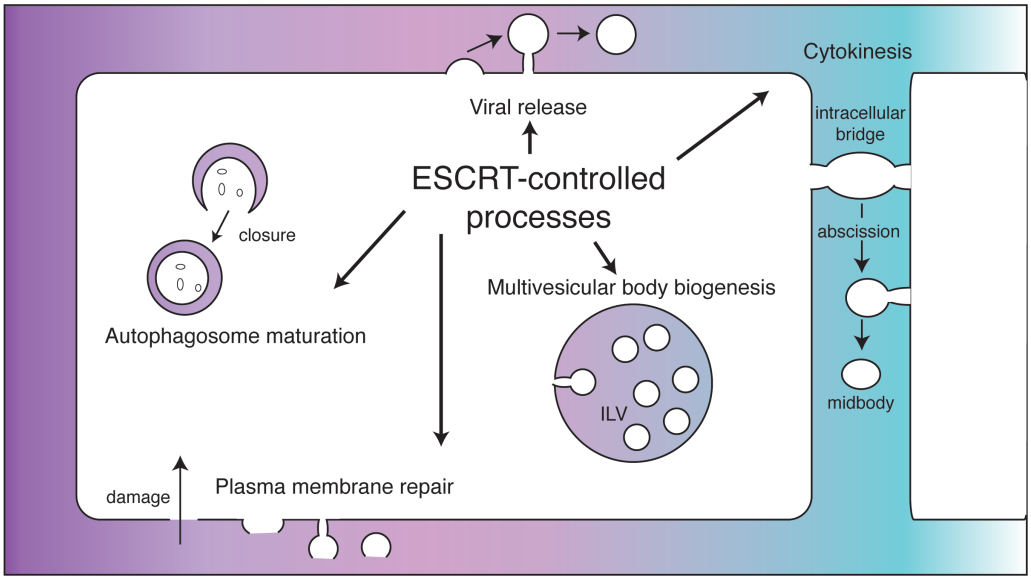

Figure 1.1 ESCRT-controlled biological processes
The ESCRT machinery controls a wide variety of membrane restructuring events in the cell, which are labeled in the figure. All of these processes are related by the fact that they require the budding of membrane away from the cytosol.

1.1 ESCRT and Human Disease

Given that dysfunction in the ESCRT machinery leads to human diseases, understanding its cell biology will likely provide tractable pharmacological targets. The ESCRT machinery is best understood in its role in endolysosomal trafficking, which controls the degradation of cell surface receptors. Clearly, dysfunction in controlling receptor homeostasis can lead to disastrous effects for an organism(1). For example, many adherens and tight junction proteins are degraded via the MVB pathway(2-4). Imbalance of the degradation of these

proteins can lead to the loss of proper cell polarization, which is particularly important for epithelial cells. When epithelial cells lose polarity, the result is the epithelial to mesenchymal transition (EMT). When epithelial cells enter EMT, they become migratory, which is thought to promote metastasis(5-7). In addition, the MVB pathway controls the degradation of cellular signaling receptors, such as epidermal growth factor receptor (EGRF). Loss of ESCRT function can cause the accumulation of EGFR on the plasma membrane, which leads to hyper-activation of its downstream targets and generates a proliferative, cancerous state(8). Targeting the EGFR and its downstream targets has been used as a therapeutic measure for some lung cancers, and thus understanding the biology of the MVB pathway may potentially lead to new treatments(9).

In mammalian cells, ESCRT function is also tied to cancer biogenesis through their control of abscission during cytokinesis. Incomplete division of daughter cells can lead to multinucleated cells, which are believed to be a source of tumorigenesis and aid in resistance to treatments(10,11). The ESCRT proteins function to resolve the intercellular bridge which separates the cells and releases the midbody (a protein-rich structure in the middle of the intercellular bridge)(12). Interestingly, this appears to be the most ancient function of the ESCRT proteins as a family of crenarchaea, *Sulfolobus*, have a subset of the ESCRT proteins, but lack an endosomal system(13,14). It has been shown that these ESCRT homologs localize at the site of cell division, in a similar manner as their mammalian counterparts, to aid in the completion of cell division(15,16). Most

components of the ESCRT machinery are recruited to the intercellular bridge to complete abscission by providing the force necessary to close off the membrane(17-19). Many of these ESCRT proteins are indispensible for their roles in cytokinesis, however, our understanding of their specific functions for abscission is still unclear.

Many viruses have insidiously evolved the ability to coax the ESCRT machinery to aid in their egress from their cellular hosts. ESCRT proteins control the membrane fission event to allow fully matured viruses to be released from cells. While it is best understood for retroviruses (e.g. HIV-1), many other types of viruses use a similar strategy(20). Viral proteins are often sufficient for generating membrane curvature, and as such, they only recruit a subset of the ESCRT proteins to complete membrane fission(21,22). These viruses produce viral proteins with “late-assembly domains” in order to engage early ESCRT components, which can then prompt ESCRT-mediated membrane fission(23). For example, HIV-1 Gag proteins contain a motif that specifically recognizes the ESCRT nucleating complex, ESCRT-I. In turn, ESCRT-I recruits only downstream ESCRT components that are necessary for membrane fission (ESCRT-III and VPS4), but bypasses others (ESCRT-II)(21,24). Deconstructing how these viruses utilize the ESCRT proteins to release from host cells will allow us to directly target and prevent viral infection.

1.3 Function of the ESCRT Machinery

1.3.1 Multivesicular body pathway

ESCRT function is best understood within the context of the endolysosomal trafficking pathway and I will use this as a reference for describing our current understanding of how the ESCRT machinery functions.

MVBs are unique endosomal organelles that play a critical role in maintaining cellular homoeostasis. They were first observed in the 1950s from electron micrograph studies, although their exact nature was unknown(25-27). Sotelo and Porter later described MVBs as “a vesicular structure, containing a large number of small vesicles” inside the lumen of an endosomal structure(28). These intralumenal vesicles (ILVs) were partially egressed from the limiting membrane, which was the first evidence that ILV formation has an unusual topology and can be described as budding away from the cytosol(27). More importantly, ILVs were later found to contain epidermal growth factor receptor, which effectively silences the activity of the receptor(29). It has since been demonstrated that an array of integral membrane proteins are sorted into ILVs(2-4,30,31). Once mature, MVBs fuse with the vacuole (lysosome in metazoan), which leads to the degradation of its luminal contents as the final step in the endolysosomal pathway(32)(Figure 1.2).

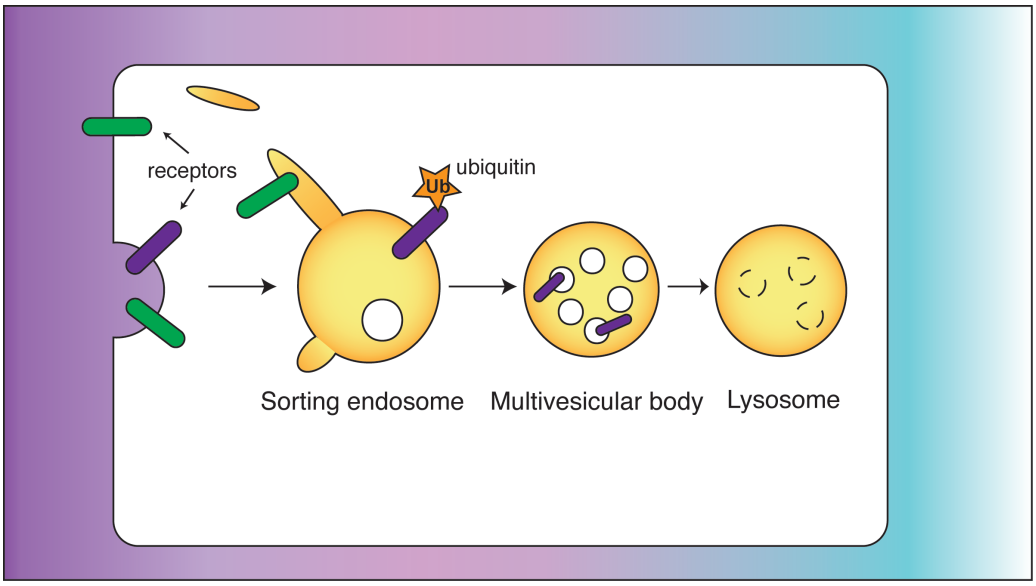

Figure 1.2 Cell surface receptor down-regulation via the MVB pathway
A cartoon showing the process of cell surface receptor down-regulation via the MVB pathway. Receptors are colored green and purple. Through endocytosis, cell surface receptors are brought into the early endosome. Some receptors, like the one colored in green, are recycled back to the plasma membrane. Others, like the one colored in purple, become ubiquitinated (orange star), which serves as a signal for internalization of this receptor into an ILV and formation of the late endosome or the MVB. The MVB then fuses with the lysosome to degrade its luminal contents

Genetic screens in *Saccharomyces cerevisiae* were performed to identify mutations in gene products that caused vacuolar protein sorting (vps) defects(33-37). Tom Stevens and colleagues observed that mutations within a certain subclass of vps genes gave rise to a unique vacuolar phenotype, which they termed as “class E” genes(38). The class E phenotype is characterized by the appearance of an aberrant structure, comprised of stacked cisternae with accumulated proteins and lipids that have not been properly delivered to the vacuole for degradation(39,40). Seminal work by Scott Emr’s group identified that the products of several of the “class E” genes work together in a molecular complex to target cellular receptors for degradation via the MVB pathway in a

ubiquitin-dependent manner(41). This complex was called the endosomal sorting complexes required for transport-I (ESCRT-I).

Further work revealed that other “class E” gene products form additional ESCRT complexes, which work as distinct molecular assemblies, with each having a clearly defined role in MVB biogenesis. Currently, the ESCRT machinery can be grouped into five sub-complexes: ESCRT-0, -I, -II, -III and the AAA-ATPase Vps4. They are thought to be recruited in a sequential manner to the endosomal membrane for their function(42-44). In terms of yeast MVB biogenesis, the ESCRT machinery functions in the following steps: cargo selection and sequestering, membrane deformation, and abscission. Here, I define cargo as any protein that gets sorted into the MVB by the ESCRT complexes. While much of the early understanding of the ESCRT complexes was achieved in yeast, it has been subsequently demonstrated that they are well conserved across eukaryotes (45-47). Therefore, MVB biogenesis in yeast has served as an excellent model of ESCRT function by eliminating much of the complexity from possible redundancy, due to isoform and splice variants seen in higher species.

For a cell receptor to be targeted for degradation via the MVB pathway, it first must be ubiquitinated(31,48,49). Monoubiquitination of the cytoplasmic tail of a receptor has been shown to be sufficient for entering the MVB pathway(50-52). The trafficking of polyubiquitinated substrates has also been observed in

some cases(53,54). However, recent data has emerged that suggested cargo could enter the MVB in a ubiquitin-independent manner as well. For example, aquaporin AQP2, the G-protein-coupled receptor PAR1, and interleukin-2 receptor β-chain can all be efficiently sorted into ILVs without ubiquitination(55-57). These data suggested that interaction with the ESCRT proteins alone could directly result in a protein being identified as an ESCRT cargo. Indeed, using a chimeric substrate, Mageswaran et al. showed that binding to the limiting membrane of the endosome while having a loose association with the ESCRT proteins was sufficient for proteins to be delivered into ILVs(58). This model also helps explain why some soluble, yet ubiquitinated, proteins can also be targeted as cargoes for the ESCRT machinery, since membrane association was initially thought to be essential for cargo processing(59-61). It seems that ubiquitination only serves to increase the affinity for the ESCRT machinery, since most early-acting ESCRT proteins (ESCRT-0, -I, and –II) contain ubiquitin-binding domains(62-64). Membrane proteins at the limiting membrane of the endosome can thus avoid ESCRT processing, unless their interaction is increased through ubiquitination. While ubiquitination may not be an absolute requirement for cargo processing, more often than not, it serves as a signal for the ESCRT proteins to identify cargoes.

1.3.2 ESCRT-0

The first critical step in the MVB pathway is the selection of ubiquitinated cargo by the ESCRT-0 complex (65). Two proteins comprise the ESCRT-0 complex, Vps27 and Hse1 (has symptoms of E class-1) (in human: Hrs

(hepatocyte growth factor-regulated tyrosine kinase substrate) and STAM1/2 (signal transducing adaptor molecule1/2)) (Table 1.1). The complex functions as an ~8 nm long heterodimer of a 1:1 stoichiometry that binds through coiled-coil interactions and two domain-swapped GAT (GGAs and Tom1) domains(66-68) (Figure 1.3). Loss of either protein causes defects in MVB biogenesis(69-71). Between the two proteins, there are five ubiquitin-binding sites –three ubiquitin interacting motifs (UIM)s and two VHS (Vps27, Hrs, and STAM1/2) domains - that can mediate selection and clustering of cargo(68,72) (Figure 1.3). Hrs/Vps27 contains a FYVE (Fab-1, YGL023, Vps27, and EEA1) domain towards its N-terminus that has a unique affinity for PI(3)P (phosphatidylinositol 3-phospate)(73,74). PI(3)P is specifically enriched on the late endosomes (the site of cargo sorting) as well as on ILVs(75). The FYVE domain helps the ESCRT-0 complex localize to the endosomal membrane(76). STAM/Hse1 has a SH3 domain that can recruit deubiquitinating enzymes (DUBs), such as AMSH (associated molecule with the SH3 domain of STAM) and UBPY (ubiquitin-specific processing protease Y)(77,78). Loss of the deubiquitinase activity of either enzyme can greatly influence cargo fate(79-82). This adds an additional regulatory step in cargo processing due to the fact that these DUBs can alter the ubiquitination state of various cargoes, where loss of a ubiquitin tag allows the cargo to diffuse away from the site of ILV formation. Another interesting observation about the ESCRT-0 complex is that it forms higher oligomeric structures on the membrane, effectively increasing the multiplicity of ESCRT-0 function(83). This could form a lattice around cargo to cluster them on a specific

Table 1.1 ESCRT proteins in yeast and human and their structural moieties

Yeast protein	Human protein	Domains and Motifs
ESCRT-0		
Vps27	Hrs	GAT, FYVE, proline-rich motif, UIM, VHS
Hse1	STAM 1/2	GAT, SH3, UIM, UIM, VHS
ESCRT-I		
Vps23	Tsg 101	coiled-coil, UEV
Vps28	Vps28	
Vps37	Vps37 A,B,C	coiled-coil
Mvb12	Mvb12 A,B; UBAP1	coiled-coil
ESCRT-II		
Vps22	EAP30	
Vps36	EAP45	GLUE (NFZ in yeast)
Vps25	EAP25	winged-helix
ESCRT-III core		
Vps20	CHMP6	MIM2
Snf7 (Vps32)	CHMP4 A,B,C	MIM2
Vps24	CHMP3	MIM1
Vps2	CHMP2 A,B	MIM1
ESCRT-III related		
Did2	CHMP1 A,B	MIM1
Ist1	IST1	MIM1, MIM2
Vps60	CHMP5	MIM5
Vfa1	--	MIM2
Vps4 complex		
Vps4	VPS4 A,B	MIT, AAA, β-domain
Vta1	LIP5	MIT, MIT, VSL

zone on the endosomal membrane. Together, ESCRT-0 uses a variety of mechanisms to control the proper sorting of cargo at the endosomal membrane.

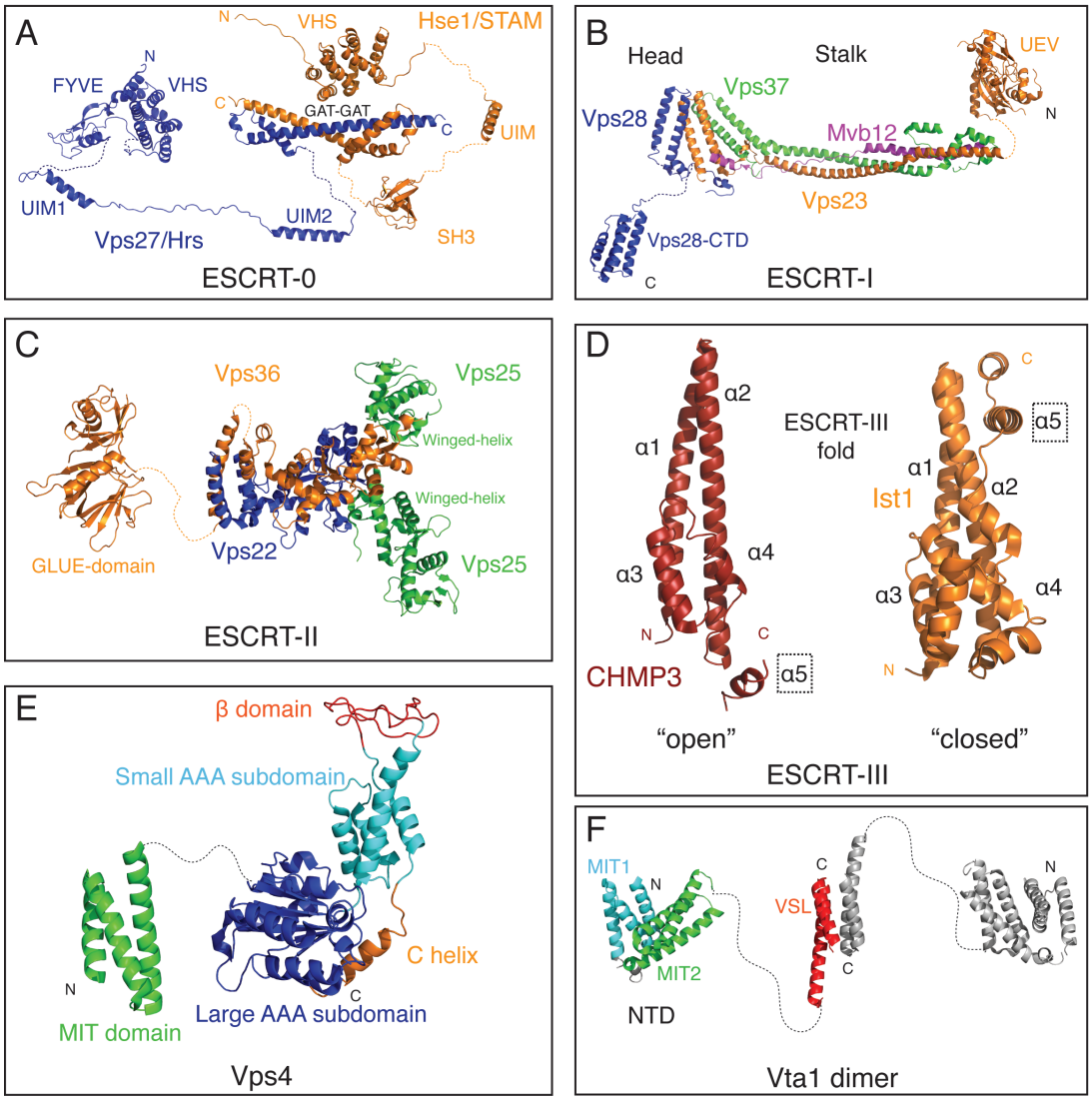

Figure 1.3 Structures of proteins that form the ESCRT machinery
(A) A modeled ESCRT-0 complex. Pieced together from the Hrs FYVE domain (PDB code: 1DVP), the tandem UIM domains of Vps27 (PDB code: 1Q0V), the STAM2 VHS domain (PDB code: 1X5B), the Vps27 UIM1 domain (PDB code: 1O06), the STAM2 SH3 domain (PDB code: 1UJ0), and the Vps27/Hse1 complex structure (PDB code: 2PJW).

(B) A modeled ESCRT-I complex. Pieced together from the Vps23 UEV domain (PDB code: 1UZX), the Vps28 CTD (PDB code: 2J9V) and the ESCRT-I complex structure (PDB ID: 2P22).

(C) A modeled ESCRT-II complex. Pieced together from the ESCRT-II complex (PDB code: 3CUQ) and the Vps36 GLUE domain (PDB code: 2J9V)

(D) ESCRT-III protein structures. On the left is the partial structure of CHMP3 with the helices labeled α1-α5 (PDB code: 2GD5). Note the position of the α5 helix, which suggests an "open" conformation. On the right is the partial structure of Ist1 with helices labeled α1-α5 (PDB code: 3GGY). Note position of the α5 helix, which abuts α2 helix and suggests a "closed" conformation. The ESCRT-III fold is represented by α1-α4 of both structures.

(E) A modeled Vps4 monomer structure. Pieced together the Vps4 MIT domain (PDB code: 2V6X) and the Vps4 AAA ATPase domain (PDB code: 2QPA). The MIT domain is colored green, the large AAA subdomain in blue, the small AAA subdomain in cyan, the β domain in red, and the C helix in orange.

(F) A modeled Vta1 dimer structure. Pieced together from the Vta1NTD structure (PDB code: 2RKK) and the Vta1 VSL structure (PDB code: 2RKL). The MIT1 domain is colored in cyan, the MIT2 is colored in green, the VSL is colored in red. The corresponding modeled in dimer is colored in gray.

1.3.3 ESCRT-I

The ESCRT-I complex has been well studied in yeast, as it was the first ESCRT sub-complex to be identified(41). It is comprised of four proteins: Vps23, Vps28, Vps37 and Mvb12 (multivesicular body 12) that exist in a complex with 1:1:1:1 stoichiometry(41,84,85). This complex is conserved in human as well: Tsg101, hVps28, Vps37, and hMvb12, respectively, although Vps37 has three isoforms and hMvb12 has two isoforms(46,86-89) (Table 1.1). UBAP1 (Ubiquitin-associated protein 1) has also been shown to have an overlapping function with hMvb12 in the MVB pathway, however it is more prominently involved in processing ubiquitinated cargo(90,91). Based on structural studies, we can build a complete model of the yeast ESCRT-I complex. It consists of a "stalk" formed by Vps23, Vps37 and Mvb12 via antiparallel coiled-coil interaction(92) and a globular 'head' group formed by Vps23, Vps28 and Vps37 at one end of the complex(93,94) (Figure 1.3). This complex can engage

ubiquitin, through the Vps23 UEV (ubiquitin E2 variant) domain on its N-terminus. A current model suggests that this ESCRT-I interaction with ubiquitin influences cargo sorting(41,95,96). Further structural studies with small-angle X-ray scattering (SAXS) revealed that the ESCRT-I complex is elongated (~22.5 ηm) and highly flexible relative to the stalk(97). The elongated structure contributes to the bifurcation of function, as one end needs to engage ESCRT-0 while the other can bind ESCRT-II.

1.3.4 ESCRT-II

The ESCRT-I complex recruits the next complex in the pathway, ESCRT-II. ESCRT-II itself is a heterocomplex: one subunit of Vps22 (in human: EAP30 (ELL-associated protein of 30 kDa)), one subunit of Vps36 (EAP45) and two subunits of Vps25 (EAP25)(98-101) (Table 1.1). The ~5 nm complex adopts a Y-shaped structure, where Vps22 and Vps36 form the base of the complex and each arm binds a copy of Vps25 (Figure 1.3). As highlighted above, binding of ubiquitinated cargo is a critical function for early-acting ESCRT complexes. While both yeast and human ESCRT-II homologs, Vps36 and EAP45, harbor a GLUE (GRAM-like ubiquitin-binding in EAP45) domain that recognizes ubiquitin, it apparently does so by two different mechanisms (Figure 1.3). Within the Vps36 GLUE domain, there are two NZF (Npl4-type zinc finger) inserts, where one binds to ESCRT-I and the other binds to ubiquitin(102,103). However, for human EAP45, the GLUE domain does not contain NZF inserts, but can still bind to ubiquitin directly(104-106). Through its interaction with ubiquitin, it is thought that ESCRT-II can influence cargo selection.

Also essential for ESCRT-II function, the two Vps25 arms directly bind to Vps20, a core ESCRT-III protein, to activate the ESCRT-III complex(107). This is most likely to be the most critical role of ESCRT-II in MVB biogenesis, as ESCRT-II overexpression can rescue ESCRT sorting defect for ESCRT-I deletion mutants(108). In addition, perturbations to one of the Vps25 binding sites can lead to the retrograde trafficking of cargo proteins(109). These data highlight the importance of ESCRT-II in cargo sequestering.

Recent work has put forward the idea that ESCRT-I and ESCRT-II work together in a supercomplex. From *in vitro* reconstitution experiments with GUVs (giant unilamellar vesicles), recombinantly purified ESCRT-I and ESCRT-II appeared to co-localize and cause membrane deformation(110). This suggested that the supercomplex can provide a mechanism for nascent vesicle budding. However, the field remains unconvinced of ESCRT-I and –II's role in membrane deformation in the cell, as argued by Schuh and Audhya(44). While purified yeast ESCRT–I and –II form a stable complex *in vitro*(102), this complex has not been detected in yeast cell extract (41,108). Attempts to reproduce GUV membrane restructuring with an ESCRT-I and –II supercomplex from either *C. elegans* or human failed to induce bud formation(44,111). Additionally, the size of the budding neck formed by the yeast supercomplex *in vitro* is two orders of magnitude larger than what is typically seen *in vivo*(112). Experiments investigating the effect of other ESCRT proteins in the presence of GUVs also

see spontaneous membrane structural change(113,114). Thus, it appears that membrane deformation is not the primary role of the ESCRT-I and –II supercomplex.

Instead of controlling membrane deformation, it is more likely that the early-acting ESCRT complexes (-0, -I and –II) are more important for cargo selection and sequestration. As discussed above, at least one component of each early ESCRT complex contains ubiquitin-binding domain. The fact that these ESCRT complexes are recruited sequentially suggests that this process has delineated steps. ESCRT-0 nucleates the entire process by recognizing ubiquitinated cargo. The recruitment of ESCRT-I and subsequently ESCRT-II can then begin to define the geometry of the nascent vesicle. Since ESCRT-I can form higher order oligomeric species on the membrane, the early-acting ESCRT complexes can expand greatly outside of their predefined geometry to encapsule/capture cargo. The precise stoichiometry of the early ESCRT complexes is currently unknown and remains of great interest to the field.

1.3.5 ESCRT-III

The ESCRT-III complex is made up of four “core” proteins, in yeast they are Vps20, Vps32 (Snf7 (sucrose non-fermenting 7) is the name I will use), Vps24, and Vps2(115) (Table 1.1). The deletion of core ESCRT-III proteins yields a strong class E phenotype(38). Other “non-core” ESCRT-III proteins have been subsequently identified and will be discussed later. In human, the ESCRT-III proteins are called CHMPs (charged multivesicular body proteins),

with the analogous core ESCRT-III proteins being: CHMP6, CHMP4, CHMP3, and CHMP2, respectively (Table 1.1). As seen with the early-acting ESCRT complexes, in human, various isoforms expand the complexity of the system. CHMP2 has two isoforms CHMP2A and -2B, and CHMP4 has three isoforms CHMP4A-C. These different isoforms are generally assumed to function redundantly to each other, but emerging evidence suggests tissue specific roles for different isoforms(116). Moreover, recent data has shown that CHMP4B functions predominantly in viral budding, whereas CHMP4C is more involved in cytokinesis(117).

All ESCRT-III proteins adopt a similar structure fold. There have been crystal structures for truncated CHMP3 and CHMP4B(118-120). The ESCRT-III proteins adopt an ~7 nm bundle of α-helical hairpins, where helices 1 and 2 form the length and base of the protein (Figure 1.3). Helices 3 and 4 fold back as an anti-parallel bundle stacked on top of the first two helixes to create a compact fold. These four helixes form the "ESCRT-III fold," and based on secondary structure prediction, are present in all of the ESCRT-III proteins. The fifth helix can then fold back and abut against the ESCRT-III fold opposite helices 3 and 4(120,121). The position of the fifth helix is critical for determining whether the ESCRT-III protein is in an active or inactive state. When helix 5 binds to the ESCRT-III fold, the protein is in a "closed", autoinhibited, monomeric and cytosolic state (Figure 1.3). Conversely, when helix 5 is relieved from contact with the ESCRT-III fold, the ESCRT-III protein is in an active, "open"

conformation and polymerizes on the endosomal membrane(115,119-122) (Figure 1.3). This is evidenced by the fact that ESCRT-III truncations lacking regions outside of the ESCRT-III fold form spiral filaments on the membrane that cause exaggerated membrane deformation(123,124). To return to the closed state, ESCRT-III proteins are removed from the membrane through the enzymatic action of Vps4. Vps4 contains a microtubule interacting and trafficking (MIT) domain that binds to the MIT-interaction motif (MIM) within the ESCRT-III proteins. ESCRT-III MIMs are located C-terminal to helix 5 and are free to bind MIT domain-containing proteins in solution when ESCRT-III proteins are in active states(125). There have been a number of MIMs described since their discovery and the core ESCRT-III proteins are categorized into two subclasses defined by the type of MIM they contain. Briefly, Vps20 and Snf7 contain a MIM2 and Vps24 and Vps2 contain a MIM1(126,127). The nature of MIT-MIM interactions is of great interest for this thesis, and will be discussed in more detail later.

While structurally similar, different ESCRT-III proteins function with distinct roles within the ESCRT-III oligomeric complex. The ESCRT-III proteins work in a sequential manner, beginning with Vps20/CHMP6 nucleating ESCRT-III polymer formation(128). Snf7/CHMP4 is the next subunit to be recruited. Snf7 is the most abundant ESCRT-III protein and is considered to be the major driving force in membrane deformation via its homo-oligomerization(128,129). To abridge polymerization, Vps24/CHMP3 is thought to act as a cap to Snf7 polymerization as it can attenuate Snf7 filament structure(128,129). Finally, Vps24 recruits Vps2

to the membrane, where Vps2 is then able to bring Vps4 to the membrane to promote ESCRT-III disassembly(128,129). The recruitment of Vps4 seems to be solely dependent on its interaction with Vps2, even though the other ESCRT-III members can also directly interact with Vps4(113,124).

Much work has gone into understanding the nature of the ESCRT-III polymer(113). It has been observed that many ESCRT-III proteins can form polymers, by themselves or with another ESCRT-III protein(109,123,124,130,131). For example. wild-type yeast Snf7 forms various oligomeric structures on the membrane, including patches, rings and long filaments(123). CHMP4, the human homolog of Snf7, can polymerize as well, since the removal of the inhibitory C-terminus causes CHMP4 to form planar spirals and circular arrays on a lipid membrane, which are flat in nature. At high concentrations, CHMP4 can form three-dimensional projections from membrane(109,131). This suggests that once in an active conformation, ESCRT-III proteins can assemble into a functional tubular and then a dome-like structure. A similar theme is seen with CHMP3 and CHMP2, which, when in their open conformation, can co-assemble into a helical structure about ~40 nm in diameter(124). As seen with CHMP4, overexpression of CHMP2 generates tubular extensions that bud away from the plasma membrane(130). Interestingly, the addition of CHMP3 and CHMP2 to a planar CHMP4 array can convert it to a tubular structure with a dome cap(109). Whichever the situation, it seems that ESCRT-III proteins are competent to form oligomeric, tubular protrusions.

However, each experimental condition seems to generate structures with slightly differently morphologies. A likely scenario is that, *in vivo,* the ESCRT-III polymer is a conglomerate of all the morphologies, and that there is a highly precise oligomer structure needed for proper ILV formation. In fact, recent work using deep-etch electron microscopy confirms this(132). Expression of CHMP4 or CHMP2 alone produces distinct polymer assemblies, yet interestingly, co-expression of the two proteins yielded a completely new morphology. Furthermore, the final ESCRT complex, Vps4, has also been implicated in having a direct role in shaping the ESCRT-III oligomer through direct interaction or by removing components from the membrane(109,131,133). These data highlight the fact that ESCRT-III proteins efficiently deform membrane, but high-resolution structural studies are clearly needed to understand how the ESCRT-III oligomer is constructed under physiological conditions.

1.3.6 Vps4

Of all the class E proteins, Vps4 has always gathered a great deal of attention due to the fact that it is the only enzyme within the ESCRT machinery(134). Vps4 is highly conserved, from archaea to human, and functions in all known ESCRT mediated processes(13-15,135). In both yeast and human, removal of Vps4 causes severe defects in MVB biogenesis and fails to recycle the ESCRT machinery from the endosomal membrane(136,137). Human has two isoforms of Vps4, VPS4A and VPSB, which are 80% identical to each other and 60% identical to yeast(138)(Table 1.1). In fact, VPSB can compliment Vps4 function in *Δvps4* yeast strains(139). Due to its high level of

conservation and the critical function in the ESCRT pathway, much focus has gone into understanding the molecular mechanism of how Vps4 works.

Vps4 belongs to a family of proteins known as the ATPase Associated with various cellular Activities (AAA ATPases). As such, hydrolysis of ATP allows the ATPases to exert a mechanical force to physically restructure their substrates in some capacity(140-143). AAA ATPases fall into one of the two classes, type–I or type–II, where they contain either one or two ATP binding cassettes. A number of groups have determined crystal structures of the Vps4 ATPase binding domain in different nucleotide states and from various sources(144-147). Vps4 contains one ATPase binding cassette, comprising of a large and small AAA subdomain, and is therefore a type-I AAA ATPase (Figure 1.3). The ATP binds between these two subdomains, similar to other AAA ATPases, via a Walker A/B motif(148). The Walker motifs are conserved structural elements that bind ATP or GTP(149). Inserted within the small AAA subdomain is a small motif of a three anti-parallel beta sheets. This “β-domain” is unique to Vps4 when compared with other AAA ATPases, and functions to bind a cofactor of Vps4, Vta1 (Vps twenty associated-1)(147) (Figure 1.3). Vps4 orthologs from simpler organisms that do not contain Vta1 also lack a β-domain, indicating a clear evolutionary relationship for this protein-protein interaction(144,150). Beyond the small AAA subdomain is a C-terminal helix that abuts the large AAA subdomain (Figure 1.3). The C-terminal helix is critical for

the stability of the large AAA subdomain, and perturbations to the structure of this helix completely destabilize Vps4(146,147,151).

There are two other structural components to Vps4 outside of the ATPase domain, the MIT domain and a linker. To date, there has been no successful attempt at crystallizing a full-length Vps4 protein. The MIT domain is at the N-terminus of Vps4 and is responsible for binding to ESCRT-III proteins(152). The Vps4 MIT domain can bind to two different structural motifs with ESCRT-III, MIM1 and MIM2 (126,127). The linker has recently emerged as having a critical role in Vps4 function. It is thought to act in an inhibitory capacity to Vps4 ATPase activity. Substrate binding to the MIT domain relieves this autoinhibition(153,154). In addition, the linker may contain a secondary binding site for ESCRT-III proteins(154). Current models predict that the MIT domain and the linker work together to coordinate the removal of ESCRT-III proteins through their direct interactions.

Key to Vps4 function is its ability to self-assemble into a higher oligomeric structure. In the absence of nucleotide, Vps4 remains in a catalytically inactive, monomeric state and upon ATP binding forms a catalytically active oligomer. While there has been some discrepancy whether inactive Vps4 actually exists as a dimer(145,148,155), our group has been able to observe only the monomeric form of Vps4(121,146). Regardless of the quaternary structure in the absence of ATP, this state is the non-functional form of Vps4. Attempts at capturing a stable

oligomer have proven difficult, since Vps4 readily converts ATP into ADP and then would disassemble into the monomer structure(148). To overcome this challenge, a mutant form has been used in many studies, with a mutation in the Walker B motif, E223Q, which is able to bind but not hydrolyze ATP (134,156,157). This traps the Vps4 in its oligomeric state. Electron microscopy study showed that the Vps4 E233Q mutant could assemble into a two-ringed dodecameric structure(155,158,159). However, recent work has found that the E233Q oligomer is non-physiological and that the preferred structure of Vps4 oligomer is in fact a hexametric ring(144). This is a more logical structure of the oligomer, as other type-I AAA ATPases also adopt single-ringed hexamers in their functional states(160,161). Furthermore, it is easier to reconcile how all the MIT domains in Vps4 can orient in the same direction for ESCRT-III interaction in a single-ring hexameric structure(162).

Unfortunately, a high-resolution structure of the Vps4 oligomer still remains elusive. The current model of the Vps4 oligomer is based on the p97 (a AAA ATPase whose D1 domain forms a single-ringed hexameric structure) oligomeric structure(146,161). While the p97 based model is useful in certain ways, we cannot truly understand the mechanism by which Vps4 removes ESCRT-III proteins from the membrane without a high-resolution structure. Other AAA ATPases, like ClpX (caseinolytic peptidase X), remodel their substrate by moving the protein substrate through a central pore in the hexamer(163,164). It has been proposed that Vps4 does so in a similar manner.

Mutating residues that are predicted to be in the central pore of the Vps4 oligomer (modeled from the p97 structure) have been shown to disrupt its function in HIV budding(145). Perturbations in the central pore of human VPS4A have also been shown to cause deficiency in ATPase activity due to a loss of ESCRT-III interaction(154). While these data do support a model where the ESCRT-III proteins are threaded through a central hole, they do not rule out other possible mechanisms(165).

1.3.7 Vta1

While Vps4 can self-assemble, this is not an efficient process and, *in vivo*, it is aided by its co-factor Vta1 (in human: LIP5 (lyst-interacting protein 5))(156,166) (Table 1.1). Vta1 contains two domains that are connected by a flexible linker (Figure 1.3). At the N-terminus are two tandem MIT domains that also bind to various ESCRT-III proteins(167,168). The first MIT domain is only competent to bind MIM1 elements(169,170) and the second MIT domain uniquely binds Vps60, an ESCRT-III protein, by a distinct MIT-MIM5 interaction(167,171). At the C-terminus is the VSL (Vta1-SBP1-LIP5) domain that allows for the dimerization of Vta1 and directly binds to the Vps4 β-domain(147,156,168,172,173). Vta1 dimer formation is critical for binding to Vps4 and the interaction between the two proteins is ATP-dependent in yeast(168). Recent work has also identified new interactions that further stimulate Vps4 ATPase activity, called the VSE (Vps4 stimulatory element)(174,175). The VSE is proximal to the VSL and could be thought of as one continuous domain. However, it is unclear whether there is a VSE-like

region in the human LIP5. Through its interaction via the VSL domain and the VSE, Vta1 greatly stimulates Vps4 activity by stabilizing the oligomer. Interestingly, the Vta1 linker region inhibits Vps4 stimulation, but this inhibition is relieved upon ESCRT-III binding to the N-terminal domain(175,176). These data suggest an important role for the linker in communicating inputs at the N-terminal MIT domains and conferring the information to the VSL. The mechanism by which this occurs is unknown and whether it is conserved in human will be discussed in Chapter 3.

Given that Vta1 is effective in driving Vps4 ATP hydrolysis, it can be thought of as an inherent part of a functional complex with Vps4 *in vivo*. For yeast Vps4 to self-assemble and have significant ATPase activity *in vitro*, protein concentrations must be greater than ~0.5 μM, but Vps4 concentration in the yeast cell is ~0.2 μM(148). This suggests that additional factors aid in Vps4 oligomerization *in vivo* such as Vta1. This process is conserved in plants as well, as the *Arabidopsis thaliana*(At) ortholog of Vps4 undergoes a five fold increase in ATPase activity in the presence of AtVta1(177). Human VPS4 is a much weaker ATPase at a similar protein concentration, which suggests that human LIP5 is necessary to promote oligomer formation *in vivo*, as well(154). Through its own MIT domains, Vta1 can also potentially aid in the recruitment of Vps4 to the endosomal membrane(178). Therefore, the role of Vta1 in the ESCRT pathway is to help recruit Vps4 to the endosomal membrane and drive Vps4 oligomer assembly(133).

Like other ESCRT proteins, Vta1 depletion in yeast cells causes a class E phenotype, albeit to a much milder degree(156,179). Deletion of non-core ESCRT-III proteins in conjunction with a Vta1 deletion, however, yields a synthetic phenotype that is comparable to a classic class E phenotype(180). Further studies using electron tomography found that Vta1 deletion mutant alone perturbed MVB formation and is exacerbated by synthetic mutations with other ESCRT-III proteins(133). In mammalian cells, LIP5 seems to have an integral role in other processes as well. Polarization of epithelial cells requires rapid turnover of cell-surface receptors, and interestingly, LIP5 has a pronounced increase of expression in these cells suggesting a link between these two observations(181). ESCRT proteins control HIV-1 release, but this can be prevented by the expression of the interferon-stimulated gene 15 (ISG15), a ubiquitin-like moiety. The Leis group has identified that LIP5 becomes conjugated with ISG15. It was suggested that conjugation prevents association of LIP5 with VPS4 and stops viral proliferation(182,183). These observations offer exciting possibilities for targeting LIP5 for therapeutics. In mammalian cells, it has been shown that LIP5 also has a direct role in cargo processing, a role that has been classically associated with early-acting ESCRT complexes. Depletion of LIP5 by siRNA caused altered kinetics for ubiquitinated cargo processing(184). Two cargos, epidermal growth factor receptor and aquaporin 2, have been suggested to have a physical interaction with LIP5 that facilitated their trafficking

through the ESCRT pathway(55,184). It will be interesting to explore whether other cargos enter ILVs by this non-canonical mechanism.

1.3.8 Current model of vesicle formation

The degree of conservation for different ESCRT complexes gives clues for their relative importance in vesicle formation. Phylogenetic analysis can only identify ESCRT-0 homologs in the broad clade of opisthokonts (animal, fungi and unicellular eukaroyotes), suggesting alternative mechanisms for cargo clustering in other organisms(185). This is not entirely unexpected as - even in human - alternative factors can activate downstream ESCRT complexes for some ESCRT-mediated events. A mammalian protein called ALIX has been shown to directly recruit ESCRT-III components in both cytokinesis and viral budding while completely bypassing ESCRT-I and –II function(17,19,186,187). In other species, ESCRT-I and –II are dispensable as three taxa of apicomplexan (parasitic protist) are completely devoid of any ESCRT-I or ESCRT-II components(47). However, all eukaryotes contain at least one ESCRT-III core protein from each subclass (containing a MIM1 or MIM2) and Vps4(47). This suggests, at least evolutionarily, that ESCRT-III and Vps4 are the minimal machinery to accomplish vesicle formation.

As discussed above, there is a growing consensus that early-acting ESCRT complexes (-0,-I, and –II) primarily function to sequester cargo and that membrane deformation and abscission is carried out by late-acting ESCRT complexes (ESCRT-III and Vps4-Vta1). When understanding ESCRT mediated

vesicle formation, two facts should be considered: first, the control of vesicle formation must be precise since it consistently generates uniformly-sized ILVs(39,133); second, the process is amenable to generate vesicles in topologically related but geometrically distinct events (MVB biogenesis, viral budding, cytokinesis, etc.). Our current understanding of the ESCRT-III polymerization process may shed light on these two observations. Snf7, *in vitro* or *in vivo*, has been shown to be potent at membrane deformation and Vps24 or a Vps24-Vps2 complex can form filament structures as well. Interestingly, co-expression of human Snf7 and Vps2 yielded polymer structures distinct from polymers formed by the individual component(132). The diversity in oligomeric structures of ESCRT-III suggests that there may be an optimal oligomeric geometry for abscission. The fact that *in vivo* Vps4 is necessary for the final steps of abscission also suggests that removal of ESCRT-III proteins by Vps4 may play an important role for the precise timing of abscission(18,188,189).

Studies with human Vps24-Vps2 heteropolymer gave insights to a structure that was capable of generating vesicles. Recombinant human Vps24-Vps2 formed helical tubes that are ultimately capped by a “dome”-like structure(124). This structure gave rise to a computational model where the predicted tension generated by ESCRT-III proteins binding to the highly curved membrane could lower the activation energy barrier for membrane scission(190). Due to the propensity of Snf7 to generate or stabilize tubular membrane curvature(131,191), it would form the base of the dome that is capped by the

Vps24-Vps2 filaments to complete the dome hemisphere. What is attractive about this model is that Snf7 would define the boundaries of the nascent vesicle through its interaction with upstream components. The ESCRT-II-Vps20 complex has been shown to have a preference for binding highly curved membrane(114). Furthermore, both “arms” of the Y-shaped ESCRT-II complex nucleate ESCRT-III polymerization and this action is thought to help encircle cargo proteins(109). Therefore, once cargo is properly clustered, Snf7 can polymerize and define the area of membrane that will eventually become a new vesicle. Consistent with this model is that loss of Snf7 allows for the retrograde trafficking of cargo back to the plasma membrane, where loss of Vps24 does not(128).

The necessity of Vps4 ATPase activity also indicates that dome formation alone is not sufficient for vesicle formation *in vivo*. There are a few models that offer insight to the role that Vps4 ultimately plays in the process. One is that the Vps4-Vta1 complex selectively removes ESCRT-III substrates to achieve an optimal geometry for dome-mediated scission, if dome assembly alone is sufficient for membrane scission as *in vitro* experiments seem to have suggested(110). There is evidence that Vps4 could affect the dome structure, since Vps4 binding to Snf7 polymers has been shown to induce curvature(131). Furthermore, Vps4 has a preference for the MIMs of Snf7 and Vps2 for ILV formation indicating a coordinated restructuring of the dome(192). Along the same line another model suggests that, due to the high affinity of the ESCRT-III

polymer for the membrane and for each other, removal of any protein might destabilize the highly curved membrane and cause membrane “buckling(193).” Dynamin, a GTPase responsible for endocytosis, follows a similar mechanism, where the release of a dynamin polymer from a membrane tubule is sufficient to generate the nascent vesicle(174). Interestingly, several other AAA-ATPases use an analogous strategy for disassembly of polymeric substrates. Eerily similar to the Vps4-ESCRT relationship, the N-terminal MIT-domains of Katanin and Spastin bind the C-terminal acidic tail of α/β tubulin, and through ATP hydrolysis, exerts a mechanical force sufficient to disassemble microtubules(160,194). In the type VI secretion system of gram-negative bacteria, the AAA-ATPase ClpV is responsible for the breakdown of large VipA/VipB polymers(195). Analogous to the Vps2, Snf7 and Vps4 relationship, ClpV only engages VipB for disassembly of the VipA/VipB heteropolymer(196). Current models are not mutually exclusive and further experiments are needed to help deconvolute this complex process.

1.4 Regulators of Vps4 Function

Outside of the “core” ESCRT-III proteins, a number of “non-core” ESCRT-III proteins that a similar fold, but do not seem to be essential for MVB biogenesis. However, these other non-core ESCRT-III proteins, Did2, Ist1, Vps60 and Vfa1 do have subtle effects on MVB biogenesis and other ESCRT-mediated processes. This discussion will now shift to these other regulatory ESCRT proteins and describe what functions these proteins may have in the ESCRT-controlled functions.

1.4.1 CHMP1-IST1 (Did2-Ist1)

First characterized in human, CHMP1 was found to engage in the MVB biogenesis. Its depletion caused enlarged MVBs, which is the predominant hallmark of MVB dysfunction in human(197). Bioinformatics analyses identified that CHMP1 contains two isoforms in human, CHMP1A and -1B(198)(Table 1.1). While some functional differences have been identified, these two proteins are thought to be redundant for their function in the MVB pathway. The yeast homolog of CHMP1 is Did2, and was not initially identified as an ESCRT protein due to its weak class E phenotype upon deletion. Later, yeast two-hybrid analysis found that Did2 interacts with the Vps4-Vta1 complex, suggesting a role as an important player in the MVB pathway(199). The interaction between Did2 and the Vps4-Vta1 complex is thought to bring Vps4-Vta1 complex to the endosomal membrane(39,173). Did2 interaction with either Vps4 or Vta1 stimulates Vps4 ATPase activity, presumably by stabilizing the Vps4 oligomeric structure directly or through Vta1(154,176). For Vta1-dependent stimulation of Vps4, Did2 binding is thought to cause a conformational change in Vta1 N-terminal domain to relieve the autoinhibition by the Vta1 linker(180). Since loss of Did2 in yeast only leads to a moderate defect in MVB biogenesis, it suggests a nuanced role for Did2, most likely regulation of Vps4 function(39,133).

The Did2-Vps4 interaction has been characterized extensively. One of the first structures of a MIT-MIM interaction came from human CHMP1A-VPS4A complex(200). The molecular details of this interaction are well conserved

between human and yeast. For the Did2-Vta1 interaction, however, the picture seems a bit unclear. The Did2-Vta1 interaction binds using a MIT-MIM type of interaction, where the Did2 MIM binds to the second of the two MIT domains in Vta1 N-terminal domain(176). Interestingly, human CHMP1B binds to the first MIT domain in LIP5(167). The nature of CHMP1B/Did2 binding to LIP5 (Vta1) will be addressed in Chapter 2.

Further pursuits in understanding Did2 function revealed that it works with another late-acting ESCRT-III protein Ist1. Ist1 was initially identified as a Vps4 interacting protein and further characterization found that it contains two Vps4 binding sites(201). One is at the C-terminus, which contains a MIM that strongly associates with Vps4 and the other is a lower affinity interaction site within the ESCRT-III fold that inhibits Vps4 oligomerization(201). During starvation trafficking through the MVB pathway is at its highest, and interestingly, Ist1 expression is at its lowest further supporting an inhibitory role for Ist1 in yeast(202). So far, Ist1 is the only ESCRT-III protein shown to have an inhibitory affect on Vps4. Structural pursuits of Ist1 have been quite fruitful(120,121). Along with Vps24, all of our structural understanding of the ESCRT-III fold comes from these two proteins. In the crystal structure of Ist1, it was revealed that helix α5 interacts with the ESCRT-III fold, which provided the first structural evidence of the conformational switch between active and inactive conformation of ESCRT-III proteins. Outside of the ESCRT-III fold, human IST1 is thought to contain two MIMs, a proximal MIM2 and a more distal MIM1. While it is been

suggested that the MIT domain of human Vps4 could engage both MIMs simultaneously, this has only been determined somewhat indirectly(120).

Within the ESCRT pathway, most evidence indicates that Ist1 and Did2 function as a heterodimer to regulate Vps4(120,121,169,180,201). In both human and yeast, deletion of Ist1 does not have a large effect on the ubiquitinated cargo processing, but electron tomography reveals that their respective deletion perturbs MVB biogenesis(133,169). When examining Ist1 function with other late-acting ESCRT-III proteins, Ist1 exhibits a synthetic phenotype in a *Δist1Δvta1* or *ΔistΔvps60* strain but not a *Δist1Δdid2* strain(180). This suggests that Did2 and Ist1 work in a complex for Vps4 recruitment. Furthermore, ablation of the Did2-Ist1 interface has a measureable effect on cargo sorting(121). Ist1 has a high affinity for Vps4 when compared to other ESCRT-III proteins, most likely due to its two binding sites (through the ESCRT-III fold and the C-terminal MIM), and has been proposed to bind a monomeric Vps4 in the cytoplasm(201). This was supported by the fact that the recruitment of Ist1 to the endosome is dependent on its interaction with Did2(178,201). Together, the Ist1-Did2 complex would hold Vps4 in the cytoplasm, and once ESCRT processing reaches a certain time point or step, this complex is then recruited to the endosomal membrane to allow for Vps4 activation.

A low-resolution crystal structure has been determined for the Ist1-Did2 complex(121). As predicted by yeast two-hybrid analyses, the Did2 MIM binds to

the Ist1 ESCRT-III fold. It binds in a perpendicular fashion to the ESCRT-III fold and in parallel to the Ist1 α5. This suggests Did2 MIM may bind Ist1 by displacing the MIM of IST1 (helix α6) and allow for a tripartite complex to form with Vps4. This has been proposed to be the inhibitory state of Vps4, in complex with Did2 and Ist1(178). When recruited to the membrane, the ESCRT-III polymer would displace the Did2-Ist1 complex from Vps4 due to avidity from the membrane localized ESCRT-III MIMs. Another interesting observation is that human Ist1 and Did2 can form polymer structures *in vitro(120)*. It is possible that once free from Vps4, Ist1 and Did2 could join the ESCRT-III polymer structure and contribute to vesicle formation. Further studies are needed to understand the exact role the Ist1 and Did2 polymers play *in vivo*.

In addition to its important role in MVB biogenesis, the human IST1 and CHMP1 complex is essential in two other ESCRT controlled processes, cytokinesis and viral release. In a similar fashion to MVB biogenesis, IST1 and CHMP1 are essential for VPS4 recruitment to the midbody (the site of cytokinesis). Loss of either component leads to multinucleated cells(120,121,203). In addition to VPS4 recruitment, CHMP1 and IST1 can also bring other MIT containing proteins to the midbody. AMSH, UBPY, Spastin, Spartin, and MITD1 all have MIT domains and can participate in cytokinesis by removing ubiquitin(169,204-206), proteolytic cleavage of microtubules(169,207-209) or limiting the association with VPS4(210,211). With regard to HIV viral release, IST1 function seems to be dispensable while CHMP1 has an essential

role(24,111). This has been seen for human cytomegalovirus as well, suggesting the role for CHMP1 in viral release may be conserved(212). It is thought that CHMP1 recruits VPS4 to the plasma membrane to complete abscission for budding viruses, just like in MVB biogenesis. It will be interesting to see why the requirements for viral release are different from the other ESCRT-mediated processes.

Recent work has identified ESCRT function to be important in the repair of micro-wounds to the plasma membrane(213). Briefly, small wounds that occur in the plasma membrane must be excised to retain membrane integrity. When the hole is produced, there is an influx of calcium into the cell due to the concentration gradient. The calcium influx, through a cascade of events whose mechanisms are unknown, brings the ESCRT machinery to the site of damage and buds the damaged membrane away as a microvesicle into the extracellular matrix. Interestingly, CHMP1B and IST1 form a ternary complex with the autolytic protease Calpain-7, a protein that can possibly bind calcium(214). Calpain-7 contains tandem MIT domains, and is the binding site for IST1 MIM(215). Calpain-7 also binds to the α2 helix of CHMP1B in an unconventional manner(214). Binding to this region of CHMP1B allows for the formation of a ternary complex between Calpain-7. IST1 and CHMP1B. Indeed, it has been shown that the presence of both IST1 and CHMP1B elevated Calpain-7 protease activity as compared to with just one ESCRT-III component or Calpain-7 alone(214). It is unknown whether the calcium binding of Calpain-7 is important

for plasma membrane repair, but it would offer an attractive model where the three-protein complex senses the calcium influx and is recruited to the site of damage. Additional work on Calpain-7 further revealed that ALIX, a protein that nucleates ESCRT-III polymerization in membrane repair, can act as a substrate and aid in Calpain-7 recruitment to the site of damage(213,216). IST1 and CHMP1B would then recruit VPS4, which is necessary to complete microvesicle release of the damaged membrane (Figure 1).

Interestingly, the CHMP proteins were not originally identified as members of the ESCRT pathway, but for their roles in chromatin remodeling. CHMP1 was initially called chromatin modifiying protein-1, but whether it actually carries out a specific chromatin remodeling event has not been explicitly tested(217). However, CHMP1A does have tumor suppressive properties, and this has been directly tied to its localization to the nucleus(218). Higher expression levels have been shown to inhibit tumor growth in both pancreatic and renal tumors(218-220). Similarly, in zebrafish cell proliferation has been directly linked to CHMP1A nuclear localization(221). While none of these observations has been directly linked to ESCRT function, it expands potential for understanding CHMP1 regulation as a tumor suppressor gene.

1.4.2 CHMP5 (Vps60)

Early work identified that loss of Vps60 in yeast caused mild endosomal trafficking defects. Through sequence analysis, it was classified as a *bona fide* ESCRT-III protein(222). Unlike other ESCRT-III proteins, Vps60 is found to bind

to only one ESCRT protein, Vta1(176). They function together in MVB biogenesis (133,176,179,180). Deletion of Vps60 and Ist1 or Did2 leads to a synthetic class E phenotype, while a *Δvps60Δvta1* strain does not exacerbate vacuolar defects(180). This result supports the model that these two proteins function as a complex in the ESCRT pathway. This interaction is conserved in human as well, in a LIP5-CHMP5 complex. Indeed, CHMP5 and LIP5 interact with high-affinity and forms a stable complex in the cytoplasm(170). Loss of CHMP5 has been reported to have different outcomes for cargo processing. Early reports did not see a dramatic effect in receptor trafficking with a loss of CHMP5(184). Subsequent studies, however, did find that CHMP5 depletion in human cells could alter both MVB biogenesis and the kinetics of cell surface receptor down regulation(223). More indirect evidence for CHMP5's role in MVB biogenesis comes from the fact that a loss of CHMP5 function causes abnormal morphogenesis of epithelial cells in *Drosphilila*(224). It is presumed that alteration of the MVB biogenesis kinetics, and consequently cell surface receptor down regulation, is the cause of this morphological change. As with yeast, deletion of Vps60 only yields subtle defects in membrane protein trafficking and this phenotype is only observed under stringent experimental conditions.

Much work has gone into understanding the nature of the Vta1-Vps60 interaction. As with all other ESCRT-III proteins, Vps60 is predicted to have an ESCRT-III fold consisting of five alpha helices. Vps60 binds to the second MIT domain of Vta1, but to achieve maximal binding, two helices α4 and α5, are

required in yeast and human(168,170). This is unique as for all other previously studied ESCRT-III interactions, a single helix or extended coil was sufficient for MIT binding(225). This interaction regulates Vps4 ATPase activity through Vta1(176). Like Did2, Vps60 binding to Vta1 is thought to cause conformational changes that relieve the inhibitory properties of the Vta1 linker to stimulate Vps4 at least in yeast(175).

At the beginning of this thesis study, only the N-terminal ESCRT-III binding domain of Vta1 (Vta1NTD) had been structurally determined. In collaboration with Prof. Chunyang Cao's group at Institute of Organic Chemistry, Chinese Academy of Science, we determined an NMR solution structure of the Vta1NTD-Vps60 (α4-α5) structure that is discussed in the appendix. The Sundquist group determined the NMR structure of the LIP5NTD-CHMP5 (residues 139-195) complex, while were we able to determine a ternary complex crystal structure of CHMP1B (MIM)-LIP5NTD-CHMP5 (residues 139-195). These two structures will be discussed further in Chapter 3. There is also a reported structure of the extreme C-terminus of CHMP5, a region outside of the LIP5 binding interface, bound to Brox, a protein with an unclear role in HIV-1 release(226,227). This peptide fragment of CHMP5 forms a small β-hairpin that was unpredicted by secondary structure predictions. Unfortunately, no functional assessment has been attributed to this complex, but it will be interesting to see if it can form larger complexes with LIP5 and other ESCRT proteins.

CHMP5 also has regulatory functions outside of MVB biogenesis. Currently, no study has explicitly examined what role CHMP5 has in cytokinesis, but CHMP5 is recruited to the site of abscission(226,227). For HIV-1 viral release, CHMP5 silencing increased the amount of released viral particles(184). However, subsequent studies saw that loss of CHMP5 had little effect on viral release(24). While CHMP5's role in HIV-1 release remains unclear, it contributes to the release of avian sarcoma leukosis virus. Just like with LIP5, ISG15ylation of CHMP5 inhibits the release of viral particles(183). Several ESCRT components can be ISG15ylated, but many of them require the ISG15ylation of CHMP5 first(182). The fact that CHMP5 functions in an upstream role in this process warrants more investigation. CHMP5 has been shown to have another role outside of MVB biogenesis, as it has been reported to be an oncogene in acute myeloid leukema (AML). Regulation of CHMP5 levels was correlated with cascade of caspase activation, which ultimately controls apoptotic cell death(228). In AML, CHMP5 expression is upregulated, and its silencing causes cell death for the cancerous cells(229). The mechanism by which CHMP5 functions as an oncogene is unclear or if its deregulation functions in a similar manner as CHMP1B in a cancer-activating pathway.

1.4.3 Vfa1

Vfa1 was initially identified in a novel approach to look for proteins that affect vacuolar transport. By overexpressing all the proteins in the yeast genome, the Ungermann group observed many genes whose perturbation can lead to altered receptor trafficking. The product of one of the identified genes

interacted with Vps4, and was thus termed Vfa1 (Vps4-associated-1). Overexpression of Vfa1 causes swollen vacuoles, a class D phenotype – as opposed to a class E phenotype that is typically observed in ESCRT dysfunction(230). Vfa1 can also be recruited to an aberrant class E structure in a dominant-negative ESCRT background, but its localization to this compartment was dependent on its interaction with Vps4(230). Therefore, the nature of the Vps4-Vfa1 relationship added a previously unknown layer of complexity to the ESCRT system. The biochemical and biophysical properties of Vfa1 regulation of Vps4 are detailed in Chapter 4.

1.5 Communication between ESCRT Complexes and Membrane

One of the most critical aspects of ESCRT function is the ESCRT complexes respective ability to sequentially recruit one another to the endosomal membrane. Interpreting and defining how each complex can bind and associate with downstream complexes has been an important focus for the field. I will now focus on our current understanding of the communication between various ESCRT complexes and membrane.

1.5.1 Early-acting ESCRT complexes

After cargo selection and clustering, ESCRT-0 must recruit the next ESCRT complex, ESCRT-I, to the membrane. Hrs/Vps27 of the ESCRT-0 complex directly binds to the ESCRT-I complex through its distinct and internal proline-rich motif(62,70,231,232), where it recognizes the UEV of Tsg101/Vps23 (70,93) (Figure 1.3). In both metazoa and yeast, this interaction is essential for ESCRT-I localization(69,70) and any perturbation to this interaction decreases

the efficiency of MVB biogenesis(62,70). Through its FYVE domain, ESCRT-0 also maintains high-affinity interaction with the endosomal membrane, but ESCRT-I only directly associates with the membrane via weak electrostatic interaction. The prevailing model is that ESCRT-0 is responsible for anchoring the ESCRT-I complex to the endosomal membrane(76,92).

At the other end of the ESCRT-I complex, the CTD (C-terminal domain) of Vps28 nucleates the downstream ESCRT-II complex formation(94,102) (Figure 1.3). The Vps36/EAP45 GLUE domain from the ESCRT-II complex directly binds to Vps28(94,102) (Figure 1.3). Importantly, the GLUE domain also binds specifically to PI(3)P that helps partially localize the ESCRT-II complex to the endosomal membrane(104). Within the Vps36 GLUE domain, there are two NZF (Npl4-type zinc finger) inserts, where one binds to ESCRT-I and the other binds to ubiquitin(102,103). However, for human EAP45, the GLUE domain lacks NZF inserts(104-106). Vexing to the field, it is still not known how human EAP45 can directly interact with ESCRT-I. Although the specifics of this interaction remain nebulous, it is clear that the GLUE domain is an essential factor for maintaining the ESCRT-I and ESCRT-II interface.

1.5.2 Late-acting ESCRT complexes

As mentioned above, the two arms of the ESCRT-II complex, Vps25, nucleate ESCRT-III oligomerization. A high-resolution crystal structure revealed that Vps25 contains a winged-helix domain that provides the minimal binding surface for ESCRT-III(107). Vps25 binds to the first helix of the ESCRT-III

protein Vps20 with micromolar affinity, but does not contribute significantly to Vps20's affinity for endosomal membrane(107). Furthermore, while this interaction is important for normal MVB biogenesis, data suggest that its role for directing ESCRT-III membrane association can be circumvented, as seen in HIV-1 budding or cytokinesis(98,233).

In order to be active, the ESCRT-III complex must be associated with the endosomal membrane. The ESCRT-III proteins do not have a ubiquitin-binding domain, so cargo is unlikely to contribute to ESCRT-III membrane association. Instead, the bottom of the ESCRT-III fold is highly basic, contrary to the acidic helix 5 and MIM, and aids in membrane binding(191). Besides ESCRT-II recruitment of Vps20 to the membrane, Vps20 can also undergo myristoylation to further tether itself to the membrane(234). Recently, a new mechanism for anchoring ESCRT-III proteins to the membrane has emerged. At the very N-terminus of ESCRT-III proteins is a small ANCHR (amphipathic N-terminus containing hydrophobic residues) motif(191). One half of the helix is polar and can electrostatically interact with the negatively charged lipid head groups of the membrane. The other hydrophobic half inserts itself into the lipid bilayer, and is functionally important for sensing membrane curvature as well(191). Understanding how ESCRT-III proteins interact with the membrane has yielded significant clues as to how the ESCRT-III polymer sculptures the membrane.

1.5.3 MIT-MIM interactions

A predominant feature of the ESCRT-III complex regulation is the communication between their MIMs and with various MIT domains. This is primarily understood through ESCRT-III interaction with Vps4, but has been described for other MIT containing proteins as well. To date, four MIT-MIM interactions have been described. A fifth unique MIT-MIM interaction has been found between the second MIT domain of Vta1/LIP5 and Vps60/CHMP5, and will be discussed further in Chapter 3 and the appendix. The MIT domain was first described as a putative domain within the SNX15 protein. It was noted that this domain had homology with a variety of other proteins loosely associated with ESCRT function(235,236). Later, a MIT domain was found within Vps4 and is the domain by which it recognizes ESCRT-III proteins(152). The first structure of the MIT domain showed it is approximately 80 amino acids long and is folded into an antiparallel three-helix bundle(127,152,200). It was postulated that each groove between the helices is capable of binding ESCRT-III ligands. The first MIT-MIM structures were determined for the VPS4A-CHMP1A complex and the Vps4-Vps2 complex, and both structures showed that the MIM bound as an amphipathic three-turn helix between helixes α2 and α3 of the MIT domain(200). Sequence alignment predicted that many ESCRT-III proteins have a similar sequence at their C-terminal ends, including Vps24, Vps2, Did2, and Ist1. The consensus sequence motif is (D/E)xxLxxRLxxL(K/R), where x is any residue. This type of MIM is defined a MIM1. As seen in all MIT-MIM1 structures, a majority of the binding energy comes from the Van der Waals contacts made by

the conserved leucines with the hydrophobic grove formed by the MIT helices α2 and α3(127,200). The peripheral hydrophilic contacts also contribute a modest amount of affinity, but are more critical for specificity for a particular MIT domain.

Vps4 MIT also recognizes another type of MIM using the groove between the α1-α3 helices. Here, ESCRT-III proteins Vps20 and Snf7 bind using a different sequence motif called MIM2. The MIM2 has a conserved sequence of (L/V)Px(V/L)P motif, which binds to the grove as an extended coil, and not as a small helix(126). In the structure of MIT-MIM2, the prolines make extensive hydrophobic contacts with the groove. Comparing the two binding sites, the α1-α3 groove is much narrower than the α2-3 groove and presumably prevents helical MIMs from binding. To date, a binding partner for the α1-α2 helical groove has not been identified and will be interesting to see if one exists.

MIT domains within other proteins utilize similar binding sites to interact with MIMs but use distinct mechanisms. CHMP1B recruits the protein Spastin via a MIM-MIT interaction to the midbody during cytokinesis to cleave microtubules(237). Interestingly, the same CHMP1B residues that bind to VPS4 as a MIM1 bind to Spastin as well. However, instead of binding at the groove of α2-α3, CHMP1B binds between α1-α3 of Spastin MIT, which would be the site of MIM2 binding for Vps4(207). Since CHMP1B binding to Spastin is different from either MIM1 (wrong site) or MIM2 (as a helix), this type of MIT-MIM interaction has been defined as a MIM3. The Spastin α1-α3 groove is wider than the Vps4

groove and thus can accommodate a helical MIM. Furthermore, CHMP1B forms a five-turn helix when interacting with Spastin, which is much longer than what is necessary for CHMP1B to bind as a MIM1. Spartin, a protein related to Spastin, is also recruited to the midbody, and is thought to interact with IST1 through a MIT-MIM3 interaction(208). Work from our group has now shown that IST1 does interact with the Spartin MIT at the α1-α3 groove, but as a much shorter helix than CHMP1B (E. Guo, unpublished data).

The fourth type of MIT-MIM interaction is seen in a complex between CHMP3 and AMSH. AMSH, a deubiquitinase recruited by ESCRT proteins during cytokinesis, contains a MIT domain that binds CHMP3(193,223). CHMP3 uses the same residues to bind AMSH as for VPS4. While CHMP3 binds to the equivalent α2-α3 pocket of AMSH, just as it would for Vps4, the critical residues for this interaction are polar not hydrophobic(238). This different binding mode was called a MIM4 with the consensus binding sequence being ExxxExxΦxxΦxxRLxTLRx, where x represents any residue and Φ is any hydrophobic residue.

A common theme of MIT-MIM binding is that it serves to recruit factors in the cell to carry out various functions. Evolution has diversified the MIT domains to bind similar peptide sequences in a variety of different ways. In fact, most MIT domains are not easily detectable by sequence homology alone and it often requires structure determination to conclusively categorize a MIT domain. Thus,

more effort is needed to understand and decode the complex MIT-MIM interactions.

1.6 Scope of the Thesis

The ESCRT machinery serves to complete a distinct set of membrane restructuring events, which is essential for a variety of cellular processes. Deregulation of ESCRT protein can lead to various pathogenic states, particularly in the case of Vps4. Since all ESCRT processes require Vps4 activity, it has been a great source of interest to the field to detail how it is regulated. Currently, there is a dearth of understanding concerning how ESCRT-III proteins work with Vps4 to control ESCRT function. My thesis has focused on how the ESCRT-III proteins either directly, by binding to Vps4, or indirectly, through interactions with Vps4's cofactor LIP5, regulate Vps4 using biochemical and structural methods. In Chapter 2, I will examine the structure of LIP5 and LIP5 in complex with CHMP1B and compare how this interaction contributes to VPS4 regulation. In Chapter 3, I will detail how the ternary complex of LIP5-CHMP1B-CHMP5 uncovered a novel mechanism of LIP5 regulation, and explore the structural requirements of LIP5 stimulation of VPS4. In Chapter 4, I will describe how Vfa1 is a *bona fide* ESCRT-III protein that can potently stimulate Vps4 ATPase activity. Finally in Chapter 5, I will discuss the insights we have gained on Vps4 function, and expand on how this might relate to Vps4 function within the cell. I believe that this thesis work has contributed to our knowledge of Vps4 regulation by ESCRT-III proteins, and has allowed us to better understand how these proteins collectively work together to control ESCRT function in the cell.

1.7 References

1. Mattissek, C., and Teis, D. (014) The role of the endosomal sorting complexes required for transport (ESCRT) in tumorigenesis. *Mol Membr Biol* **31**, 111-119

2. Babst, M. (2005) A protein's final ESCRT. *Traffic* **6**, 2-9

3. Lobert, V. H., Brech, A., Pedersen, N. M., Wesche, J., Oppelt, A., Malerod, L., and Stenmark, H. (2010) Ubiquitination of alpha 5 beta 1 integrin controls fibroblast migration through lysosomal degradation of fibronectin-integrin complexes. *Dev Cell* **19**, 148-159

4. Tu, C., Ortega-Cava, C. F., Winograd, P., Stanton, M. J., Reddi, A. L., Dodge, I., Arya, R., Dimri, M., Clubb, R. J., Naramura, M., Wagner, K. U., Band, V., and Band, H. (2010) Endosomal-sorting complexes required for transport (ESCRT) pathway-dependent endosomal traffic regulates the localization of active Src at focal adhesions. *Proc Natl Acad Sci U S A* **107**, 16107-16112

5. Boyer, B., Valles, A. M., Tucker, G. C., Delouvee, A., and Thiery, J. P. (1993) Involvement of cell motility in tumor progression. *Symp Soc Exp Biol* **47**, 183-195

6. Dukes, J. D., Fish, L., Richardson, J. D., Blaikley, E., Burns, S., Caunt, C. J., Chalmers, A. D., and Whitley, P. (2011) Functional ESCRT machinery is required for constitutive recycling of claudin-1 and maintenance of polarity in vertebrate epithelial cells. *Mol Biol Cell* **22**, 3192-3205

7. Gotzmann, J., Mikula, M., Eger, A., Schulte-Hermann, R., Foisner, R., Beug, H., and Mikulits, W. (2004) Molecular aspects of epithelial cell plasticity: implications for local tumor invasion and metastasis. *Mutat Res* **566**, 9-20

8. Brankatschk, B., Wichert, S. P., Johnson, S. D., Schaad, O., Rossner, M. J., and Gruenberg, J. (2012) Regulation of the EGF transcriptional response by endocytic sorting. *Sci Signal* **5**, ra21

9. Zhang, Z., Stiegler, A. L., Boggon, T. J., Kobayashi, S., and Halmos, B. (2010) EGFR-mutated lung cancer: a paradigm of molecular oncology. *Oncotarget* **1**, 497-514

10. Weihua, Z., Lin, Q., Ramoth, A. J., Fan, D., and Fidler, I. J. (2011) Formation of solid tumors by a single multinucleated cancer cell. *Cancer* **117**, 4092-4099

11. Ariizumi, T., Ogose, A., Kawashima, H., Hotta, T., Umezu, H., and Endo, N. (2009) Multinucleation followed by an acytokinetic cell division in

myxofibrosarcoma with giant cell proliferation. *J Exp Clin Cancer Res* **28**, 44

12. Guizetti, J., and Gerlich, D. W. (2012) ESCRT-III polymers in membrane neck constriction. *Trends Cell Biol* **22**, 133-140

13. Lindas, A. C., Karlsson, E. A., Lindgren, M. T., Ettema, T. J., and Bernander, R. (2008) A unique cell division machinery in the Archaea. *Proc Natl Acad Sci U S A* **105**, 18942-18946

14. Makarova, K. S., Yutin, N., Bell, S. D., and Koonin, E. V. (2010) Evolution of diverse cell division and vesicle formation systems in Archaea. *Nat Rev Microbiol* **8**, 731-741

15. Samson, R. Y., Obita, T., Freund, S. M., Williams, R. L., and Bell, S. D. (2008) A role for the ESCRT system in cell division in archaea. *Science* **322**, 1710-1713

16. Samson, R. Y., Obita, T., Hodgson, B., Shaw, M. K., Chong, P. L., Williams, R. L., and Bell, S. D. (2011) Molecular and structural basis of ESCRT-III recruitment to membranes during archaeal cell division. *Mol Cell* **41**, 186-196

17. Carlton, J. G., and Martin-Serrano, J. (2007) Parallels between cytokinesis and retroviral budding: a role for the ESCRT machinery. *Science* **316**, 1908-1912

18. Elia, N., Sougrat, R., Spurlin, T. A., Hurley, J. H., and Lippincott-Schwartz, J. (2011) Dynamics of endosomal sorting complex required for transport (ESCRT) machinery during cytokinesis and its role in abscission. *Proc Natl Acad Sci U S A* **108**, 4846-4851

19. Morita, E., Sandrin, V., Chung, H. Y., Morham, S. G., Gygi, S. P., Rodesch, C. K., and Sundquist, W. I. (2007) Human ESCRT and ALIX proteins interact with proteins of the midbody and function in cytokinesis. *EMBO J* **26**, 4215-4227

20. Weissenhorn, W., Poudevigne, E., Effantin, G., and Bassereau, P. (2013) How to get out: ssRNA enveloped viruses and membrane fission. *Curr Opin Virol* **3**, 159-167

21. Weiss, E. R., and Gottlinger, H. (2011) The role of cellular factors in promoting HIV budding. *J Mol Biol* **410**, 525-533

22. Martin-Serrano, J., and Neil, S. J. (2011) Host factors involved in retroviral budding and release. *Nat Rev Microbiol* **9**, 519-531

23. McCullough, J., Colf, L. A., and Sundquist, W. I. (2013) Membrane fission reactions of the mammalian ESCRT pathway. *Annu Rev Biochem* **82**, 663-692

24. Morita, E., Sandrin, V., McCullough, J., Katsuyama, A., Baci Hamilton, I., and Sundquist, W. I. (2011) ESCRT-III protein requirements for HIV-1 budding. *Cell Host Microbe* **9**, 235-242

25. Palade, G. E. (1955) Studies on the endoplasmic reticulum. II. Simple dispositions in cells in situ. *J Biophys Biochem Cytol* **1**, 567-582

26. Palay, S. L., and Palade, G. E. (1955) The fine structure of neurons. *J Biophys Biochem Cytol* **1**, 69-88

27. Sager, R., and Palade, G. E. (1957) Structure and development of the chloroplast in Chlamydomonas. I. The normal green cell. *J Biophys Biochem Cytol* **3**, 463-488

28. Sotelo, J. R., and Porter, K. R. (1959) An electron microscope study of the rat ovum. *J Biophys Biochem Cytol* **5**, 327-342

29. Haigler, H. T., McKanna, J. A., and Cohen, S. (1979) Direct visualization of the binding and internalization of a ferritin conjugate of epidermal growth factor in human carcinoma cells A-431. *J Cell Biol* **81**, 382-395

30. Katzmann, D. J., Odorizzi, G., and Emr, S. D. (2002) Receptor downregulation and multivesicular-body sorting. *Nat Rev Mol Cell Biol* **3**, 893-905

31. Raiborg, C., and Stenmark, H. (2009) The ESCRT machinery in endosomal sorting of ubiquitylated membrane proteins. *Nature* **458**, 445-452

32. Futter, C. E., Pearse, A., Hewlett, L. J., and Hopkins, C. R. (1996) Multivesicular endosomes containing internalized EGF-EGF receptor complexes mature and then fuse directly with lysosomes. *J Cell Biol* **132**, 1011-1023

33. Bankaitis, V. A., Johnson, L. M., and Emr, S. D. (1986) Isolation of yeast mutants defective in protein targeting to the vacuole. *Proc Natl Acad Sci U S A* **83**, 9075-9079

34. Rothman, J. H., and Stevens, T. H. (1986) Protein sorting in yeast: mutants defective in vacuole biogenesis mislocalize vacuolar proteins into the late secretory pathway. *Cell* **47**, 1041-1051

35. Banta, L. M., Robinson, J. S., Klionsky, D. J., and Emr, S. D. (1988) Organelle assembly in yeast: characterization of yeast mutants defective in vacuolar biogenesis and protein sorting. *J Cell Biol* **107**, 1369-1383

36. Robinson, J. S., Klionsky, D. J., Banta, L. M., and Emr, S. D. (1988) Protein sorting in Saccharomyces cerevisiae: isolation of mutants defective in the delivery and processing of multiple vacuolar hydrolases. *Mol Cell Biol* **8**, 4936-4948

37. Rothman, J. H., Howald, I., and Stevens, T. H. (1989) Characterization of genes required for protein sorting and vacuolar function in the yeast Saccharomyces cerevisiae. *EMBO J* **8**, 2057-2065

38. Raymond, C. K., Howald-Stevenson, I., Vater, C. A., and Stevens, T. H. (1992) Morphological classification of the yeast vacuolar protein sorting mutants: evidence for a prevacuolar compartment in class E vps mutants. *Mol Biol Cell* **3**, 1389-1402

39. Nickerson, D. P., West, M., and Odorizzi, G. (2006) Did2 coordinates Vps4-mediated dissociation of ESCRT-III from endosomes. *J Cell Biol* **175**, 715-720

40. Rieder, S. E., Banta, L. M., Kohrer, K., McCaffery, J. M., and Emr, S. D. (1996) Multilamellar endosome-like compartment accumulates in the yeast vps28 vacuolar protein sorting mutant. *Mol Biol Cell* **7**, 985-999

41. Katzmann, D. J., Babst, M., and Emr, S. D. (2001) Ubiquitin-dependent sorting into the multivesicular body pathway requires the function of a conserved endosomal protein sorting complex, ESCRT-I. *Cell* **106**, 145-155

42. Hanson, P. I., and Cashikar, A. (2012) Multivesicular body morphogenesis. *Annu Rev Cell Dev Biol* **28**, 337-362

43. Henne, W. M., Buchkovich, N. J., and Emr, S. D. (2011) The ESCRT pathway. *Dev Cell* **21**, 77-91

44. Schuh, A. L., and Audhya, A. (2014) The ESCRT machinery: From the plasma membrane to endosomes and back again. *Crit Rev Biochem Mol Biol*

45. Babst, M., Odorizzi, G., Estepa, E. J., and Emr, S. D. (2000) Mammalian tumor susceptibility gene 101 (TSG101) and the yeast homologue, Vps23p, both function in late endosomal trafficking. *Traffic* **1**, 248-258

46. Bishop, N., and Woodman, P. (2001) TSG101/mammalian VPS23 and mammalian VPS28 interact directly and are recruited to VPS4-induced endosomes. *J Biol Chem* **276**, 11735-11742

47. Leung, K. F., Dacks, J. B., and Field, M. C. (2008) Evolution of the multivesicular body ESCRT machinery; retention across the eukaryotic lineage. *Traffic* **9**, 1698-1716

48. Bonifacino, J. S., and Traub, L. M. (2003) Signals for sorting of transmembrane proteins to endosomes and lysosomes. *Annu Rev Biochem* **72**, 395-447

49. Saksena, S., and Emr, S. D. (2009) ESCRTs and human disease. *Biochem Soc Trans* **37**, 167-172

50. Haglund, K., Sigismund, S., Polo, S., Szymkiewicz, I., Di Fiore, P. P., and Dikic, I. (2003) Multiple monoubiquitination of RTKs is sufficient for their endocytosis and degradation. *Nat Cell Biol* **5**, 461-466

51. MacDonald, C., Buchkovich, N. J., Stringer, D. K., Emr, S. D., and Piper, R. C. (2012) Cargo ubiquitination is essential for multivesicular body intralumenal vesicle formation. *EMBO Rep* **13**, 331-338

52. Urbanowski, J. L., and Piper, R. C. (2001) Ubiquitin sorts proteins into the intralumenal degradative compartment of the late-endosome/vacuole. *Traffic* **2**, 622-630

53. Duncan, L. M., Piper, S., Dodd, R. B., Saville, M. K., Sanderson, C. M., Luzio, J. P., and Lehner, P. J. (2006) Lysine-63-linked ubiquitination is required for endolysosomal degradation of class I molecules. *EMBO J* **25**, 1635-1645

54. Huang, F., Kirkpatrick, D., Jiang, X., Gygi, S., and Sorkin, A. (2006) Differential regulation of EGF receptor internalization and degradation by multiubiquitination within the kinase domain. *Mol Cell* **21**, 737-748

55. van Balkom, B. W., Boone, M., Hendriks, G., Kamsteeg, E. J., Robben, J. H., Stronks, H. C., van der Voorde, A., van Herp, F., van der Sluijs, P., and Deen, P. M. (2009) LIP5 interacts with aquaporin 2 and facilitates its lysosomal degradation. *J Am Soc Nephrol* **20**, 990-1001

56. Dores, M. R., Chen, B., Lin, H., Soh, U. J., Paing, M. M., Montagne, W. A., Meerloo, T., and Trejo, J. (2012) ALIX binds a YPX(3)L motif of the GPCR PAR1 and mediates ubiquitin-independent ESCRT-III/MVB sorting. *J Cell Biol* **197**, 407-419

57. Yamashita, Y., Kojima, K., Tsukahara, T., Agawa, H., Yamada, K., Amano, Y., Kurotori, N., Tanaka, N., Sugamura, K., and Takeshita, T. (2008) Ubiquitin-independent binding of Hrs mediates endosomal sorting of the interleukin-2 receptor beta-chain. *Journal of Cell Science* **121**, 1727-1738

58. Mageswaran, S. K., Dixon, M. G., Curtiss, M., Keener, J. P., and Babst, M. (2014) Binding to any ESCRT can mediate ubiquitin-independent cargo sorting. *Traffic* **15**, 212-229

59. Gibbings, D. J., Ciaudo, C., Erhardt, M., and Voinnet, O. (2009) Multivesicular bodies associate with components of miRNA effector complexes and modulate miRNA activity. *Nat Cell Biol* **11**, 1143-1149

60. Ikeda, H., and Kerppola, T. K. (2008) Lysosomal localization of ubiquitinated Jun requires multiple determinants in a lysine-27-linked polyubiquitin conjugate. *Mol Biol Cell* **19**, 4588-4601

61. Taelman, V. F., Dobrowolski, R., Plouhinec, J. L., Fuentealba, L. C., Vorwald, P. P., Gumper, I., Sabatini, D. D., and De Robertis, E. M. (2010) Wnt signaling requires sequestration of glycogen synthase kinase 3 inside multivesicular endosomes. *Cell* **143**, 1136-1148

62. Bilodeau, P. S., Winistorfer, S. C., Kearney, W. R., Robertson, A. D., and Piper, R. C. (2003) Vps27-Hse1 and ESCRT-I complexes cooperate to increase efficiency of sorting ubiquitinated proteins at the endosome. *J Cell Biol* **163**, 237-243

63. Mizuno, E., Kawahata, K., Kato, M., Kitamura, N., and Komada, M. (2003) STAM proteins bind ubiquitinated proteins on the early endosome via the VHS domain and ubiquitin-interacting motif. *Mol Biol Cell* **14**, 3675-3689

64. Pornillos, O., Alam, S. L., Rich, R. L., Myszka, D. G., Davis, D. R., and Sundquist, W. I. (2002) Structure and functional interactions of the Tsg101 UEV domain. *EMBO J* **21**, 2397-2406

65. Bishop, N., Horman, A., and Woodman, P. (2002) Mammalian class E vps proteins recognize ubiquitin and act in the removal of endosomal protein-ubiquitin conjugates. *J Cell Biol* **157**, 91-101

66. Asao, H., Sasaki, Y., Arita, T., Tanaka, N., Endo, K., Kasai, H., Takeshita, T., Endo, Y., Fujita, T., and Sugamura, K. (1997) Hrs is associated with STAM, a signal-transducing adaptor molecule. Its suppressive effect on cytokine-induced cell growth. *J Biol Chem* **272**, 32785-32791

67. Prag, G., Watson, H., Kim, Y. C., Beach, B. M., Ghirlando, R., Hummer, G., Bonifacino, J. S., and Hurley, J. H. (2007) The Vps27/Hse1 complex is a GAT domain-based scaffold for ubiquitin-dependent sorting. *Dev Cell* **12**, 973-986

68. Bilodeau, P. S., Urbanowski, J. L., Winistorfer, S. C., and Piper, R. C. (2002) The Vps27p Hse1p complex binds ubiquitin and mediates endosomal protein sorting. *Nat Cell Biol* **4**, 534-539

69. Bache, K. G., Brech, A., Mehlum, A., and Stenmark, H. (2003) Hrs regulates multivesicular body formation via ESCRT recruitment to endosomes. *J Cell Biol* **162**, 435-442

70. Katzmann, D. J., Stefan, C. J., Babst, M., and Emr, S. D. (2003) Vps27 recruits ESCRT machinery to endosomes during MVB sorting. *J Cell Biol* **162**, 413-423

71. Razi, M., and Futter, C. E. (2006) Distinct roles for Tsg101 and Hrs in multivesicular body formation and inward vesiculation. *Mol Biol Cell* **17**, 3469-3483

72. Ren, X., and Hurley, J. H. (2010) VHS domains of ESCRT-0 cooperate in high-avidity binding to polyubiquitinated cargo. *EMBO J* **29**, 1045-1054

73. Gillooly, D. J., Simonsen, A., and Stenmark, H. (2001) Cellular functions of phosphatidylinositol 3-phosphate and FYVE domain proteins. *Biochem J* **355**, 249-258

74. Stahelin, R. V., Long, F., Diraviyam, K., Bruzik, K. S., Murray, D., and Cho, W. (2002) Phosphatidylinositol 3-phosphate induces the membrane penetration of the FYVE domains of Vps27p and Hrs. *J Biol Chem* **277**, 26379-26388

75. Gillooly, D. J., Morrow, I. C., Lindsay, M., Gould, R., Bryant, N. J., Gaullier, J. M., Parton, R. G., and Stenmark, H. (2000) Localization of phosphatidylinositol 3-phosphate in yeast and mammalian cells. *EMBO J* **19**, 4577-4588

76. Raiborg, C., Bremnes, B., Mehlum, A., Gillooly, D. J., D'Arrigo, A., Stang, E., and Stenmark, H. (2001) FYVE and coiled-coil domains determine the specific localisation of Hrs to early endosomes. *J Cell Sci* **114**, 2255-2263

77. Kato, M., Miyazawa, K., and Kitamura, N. (2000) A deubiquitinating enzyme UBPY interacts with the Src homology 3 domain of Hrs-binding protein via a novel binding motif PX(V/I)(D/N)RXXKP. *J Biol Chem* **275**, 37481-37487

78. Tanaka, N., Kaneko, K., Asao, H., Kasai, H., Endo, Y., Fujita, T., Takeshita, T., and Sugamura, H. (1999) Possible involvement of a novel STAM-associated molecule "AMSH" in intracellular signal transduction mediated by cytokines. *Journal of Biological Chemistry* **274**, 19129-19135

79. Bowers, K., Piper, S. C., Edeling, M. A., Gray, S. R., Owen, D. J., Lehner, P. J., and Luzio, J. P. (2006) Degradation of endocytosed epidermal growth factor and virally ubiquitinated major histocompatibility complex class I is independent of mammalian ESCRTII. *Journal of Biological Chemistry* **281**, 5094-5105

80. McCullough, J., Row, P. E., Lorenzo, O., Doherty, M., Beynon, R., Clague, M. J., and Urbe, S. (2006) Activation of the endosome-associated ubiquitin isopeptidase AMSH by STAM, a component of the multivesicular body-sorting machinery. *Curr Biol* **16**, 160-165

81. Row, P. E., Prior, I. A., McCullough, J., Clague, M. J., and Urbe, S. (2006) The ubiquitin isopeptidase UBPY regulates endosomal ubiquitin dynamics and is essential for receptor down-regulation. *Journal of Biological Chemistry* **281**, 12618-12624

82. Mizuno, E., Iura, T., Mukai, A., Yoshimori, T., Kitamura, N., and Komada, M. (2005) Regulation of epidermal growth factor receptor down-regulation by UBPY-mediated deubiquitination at endosomes. *Molecular Biology of the Cell* **16**, 5163-5174

83. Mayers, J. R., Fyfe, I., Schuh, A. L., Chapman, E. R., Edwardson, J. M., and Audhya, A. (2011) ESCRT-0 Assembles as a Heterotetrameric Complex on Membranes and Binds Multiple Ubiquitinylated Cargoes Simultaneously. *Journal of Biological Chemistry* **286**, 9636-9645

84. Chu, T., Sun, J., Saksena, S., and Emr, S. D. (2006) New component of ESCRT-I regulates endosomal sorting complex assembly. *J Cell Biol* **175**, 815-823

85. Curtiss, M., Jones, C., and Babst, M. (2007) Efficient cargo sorting by ESCRT-I and the subsequent release of ESCRT-I from multivesicular bodies requires the subunit Mvb12. *Mol Biol Cell* **18**, 636-645

86. Bache, K. G., Slagsvold, T., Cabezas, A., Rosendal, K. R., Raiborg, C., and Stenmark, H. (2004) The growth-regulatory protein HCRP1/hVps37A is a subunit of mammalian ESCRT-I and mediates receptor down-regulation. *Mol Biol Cell* **15**, 4337-4346

87. Eastman, S. W., Martin-Serrano, J., Chung, W., Zang, T., and Bieniasz, P. D. (2005) Identification of human VPS37C, a component of endosomal sorting complex required for transport-I important for viral budding. *J Biol Chem* **280**, 628-636

88. Morita, E., Sandrin, V., Alam, S. L., Eckert, D. M., Gygi, S. P., and Sundquist, W. I. (2007) Identification of human MVB12 proteins as ESCRT-I subunits that function in HIV budding. *Cell Host Microbe* **2**, 41-53

89. Stuchell, M. D., Garrus, J. E., Muller, B., Stray, K. M., Ghaffarian, S., McKinnon, R., Krausslich, H. G., Morham, S. G., and Sundquist, W. I. (2004) The human endosomal sorting complex required for transport (ESCRT-I) and its role in HIV-1 budding. *J Biol Chem* **279**, 36059-36071

90. Stefani, F., Zhang, L., Taylor, S., Donovan, J., Rollinson, S., Doyotte, A., Brownhill, K., Bennion, J., Pickering-Brown, S., and Woodman, P. (2011) UBAP1 is a component of an endosome-specific ESCRT-I complex that is essential for MVB sorting. *Curr Biol* **21**, 1245-1250

91. Wunderley, L., Brownhill, K., Stefani, F., Tabernero, L., and Woodman, P. (2014) The molecular basis for selective assembly of the UBAP1-containing endosome-specific ESCRT-I complex. *J Cell Sci* **127**, 663-672

92. Kostelansky, M. S., Schluter, C., Tam, Y. Y. C., Lee, S., Ghirlando, R., Beach, B., Conibear, E., and Hurley, J. H. (2007) Molecular architecture and functional model of the complete yeast ESCRT-I heterotetramer. *Cell* **129**, 485-498

93. Kostelansky, M. S., Sun, J., Lee, S., Kim, J., Ghirlando, R., Hierro, A., Emr, S. D., and Hurley, J. H. (2006) Structural and functional organization of the ESCRT-I trafficking complex. *Cell* **125**, 113-126

94. Teo, H., Gill, D. J., Sun, J., Perisic, O., Veprintsev, D. B., Vallis, Y., Emr, S. D., and Williams, R. L. (2006) ESCRT-I core and ESCRT-II GLUE domain structures reveal role for GLUE in linking to ESCRT-I and membranes. *Cell* **125**, 99-111

95. Sundquist, W. I., Schubert, H. L., Kelly, B. N., Hill, G. C., Holton, J. M., and Hill, C. P. (2004) Ubiquitin recognition by the human TSG101 protein. *Mol Cell* **13**, 783-789

96. Teo, H., Veprintsev, D. B., and Williams, R. L. (2004) Structural insights into endosomal sorting complex required for transport (ESCRT-I) recognition of ubiquitinated proteins. *J Biol Chem* **279**, 28689-28696

97. Boura, E., Rozycki, B., Herrick, D. Z., Chung, H. S., Vecer, J., Eaton, W. A., Cafiso, D. S., Hummer, G., and Hurley, J. H. (2011) Solution structure of the ESCRT-I complex by small-angle X-ray scattering, EPR, and FRET spectroscopy. *Proc Natl Acad Sci U S A* **108**, 9437-9442

98. Langelier, C., von Schwedler, U. K., Fisher, R. D., De Domenico, I., White, P. L., Hill, C. P., Kaplan, J., Ward, D., and Sundquist, W. I. (2006) Human ESCRT-II complex and its role in human immunodeficiency virus type 1 release. *J Virol* **80**, 9465-9480

99. Hierro, A., Sun, J., Rusnak, A. S., Kim, J., Prag, G., Emr, S. D., and Hurley, J. H. (2004) Structure of the ESCRT-II endosomal trafficking complex. *Nature* **431**, 221-225

100. Im, Y. J., and Hurley, J. H. (2008) Integrated structural model and membrane targeting mechanism of the human ESCRT-II complex. *Dev Cell* **14**, 902-913

101. Teo, H., Perisic, O., Gonzalez, B., and Williams, R. L. (2004) ESCRT-II, an endosome-associated complex required for protein sorting: crystal structure and interactions with ESCRT-III and membranes. *Dev Cell* **7**, 559-569

102. Gill, D. J., Teo, H., Sun, J., Perisic, O., Veprintsev, D. B., Emr, S. D., and Williams, R. L. (2007) Structural insight into the ESCRT-I/-II link and its role in MVB trafficking. *EMBO J* **26**, 600-612

103. Alam, S. L., Sun, J., Payne, M., Welch, B. D., Blake, B. K., Davis, D. R., Meyer, H. H., Emr, S. D., and Sundquist, W. I. (2004) Ubiquitin interactions of NZF zinc fingers. *EMBO J* **23**, 1411-1421

104. Slagsvold, T., Aasland, R., Hirano, S., Bache, K. G., Raiborg, C., Trambaiolo, D., Wakatsuki, S., and Stenmark, H. (2005) Eap45 in mammalian ESCRT-II binds ubiquitin via a phosphoinositide-interacting GLUE domain. *J Biol Chem* **280**, 19600-19606

105. Alam, S. L., Langelier, C., Whitby, F. G., Koirala, S., Robinson, H., Hill, C. P., and Sundquist, W. I. (2006) Structural basis for ubiquitin recognition by the human ESCRT-II EAP45 GLUE domain. *Nat Struct Mol Biol* **13**, 1029-1030

106. Hirano, S., Suzuki, N., Slagsvold, T., Kawasaki, M., Trambaiolo, D., Kato, R., Stenmark, H., and Wakatsuki, S. (2006) Structural basis of ubiquitin recognition by mammalian Eap45 GLUE domain. *Nat Struct Mol Biol* **13**, 1031-1032

107. Im, Y. J., Wollert, T., Boura, E., and Hurley, J. H. (2009) Structure and function of the ESCRT-II-III interface in multivesicular body biogenesis. *Dev Cell* **17**, 234-243

108. Babst, M., Katzmann, D. J., Snyder, W. B., Wendland, B., and Emr, S. D. (2002) Endosome-associated complex, ESCRT-II, recruits transport machinery for protein sorting at the multivesicular body. *Dev Cell* **3**, 283-289

109. Henne, W. M., Buchkovich, N. J., Zhao, Y., and Emr, S. D. (2012) The endosomal sorting complex ESCRT-II mediates the assembly and architecture of ESCRT-III helices. *Cell* **151**, 356-371

110. Wollert, T., and Hurley, J. H. (2010) Molecular mechanism of multivesicular body biogenesis by ESCRT complexes. *Nature* **464**, 864-869

111. Boura, E., Ivanov, V., Carlson, L. A., Mizuuchi, K., and Hurley, J. H. (2012) Endosomal sorting complex required for transport (ESCRT) complexes

induce phase-separated microdomains in supported lipid bilayers. *J Biol Chem* **287**, 28144-28151

112. Richter, C., West, M., and Odorizzi, G. (2007) Dual mechanisms specify Doa4-mediated deubiquitination at multivesicular bodies. *EMBO J* **26**, 2454-2464

113. Wollert, T., Wunder, C., Lippincott-Schwartz, J., and Hurley, J. H. (2009) Membrane scission by the ESCRT-III complex. *Nature* **458**, 172-177

114. Fyfe, I., Schuh, A. L., Edwardson, J. M., and Audhya, A. (2011) Association of the endosomal sorting complex ESCRT-II with the Vps20 subunit of ESCRT-III generates a curvature-sensitive complex capable of nucleating ESCRT-III filaments. *J Biol Chem* **286**, 34262-34270

115. Babst, M., Katzmann, D. J., Estepa-Sabal, E. J., Meerloo, T., and Emr, S. D. (2002) Escrt-III: an endosome-associated heterooligomeric protein complex required for mvb sorting. *Dev Cell* **3**, 271-282

116. Lee, J. A., Liu, L., Javier, R., Kreitzer, A. C., Delaloy, C., and Gao, F. B. (2011) ESCRT-III subunits Snf7-1 and Snf7-2 differentially regulate transmembrane cargos in hESC-derived human neurons. *Mol Brain* **4**, 37

117. Carlton, J. G., Agromayor, M., and Martin-Serrano, J. (2008) Differential requirements for Alix and ESCRT-III in cytokinesis and HIV-1 release. *Proc Natl Acad Sci U S A* **105**, 10541-10546

118. Martinelli, N., Hartlieb, B., Usami, Y., Sabin, C., Dordor, A., Miguet, N., Avilov, S. V., Ribeiro, E. A., Jr., Gottlinger, H., and Weissenhorn, W. (2012) CC2D1A is a regulator of ESCRT-III CHMP4B. *J Mol Biol* **419**, 75-88

119. Muziol, T., Pineda-Molina, E., Ravelli, R. B., Zamborlini, A., Usami, Y., Gottlinger, H., and Weissenhorn, W. (2006) Structural basis for budding by the ESCRT-III factor CHMP3. *Dev Cell* **10**, 821-830

120. Bajorek, M., Schubert, H. L., McCullough, J., Langelier, C., Eckert, D. M., Stubblefield, W. M., Uter, N. T., Myszka, D. G., Hill, C. P., and Sundquist, W. I. (2009) Structural basis for ESCRT-III protein autoinhibition. *Nat Struct Mol Biol* **16**, 754-762

121. Xiao, J., Chen, X. W., Davies, B. A., Saltiel, A. R., Katzmann, D. J., and Xu, Z. (2009) Structural basis of Ist1 function and Ist1-Did2 interaction in the multivesicular body pathway and cytokinesis. *Mol Biol Cell* **20**, 3514-3524

122. Zamborlini, A., Usami, Y., Radoshitzky, S. R., Popova, E., Palu, G., and Gottlinger, H. (2006) Release of autoinhibition converts ESCRT-III

components into potent inhibitors of HIV-1 budding. *Proc Natl Acad Sci U S A* **103**, 19140-19145

123. Ghazi-Tabatabai, S., Saksena, S., Short, J. M., Pobbati, A. V., Veprintsev, D. B., Crowther, R. A., Emr, S. D., Egelman, E. H., and Williams, R. L. (2008) Structure and disassembly of filaments formed by the ESCRT-III subunit Vps24. *Structure* **16**, 1345-1356

124. Lata, S., Schoehn, G., Jain, A., Pires, R., Piehler, J., Gottlinger, H. G., and Weissenhorn, W. (2008) Helical structures of ESCRT-III are disassembled by VPS4. *Science* **321**, 1354-1357

125. Rozycki, B., Kim, Y. C., and Hummer, G. (2011) SAXS ensemble refinement of ESCRT-III CHMP3 conformational transitions. *Structure* **19**, 109-116

126. Kieffer, C., Skalicky, J. J., Morita, E., De Domenico, I., Ward, D. M., Kaplan, J., and Sundquist, W. I. (2008) Two distinct modes of ESCRT-III recognition are required for VPS4 functions in lysosomal protein targeting and HIV-1 budding. *Dev Cell* **15**, 62-73

127. Obita, T., Saksena, S., Ghazi-Tabatabai, S., Gill, D. J., Perisic, O., Emr, S. D., and Williams, R. L. (2007) Structural basis for selective recognition of ESCRT-III by the AAA ATPase Vps4. *Nature* **449**, 735-739

128. Teis, D., Saksena, S., and Emr, S. D. (2008) Ordered assembly of the ESCRT-III complex on endosomes is required to sequester cargo during MVB formation. *Dev Cell* **15**, 578-589

129. Saksena, S., Wahlman, J., Teis, D., Johnson, A. E., and Emr, S. D. (2009) Functional reconstitution of ESCRT-III assembly and disassembly. *Cell* **136**, 97-109

130. Bodon, G., Chassefeyre, R., Pernet-Gallay, K., Martinelli, N., Effantin, G., Hulsik, D. L., Belly, A., Goldberg, Y., Chatellard-Causse, C., Blot, B., Schoehn, G., Weissenhorn, W., and Sadoul, R. (2011) Charged multivesicular body protein 2B (CHMP2B) of the endosomal sorting complex required for transport-III (ESCRT-III) polymerizes into helical structures deforming the plasma membrane. *J Biol Chem* **286**, 40276-40286

131. Hanson, P. I., Roth, R., Lin, Y., and Heuser, J. E. (2008) Plasma membrane deformation by circular arrays of ESCRT-III protein filaments. *J Cell Biol* **180**, 389-402

132. Cashikar, A. G., Shim, S., Roth, R., Maldazys, M. R., Heuser, J. E., and Hanson, P. I. (2014) Structure of cellular ESCRT-III spirals and their relationship to HIV budding. *Elife*, e02184

133. Nickerson, D. P., West, M., Henry, R., and Odorizzi, G. (2010) Regulators of Vps4 ATPase activity at endosomes differentially influence the size and rate of formation of intralumenal vesicles. *Mol Biol Cell* **21**, 1023-1032

134. Babst, M., Sato, T. K., Banta, L. M., and Emr, S. D. (1997) Endosomal transport function in yeast requires a novel AAA-type ATPase, Vps4p. *EMBO J* **16**, 1820-1831

135. Hobel, C. F., Albers, S. V., Driessen, A. J., and Lupas, A. N. (2008) The Sulfolobus solfataricus AAA protein Sso0909, a homologue of the eukaryotic ESCRT Vps4 ATPase. *Biochem Soc Trans* **36**, 94-98

136. Bishop, N., and Woodman, P. (2000) ATPase-defective mammalian VPS4 localizes to aberrant endosomes and impairs cholesterol trafficking. *Mol Biol Cell* **11**, 227-239

137. Fujita, H., Yamanaka, M., Imamura, K., Tanaka, Y., Nara, A., Yoshimori, T., Yokota, S., and Himeno, M. (2003) A dominant negative form of the AAA ATPase SKD1/VPS4 impairs membrane trafficking out of endosomal/lysosomal compartments: class E vps phenotype in mammalian cells. *J Cell Sci* **116**, 401-414

138. Scheuring, S., Rohricht, R. A., Schoning-Burkhardt, B., Beyer, A., Muller, S., Abts, H. F., and Kohrer, K. (2001) Mammalian cells express two VPS4 proteins both of which are involved in intracellular protein trafficking. *J Mol Biol* **312**, 469-480

139. Scheuring, S., Bodor, O., Rohricht, R. A., Muller, S., Beyer, A., and Kohrer, K. (1999) Cloning, characterisation, and functional expression of the Mus musculus SKD1 gene in yeast demonstrates that the mouse SKD1 and the yeast VPS4 genes are orthologues and involved in intracellular protein trafficking. *Gene* **234**, 149-159

140. Erzberger, J. P., and Berger, J. M. (2006) Evolutionary relationships and structural mechanisms of AAA+ proteins. *Annu Rev Biophys Biomol Struct* **35**, 93-114

141. Iyer, L. M., Leipe, D. D., Koonin, E. V., and Aravind, L. (2004) Evolutionary history and higher order classification of AAA+ ATPases. *J Struct Biol* **146**, 11-31

142. Frickey, T., and Lupas, A. N. (2004) Phylogenetic analysis of AAA proteins. *J Struct Biol* **146**, 2-10

143. Ogura, T., and Wilkinson, A. J. (2001) AAA+ superfamily ATPases: common structure--diverse function. *Genes Cells* **6**, 575-597

144. Monroe, N., Han, H., Gonciarz, M. D., Eckert, D. M., Karren, M. A., Whitby, F. G., Sundquist, W. I., and Hill, C. P. (2014) The oligomeric state of the active Vps4 AAA ATPase. *J Mol Biol* **426**, 510-525

145. Gonciarz, M. D., Whitby, F. G., Eckert, D. M., Kieffer, C., Heroux, A., Sundquist, W. I., and Hill, C. P. (2008) Biochemical and structural studies of yeast Vps4 oligomerization. *J Mol Biol* **384**, 878-895

146. Xiao, J., Xia, H., Yoshino-Koh, K., Zhou, J., and Xu, Z. (2007) Structural characterization of the ATPase reaction cycle of endosomal AAA protein Vps4. *J Mol Biol* **374**, 655-670

147. Scott, A., Chung, H. Y., Gonciarz-Swiatek, M., Hill, G. C., Whitby, F. G., Gaspar, J., Holton, J. M., Viswanathan, R., Ghaffarian, S., Hill, C. P., and Sundquist, W. I. (2005) Structural and mechanistic studies of VPS4 proteins. *EMBO J* **24**, 3658-3669

148. Babst, M., Wendland, B., Estepa, E. J., and Emr, S. D. (1998) The Vps4p AAA ATPase regulates membrane association of a Vps protein complex required for normal endosome function. *EMBO J* **17**, 2982-2993

149. Hanson, P. I., and Whiteheart, S. W. (2005) AAA+ proteins: have engine, will work. *Nat Rev Mol Cell Biol* **6**, 519-529

150. Hill, C. P., and Babst, M. (2012) Structure and function of the membrane deformation AAA ATPase Vps4. *Biochim Biophys Acta* **1823**, 172-181

151. Vajjhala, P. R., Nguyen, C. H., Landsberg, M. J., Kistler, C., Gan, A. L., King, G. F., Hankamer, B., and Munn, A. L. (2008) The Vps4 C-terminal helix is a critical determinant for assembly and ATPase activity and has elements conserved in other members of the meiotic clade of AAA ATPases. *FEBS J* **275**, 1427-1449

152. Scott, A., Gaspar, J., Stuchell-Brereton, M. D., Alam, S. L., Skalicky, J. J., and Sundquist, W. I. (2005) Structure and ESCRT-III protein interactions of the MIT domain of human VPS4A. *Proc Natl Acad Sci U S A* **102**, 13813-13818

153. Shestakova, A., Curtiss, M., Davies, B. A., Katzmann, D. J., and Babst, M. (2013) The linker region plays a regulatory role in assembly and activity of the Vps4 AAA ATPase. *J Biol Chem* **288**, 26810-26819

154. Merrill, S. A., and Hanson, P. I. (2010) Activation of human VPS4A by ESCRT-III proteins reveals ability of substrates to relieve enzyme autoinhibition. *J Biol Chem* **285**, 35428-35438

155. Hartmann, C., Chami, M., Zachariae, U., de Groot, B. L., Engel, A., and Grutter, M. G. (2008) Vacuolar protein sorting: two different functional states of the AAA-ATPase Vps4p. *J Mol Biol* **377**, 352-363

156. Azmi, I., Davies, B., Dimaano, C., Payne, J., Eckert, D., Babst, M., and Katzmann, D. J. (2006) Recycling of ESCRTs by the AAA-ATPase Vps4 is regulated by a conserved VSL region in Vta1. *J Cell Biol* **172**, 705-717

157. Whiteheart, S. W., Rossnagel, K., Buhrow, S. A., Brunner, M., Jaenicke, R., and Rothman, J. E. (1994) N-ethylmaleimide-sensitive fusion protein: a trimeric ATPase whose hydrolysis of ATP is required for membrane fusion. *J Cell Biol* **126**, 945-954

158. Landsberg, M. J., Vajjhala, P. R., Rothnagel, R., Munn, A. L., and Hankamer, B. (2009) Three-dimensional structure of AAA ATPase Vps4: advancing structural insights into the mechanisms of endosomal sorting and enveloped virus budding. *Structure* **17**, 427-437

159. Yu, Z., Gonciarz, M. D., Sundquist, W. I., Hill, C. P., and Jensen, G. J. (2008) Cryo-EM structure of dodecameric Vps4p and its 2:1 complex with Vta1p. *J Mol Biol* **377**, 364-377

160. Roll-Mecak, A., and Vale, R. D. (2008) Structural basis of microtubule severing by the hereditary spastic paraplegia protein spastin. *Nature* **451**, 363-367

161. Zhang, X., Shaw, A., Bates, P. A., Newman, R. H., Gowen, B., Orlova, E., Gorman, M. A., Kondo, H., Dokurno, P., Lally, J., Leonard, G., Meyer, H., van Heel, M., and Freemont, P. S. (2000) Structure of the AAA ATPase p97. *Mol Cell* **6**, 1473-1484

162. Hurley, J. H., and Yang, B. (2014) Making sense of Vps4. *J Mol Biol* **426**, 503-506

163. Weber-Ban, E. U., Reid, B. G., Miranker, A. D., and Horwich, A. L. (1999) Global unfolding of a substrate protein by the Hsp100 chaperone ClpA. *Nature* **401**, 90-93

164. Reid, B. G., Fenton, W. A., Horwich, A. L., and Weber-Ban, E. U. (2001) ClpA mediates directional translocation of substrate proteins into the ClpP protease. *Proc Natl Acad Sci U S A* **98**, 3768-3772

165. Davies, B. A., Azmi, I. F., Payne, J., Shestakova, A., Horazdovsky, B. F., Babst, M., and Katzmann, D. J. (2010) Coordination of substrate binding and ATP hydrolysis in Vps4-mediated ESCRT-III disassembly. *Mol Biol Cell* **21**, 3396-3408

166. Vajjhala, P. R., Wong, J. S., To, H. Y., and Munn, A. L. (2006) The beta domain is required for Vps4p oligomerization into a functionally active ATPase. *FEBS J* **273**, 2357-2373

167. Skalicky, J. J., Arii, J., Wenzel, D. M., Stubblefield, W. M., Katsuyama, A., Uter, N. T., Bajorek, M., Myszka, D. G., and Sundquist, W. I. (2012) Interactions of the human LIP5 regulatory protein with endosomal sorting complexes required for transport. *J Biol Chem* **287**, 43910-43926

168. Xiao, J., Xia, H., Zhou, J., Azmi, I. F., Davies, B. A., Katzmann, D. J., and Xu, Z. (2008) Structural basis of Vta1 function in the multivesicular body sorting pathway. *Dev Cell* **14**, 37-49

169. Agromayor, M., Carlton, J. G., Phelan, J. P., Matthews, D. R., Carlin, L. M., Ameer-Beg, S., Bowers, K., and Martin-Serrano, J. (2009) Essential role of hIST1 in cytokinesis. *Mol Biol Cell* **20**, 1374-1387

170. Shim, S., Merrill, S. A., and Hanson, P. I. (2008) Novel interactions of ESCRT-III with LIP5 and VPS4 and their implications for ESCRT-III disassembly. *Mol Biol Cell* **19**, 2661-2672

171. Yang, Z., Vild, C., Ju, J., Zhang, X., Liu, J., Shen, J., Zhao, B., Lan, W., Gong, F., Liu, M., Cao, C., and Xu, Z. (2012) Structural basis of molecular recognition between ESCRT-III-like protein Vps60 and AAA-ATPase regulator Vta1 in the multivesicular body pathway. *J Biol Chem* **287**, 43899-43908

172. Yang, D., and Hurley, J. H. (2010) Structural role of the Vps4-Vta1 interface in ESCRT-III recycling. *Structure* **18**, 976-984

173. Lottridge, J. M., Flannery, A. R., Vincelli, J. L., and Stevens, T. H. (2006) Vta1p and Vps46p regulate the membrane association and ATPase activity of Vps4p at the yeast multivesicular body. *Proc Natl Acad Sci U S A* **103**, 6202-6207

174. Bashkirov, P. V., Akimov, S. A., Evseev, A. I., Schmid, S. L., Zimmerberg, J., and Frolov, V. A. (2008) GTPase cycle of dynamin is coupled to membrane squeeze and release, leading to spontaneous fission. *Cell* **135**, 1276-1286

175. Norgan, A. P., Davies, B. A., Azmi, I. F., Schroeder, A. S., Payne, J. A., Lynch, G. M., Xu, Z., and Katzmann, D. J. (2013) Relief of autoinhibition enhances Vta1 activation of Vps4 via the Vps4 stimulatory element. *J Biol Chem* **288**, 26147-26156

176. Azmi, I. F., Davies, B. A., Xiao, J., Babst, M., Xu, Z., and Katzmann, D. J. (2008) ESCRT-III family members stimulate Vps4 ATPase activity directly or via Vta1. *Dev Cell* **14**, 50-61

177. Haas, T. J., Sliwinski, M. K., Martinez, D. E., Preuss, M., Ebine, K., Ueda, T., Nielsen, E., Odorizzi, G., and Otegui, M. S. (2007) The Arabidopsis AAA ATPase SKD1 is involved in multivesicular endosome function and interacts with its positive regulator LYST-INTERACTING PROTEIN5. *Plant Cell* **19**, 1295-1312

178. Shestakova, A., Hanono, A., Drosner, S., Curtiss, M., Davies, B. A., Katzmann, D. J., and Babst, M. (2010) Assembly of the AAA ATPase Vps4 on ESCRT-III. *Mol Biol Cell* **21**, 1059-1071

179. Shiflett, S. L., Ward, D. M., Huynh, D., Vaughn, M. B., Simmons, J. C., and Kaplan, J. (2004) Characterization of Vta1p, a class E Vps protein in Saccharomyces cerevisiae. *J Biol Chem* **279**, 10982-10990

180. Rue, S. M., Mattei, S., Saksena, S., and Emr, S. D. (2008) Novel Ist1-Did2 complex functions at a late step in multivesicular body sorting. *Mol Biol Cell* **19**, 475-484

181. Boone, M., Mobasheri, A., Fenton, R. A., van Balkom, B. W., Wismans, R., van der Zee, C. E., and Deen, P. M. (2010) The lysosomal trafficking regulator interacting protein-5 localizes mainly in epithelial cells. *J Mol Histol* **41**, 61-74

182. Kuang, Z., Seo, E. J., and Leis, J. (2011) Mechanism of inhibition of retrovirus release from cells by interferon-induced gene ISG15. *J Virol* **85**, 7153-7161

183. Pincetic, A., Kuang, Z., Seo, E. J., and Leis, J. (2010) The interferon-induced gene ISG15 blocks retrovirus release from cells late in the budding process. *J Virol* **84**, 4725-4736

184. Ward, D. M., Vaughn, M. B., Shiflett, S. L., White, P. L., Pollock, A. L., Hill, J., Schnegelberger, R., Sundquist, W. I., and Kaplan, J. (2005) The role of LIP5 and CHMP5 in multivesicular body formation and HIV-1 budding in mammalian cells. *J Biol Chem* **280**, 10548-10555

185. Herman, E. K., Walker, G., van der Giezen, M., and Dacks, J. B. (2011) Multivesicular bodies in the enigmatic amoeboflagellate Breviata anathema and the evolution of ESCRT 0. *J Cell Sci* **124**, 613-621

186. Fisher, R. D., Chung, H. Y., Zhai, Q., Robinson, H., Sundquist, W. I., and Hill, C. P. (2007) Structural and biochemical studies of ALIX/AIP1 and its role in retrovirus budding. *Cell* **128**, 841-852

187. Strack, B., Calistri, A., Craig, S., Popova, E., and Gottlinger, H. G. (2003) AIP1/ALIX is a binding partner for HIV-1 p6 and EIAV p9 functioning in virus budding. *Cell* **114**, 689-699

188. Garrus, J. E., von Schwedler, U. K., Pornillos, O. W., Morham, S. G., Zavitz, K. H., Wang, H. E., Wettstein, D. A., Stray, K. M., Cote, M., Rich, R. L., Myszka, D. G., and Sundquist, W. I. (2001) Tsg101 and the vacuolar protein sorting pathway are essential for HIV-1 budding. *Cell* **107**, 55-65

189. McNeil, P. L. (2014) Cell Biology: ESCRTing Trouble Out! *Curr Biol* **24**, R370-372

190. Fabrikant, G., Lata, S., Riches, J. D., Briggs, J. A., Weissenhorn, W., and Kozlov, M. M. (2009) Computational model of membrane fission catalyzed by ESCRT-III. *PLoS Comput Biol* **5**, e1000575

191. Buchkovich, N. J., Henne, W. M., Tang, S., and Emr, S. D. (2013) Essential N-terminal insertion motif anchors the ESCRT-III filament during MVB vesicle formation. *Dev Cell* **27**, 201-214

192. Adell, M. A., Vogel, G. F., Pakdel, M., Muller, M., Lindner, H., Hess, M. W., and Teis, D. (2014) Coordinated binding of Vps4 to ESCRT-III drives membrane neck constriction during MVB vesicle formation. *J Cell Biol* **205**, 33-49

193. Lenz, M., Crow, D. J., and Joanny, J. F. (2009) Membrane buckling induced by curved filaments. *Phys Rev Lett* **103**, 038101

194. Iwaya, N., Kuwahara, Y., Fujiwara, Y., Goda, N., Tenno, T., Akiyama, K., Mase, S., Tochio, H., Ikegami, T., Shirakawa, M., and Hiroaki, H. (2010) A common substrate recognition mode conserved between katanin p60 and VPS4 governs microtubule severing and membrane skeleton reorganization. *J Biol Chem* **285**, 16822-16829

195. Bonemann, G., Pietrosiuk, A., Diemand, A., Zentgraf, H., and Mogk, A. (2009) Remodelling of VipA/VipB tubules by ClpV-mediated threading is crucial for type VI protein secretion. *EMBO J* **28**, 315-325

196. Pietrosiuk, A., Lenherr, E. D., Falk, S., Bonemann, G., Kopp, J., Zentgraf, H., Sinning, I., and Mogk, A. (2011) Molecular basis for the unique role of the AAA+ chaperone ClpV in type VI protein secretion. *J Biol Chem* **286**, 30010-30021

197. Howard, T. L., Stauffer, D. R., Degnin, C. R., and Hollenberg, S. M. (2001) CHMP1 functions as a member of a newly defined family of vesicle trafficking proteins. *J Cell Sci* **114**, 2395-2404

198. Morita, E., and Sundquist, W. I. (2004) Retrovirus budding. *Annu Rev Cell Dev Biol* **20**, 395-425

199. Bowers, K., Lottridge, J., Helliwell, S. B., Goldthwaite, L. M., Luzio, J. P., and Stevens, T. H. (2004) Protein-protein interactions of ESCRT complexes in the yeast Saccharomyces cerevisiae. *Traffic* **5**, 194-210

200. Stuchell-Brereton, M. D., Skalicky, J. J., Kieffer, C., Karren, M. A., Ghaffarian, S., and Sundquist, W. I. (2007) ESCRT-III recognition by VPS4 ATPases. *Nature* **449**, 740-744

201. Dimaano, C., Jones, C. B., Hanono, A., Curtiss, M., and Babst, M. (2008) Ist1 regulates Vps4 localization and assembly. *Mol Biol Cell* **19**, 465-474

202. Jones, C. B., Ott, E. M., Keener, J. M., Curtiss, M., Sandrin, V., and Babst, M. (2012) Regulation of membrane protein degradation by starvation-response pathways. *Traffic* **13**, 468-482

203. Bajorek, M., Morita, E., Skalicky, J. J., Morham, S. G., Babst, M., and Sundquist, W. I. (2009) Biochemical analyses of human IST1 and its function in cytokinesis. *Mol Biol Cell* **20**, 1360-1373

204. Agromayor, M., and Martin-Serrano, J. (2006) Interaction of AMSH with ESCRT-III and deubiquitination of endosomal cargo. *J Biol Chem* **281**, 23083-23091

205. Tsang, H. T., Connell, J. W., Brown, S. E., Thompson, A., Reid, E., and Sanderson, C. M. (2006) A systematic analysis of human CHMP protein interactions: additional MIT domain-containing proteins bind to multiple components of the human ESCRT III complex. *Genomics* **88**, 333-346

206. Row, P. E., Liu, H., Hayes, S., Welchman, R., Charalabous, P., Hofmann, K., Clague, M. J., Sanderson, C. M., and Urbe, S. (2007) The MIT domain of UBPY constitutes a CHMP binding and endosomal localization signal required for efficient epidermal growth factor receptor degradation. *J Biol Chem* **282**, 30929-30937

207. Yang, D., Rismanchi, N., Renvoise, B., Lippincott-Schwartz, J., Blackstone, C., and Hurley, J. H. (2008) Structural basis for midbody targeting of spastin by the ESCRT-III protein CHMP1B. *Nat Struct Mol Biol* **15**, 1278-1286

208. Renvoise, B., Parker, R. L., Yang, D., Bakowska, J. C., Hurley, J. H., and Blackstone, C. (2010) SPG20 protein spartin is recruited to midbodies by ESCRT-III protein Ist1 and participates in cytokinesis. *Mol Biol Cell* **21**, 3293-3303

209. Reid, E., Connell, J., Edwards, T. L., Duley, S., Brown, S. E., and Sanderson, C. M. (2005) The hereditary spastic paraplegia protein spastin interacts with the ESCRT-III complex-associated endosomal protein CHMP1B. *Hum Mol Genet* **14**, 19-38

210. Lee, S., Chang, J., Renvoise, B., Tipirneni, A., Yang, S., and Blackstone, C. (2012) MITD1 is recruited to midbodies by ESCRT-III and participates in cytokinesis. *Mol Biol Cell* **23**, 4347-4361

211. Hadders, M. A., Agromayor, M., Obita, T., Perisic, O., Caballe, A., Kloc, M., Lamers, M. H., Williams, R. L., and Martin-Serrano, J. (2012) ESCRT-III binding protein MITD1 is involved in cytokinesis and has an unanticipated PLD fold that binds membranes. *Proc Natl Acad Sci U S A* **109**, 17424-17429

212. Tandon, R., AuCoin, D. P., and Mocarski, E. S. (2009) Human cytomegalovirus exploits ESCRT machinery in the process of virion maturation. *J Virol* **83**, 10797-10807

213. Jimenez, A. J., Maiuri, P., Lafaurie-Janvore, J., Divoux, S., Piel, M., and Perez, F. (2014) ESCRT machinery is required for plasma membrane repair. *Science* **343**, 1247136

214. Maemoto, Y., Osako, Y., Goto, E., Nozawa, E., Shibata, H., and Maki, M. (2011) Calpain-7 binds to CHMP1B at its second alpha-helical region and forms a ternary complex with IST1. *J Biochem* **150**, 411-421

215. Osako, Y., Maemoto, Y., Tanaka, R., Suzuki, H., Shibata, H., and Maki, M. (2010) Autolytic activity of human calpain 7 is enhanced by ESCRT-III-related protein IST1 through MIT-MIM interaction. *FEBS J* **277**, 4412-4426

216. Maemoto, Y., Kiso, S., Shibata, H., and Maki, M. (2013) Analysis of limited proteolytic activity of calpain-7 using non-physiological substrates in mammalian cells. *FEBS J* **280**, 2594-2607

217. Stauffer, D. R., Howard, T. L., Nyun, T., and Hollenberg, S. M. (2001) CHMP1 is a novel nuclear matrix protein affecting chromatin structure and cell-cycle progression. *J Cell Sci* **114**, 2383-2393

218. Li, J., Belogortseva, N., Porter, D., and Park, M. (2008) Chmp1A functions as a novel tumor suppressor gene in human embryonic kidney and ductal pancreatic tumor cells. *Cell Cycle* **7**, 2886-2893

219. You, Z., Xin, Y., Liu, Y., Sun, J., Zhou, G., Gao, H., Xu, P., Chen, Y., Chen, G., Zhang, L., Gu, L., Chen, Z., Han, B., and Xuan, Y. (2012) Chmp1A acts as a tumor suppressor gene that inhibits proliferation of renal cell carcinoma. *Cancer Lett* **319**, 190-196

220. Manohar, S., Harlow, M., Nguyen, H., Li, J., Hankins, G. R., and Park, M. (2011) Chromatin modifying protein 1A (Chmp1A) of the endosomal sorting complex required for transport (ESCRT)-III family activates ataxia telangiectasia mutated (ATM) for PanC-1 cell growth inhibition. *Cell Cycle* **10**, 2529-2539

221. Mochida, G. H., Ganesh, V. S., de Michelena, M. I., Dias, H., Atabay, K. D., Kathrein, K. L., Huang, H. T., Hill, R. S., Felie, J. M., Rakiec, D., Gleason, D., Hill, A. D., Malik, A. N., Barry, B. J., Partlow, J. N., Tan, W. H., Glader, L. J., Barkovich, A. J., Dobyns, W. B., Zon, L. I., and Walsh, C. A. (2012) CHMP1A encodes an essential regulator of BMI1-INK4A in cerebellar development. *Nat Genet* **44**, 1260-1264

222. Kranz, A., Kinner, A., and Kolling, R. (2001) A family of small coiled-coil-forming proteins functioning at the late endosome in yeast. *Mol Biol Cell* **12**, 711-723

223. Shim, J. H., Xiao, C., Hayden, M. S., Lee, K. Y., Trombetta, E. S., Pypaert, M., Nara, A., Yoshimori, T., Wilm, B., Erdjument-Bromage, H., Tempst, P., Hogan, B. L., Mellman, I., and Ghosh, S. (2006) CHMP5 is essential for late endosome function and down-regulation of receptor signaling during mouse embryogenesis. *J Cell Biol* **172**, 1045-1056

224. Berns, N., Woichansky, I., Friedrichsen, S., Kraft, N., and Riechmann, V. (2014) A genome-scale in vivo RNAi analysis of epithelial development in Drosophila identifies new proliferation domains outside of the stem cell niche. *J Cell Sci*

225. Hurley, J. H., and Yang, D. (2008) MIT domainia. *Dev Cell* **14**, 6-8

226. Mu, R., Dussupt, V., Jiang, J., Sette, P., Rudd, V., Chuenchor, W., Bello, N. F., Bouamr, F., and Xiao, T. S. (2012) Two distinct binding modes define the interaction of Brox with the C-terminal tails of CHMP5 and CHMP4B. *Structure* **20**, 887-898

227. Zhai, Q., Landesman, M. B., Robinson, H., Sundquist, W. I., and Hill, C. P. (2011) Structure of the Bro1 domain protein BROX and functional analyses of the ALIX Bro1 domain in HIV-1 budding. *PLoS One* **6**, e27466

228. Shahmoradgoli, M., Mannherz, O., Engel, F., Heck, S., Kramer, A., Seiffert, M., Pscherer, A., and Lichter, P. (2011) Antiapoptotic function of charged multivesicular body protein 5: a potentially relevant gene in acute myeloid leukemia. *Int J Cancer* **128**, 2865-2871

229. Wang, H. R., Xiao, Z. Y., Chen, M., Wang, F. L., Liu, J., Zhong, H., Zhong, J. H., Ou-Yang, R. R., Shen, Y. L., and Pan, S. M. (2012) Anti-CHMP5 single chain variable fragment antibody retrovirus infection induces programmed cell death of AML leukemic cells in vitro. *Acta Pharmacol Sin* **33**, 809-816

230. Arlt, H., Perz, A., and Ungermann, C. (2011) An overexpression screen in Saccharomyces cerevisiae identifies novel genes that affect endocytic protein trafficking. *Traffic* **12**, 1592-1603

231. Lu, Q., Hope, L. W. Q., Brasch, M., Reinhard, C., and Cohen, S. N. (2003) TSG101 interaction with HRS mediates endosomal trafficking and receptor down-regulation. *P Natl Acad Sci USA* **100**, 7626-7631

232. Pornillos, O., Higginson, D. S., Stray, K. M., Fisher, R. D., Garrus, J. E., Payne, M., He, G. P., Wang, H. E., Morham, S. G., and Sundquist, W. I. (2003) HIV Gag mimics the Tsg101-recruiting activity of the human Hrs protein. *Journal of Cell Biology* **162**, 425-434

233. Morita, E., Colf, L. A., Karren, M. A., Sandrin, V., Rodesch, C. K., and Sundquist, W. I. (2010) Human ESCRT-III and VPS4 proteins are required for centrosome and spindle maintenance. *Proc Natl Acad Sci U S A* **107**, 12889-12894

234. Yorikawa, C., Shibata, H., Waguri, S., Hatta, K., Horii, M., Katoh, K., Kobayashi, T., Uchiyama, Y., and Maki, M. (2005) Human CHMP6, a myristoylated ESCRT-III protein, interacts directly with an ESCRT-II component EAP20 and regulates endosomal cargo sorting. *Biochem J* **387**, 17-26

235. Phillips, S. A., Barr, V. A., Haft, D. H., Taylor, S. I., and Haft, C. R. (2001) Identification and characterization of SNX15, a novel sorting nexin involved in protein trafficking. *J Biol Chem* **276**, 5074-5084

236. Ciccarelli, F. D., Proukakis, C., Patel, H., Cross, H., Azam, S., Patton, M. A., Bork, P., and Crosby, A. H. (2003) The identification of a conserved domain in both spartin and spastin, mutated in hereditary spastic paraplegia. *Genomics* **81**, 437-441

237. Lumb, J. H., Connell, J. W., Allison, R., and Reid, E. (2012) The AAA ATPase spastin links microtubule severing to membrane modelling. *Biochim Biophys Acta* **1823**, 192-197

238. Solomons, J., Sabin, C., Poudevigne, E., Usami, Y., Hulsik, D. L., Macheboeuf, P., Hartlieb, B., Gottlinger, H., and Weissenhorn, W. (2011) Structural basis for ESCRT-III CHMP3 recruitment of AMSH. *Structure* **19**, 1149-1159

Chapter 2 Structural Conservation of Vps4 regulation by its co-factor Vta1 and ESCRT-III proteins

2.1 Abstract

Disassembly of endosomal sorting complexes required for transport (ESCRT) machinery from cellular membrane is a critical final step in multi-vesicular body biogenesis, retroviral release, abscission during cytokinesis and plasma membrane repair. This process requires the interaction of the ESCRT-III complex with the enzymatic Vps4-Vta1 (VPS4/LIP5 in human) complex. While it has been extensively studied in yeast, there has been a lack of understanding whether the specifics of these interactions are conserved in human proteins as well. Here we present the crystal structures of the LIP5 N-terminal domain (LIP5NTD), the region that interacts with the ESCRT-III ligands, alone and in complex with a fragment of an ESCRT-III protein, CHMP1B. The LIP5NTD contains two microtubule-interacting and trafficking (MIT) domains. We saw that, thematically, LIP5NTD and Vta1NTD share the same fold, but there are subtle differences between the two structures particularly in the second MIT domain. These differences may explain the different binding properties for yeast and human ESCRT-III proteins to this domain. Furthermore, we identified that for both yeast and human, CHMP1B interacts with the first MIT domain of LIP5. The MIT-interacting motif (MIM) of CHMP1B binds via a canonical MIT-MIM1 mode as seen for other MIT-ESCRT-III interactions. Our data redefine how the

ESCRT-III proteins bind to LIP5, and suggest a lack of conservation for ESCRT-III binding to the second MIT domain of LIP5.

2.2 Introduction

The Endosomal Sorting Complexes Required for Transport (ESCRT) proteins control and complete many essential biological processes, such as multi-vesicular body (MVB) biogenesis, enveloped virus budding, abscission during cytokinesis, and repair of small membrane wounds (1-4). These events are all topologically related by the fact that they require the budding of cellular membrane away from the cytosol, which is distinct from other well-studied protein-membrane reconstructing events like clathrin-mediated endocytosis (5). MVB biogenesis is the best understood process of all the ESCRT-controlled functions, and was initially characterized in yeast (6). Although predominantly studied in this context, it has been shown that the ESCRT proteins are well-conserved from archaea to human and are thought to function through similar mechanisms regardless of protein origin (7).

The ESCRT proteins function as a series of macromolecular complexes during the long process of vesicle formation (8,9). Working at the later stage of vesicle formation are two ESCRT complexes, ESCRT-III and Vps4 (in human: VPS4). The ESCRT-III complex is comprised of similarly folded proteins, whose job is to bind and deform membrane (10,11). The ESCRT-III proteins, when bound to the membrane, are thought to undergo conformational changes that expose a C-terminal region that can now bind to the AAA-ATPase Vps4. Vps4

contains a microtubule-interacting and trafficking (MIT) domain at its N-terminus that can engage with the ESCRT-III proteins (12). Structurally, MIT domains are comprised of a small three-helix bundle capable of binding ligands in the grooves between its helical grooves. In fact, the ESCRT-III proteins have evolved to bind at discreet grooves on the surface of the Vps4 MIT domain using two different sequence motifs, commonly referred to as MIT-interacting motifs (MIMs) (13-15). Through this MIT-MIM interaction ESCRT-III recruits Vps4 to the membrane, and where ATP hydrolysis provides the energy necessary to complete membrane scission(16).

Vps4, however, is an inefficient enzyme that must undergo oligomerization to form a functional and active species (17). Upon ATP binding, Vps4 monomers form a high-ordered, hexameric, and single-ringed species that is functionally active (18). Biochemical studies have shown that this oligomer is unstable and requires additional factors to be stabilized in this conformational state (19). One such factor is Vta1 (LIP5), an ESCRT protein that binds to a unique domain within the ATPase domain of Vps4 (20). The Vps4-Vta1 interaction has been shown to dramatically increase Vps4 ATPase activity. It is thought that Vta1 interaction helps stabilize the oligomer, which in turn increases ATPase throughput (19). Vta1 may also aid in Vps4 regulation by controlling its localization. Vta1 contains two tandem MIT domains at its N-terminus (19). The multiplicity of MIT domains within the Vps4-Vta1 complex increase its avidity in

binding the ESCRT-III ligands, thus allowing the complex to be recruited to the membrane.

Two ESCRT-III proteins, Did2 (CHMP1A and CHMP1B) and Vps60 (CHMP5) are thought to have specialized roles in recruiting the Vps4-Vta1 complex. Loss of either Did2 or Vps60 leads to altered kinetics for receptor degradation through the MVB pathway, presumably due to the development of MVBs with unusual morphology (21,22). Did2 can bind to either the Vps4 MIT or the Vta1 MIT domains, and both interactions increase Vps4 ATPase activity (23,24). It seems that Vps60 can only interact with Vta1 and not with Vps4 (25,26). With regards to VPS4 binding in human, the CHMP1A MIM was found to form a small helix that binds between the second and third helices of the Vps4 MIT, which has since been classified as a MIT-MIM1 interaction (15). The specifics of this interaction are thought to be conserved in yeast as well. In yeast, Did2 binding to Vta1 has been mapped to the second MIT domain where it is assumed to interact by a canonical MIT-MIM1 mechanism (23). Although, it is not known whether the human orthologs of Did2 and Vta1 bind using the same mechanism.

Currently, there is a significant gap between our understandings of ESCRT function in yeast versus in human. Vta1 and LIP5 have low sequence homology, which suggests the possibility that ESCRT-III proteins regulate Vta1 and LIP5 by different mechanisms. To this end, we determined the crystal

structure of the LIP5 N-terminal domain (LIP5NTD). We found that, overall, the N-terminal domains of LIP5 and Vta1 adopt a similar fold. However, some structural differences indicate a possible alternative mechanism of regulation. We also investigated the nature of interaction between Did2 and Vta1, and between CHMP1B and LIP5. To our surprise, we found that regardless of protein origin, the ESCRT-III protein bound to MIT1 of Vta1/LIP5, while Vps60 binds to MIT2. The high-resolution crystal structure of LIP5NTD-CHMP1B showed that this interaction indeed occurs via a canonical mode of MIT-MIM1 interaction. From our biochemical and structural analysis, regulation by the ESCRT-III proteins for the Vta1/LIP5 MIT1 domain seems to be conserved, while regulation of MIT2 is divergent.

2.3 Results

2.3.1 The crystal structure of the N-terminal domain of LIP5

Due to the low sequence homology between yeast Vta1 and human LIP5 (approximately 22% identity) (Figure 2.1), we sought to determine the crystal structure of the N-terminal domain of LIP5 (LIP5NTD, residues 1-162) to identify the extent of conservation between the two structures. The LIP5NTD structure was determined by single-wavelength anomalous diffraction (SAD) method and refined to a 3.0Å resolution with an R-factor of 24.8% and a free R-factor of 28.6% (Table 2.1).

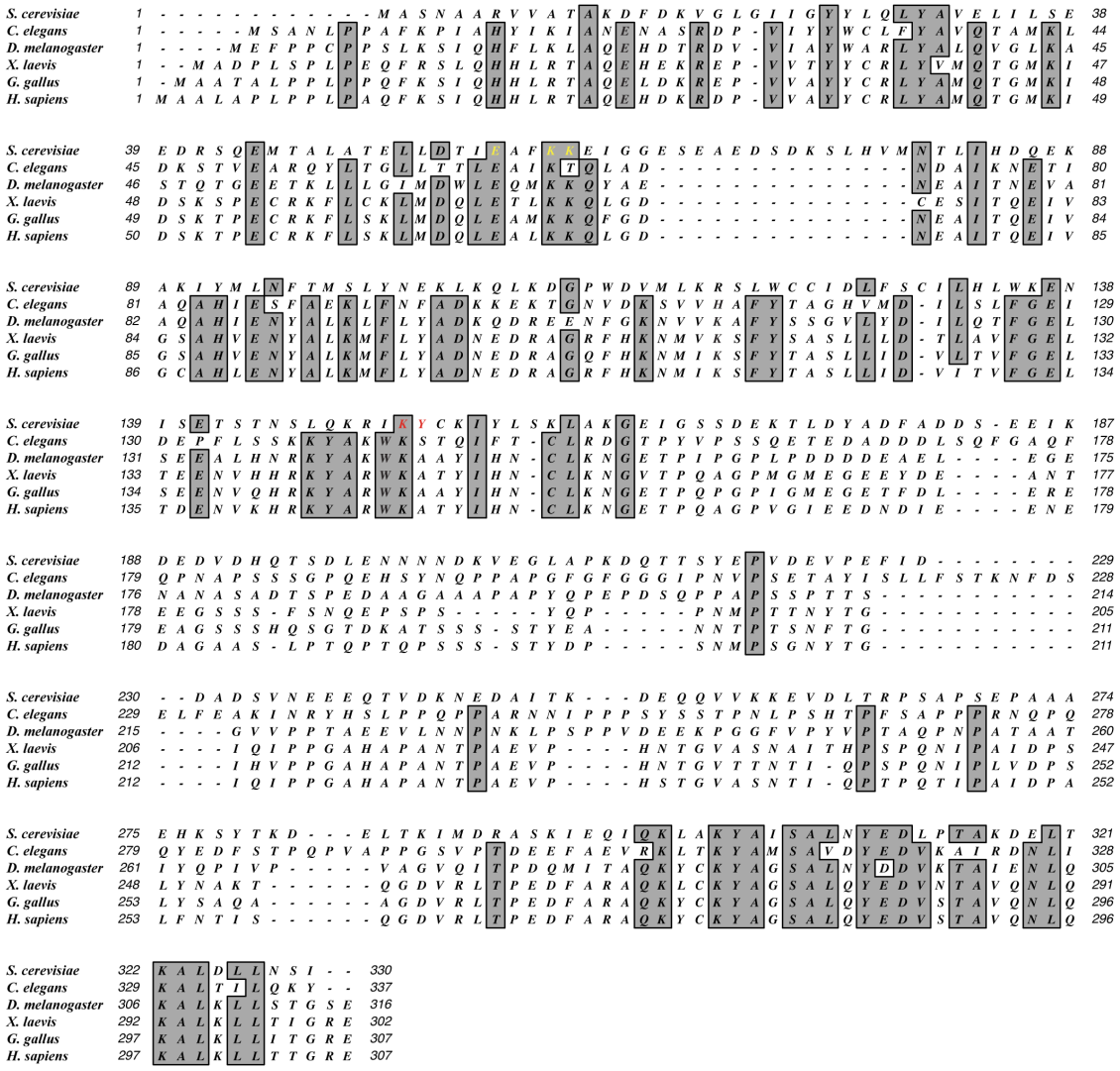

Figure 2.1 Sequence alignment of Vta1/LIP5
Vta1 residues predicted to be important for binding the ESCRT-III proteins to the MIT1 are colored in yellow. Vta1 MIT2 residues that are important for Vps60 are colored in red.

In the crystal structure, there are three molecules in the asymmetric unit (ASU). The electron density quality for the three molecules varies at different regions of the protein structure. Only molecule A had sufficient electron density

Table 2.1 Crystallographic data statistics

	LIP5NTD		LIP5NTD/CHMP1B
	Native	SeMet	Native
Data Collection			
Space group	$P6_522$	$P6_522$	$P2_12_12_1$
Unit cell parameters:			
a, b, c (Å)	76.4, 76.4, 355.9	76.1, 76.1, 355.1	52.8, 55.2, 194.9
α, β, γ (°)	90.0, 90.0, 120.0	90.0, 90.0, 120.0	90.0, 90.0, 90.0
Molecules/ASU	3	3	2
Wavelength (Å)	0.9792	0.9792	0.9787
Resolution (Å)	3.0	3.3	2.2
Unique reflections	13124	9907	29702
Redundancy[1]	6.9 (7.1)	18.3 (19.0)	7.3 (7.4)
Completeness (%)	98.8 (99.8)	98.2 (99.1)	99.9 (100)
Average I/σ (I)	18.8 (3.6)	22.4 (5.0)	19.4 (3.2)
R_{merge}	0.10 (0.60)	0.16 (0.56)	0.11 (0.55)
Refinement			
Residues in the structure			
LIP5	3-158		1-162
CHMP1B			183-199
Resolution range (Å)	50.0-3.0		50.0-2.2
R_{work} (%)	25.0		19.6
R_{free} (%)	28.7		22.7
RMS deviations			
Bond lengths (Å)	0.010		0.009
Bond angles (°)	1.06		1.22
B-factor average (A^2)	71.1		37.6
Ramachandran plot			
Most favored (%)	97.7		98.0
Allowed (%)	1.2		1.7
Outliers (%)	1.2		0.3
PDB accession code	4TXP		4TXQ

[1] Values in parentheses are for the specified high-resolution bin.

to build a continuous model. In the final model, residue 4 is missing for molecule B and residues 4 and 7 are missing for molecule C. By aligning molecule A to B, A to C and B to C based on their visible Cα positions, we determined that the root mean squire deviations (r.s.m.d) were 0.22, 0.37, and 0.36 $Å^2$, respectively (Figure 2.2B). In the following structure description and analysis, we use molecule A as a structure representative for the LIP5NTD structure.

A

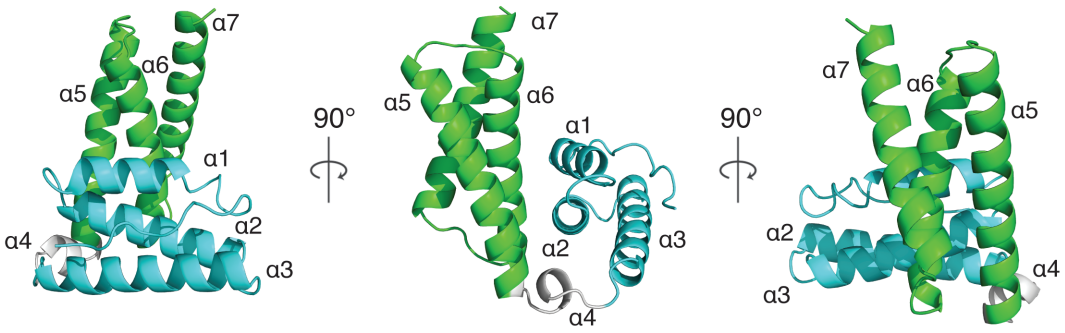

B

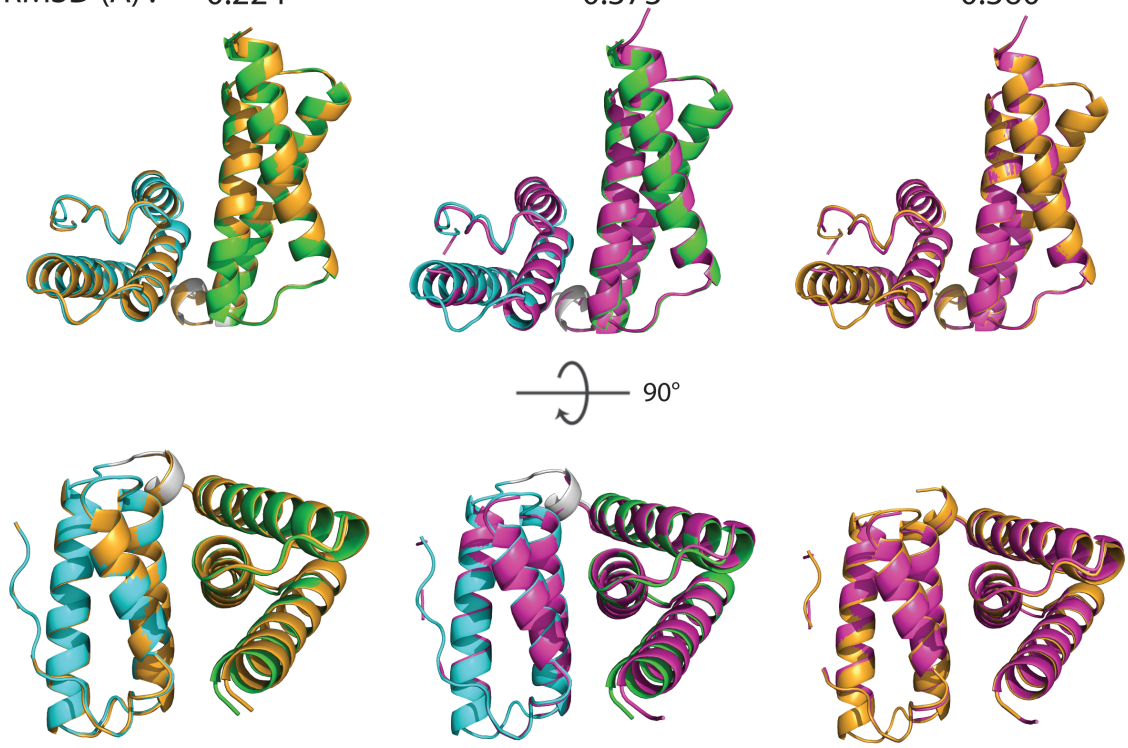
Molecule:
A + B
A + C
B + C
RMSD (Å) :
0.224
0.373
0.360
90°

C

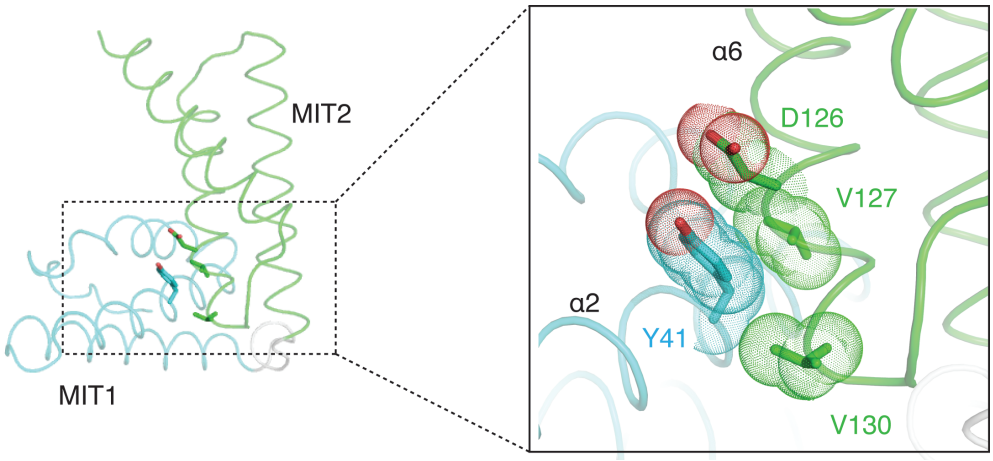
MIT2
MIT1
α6
D126
V127
α2
Y41
V130

D

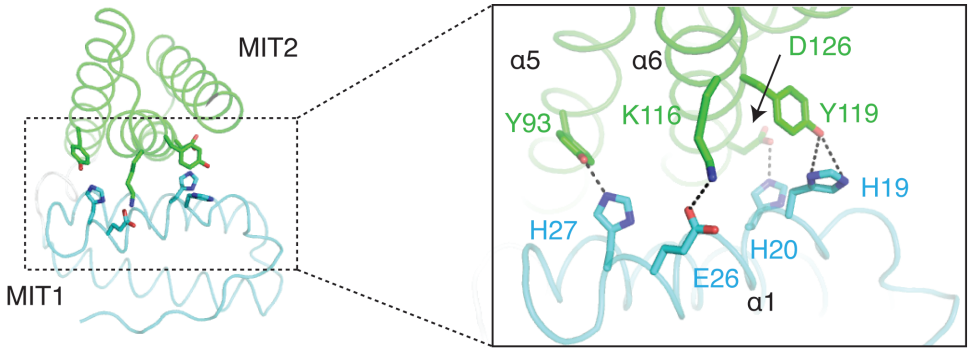

Figure 2.2 The crystal structure of LIP5NTD
(A) Overview of the LIP5NTD structure. Cartoon representation of LIP5NTD (1-162) in three orthogonal views. MIT1, MIT2 and the short linker between the two MIT domains of LIP5NTD are colored cyan, green and white, respectively. Helices of LIP5NTD are labeled α1-α7. (B) Molecules in the asymmetric unit have good agreement with each other. Molecules in the asymmetric unit were aligned to one another based on their Cα positions, where the root mean squared deviation is noted above the alignment (RMSD, Å). Molecule A has the same coloring scheme described in Figure 1A, molecule B is colored in magenta, and molecule C is colored in orange. (C) An example of van der Waals contacts at MIT domain interface with the same coloring scheme as described in Figure 1 except atoms are colored as such: carbon atoms of MIT1, cyan; carbon atoms of MIT2, green; oxygen, red; nitrogen, blue. Side chains that are found to make hydrophilic intramolecular interactions are represented as sticks, except critical side chains are shown as sticks with their van der Waals surfaces in dot representation. (D) Hydrophillic intramolecular interactions stabilize MIT1-MIT2 interface. Left panel, overview of loop representation of LIP5NTD. Right panel, zoom-in view of the side chains involved in hydrophilic interactions and uses the same coloring scheme as described in Figure 2C. Hydrogen bonds are represented by dashed lines.

Not surprisingly, LIP5NTD contains two easily identifiable MIT domains, MIT1 and MIT2. Each MIT domain contains a three-helix bundle that is oriented nearly perpendicular to each other (Figure 2.2A). MIT1 contains helices α1-α3 (residues 16-74) and MIT2 contains helices α5-α7 (residues 83-162). Connecting these two domains is a small one-turn helix (α4, residues 75-82). Interestingly, we observed an N-terminal extended loop (residues 3-15)

positioned in the groove between helices α1 and α3 that could occlude any possible ligand binding to this groove.

MIT1 and MIT2 interact through an extensive surface area, where many of the residues from α1-α2 of MIT1 and α5-α6 of MIT2 contribute to stabilize the interface. Hydrophobic interactions predominate, for example Tyr41 from the MIT1 makes van der Waals contacts with three residues from the MIT2: Asp126, Val127 and Val130 (Figure 2.2C). Additional contributions to the stability of this interface come from several hydrophilic interactions as well. Three histidines from the MIT1, His19, His20, and His27, form hydrogen bond interactions with Tyr119, Asp126, and Tyr93, respectively, from the MIT2 (Figure 2.2D). A salt bridge between Glu26 and Lys116, which is conserved across metazoa, is also seen at the interface (Figure 2.1 and Figure 2.2D). The high conservation of this salt bridge indicates a potential functional importance for this interaction. A list of all the intramolecular interactions between MIT1 and MIT2 can be found in Table 2.2.

2.3.2 Comparing the LIP5NTD crystal structure to the Vta1NTD crystal structure and the LIP5NTD solution structure

The crystal structure of the N-terminal domain of yeast Vta1 (Vta1NTD, residues 1-167) was reported previously (19,23). While the sequence conservation between Vta1 and LIP5 is low, the overall structural folds are similar. We aligned the Vta1NTD structure (pdb code: 2RKK) with our LIP5NTD

Table 2.2 Tabulation of the intramolecular interactions within LIP5

MIT1	MIT2
Hydrogen bond interactions	
H19 ND1	Y119 OH
H19 NE2	Y119 OH
H20 NE2	D126 OD2
E26 OE1	K116 NZ
E26 OE2	K116 NZ
H27 NE2	Y93 OH
Van der Waals interactions	
H19	Y119, L123
T23	T120
H27	Y93
V34	Y93
Y37	L90, V127
C38	V127
Y41	D126, V127, V130,

structure (Figure 2.3A). The Vta1 structure contains two molecules in the ASU. By aligning the Cα positions between these two structures and LIP5NTD, we saw the r.m.s.d between the structures was 3.4 Å and 3.8 Å, respectively.

The high r.m.s.d suggests that there are some outstanding differences between the two structures. Due to the low-resolution (~3Å) of both structures, we only note major structural differences. These differences are localized to four major areas. First is the aforementioned N-terminal extended loop that exists in the LIP5NTD structure (Figure 2.3A). This stretch of sequence is a conserved feature in metazoan LIP5 but not yeast Vta1 (Figure 2.1). In addition, the α4 linker that connects the two MIT domains is significantly longer and disordered in the Vta1 structure, but we saw clear electron density for a one-turn helix in the LIP5 structure (Figure 2.3A). We also observed that in the MIT2 fold, the turn between helices α6-α7 occurs much earlier in LIP5 by about 4.6Å. Beyond that, we saw other subtle helix positional differences between the two structures. The

A

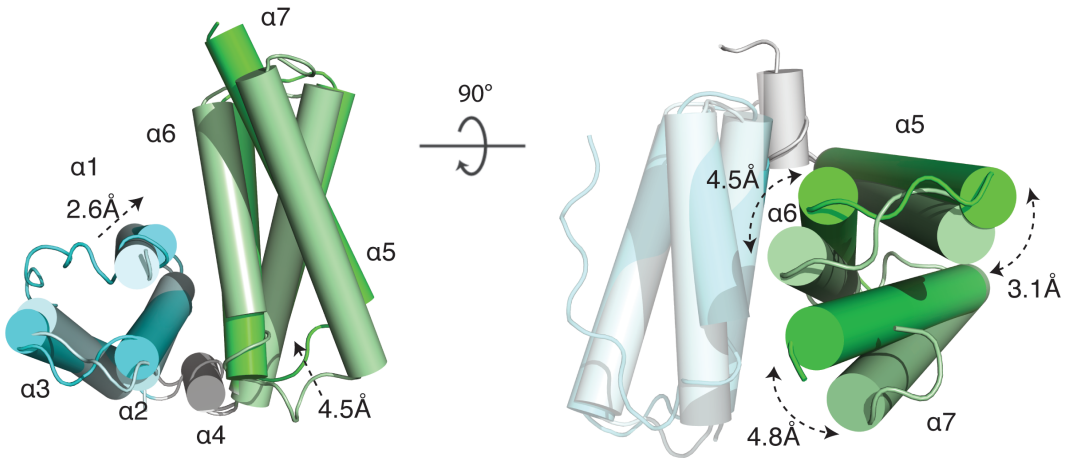
α7
α6
α1
2.6Å
α5
α3
α2
α4
4.5Å
90°
α5
4.5Å
α6
3.1Å
4.8Å
α7

B

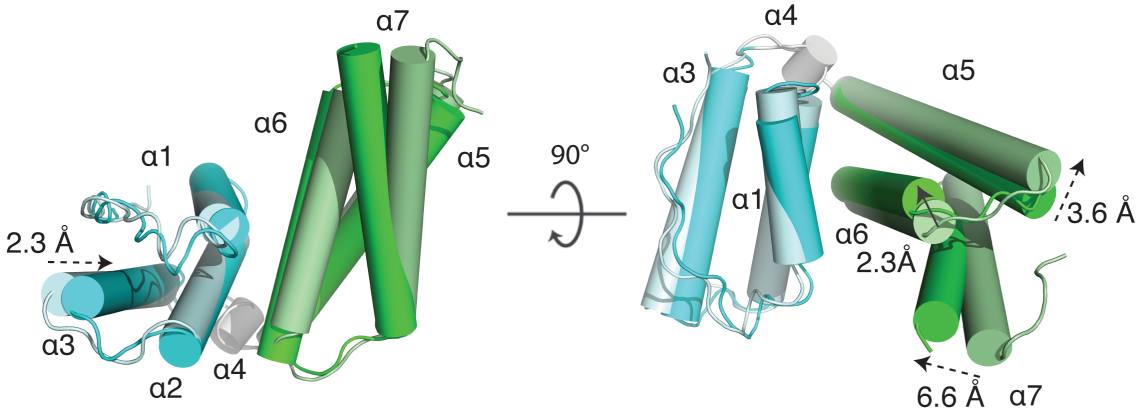
α7
α6
α1
α5
2.3 Å
α3
α2
α4
90°
α4
α3
α5
α1
3.6 Å
α6
2.3Å
6.6 Å
α7

C

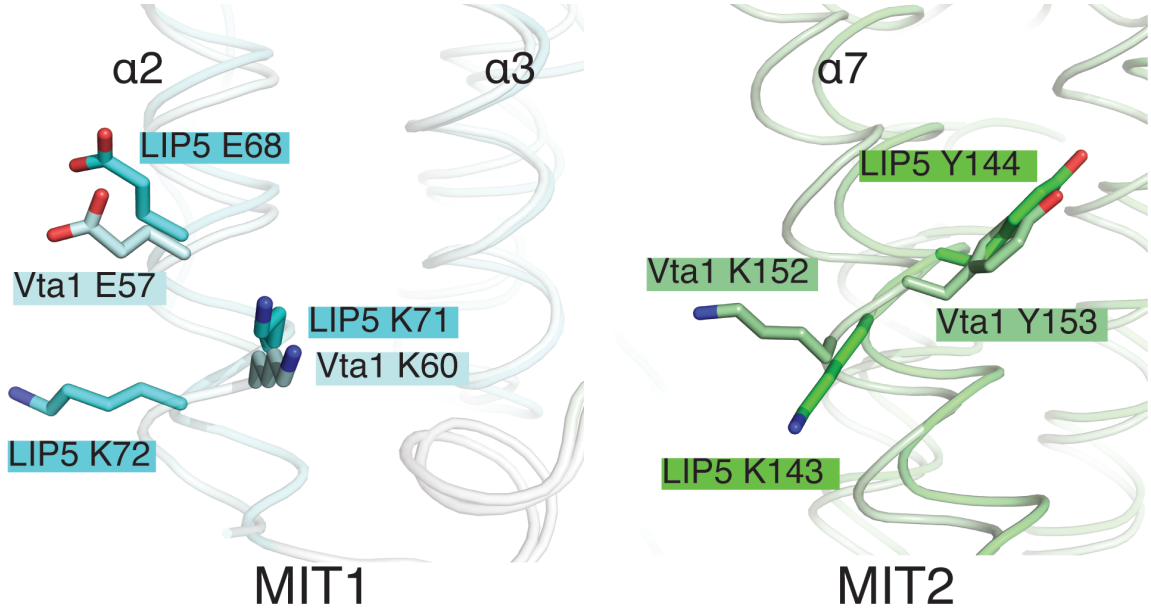

Figure 2.3 Structural differences and similarities between the LIP5NTD crystal structure, the Vta1NTD crystal structure and the LIP5NTD solution structure

(A) Two orthogonal views of the superimposition of Vta1NTD and LIP5NTD. LIP5 is colored in the same schematic as described in Figure 2A and Vta1 (PDB code: 2RKK) is colored similarly but pale. Positional differences between the structures are labeled with arrows. Helices are labeled α1-α7. (B) Two orthogonal views of the superimposition of the LIP5NTD crystal structure and the LIP5NTD solution structure. LIP5 from the crystal structure is colored in the same schematic as described in Figure 2A and LIP5 from the solution structure (PDB code: 2LXL) is colored similarly but pale. Positional differences between the structures are labeled with arrows. Helices are labeled α1-α7. (C) Residues predicted to be essential for ESCRT-III binding. The left panel shows the superimposition of α2-α3 groove surface of LIP5 and Vta1. Side chains that were structurally conserved and predicted to prevent MIM1 binding are shown, with LIP5 residues in cyan and Vta1 residues in pale cyan. The right panel shows the superimposition of the MIT2 domains of LIP5 (green) and Vta1 (pale green). Vta1 residues that are important for Vps60 binding and residues from LIP5 that are structurally conserved are shown. The following atoms are additionally colored: oxygen, red; nitrogen, blue; sulfur, orange.

two MIT1 domains superimpose very well, where we only saw helix α1 of LIP5 being about 2.6Å closer to the MIT2 (Figure 2.3A). However, there is larger

positional difference in the MIT2. Helix α7 of LIP5 seems to be the driving force behind the relative shift of its MIT2, where it is about 4.8Å closer to the MIT1. This positions α6 in a more perpendicular orientation relative to the MIT1 by 4.5Å, and consequently forces helix α5 to shift outwards by 3.1Å relative to the overall structure.

We also compared our LIP5NTD crystal structure to a recent solution NMR structure of LIP5NTD (PDB code: 2LXL) (27). Aligning the two structures based on their Cα positions generates a r.m.s.d. of 1.3 Å, which suggests good agreement between the two independently determined LIP5NTD structures. For the MIT1 domain, the two structures are nearly superimposable except for a 2.3Å positional difference in helix α1 (Figure 2.3B). In MIT2, we saw more substantial conformational differences. Helices α5 and α6 in the crystal structure have a 3.6 Å and 2.3 Å shift, respectively, relative to their solution structure counterparts (Figure 2.3B). There is also positional difference in the position of helix α7 between the two structures, where it shifts by 6.6Å. While some differences exist we propose that thematically, these two structures are the same

2.3.3 ESCRT-III binding to LIP5/Vta1

Previous work has mapped the binding sites of Did2 and Vps60 to the second MIT domain of Vta1 ((23), appendix). By comparing our LIP5 structure to Vta1, we looked to see whether the binding surface for these ESCRT-III proteins is conserved in human. Vta1 Lys152 has been previously shown to be critical for binding both Did2 and Vps60 (23). From the alignment, we see that LIP5 Lys143

is oriented in an equivalent position, suggesting the residue can be utilized to bind CHMP1B and CHMP5 by LIP5 in a similar manner. However, when site-directed mutagenesis and binding analysis were used to investigate the contribution of this residue for binding the two ESCRT-III proteins, no effect was seen for K143A mutation (data not shown). Therefore, we made an additional mutation of a highly conserved tyrosine, Y144A, hoping to further perturb the binding interface (Figure 2.3C). We termed these MIT2 domain mutations LIP5-MUT2 (K143A, Y144A). The equivalent mutations on Vta1 are K152A, Y153A (Figure 2.3C). We also made a series of alanine mutations to residues in the MIT1 domain (E68A, K71A, K72A), termed LIP5 MUT1. Based on the assumption that LIP5 can bind the ESCRT-III proteins via a MIT-MIM1 binding mode, these residues would be essential for maintaining the LIP5 and ESCRT-III interaction. (14,15) (Figure 2.1 and Figure 2.3C).

Using Glutathione S-Transferase (GST) pulldown analysis, we tested whether GST-tagged CHMP1B or CHMP5 could interact with LIP5, LIP5 MUT1 or LIP5 MUT2 (Figure 4A). To our surprise, CHMP1B failed to bind LIP5 MUT1, but retained full capacity to bind LIP5 MUT2 compared to the wild-type protein. The LIP5 MUT1 mutations block binding to the LIP5 α2-α3 helical groove, suggesting CHMP1B binds as a MIM1 (14,15). We also saw that neither LIP5 MUT1 nor LIP5 MUT2 seemed to dramatically affect CHMP5 binding. Further studies investigating the LIP5-CHMP5 interaction clearly showed that LIP5 Lys143 and Tyr144 are not involved in the LIP5-CHMP5 binding interface ((27),

also in Chapter 3), and could explain why we do not see a loss of binding in our assay.

A

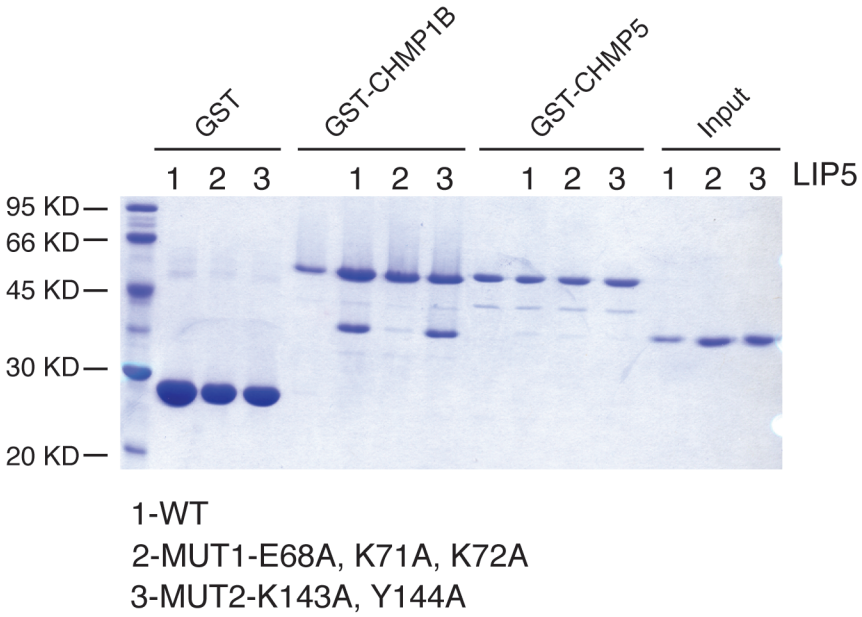

B

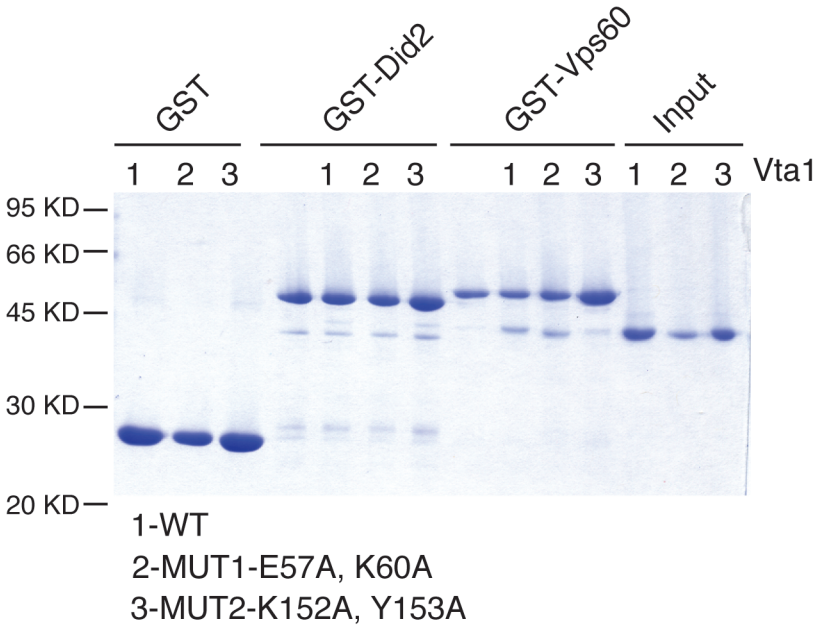

Figure 2.4 GST-pulldown analysis of LIP5/Vta1 for ESCRT-III binding

(A) ESCRT-III binding to LIP5. GST-CHMP1B and GST-CHMP5 were used to analyze their interactions with LIP5, LIP5 MUT1, and LIP5 MUT2 (listed 1-3). (B) ESCRT-III binding to Vta1. GST-Did2 and GST-Vps60 were used to analyze their interactions with Vta1, Vta1 MUT1, and Vta1 MUT2 (listed 1-3). Proteins retained on the beads were analyzed by SDS-PAGE and visualized by Coomassie staining.

Since the mechanism of binding was different between yeast and human proteins, we wanted to validate the binding site of Did2 and Vps60 on Vta1 by GST pulldown analysis. A similar experiment was performed as described above, but this time we used Vta1, Vta1 MUT1 (E57A, K60A) and Vta1 MUT2 (K152A, Y153A), which are equivalent to the LIP5 mutations (Figure 2.3B). We observed again, that Did2 failed to bind Vta1 MUT1, but could interact with Vta1 and Vta1 MUT2 (Figure 2.4B). As expected, the Vps60 binding site of Vta1 appears to be on MIT2, as only mutations on MIT2 (Vta1 MUT2) lead to loss of interaction with GST-Vps60 (Figure 2.4B). These data suggest that the previous notion that both Did2 and Vps60 bind to MIT2 of Vta1 needs to be reexamined and that the interaction between CHMP1B/Did2 and LIP5/Vta1 is well-conserved, but the CHMP5/Vps60 binding interface seems to be divergent.

2.3.4 The Crystal structure of LIP5NTD-CHMP1B

To determine whether CHMP1B does in fact bind LIP5 as a MIM1, we determined the crystal structure of LIP5NTD in complex with $CHMP1B^{176-199}$, a fragment that is necessary and sufficient for binding LIP5NTD. The LIP5NTD-$CHMP1B^{176-199}$ complex structure was solved by molecular replacement using the above-determined crystal structure of LIP5NTD as a search model (Table 2.1). The structure was refined to 2.2 Å with an R-factor of 19.3% and a free R-factor of 22.7%. Binding of CHMP1B does not cause significant change in the overall

structure of LIP5NTD. When the LIP5NTD molecules in the apo- and CHMP1B-complex structures were compared, the alignment showed an RMSD of 0.34 Å between the Cα positions of the two structures.

2.3.5 CHMP1B binds to the MIT1 domain of LIP5

The CHMP1B binding site of LIP5 is located on the MIT1 domain. CHMP1B forms a three-turn helix and sits on the surface groove formed by helices α2 and α3 of the LIP5 MIT1 (Figure 2.5A). The binding mode of CHMP1B to LIP5 is similar to the binding observed in the VPS4A-CHMP1A complex structure (15), which is also more generally known as the MIT-MIM1 binding mode. As seen in other MIT-MIM1 structures, the cognate MIT domain presents an overall hydrophobic surface, which is necessary for tight binding (Figure 2.5B). The binding between the two molecules buries approximately 624 $Å^2$ of surface area.

A

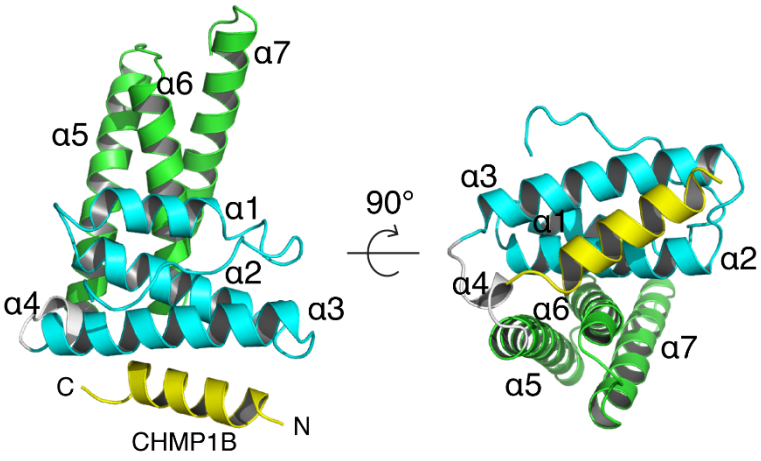

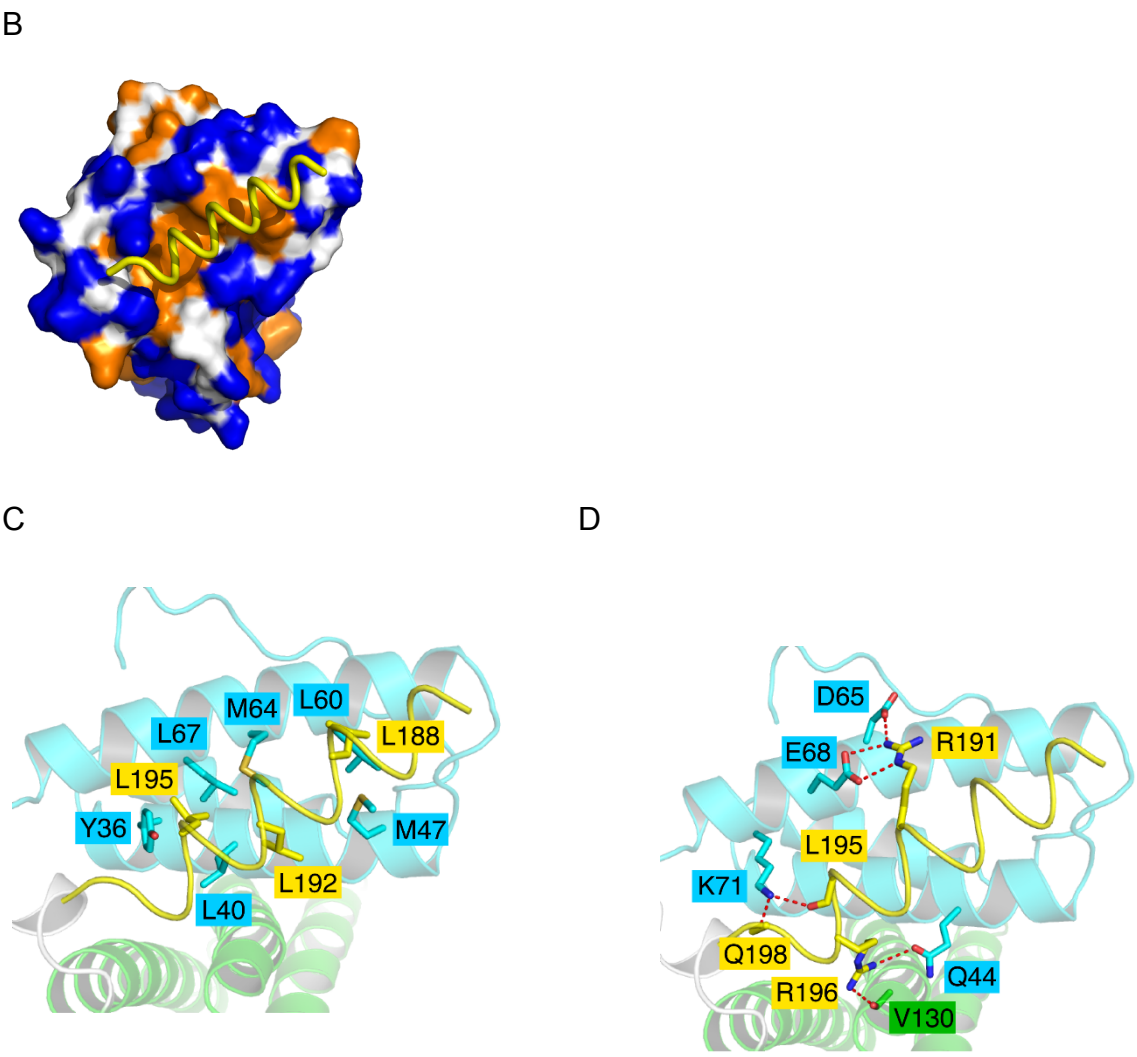

Figure 2.5 The crystal structure of LIP5NTD-CHMP1B complex.
(A) An overview of the LIP5NTD-CHMP1B complex structure. Cartoon representation of LIP5NTD (residues 1-162) in complex with CHMP1B (residues 176-199) in two orthogonal views. CHMP1B is colored in yellow and LIP5 is colored the same as in Figure 1A. Helices of LIP5NTD are labeled α1-α7. (B) The CHMP1B-binding surface of LIP5NTD is hydrophobic. LIP5NTD is shown as a surface representation and colored based on the underlying atoms: hydrophobic side chain atoms, orange; polar and charged side chain atoms, blue; and main chain atoms, white. CHMP1B is shown as a yellow coil. (C), (D) Detailed interactions at LIP5NTD-CHMP1B interface. Zoom-in cartoon representation showing residues involved in hydrophobic (C) and polar (D) interactions between LIP5NTD and CHMP1B. Residues that make distinct contacts are shown as stick models. Hydrogen bonds are denoted as dashed lines. Coloring schemes are the same as in (A) except for the following atoms: oxygen, red; nitrogen, blue; sulfur, orange.

The bound peptide in the canonical MIT-MIM1 structure often utilizes a series of conserved aliphatic residues, in many cases leucines, for binding (14,15). In the LIP5NTD-CHMP1B$^{176-199}$ structure, Leu188, Leu192, and Leu195 of CHMP1B make intimate contacts with LIP5, whose binding surface consists of Tyr36, Leu40 and Met47 from helix α2 and Leu60, Met64, Leu67 from helix α3 (Figure 2.5C). In addition to the leucines, two polar residues of CHMP1B, Arg191 and Arg196, are also seen at the binding interface, with their aliphatic portion of the side chains contributing to hydrophobic binding and terminal groups contributing to polar interactions (Figure 2.5D). Arg191 forms two salt bridges with Asp65 and Glu68 of LIP5, and Arg196 makes one hydrogen bond interaction with Gln44. Interestingly, Arg196 also makes a lone interaction with the MIT2 domain. Here, a hydrogen bond is formed between its side chain and the main chain carbonyl oxygen atom of Val130. A tabulated list of all interactions is shown in Table 2.3.

Table 2.3 Interaction table for LIP5NTD-CHMP1B MIM structures

CHMP1B	**LIP5**
Hydrogen bond interactions	
R191NE	E68 OE2
R191 NH2	E68 OE1
R191 NH2	D65 OD1
L195 O	K71 NZ
R196 NH1	Q44 OE1
R196 NH2	V130 O
Q198 O	K71 NZ
Van der Waals interactions	
L188	M47, L60, S61
R191	M64
L192	L40, Q44, M47, M64
L195	Y36, L40, M64, L67, K71
R196	L40

To evaluate the contribution of individual residues to the overall stability of the LIP5-CHMP1B complex, site-directed mutagenesis and GST pulldown analysis were performed. We used GST-tagged CHMP1B$^{176-199}$ to test its binding to LIP5 and various LIP5 mutants including LIP5 L40A, LIP5 Q44A, LIP5 M64A, LIP5 E68A and LIP5 MUT1. Among the mutants, M64A has been previously shown to disrupt CHMP1B binding (27). We observed that both L40A and E68A affected CHMP1B binding to a similar extent as M64A, whereas Q44A had little effect on CHMP1B binding (Figure 2.6A). However, to completely abolish the binding of CHMP1B, multiple mutations were required on the LIP5 surface.

A

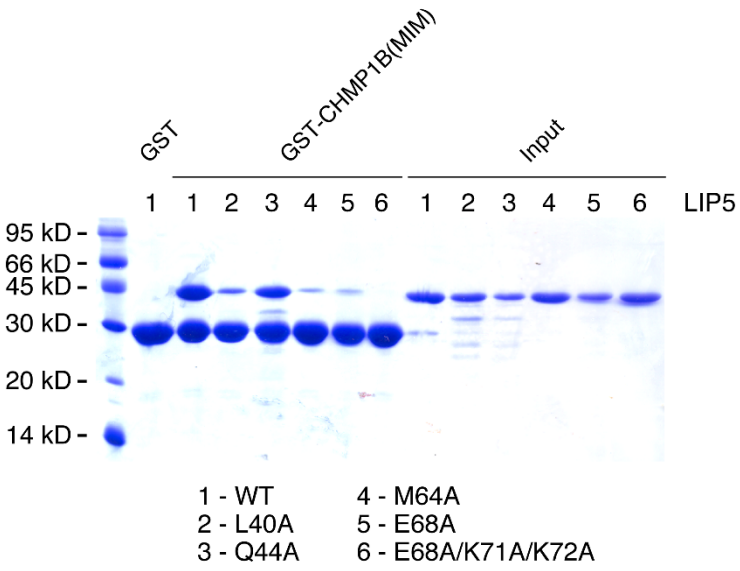

B

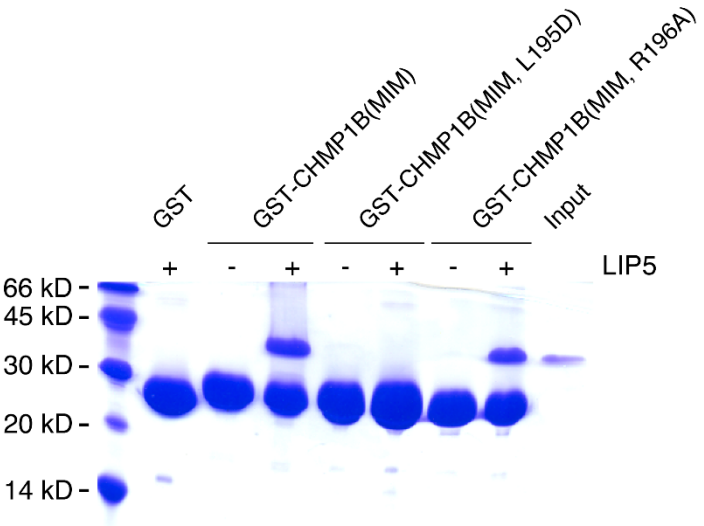

Figure 2.6 Critical residues at the LIP5NTD-CHMP1B interface.
(A) Critical residues on LIP5. GST-CHMP1B$^{176-199}$ was used to analyze its interaction with LIP5 and various LIP5 mutants (listed as 2-6). (B) Critical residues on CHMP1B. GST-CHMP1B$^{176-199}$, GST-CHMP1B$^{176-199, L195D}$ or GST-CHMP1B$^{176-199, R196A}$ was used to analyze its interaction with LIP5.

We also mutated two CHMP1B residues, Leu195 and Arg196, to evaluate their importance to LIP5 binding. The ability of GST-tagged CHMP1B$^{176-199}$, CHMP1B$^{176-199/L195D}$ or CHMP1B$^{176-199/R196A}$ to bind LIP5 was examined. As seen in Figure 2.6B, L195D was not able to bind LIP5, demonstrating the importance of hydrophobic interaction to the overall binding. In contrast, R196A bound LIP5 to the same extent as the wild-type protein, suggesting that the peripheral polar interaction contributes to a lesser degree to the overall stability of the complex.

2.4 Discussion

ESCRT function is central to MVB biogenesis, where the final steps are regulated by the AAA-ATPase VPS4. VPS4 has evolved a cofactor, LIP5, which can increase its activity and promote its association with the ESCRT-III

components. While much of our knowledge about human LIP5 function was originally derived from studies in yeast, there is always the question how conserved the mechanism of VPS4 regulation really is. Here, we have investigated the structure of LIP5NTD and revealed it to be structurally homologous to its yeast counterpart, Vta1. However, our studies also showed that the mechanism by which it binds to some of the ESCRT-III components may have diverged. The crystal structure of LIP5NTD in complex with CHMP1B MIM revealed canonical MIT-MIM1 binding mode between the two proteins. Together, this work has identified key similarities and differences between Vta1 and LIP5, pointing to the potential mechanistic differences that may exist between yeast and human systems.

2.4.1 LIP5NTD comparison to Vta1NTD

Our structural analysis was able to see that, despite low conservation between LIP5 and Vta1, the N-terminal domains of each protein adopt a similar fold. However, LIP5 contains a N-terminal extended coil that binds in the α1-α3 helical pocket (Figure 2.2A). This structural feature potentially has physiological consequences. In the case of Vps4 MIT domain, it can bind two ESCRT-III ligands, MIM1 in its α2-α3 pocket and MIM2 in its α1-α3 pocket (13-15,28). The MIM2 uses the consensus sequence of Φ-P-X-Φ-P (where Φ is a hydrophobic residue, and X is any residue) to bind this pocket as an extended coil (28). LIP5 residues Leu2, Leu7, Pro8, Leu10, and Pro11 mimic the MIM2 sequence to make hydrophobic contacts in this pocket. Other studies have shown that ESCRT-III MIM2 containing proteins cannot bind LIP5 (27). Most likely, this N-

terminal coil may function *in vivo* to prevent interactions with these MIM2-containing ligands.

Although similar, we have observed structural differences between Vta1NTD and LIPNTD. As seen in Figure 2.3A, the LIP5 MIT2 globally undergoes approximately a 4 Å rotation relative to the Vta1 MIT2. This movement increases surface area of the MIT1-MIT2 interface, which allows for a more extensive interaction. In fact, this allows for the formation of a salt bridge between LIP5 Glu-26 and Lys-116, which we will describe in Chapter 3 to be important for sensing the binding of CHMP5. While not explicitly tested, we believe that the structural differences between the two orthologous proteins may account for the functional differences.

2.4.2 ESCRT-III binding to the MIT2 domain

We also investigated whether the mechanisms of ESCRT-III binding are conserved in LIP5. Yeast proteins, Did2 and Vps60, were initially found to bind to the Vta1 MIT2 (23). We were keenly interested in seeing if LIP5 uses a similar binding strategy to interact with CHMP1B and CHMP5, the respective orthologs of Did2 and Vps60. One of the key residues for this interaction, Vta1 Lys152, is structurally conserved in the LIP5 structure as residue Lys143 (Figure 2.3B). However, mutation of this residue and a structurally conserved tyrosine does not ablate CHMP5 binding (Figure 2.4A). LIP5 and CHMP5 bind with a very high affinity, ~100 pm, so one could argue that our assay was not sensitive enough for detecting the effect of mutating these two residues even if they are part of the

binding interface (24,27). However, our structural work on the LIP5-CHMP5 complex as described in Chapter 3 will show that these residues are not in the binding interface. While these residues are important for the Vta1-Vps60 binding , the same cannot be said true for LIP5 and CHMP5. Clearly, the binding interface between Vta1-Vps60 and LIP5-CHMP5 has diverged during evolution.

2.4.3 CHMP1B binding to LIP5NTD

Our work led us to test whether CHMP1B binds to the MIT2 of LIP5 as well. GST-pull-down analysis showed that GST-CHMP1B binds LIP5 MUT2 to a similar amount as wild-type (Figure 2.4A). Interestingly, GST-CHMP1B failed to bind LIP5 MUT1 (Figure 2.4A). Since residues mutated in LIP5 MUT1 stabilize MIM1-binding elements, this suggested that CHMP1B binds to LIP5 as a MIM1. This prompted us to test whether Did2 does in fact bind to Vta1 MIT2. Sequence analysis predicted that Did2 would bind MIT domains as a MIM1, mainly through hydrophobic contacts (14,15). MIM1 has been shown to bind between the α2-α3 helical groove of the MIT domain. This would correspond to helices α6-α7 in the MIT2 domain of Vta1. If that were the case, Lys155 in the α6-α7 groove would prevent any binding by a hydrophobic MIM1 element. Indeed, we found that Did2 binds to the Vta1 MUT2, but not Vta1 MUT1 (Figure 2.4B). This establishes that CHMP1B and Did2 bind to the same region of LIP5/Vta1 and this interaction is well-conserved in MIT1. These data are consistent with our current understanding of ESCRT-III regulation of MIT domain containing protein. Most interestingly since the binding sites of MIM1 containing ESCRT-III proteins, like

Did2, and Vps60 do not overlap, it should be possible to explore how these proteins simultaneously regulate Vta1.

A number of human MIM1-containing ESCRT-III proteins including CHMP1A, -1B, CHMP2, CHMP3 and IST1 have been previously shown to bind to LIP5 (24,29). The crystal structure of the LIP5NTD-CHMP1B complex confirmed that CHMP1B binds to LIP5 MIT1 as a MIM1. This predicts that other MIM1-containing ESCRT-III proteins will bind to LIP5 in the same way. Since binding of CHMP1B MIM1 to LIP5 does not induce significant conformational change in LIP5, this suggests that interaction between LIP5 and MIM1-containing ESCRT-III proteins likely serve to recruit the VPS4-LIP5 complex to the ESCRT-III bound membrane.

Taken together, the structural analysis of LIP5NTD and the LIP5NTD-CHMP1B MIM structures have illustrated important insights on ESCRT-III regulation of LIP5. While previous work in understanding ESCRT-III function in yeast does not need to be dramatically reinterpreted, it does highlight that differences do exist between yeast and human systems. Earlier reports showed that Vta1 stimulation of Vps4 ATPase activity is potentiated by ESCRT-III binding, and it will be interesting to see whether this mechanism is conserved in human. The fact that there appears to be two different binding mechanisms for binding to MIT2 by the two orthologs CHMP5/Vps60 suggests that the allosteric

regulation of the LIP5/Vps60 might be different. Further functional assays are needed to deconvolute the complicated mechanism of LIP5/Vta1 regulation.

2.5 Methods

2.5.1 Cloning, Expression, and Purification

DNA sequences encoding for various proteins and protein fragments were amplified from cDNAs (ATCC®) and cloned into a modified pET28b vector to generate N-terminal His_6-SUMO tagged fusion proteins. Point mutations were generated using a standard PCR mutagenesis protocol (Stratagene). Proteins were expressed in *Escherichia coli* Rosetta(DE3), where cells were grown at 37°C to log phase in standard LB media and induced with 0.2 mM Isopropyl β-D-1-thiogalactopyranoside followed by an additional 16-20h growth at 16°C. Seleno-methionyl $LIP5^{1-162}$ derivative was expressed in *E. coli* B834(DE3) using a minimal medium where methionine was replaced with seleno-methionines.

All proteins were purified using a similar protocol with adjustment made when necessary. Cells were pelleted and lysed by sonication in buffer A (25 mM Tris pH 8.0, 300 mM NaCl, 5 mM 2-mercaptoethanol, and 10 µg/mL (w/v) phenylmethylsulfonyl fluoride). Cell lysate was cleared by centrifugation and supernatant was loaded onto a Ni^{2+}-nitrilotriacetic acid affinity column, washed with buffer A and eluted with buffer A supplemented with 250 mM imidazole. Eluate was collected, digested with ULP1 to cleave the His_6-SUMO tag while being dialyzed against 50 mM Tris pH 8.0, 25 mM NaCl overnight. A moderate precipitation formed for $LIP5^{1-162}$ during dialysis, which was determined to be

nucleic acid and could be cleared by centrifugation. Dialyzed protein mixture was passed over a second Ni^{2+}-nitrilotriacetic acid column to remove the His_6-SUMO tag. Proteins that would be used for GST-pull-down analysis were stored directly in -80°C.

Proteins used for crystallization were further purified. $LIP5^{1-162}$ was further purified on a Source-S (GE Healthcare) cation exchange column using buffer C (50 mM HEPES pH 7.0, 50 mM NaCl, 1mM EDTA, 1mM DTT) as a loading buffer, and eluted via a gradient with buffer C supplemented with 1M NaCl. Fractions containing the protein were pooled, concentrated and loaded onto a HiLoad™ Superdex™ 75 (GE Healthcare) column and eluted with buffer C. For the LIP5NTD-CHMP1B complex, the CHMP1B fragment was mixed with $LIP5^{1-162}$ in an approximately 2:1 ratio. This mixture was concentrated and loaded onto the Superdex™ 75 column, and eluted with buffer C. Complex formation was confirmed by elution position change from the gel filtration column. The CHMP1B peptide was not detectable by Coomassie blue staining.

2.5.2 Crystallization and Data Collection

Crystals of $LIP5^{1-162}$ were produced by hanging drop vapor diffusion method at 4°C. Protein at 15 mg/ml was mixed in a 1:1 ratio with a reservoir solution of 7.5-9% PEG8000, 3% 1,4-butanediol, 0.1 M cacodylate pH 7.0, 0.2 M sodium acetate to a final volume of 4 µl and equilibrated against 500 µl of the reservoir solution. Small hexagonal crystals appeared after approximately two weeks, which were then transferred into a solution containing 20% PEG8000,

20% glycerol, 8% butanediol, 0.1 M cacodylate pH 7.0, 0.2 M sodium acetate and immediately flash-frozen under liquid nitrogen. The seleno-methionyl derived LIP5$^{1-162}$ crystals were produced and harvested in a similar manner. Data were collected at Advanced Photon Source beamline 21-ID, and processed and scaled using XDS (MPI for Medical Research).

Complex crystals of LIP5-CHMP1B were grown by sitting drop vapor diffusion method at 4°C. Protein complex at 12.7 mg/ml was mixed in a 1:1 ratio with a solution of 16% MPD, 0.1 M Tris pH 9.0 and equilibrated against 500 µl of a reservoir solution of 8% MPD, 0.1 M Tris pH 9.0. Two crystals with different morphology appeared. Long needle-like crystals would appear instantly and dissolve over time. Stable diamond-like crystals would appear later and were ultimately used for data collection. Crystals were micro-dialyzed (Hampton Research) against 30% MPD, 0.1 M Tris pH 9.0 for 16-24h before flash-freezing under liquid nitrogen. Data were collected at Advanced Photon Source beamline 21-ID, and processed and scaled using HKL2000 (HKL Research Inc.)

2.5.3 Structure Determination and Refinement

The LIP5$^{1-162}$ structure was determined using single-wavelength anomalous diffraction method using the data set collected at the peak wavelength (λ=0.9792). There are three molecules in the asymmetric unit. Phenix autosol was able to find 12 out of the 15 expected selenomethionine sites (5 sites/LIP5 molecule) (30). Phases were calculated and refined. Autosol was able to build a model for one of the three molecules based on the initial electron

density map. This model was then used to search for the other two molecules against the native data set by molecular replacement as implemented in Phenix AutoMR. BUSTER was used for further structure refinement with NCS applied throughout (Global Phasing Limited). The LIP5NTD-CHMP1B structure was solved by molecular replacement as implemented in AutoMR using the refined LIP5$^{1-162}$ structure as an initial search model. Structure refinement was done in Phenix, with NCS restrictions applied to the LIP5-CHMP1B structure in the early rounds of refinement. COOT was used for model building and adjustment. Structural figures were generated with PYMOL (Schrödlinger). Structure refinement statistics are shown in Table 2.1.

2.5.4 GST Pull-down Analysis

GST pull-down analysis was performed following standard procedures in phosphate-buffered saline (PBS) solution supplemented with 1 mM DTT and 0.1% (v/v) Tween 20(31). Specific samples were also supplemented with 2 mM ATP as indicated in the figure. Purified proteins were incubated with GST alone or GST-tagged proteins immobilized on glutathione-agarose beads for 1 h at 4 °C. The beads were then washed extensively with the buffer before bound proteins were analyzed on SDS-PAGE and visualized by Coomassie blue staining.

2.6 Acknowledgements

We thank the staff at the Advanced Photon Source LS-CAT Sector 21 (21-ID-D) for access and help with data collection. Use of the Advanced Photon Source, an Office of Science User Facility operated for the U.S. Department of Energy

(DOE) Office of Science by Argonne National Laboratory, was supported by the U.S. DOE under Contract No. DE-AC02-06CH11357. Use of the LS-CAT Sector 21 was supported by the Michigan Economic Development Corporation and the Michigan Technology Tri-Corridor (Grant 085P1000817). This work was supported by a grant to Z. Xu (GM095769) from National Institutes of Health.

2.7 References

1. Hanson, P. I., and Cashikar, A. (2012) Multivesicular body morphogenesis. *Annu Rev Cell Dev Biol* **28**, 337-362

2. Hurley, J. H., and Stenmark, H. (2011) Molecular mechanisms of ubiquitin-dependent membrane traffic. *Annu Rev Biophys* **40**, 119-142

3. Jimenez, A. J., Maiuri, P., Lafaurie-Janvore, J., Divoux, S., Piel, M., and Perez, F. (2014) ESCRT machinery is required for plasma membrane repair. *Science* **343**, 1247136

4. McCullough, J., Colf, L. A., and Sundquist, W. I. (2013) Membrane fission reactions of the mammalian ESCRT pathway. *Annu Rev Biochem* **82**, 663-692

5. Kirchhausen, T., Owen, D., and Harrison, S. C. (2014) Molecular structure, function, and dynamics of clathrin-mediated membrane traffic. *Cold Spring Harb Perspect Biol* **6**, a016725

6. Katzmann, D. J., Babst, M., and Emr, S. D. (2001) Ubiquitin-dependent sorting into the multivesicular body pathway requires the function of a conserved endosomal protein sorting complex, ESCRT-I. *Cell* **106**, 145-155

7. Leung, K. F., Dacks, J. B., and Field, M. C. (2008) Evolution of the multivesicular body ESCRT machinery; retention across the eukaryotic lineage. *Traffic* **9**, 1698-1716

8. Wollert, T., and Hurley, J. H. (2010) Molecular mechanism of multivesicular body biogenesis by ESCRT complexes. *Nature* **464**, 864-869

9. Wollert, T., Wunder, C., Lippincott-Schwartz, J., and Hurley, J. H. (2009) Membrane scission by the ESCRT-III complex. *Nature* **458**, 172-177

10. Bajorek, M., Schubert, H. L., McCullough, J., Langelier, C., Eckert, D. M., Stubblefield, W. M., Uter, N. T., Myszka, D. G., Hill, C. P., and Sundquist, W. I. (2009) Structural basis for ESCRT-III protein autoinhibition. *Nat Struct Mol Biol* **16**, 754-762

11. Hanson, P. I., Roth, R., Lin, Y., and Heuser, J. E. (2008) Plasma membrane deformation by circular arrays of ESCRT-III protein filaments. *J Cell Biol* **180**, 389-402

12. Scott, A., Gaspar, J., Stuchell-Brereton, M. D., Alam, S. L., Skalicky, J. J., and Sundquist, W. I. (2005) Structure and ESCRT-III protein interactions of the MIT domain of human VPS4A. *Proc Natl Acad Sci U S A* **102**, 13813-13818

13. Kieffer, C., Skalicky, J. J., Morita, E., De Domenico, I., Ward, D. M., Kaplan, J., and Sundquist, W. I. (2008) Two distinct modes of ESCRT-III recognition are required for VPS4 functions in lysosomal protein targeting and HIV-1 budding. *Dev Cell* **15**, 62-73

14. Obita, T., Saksena, S., Ghazi-Tabatabai, S., Gill, D. J., Perisic, O., Emr, S. D., and Williams, R. L. (2007) Structural basis for selective recognition of ESCRT-III by the AAA ATPase Vps4. *Nature* **449**, 735-739

15. Stuchell-Brereton, M. D., Skalicky, J. J., Kieffer, C., Karren, M. A., Ghaffarian, S., and Sundquist, W. I. (2007) ESCRT-III recognition by VPS4 ATPases. *Nature* **449**, 740-744

16. Adell, M. A., Vogel, G. F., Pakdel, M., Muller, M., Lindner, H., Hess, M. W., and Teis, D. (2014) Coordinated binding of Vps4 to ESCRT-III drives membrane neck constriction during MVB vesicle formation. *J Cell Biol* **205**, 33-49

17. Babst, M., Wendland, B., Estepa, E. J., and Emr, S. D. (1998) The Vps4p AAA ATPase regulates membrane association of a Vps protein complex required for normal endosome function. *EMBO J* **17**, 2982-2993

18. Monroe, N., Han, H., Gonciarz, M. D., Eckert, D. M., Karren, M. A., Whitby, F. G., Sundquist, W. I., and Hill, C. P. (2014) The oligomeric state of the active Vps4 AAA ATPase. *J Mol Biol* **426**, 510-525

19. Xiao, J., Xia, H., Zhou, J., Azmi, I. F., Davies, B. A., Katzmann, D. J., and Xu, Z. (2008) Structural basis of Vta1 function in the multivesicular body sorting pathway. *Dev Cell* **14**, 37-49

20. Yang, D., and Hurley, J. H. (2010) Structural role of the Vps4-Vta1 interface in ESCRT-III recycling. *Structure* **18**, 976-984

21. Nickerson, D. P., West, M., Henry, R., and Odorizzi, G. (2010) Regulators of Vps4 ATPase activity at endosomes differentially influence the size and rate of formation of intralumenal vesicles. *Mol Biol Cell* **21**, 1023-1032

22. Nickerson, D. P., West, M., and Odorizzi, G. (2006) Did2 coordinates Vps4-mediated dissociation of ESCRT-III from endosomes. *J Cell Biol* **175**, 715-720

23. Azmi, I. F., Davies, B. A., Xiao, J., Babst, M., Xu, Z., and Katzmann, D. J. (2008) ESCRT-III family members stimulate Vps4 ATPase activity directly or via Vta1. *Dev Cell* **14**, 50-61

24. Shim, S., Merrill, S. A., and Hanson, P. I. (2008) Novel interactions of ESCRT-III with LIP5 and VPS4 and their implications for ESCRT-III disassembly. *Mol Biol Cell* **19**, 2661-2672

25. Shiflett, S. L., Ward, D. M., Huynh, D., Vaughn, M. B., Simmons, J. C., and Kaplan, J. (2004) Characterization of Vta1p, a class E Vps protein in Saccharomyces cerevisiae. *J Biol Chem* **279**, 10982-10990

26. Tsang, H. T., Connell, J. W., Brown, S. E., Thompson, A., Reid, E., and Sanderson, C. M. (2006) A systematic analysis of human CHMP protein interactions: additional MIT domain-containing proteins bind to multiple components of the human ESCRT III complex. *Genomics* **88**, 333-346

27. Skalicky, J. J., Arii, J., Wenzel, D. M., Stubblefield, W. M., Katsuyama, A., Uter, N. T., Bajorek, M., Myszka, D. G., and Sundquist, W. I. (2012) Interactions of the human LIP5 regulatory protein with endosomal sorting complexes required for transport. *J Biol Chem* **287**, 43910-43926

28. Vild, C. J., and Xu, Z. (2014) Vfa1 binds to the N-terminal microtubule-interacting and trafficking (MIT) domain of Vps4 and stimulates its ATPase activity. *J Biol Chem* **289**, 10378-10386

29. Bajorek, M., Morita, E., Skalicky, J. J., Morham, S. G., Babst, M., and Sundquist, W. I. (2009) Biochemical analyses of human IST1 and its function in cytokinesis. *Mol Biol Cell* **20**, 1360-1373

30. Adams, P. D., Afonine, P. V., Bunkoczi, G., Chen, V. B., Davis, I. W., Echols, N., Headd, J. J., Hung, L. W., Kapral, G. J., Grosse-Kunstleve, R. W., McCoy, A. J., Moriarty, N. W., Oeffner, R., Read, R. J., Richardson, D. C., Richardson, J. S., Terwilliger, T. C., and Zwart, P. H. (2010) PHENIX: a comprehensive Python-based system for macromolecular structure solution. *Acta Crystallogr D Biol Crystallogr* **66**, 213-221

31. Xiao, J., Xia, H., Yoshino-Koh, K., Zhou, J., and Xu, Z. (2007) Structural characterization of the ATPase reaction cycle of endosomal AAA protein Vps4. *J Mol Biol* **374**, 655-670

Chapter 3 Structural Basis of VPS4 Regulation by the LIP5/ESCRT-III Protein Complexes

3.1 Abstract

The AAA-ATPase VPS4 catalyzes the disassembly of the ESCRT machinery from cellular membrane, a critical final step in membrane vesiculation away from the cytoplasm. LIP5 and regulatory ESCRT-III proteins bind VPS4 and are essential for controlling its activity. Here we present structure and functional analyses of molecular interactions between human VPS4B, LIP5 and ESCRT-III proteins. The crystal structure of the LIP5 N-terminal domain (LIP5NTD) in complex with the MIT-interacting motifs (MIMs) of two ESCRT-III proteins, CHMP1B and CHMP5, was determined. While CHMP1B MIM has no effect, CHMP5 MIM can strongly inhibit LIP5-dependent stimulation of VPS4. We found that binding of CHMP5 leads to a conformational change in LIP5NTD, which may result from the insertion of a conserved CHMP5 tyrosine residue (Tyr182) at the core of LIP5 structure. We hypothesized a novel mechanism of VPS4 regulation, where CHMP5 binding disrupts a previously unknown critical interaction between LIP5NTD and VPS4.

3.2 Introduction

The endosomal sorting complex required for transport (ESCRT) machinery is responsible for catalyzing membrane fission reactions away from the cytoplasm, a process that has reverse topology as compared to classical

vesiculation processes such as endocytosis (1-4). ESCRT was initially identified in the yeast multivesicular body (MVB) biogenesis pathway (5) and was later shown to be involved in additional biologically important events in higher eukaryotic cells, including enveloped virus budding from the plasma membrane (6), resolution of the mid-body structure during cytokinesis (7) and more recently repair of small plasma membrane wounds (8). The core components of the ESCRT machinery have shown remarkable structure and functional conservation throughout eukaryotic cells. Among them, late-acting complexes ESCRT-III and Vps4 catalyze the actual membrane fission event as well as the disassembly of the machinery at the end of each reaction cycle (9-12). ESCRT-III and Vps4 are required for all known ESCRT-dependent cellular processes and are thought to constitute a minimal membrane fission machine.

ESCRT-III consists of four core subunits: Vps20 (*human ortholog*: CHMP6), Snf7 (CHMP4), Vps24 (CHMP3), and Vps2 (CHMP2) (13,14). They all exist as soluble monomeric proteins in their inactive states and polymerize into membrane-bound helical filaments when activated by upstream factors (15-19). ESCRT-III polymerization plays a critical role in membrane fission, and also exposes arrays of C-terminal tails that can bind microtubule interacting and transport (MIT) domain-containing proteins (20,21). These MIT domain-binding sequences on the ESCRT-III proteins are also known as the MIT interacting motifs (MIM). Two of the ESCRT proteins whose sequences contain MIT domains are Vps4 (VPS4) and its activator Vta1 (LIP5) (22,23).

Vps4 is an AAA-ATPase whose function in the cell is to extract the ESCRT-III subunits from the membrane-bound filaments and return them to their inactive states at the end of the membrane fission reaction cycle (24-28). There is also evidence suggesting that Vps4 directly contributes to membrane fission in some cellular processes (8,29-31). Vps4 contains an N-terminal MIT domain, a linker and a C-terminal canonical AAA-ATPase cassette (32-34). Unique to the Vps4 structure is a small motif of three anti-parallel β-sheets called the "β-domain", inserted within AAA cassette. Vps4 can exist in two quaternary structures, an inactive disassembled state and an active high-order oligomer (35). Equilibrium between the two states represents a major step of regulation in the ESCRT machinery. Binding of ATP shifts the equilibrium towards assembly and hydrolysis of ATP shifts the equilibrium towards disassembly (36). Furthermore, the ATP-dependent assembly of Vps4 is greatly promoted by Vta1 (LIP5) (37-39).

The structure of Vta1 contains two terminal domains that are connected by a ~100 residue long, non-conserved flexible linker (23,40). The N-terminus consists of two tandem MIT domains (23) and at the C-terminus is the Vta1-SBP1-LIP5 (VSL) domain that allows for the dimerization of Vta1, and which directly binds to the β-domain of Vps4 (40). Vta1 dimer formation is critical for binding to Vps4 and the interaction between the two proteins has been shown to be ATP-dependent (23,41). In yeast, Vta1 can stimulate the ATPase activity of

Vps4 by about three fold and this effect is largely attributed to the fact that interaction between the VSL domain and Vps4 stabilizes the active Vps4 assembly structure (23). The activity of Vps4 can also be regulated by other mechanisms. Recent work has identified a region immediately N-terminal to the VSL domain in yeast Vta1 that can further stimulate Vps4 activity (named VSE) by increasing the catalytic efficiency of the ATPase (42).

The ESCRT-III proteins display regulatory activity towards Vps4 as well. Binding of the Vps4 MIT domain to the high concentrations of MIM sequences displayed by membrane-bound ESCRT-III filaments can serve to recruit, assemble and activate the ATPase (25,29). Furthermore, direct interactions between ESCRT-III and the MIT domain relieve auto-inhibition imposed by the linker of Vps4 (43). Beyond the four core ESCRT-III subunits, there exist several proteins whose structural folds are similar to ESCRT-III but loss of their function does not cause severe defects in the MVB pathway (10,44). These include Did2 (CHMP1), Vps60 (CHMP5) and Ist1 (IST1), which have been implicated in the regulation of Vps4 activity and in some cases are thought to aid in the recruitment of Vps4 to the membrane (45). The regulatory role of the Did2, Vps60 and Ist1 in particular overlaps with that of Vta1. Biochemical analysis of protein-protein interactions has shown that Did2, Vps60 and Ist1 can all bind to the N-terminal domain of Vta1 (23,46). Works in the yeast have suggested that Did2 and Vps60 are allosteric ligands of Vps4 activity (38,42).

Since metazoan ESCRT machinery perform a series of additional functions not described in yeast, it is essential that the molecular mechanism of Vps4 regulation be studied in its native contexts. To this end, we performed structural and functional analyses of molecular interactions between human VPS4B, LIP5 and regulatory ESCRT-III proteins CHMP1B and CHMP5 to gain mechanistic insights into the regulation of metazoan ESCRT machinery. The atomic-resolution crystal structure of the LIP5-CHMP1B-CHMP5 complex was determined and they revealed that binding of CHMP5 leads to disruption of the interface between the two MIT domains of LIP5. Induction of this conformational change precludes LIP5 stimulation of VPS4 via a previously uncharacterized interaction, and helps explains the mechanism by which CHMP5 allosterically regulates LIP5 function in metazoan.

3.3 Results

3.3.1 Binding of CHMP5 to LIP5 inhibits its stimulatory activity towards VPS4

Yeast regulatory ESCRT-III proteins, Did2 and Vps60, have been shown to regulate the MVB pathway by stimulating Vps4 ATPase activity in a Vta1-dependent manner (38). We asked whether a similar effect could be observed in metazoan orthologs CHMP1B and CHMP5. Earlier studies on human Vps4 orthologs (VPS4A and VPS4B) indicated that they have much weaker ATPase activity than yeast Vps4 (43). Using the Malachite Green ATPase assay, we observed a similar result but our study also indicated that VPS4B is slightly more active than VPS4A and also more stable under experimental conditions (data not shown). Therefore, VPS4B was used for the rest of our experiments. To

eliminate any potential stimulation through direct interaction between VPS4B and the ESCRT-III proteins via the MIT domain, we used a MIT domain truncation mutant of VPS4B (VPS4B$^{79-444}$ or VPS4BΔMIT) which has a similar basal and LIP5 stimulated activities as the full-length protein (data not shown).

The ATPase activity of VPS4B is concentration-dependent and at sub-micromolar protein concentration we saw little basal activity (0.83 Pi/min/VPS4B) (Figure 3.1A. With the addition of LIP5, we observed a dramatic stimulation of the activity to 8.54 Pi/min/VPS4B. However, when the minimal LIP5 binding element of CHMP5 was included with LIP5 in the assay, a pronounced inhibitory effect was observed. Addition of CHMP5 reduced the LIP5 stimulated VPS4B ATPase activity to 0.67 Pi/min/VPS4B, which was near its basal level. To determine whether this inhibitory effect depended upon CHMP5 binding to LIP5, we used a previously described LIP5-binding deficient mutant of CHMP5 (L163D/L167D/L170D/L174D or L4D) (47). In Figure 3.1A, we saw that inclusion of the quadruple leucine mutant in the assay failed to reproduce a similar inhibitory effect (4.94 Pi/min/VPS4B). These data showed that while human CHMP5 regulates VPS4 ATPase activity in a LIP5-dependent manner, it has an opposite effect as compared to its yeast counterpart suggesting a potentially different mechanism of regulation. Interestingly, addition of the minimal LIP5 binding element of CHMP1B to the assay had little effect on VPS4B ATPase activity (Figure 3.1B). This suggested that CHMP1B and CHMP5 play different roles in regulating LIP5 function.

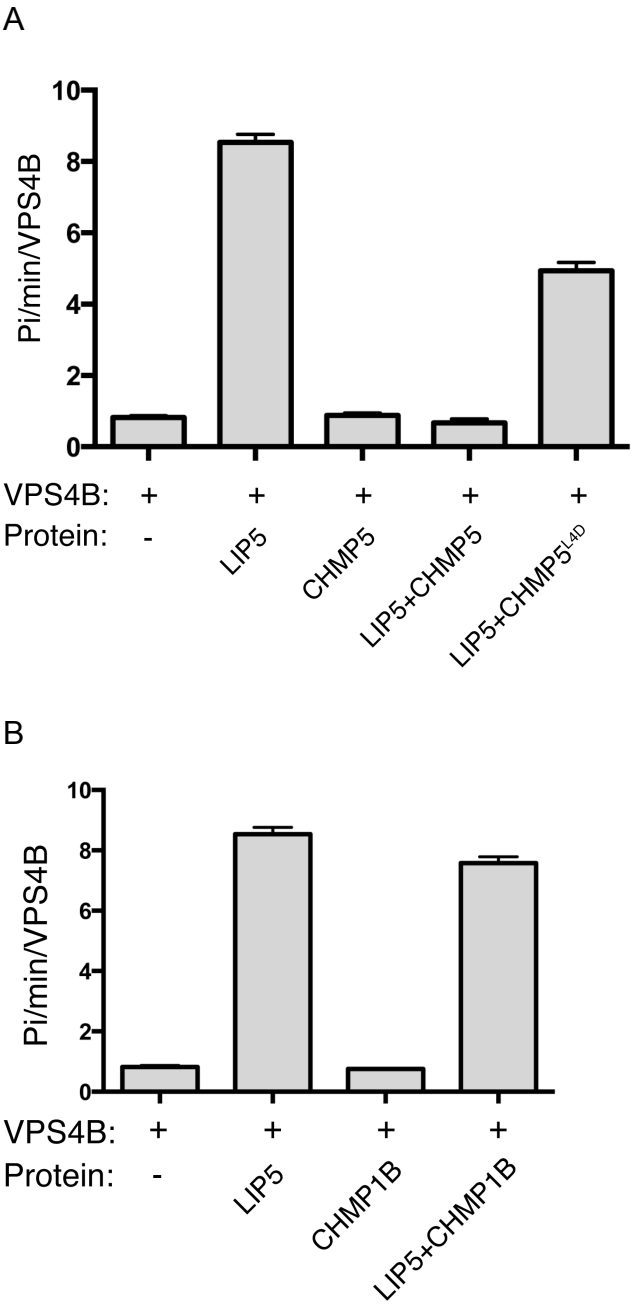

Figure 3.1 ESCRT-III proteins regulate the stimulatory activity of LIP5 on VPS4.

(A) CHMP5 MIM inhibits the stimulatory activity of LIP5. ATP hydrolysis by 0.5 μM VPS4BΔMIT (intrinsic, first column) was assayed under conditions of 2 mM ATP at 37°C (see Experimental procedures). In addition, the following proteins were incubated with Vps4: 0.5 μM LIP5 (second column), 2 μM CHMP5 MIM (third column), 0.5 μM LIP5 plus 2 μM CHMP5 MIM (fourth column), and 0.5 μM LIP5 plus 2 μM CHMP5 MIM L4D (fifth column). (B) CHMP1B MIM has no effect on LIP5 activity. The following proteins were incubated with Vps4: 0.5 μM LIP5 (second column), 2 μM CHMP1B MIM (third column), and 0.5 μM LIP5 plus 2 μM

CHMP1B MIM (fourth column). Each experiment was done in triplicate; all experiments were repeated a minimum of three times.

3.3.2 The crystal structure of LIP5NTD-CHMP1B-CHMP5

Since CHMP5 has a clear role in regulating the ability of LIP5 to stimulate VPS4 ATPase activity, we asked what the structural basis of this regulation is. In a previously determined NMR structure of LIP5NTD-CHMP5 binary complex, there is no discernable conformational change in LIP5NTD upon CHMP5 MIM binding (47). We reasoned that CHMP5-binding induced LIP5 conformational change might be small and transient thus not easily observable in the solution structure. To that end, we embarked on determining the crystal structure of the ternary complex of LIP5NTD-CHMP1B-CHMP5. The presence of CHMP1B led to the formation of crystals that diffracted to a very high resolution of 1.0 Å. The structure was determined and refined with an R-factor of 16.5% and a free R-factor of 18.1% (Table 3.1). The final model consists of LIP5 residues 4-162, CHMP1B residues 185-199 and CHMP5 residues 151-190.

In the ternary complex structure, CHMP1B forms a small helix that binds to the MIT1 domain of LIP5 and CHMP5 forms a loop-helix-turn-helix structure that wraps around the MIT2 domain but also makes significant contacts with the MIT1 domain (Figure 3.2A). Overall, the modes of both ESCRT-III proteins' binding to LIP5 largely mirror those observed in their respective binary complex structures (47). The interface between LIP5 and CHMP5 is extensive with a measured buried surface area to be 1505 $Å^2$. The CHMP5 conformation in the complex structure can be divided into three major parts (Figure 3.2B). Residues 151-159 adopt an extended loop conformation and bind across the surface of

Table 3.1 Crystallography statistics

	LIP5NTD/CHMP1B/CHMP5
	Native
Data Collection	
Space group	$P2_1$
Unit cell parameters:	
a, b, c (Å)	34.2, 60.5, 52.0
α, β, γ (°)	90.0, 90.5, 90.0
Molecules/ASU	1
Wavelength (Å)	0.9998
Resolution (Å)	1.0
Unique reflections	99846
Redundancy[1]	4.5 (3.5)
Completeness (%)	87.4 (46.1)
Average I/σ (I)	50.6 (5.4)
R_{merge}	0.05 (0.27)
Refinement	
Residues in the structure	
LIP5	4-162
CHMP1B	185-199
CHMP5	151-190
Resolution range (Å)	50.0-1.0
R_{work} (%)	16.5
R_{free} (%)	18.1
RMS deviations	
Bond lengths (Å)	0.008
Bond angles (°)	1.28
B-factor average (A^2)	8.5
Ramachandran plot	
Most favored (%)	98.8
Allowed (%)	1.2
Outliers (%)	0.0
PDB accession code	4TXR

helices 5 and 7 of LIP5NTD. Residues 160-176 form a long helix that binds across helices 6 and 7 of LIP5NTD as well as make extensive contacts with helix 1. Following a three-residue turn, residues 181-189 form a short helix that binds across the surface of helices 5 and 6 of LIP5NTD. When binding to the helices of the MIT2 domain, these CHMP5 structural elements all bind at a nearly perpendicular angle.

A

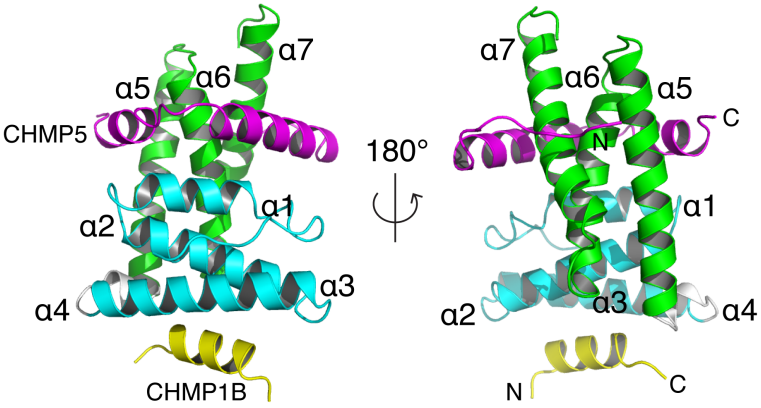

B

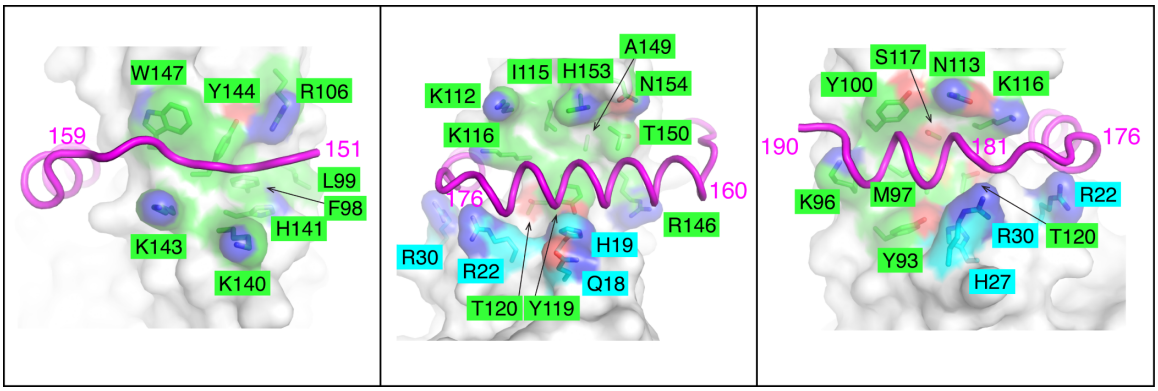

C

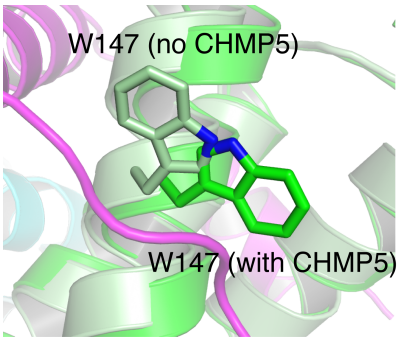

Figure 3.2 The crystal structure of LIP5NTD-CHMP1B-CHMP5 complex. (A) An overview of the LIP5NTD-CHMP1B-CHMP5 complex structure. Cartoon representation of LIP5NTD (residues 1-162) in complex with CHMP1B (residues 176-199) and CHMP5 (residues 151-190) in front (left panel) and back (right panel) views. Coloring and labeling schemes are the same as in Figure 1A except that CHMP5 is colored in magenta. (B) CHMP5 makes extensive

contacts with LIP5NTD. The interface is divided and shown in three separate panels based on three sequence segments of CHMP5: 151-159 (left), 160-176 (center) and 176-190 (right). CHMP5 is shown as a magenta coil. LIP5NTD is shown as a semi-transparent surface along with stick representation of side chains that contribute to van der Waals interactions. Surface and sticks are colored using the following schemes: carbon atoms of MIT1, cyan; carbon atoms of MIT2, green; oxygen, red; nitrogen, blue. (C) Trp147 of LIP5 flips upon binding CHMP5. Zoom-in cartoon representation showing the conformation of Trp147 before (pale green) and after (green) binding CHMP5 (magenta).

Interactions between CHMP5 and LIP5 are largely mediated by van der Waals interactions (Table 3.2). As noted previously, CHMP5 contains a "leucine-collar" that consists of six leucine residues, Leu158, Leu163, Leu167, Leu170, Leu174 and Leu183 (Figure 3.3) (47). These residues are highly conserved in metazoan CHMP5 (Figure 3.4). They bind to a conserved hydrophobic LIP5 surface that is formed by aromatic side chains and aliphatic portions of basic residues (Figure 3.2B). For example, the highly conserved Trp147 of LIP5 has been previously shown to be essential for high-affinity binding (47). Comparison between the LIP5NTD-CHMP1B and LIP5-CHMP1B-CHMP5 structures showed that the imidazole ring of the Trp147 side chain adopts a different rotamer conformation upon CHMP5 binding. It swings around the Cβ-Cγ bond by 180° to make room for CHMP5 binding (Figure 3.2C). There are only a few specific hydrogen bond interactions between CHMP5 and LIP5. CHMP5 residues involved in these interactions are clustered either at the N-terminal loop (Arg151 and Tyr153) or at the short linker between the two helices (Asp177, Asp179, Tyr182 and Asp184) (Figure 3.5). These residues are invariant among metazoan CHMP5 (Figure 3.4). There has been speculation that charge-charge interaction might contribute to high-affinity binding between the two molecules given that CHMP5 is acidic and LIP5 is basic (47). However, except for the few residues

Table 3.2 Intermolecular interactions in the CHMP5-LIP5-CHMP1B structure

CHMP5	LIP5	CHMP1B
Hydrogen bond interactions		
	R57 NH1	D186 OD1
	R57 NH2	D186 OD2
	E68 OE2	R191 NE
	E68 OE1	R191 NH2
	D65 OD1	R191 NH2
	K71 NZ	L195 O
	E83 OE2	R196 NE
	E83 OE1	R196 NH1
	Q44 OE1	R196 NH2
	V130 O	R196 NH2
	E83 N	Q198 OE1
R151 NH1	D102 OD2	
R151 NH1	N103 OD1	
S152 O	R106 NH2	
Y153 OH	D102 OD2	
E166 OE1	N154 ND2	
D177 OD2	K116 NZ	
D177 O	R22 NH2	
D179 O	K116 NZ	
Y182 OH	E26 OE2	
Y182 OH	T120 OG	
D184 OD2	R30 NE	
A186 O	K96 NZ	
A189 O	K96 NZ	
Van der Waals interactions		
	M47, R57, L60, S61, M64	L188
	M64	R191
	L40, M43, Q44, M47, M64	L192
	Y36, L40, M64, L67, K71	L195
	L40	R196
Y153	F98, L99, R106, H141, Y144	
T155	K143, W147	

CHMP5	LIP5	CHMP1B
P156	W147	
L158	W147	
L163	R146, T150	
E166	T150, N154	
L167	Y119, R146, T150	
L170	I115, Y119, A149, H153	
G171	Y119, H19	
D172	H19	
L174	R22, Y119, T120	
L175	N18, H19, R22	
Y182	N113, K116, S117	
L183	H27, R30, M97, Y93	
E185	Y100, N113	
A186	Y100	

mentioned above, most of the acidic residues of CHMP5 point away from the interface hence unlikely to contribute directly to binding.

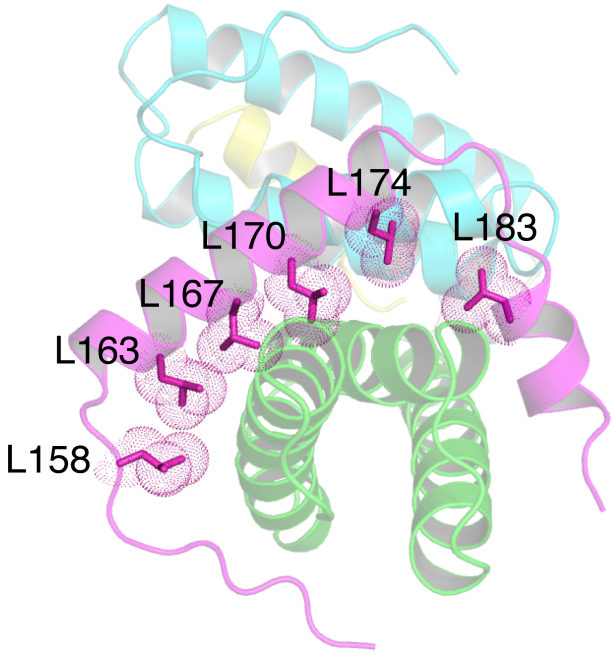

Figure 3.3 "Leucine collar" of CHMP5 mediates hydrophobic binding to LIP5.
LIP5-CHMP1B-CHMP5 complex structure is shown as a cartoon representation. Side chains of "leucine collar" residues are shown as stick models along with their van der Waals surfaces. Same coloring scheme is used throughout the manuscript.

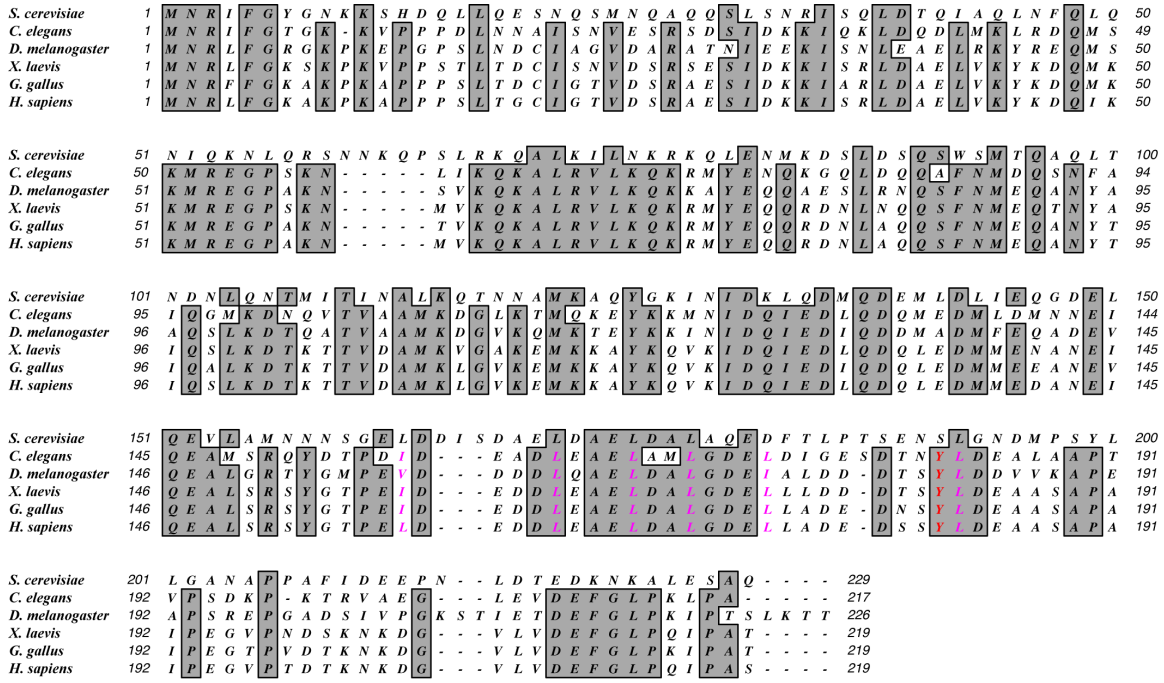

Figure 3.4 Sequence alignment of CHMP5/Vps60.
"Leucine collar" residues are colored magenta. Tyr182 is colored red.

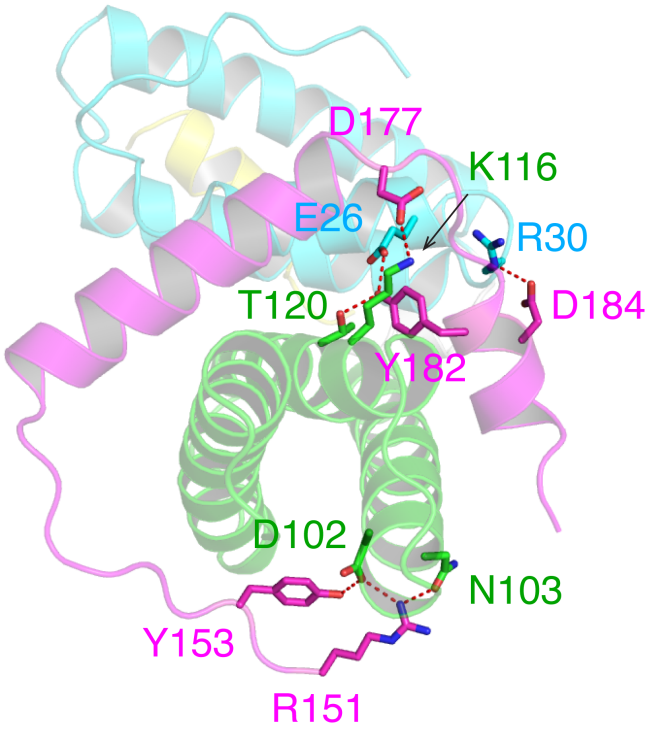

Figure 3.5 Specific hydrogen bond interactions between CHMP5 and LIP5.
CHMP5 residues involved in these interactions are clustered either at the N-terminal loop (Arg151 and Tyr153) or at the short linker between the two helices

(Asp177, Tyr182 and Asp184). Same coloring scheme is used throughout Chapter 3.

3.3.3 Conformational change in LIP5 associated with CHMP5 binding

The availability of high-resolution LIP5 complex crystal structures enabled us to examine structural change in LIP5 associated with CHMP5 binding. Overall, a moderate conformational adjustment was observed in LIP5, where the MIT2 domain moves relative to the MIT1 domain due to the presence of CHMP5 at the MIT1-MIT2 interface (Figure 3.6A). Helices 5 and 7 of the MIT2 domain are pushed outwards by about 2 Å. In the absence of CHMP5 binding, there are a number of hydrogen bonds between the two MIT domains. In particular, Glu26 of the MIT1 domain interacts with Lys116 of the MIT2 domain. Upon CHMP5 binding, the distance between Glu26 and Lys116 increases from 2.9 Å to 9.0 Å (Figure 3.6B). These residues would now form new interactions with the bound CHMP5. In the LIP5NTD-CHMP1B-CHMP5 structure, Glu26 forms hydrogen bonds with the side chain of Tyr182. Lys116 forms hydrogen bonds with the side chain of Asp177 and with the main chain carbonyl oxygen of Asp179 (Figure 6c). There are also additional interactions between CHMP5 and LIP5NTD in the vicinity including His19, Arg22 and Arg30 that stabilize the new conformation of LIP5NTD (Table 3.2).

Of particular interest is Tyr182 of CHMP5, which stands out as the potential culprit of the conformational change. In the ternary complex structure, Tyr182 drives itself between the LIP5 MIT1 and MIT2 domains, where it makes both hydrogen bond and van der Waals interactions with LIP5. In the NMR structure of the LIP5NTD-CHMP5 binary complex, five out of the ten structure

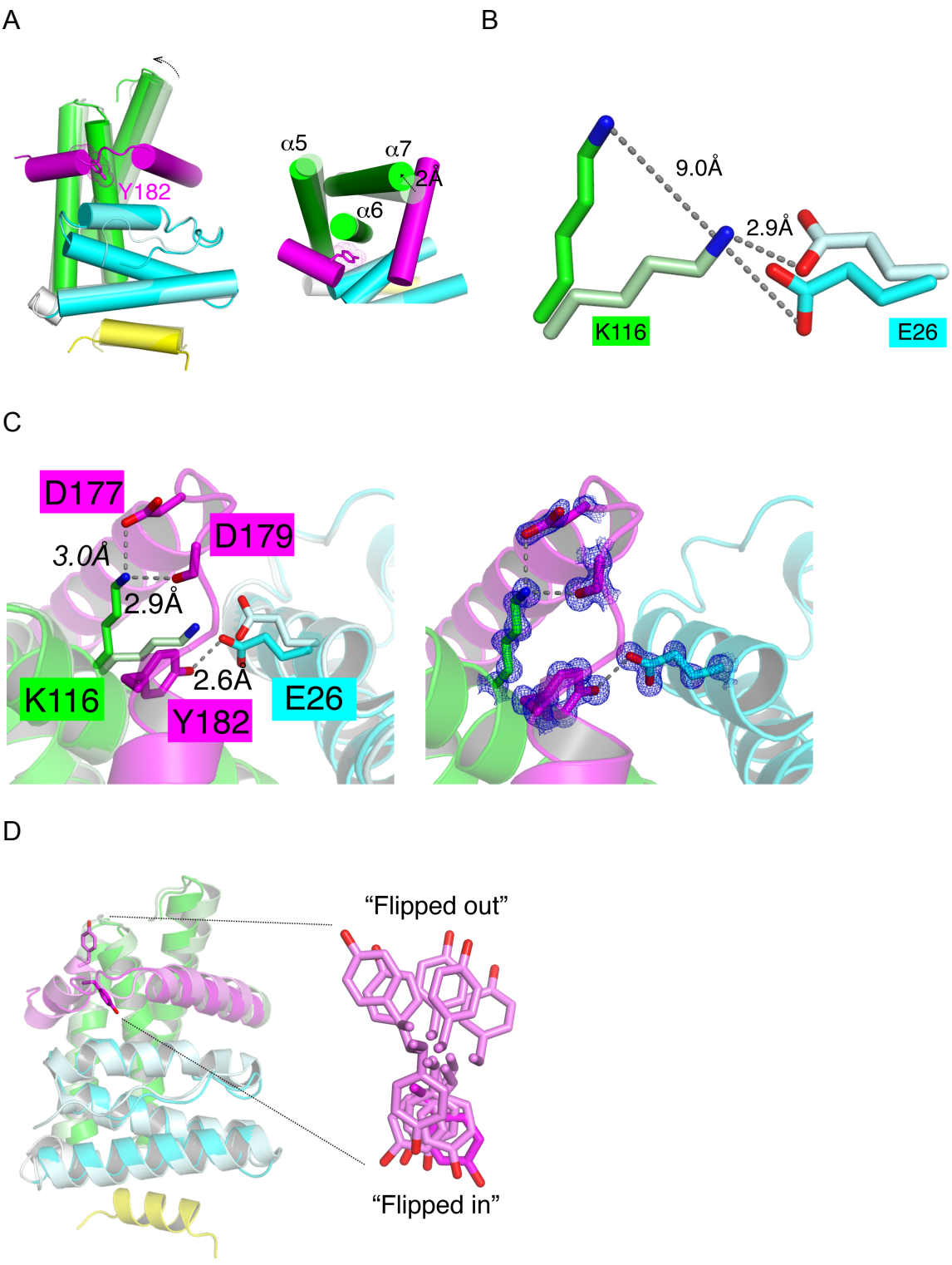

Figure 3.6 Conformational change at the LIP5 MIT domain interface. (A) Superimposition of LIP5NTD-CHMP1B structure with LIP5NTD-CHMP1B-CHMP5 structure. The coloring scheme used is the same as in Figures 1a and 4a (the binary complex has a pale color tone). The view in the right panel is

nearly orthogonal to that of the left panel and highlights the movement of the MIT domain. Helices are shown as cylinders and loops in the right panel are omitted for clarity. (B) K116-E26 salt bridge is broken in the ternary complex structure. Side chains are shown in stick representation. Carbons atoms are colored using the same scheme as in (A). (C) K116 and E26 are engaged in new interactions in the ternary complex structure. The left panel is a zoom-in view of interactions involving K116 and E26 before and after CHMP5 binding. Residues involved are shown as sticks and labeled. New hydrogen bonds are denoted as dashed lines with distances indicated. The right panel omits the binary complex structure but shows 2Fo-Fc electron density (2.0σ) associated with interacting residues in the ternary complex structure. (D) Insertion of Tyr182 at the MIT domain interface. The left panel shows superimposition of LIP5NTD-CHMP1B-CHMP5 structure with LIP5NTD-CHMP5 structure (only one of the ten NMR structure assemblies is shown). The right panel shows the conformation of Tyr182 in the two structures. Tyr182 in the ternary complex structure adopts a "flipped in" conformation. Tyr182 in the binary complex structure can adopt either a "flipped in" or "flipped out" conformation.

ensembles have the Tyr182 pointed into the LIP5 MIT domain interface and the other five are oriented towards the solvent (Figure 3.6D)(47). These data suggest that Tyr182 can exist in equilibrium between a "flipped in" or a "flipped out" conformation. Binding of CHMP1B appears to have stabilized Tyr182 in the "flipped in" conformation at the LIP5 MIT domain interface as evidenced by the well-defined electron density associated with the residue (Figure 3.6C). Interestingly, Tyr182 of CHMP5 and Glu26 of LIP5 are strictly conserved in metazoan protein sequences suggesting a potentially conserved mechanism in higher eukaryotes (Figure 3.4, 3.7).

We looked to see whether insertion of Tyr182 into the MIT domain interface might be structurally related to the inhibitory function of CHMP5 on LIP5. A significant loss of the inhibitory effect of CHMP5 was observed when Tyr182 is mutated to alanine (Figure 3.8A). Interestingly, this mutation has little effect on CHMP5 binding to LIP5 as GST-CHMP5^{Y182A} can still bind a similar amount of LIP5 as the wild-type protein (Figure 3.8B). These data suggested

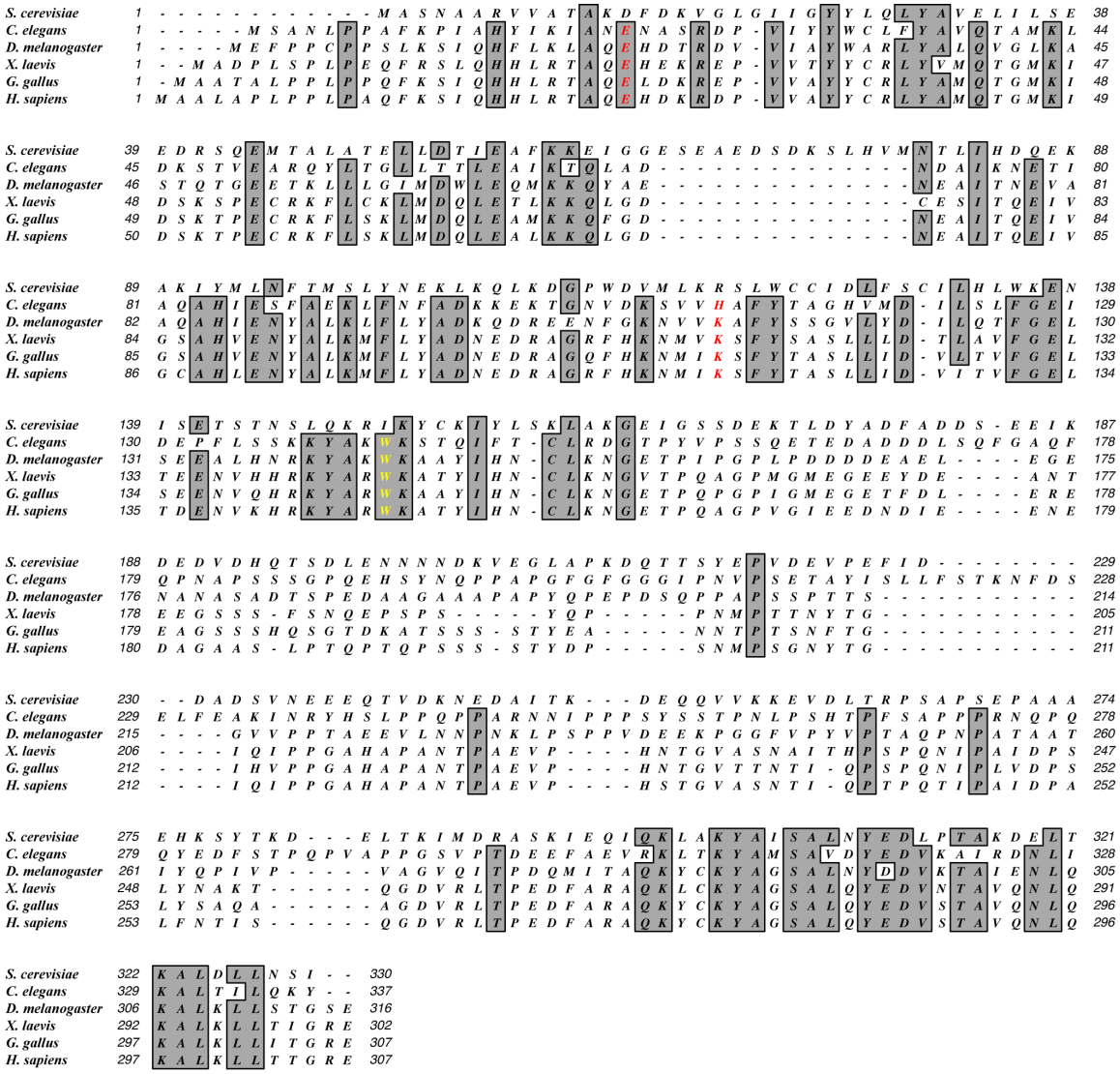

Figure 3.7 Sequence alignment of LIP5/Vta1.
Glu26 and Lys116 are colored red. Trp147 is colored yellow.

that the mere binding of CHMP5 to LIP5 is not sufficient for its inhibitory effect on LIP5 function. Instead, the inhibitory effect is predicated on the conformational change in LIP5 associated with insertion of Tyr182 at the MIT domain interface.

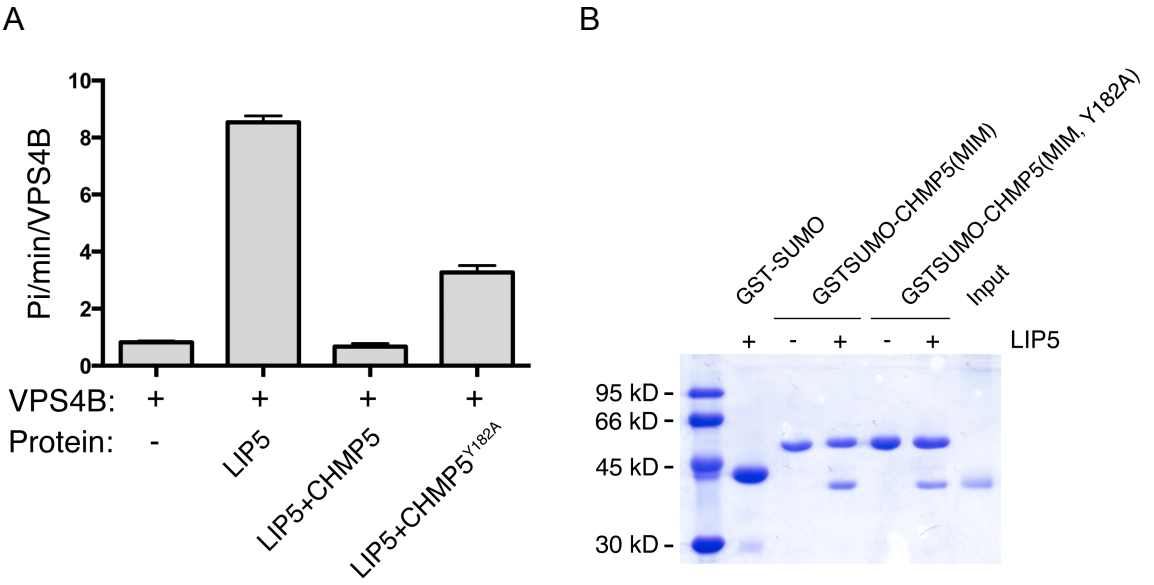

Figure 3.8 Tyr182 of CHMP5 is important for its inhibitory activity.
(A) CHMP5 Y182A abolishes its inhibitory activity towards LIP5. Protein concentration used in the ATPase assay: VPS4BΔMIT, 0.5 μM; LIP5, 0.5 μM; and CHMP5, 2 μM. (B) CHMP5 Y182A still binds LIP5. GST-SUMO, GST-SUMO-CHMP5^{MIM}, or GST-SUMO-CHMP5$^{MIM, Y182A}$ was used to analyze its interaction with LIP5. GST-SUMO was used as a tag since GST-CHMP5^{MIM} runs at a position similar to that of LIP5.

3.3.4 LIP5NTD is directly involved in stimulation of VPS4 activity

Studies in yeast suggested that the stimulatory effect of Vta1 on Vps4 is attributed to the binding of its C-terminal VSE and VSL domains to Vps4 (38,42). The unstructured linker of Vta1 acts to inhibit the function of VSE and this inhibition is relieved upon binding of the regulatory ESCRT-III proteins to the N-terminal domain of Vta1 (42). To probe whether a similar mechanism is utilized in metazoan LIP5, we generated a LIP5 truncation mutant (LIP5$^{215-307}$) that would include the putative VSE and VSL domains (Figure 3.9A). A similar yeast Vta1 truncation mutant displayed an increased stimulatory activity towards Vps4 when compared with the wide-type Vta1(42). To our surprise, LIP5$^{215-307}$ had very low

activity towards VPS4B even though its binding affinity to VPS4B did not appear to be compromised (Figure 3.9B, 3.9C).

A

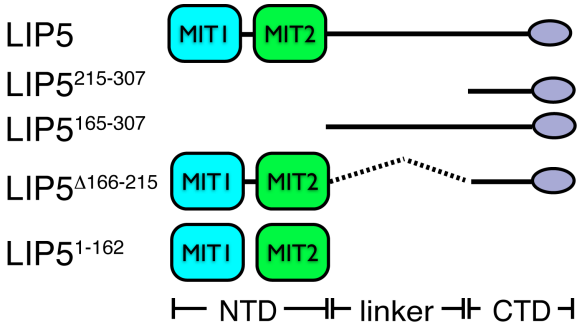

B

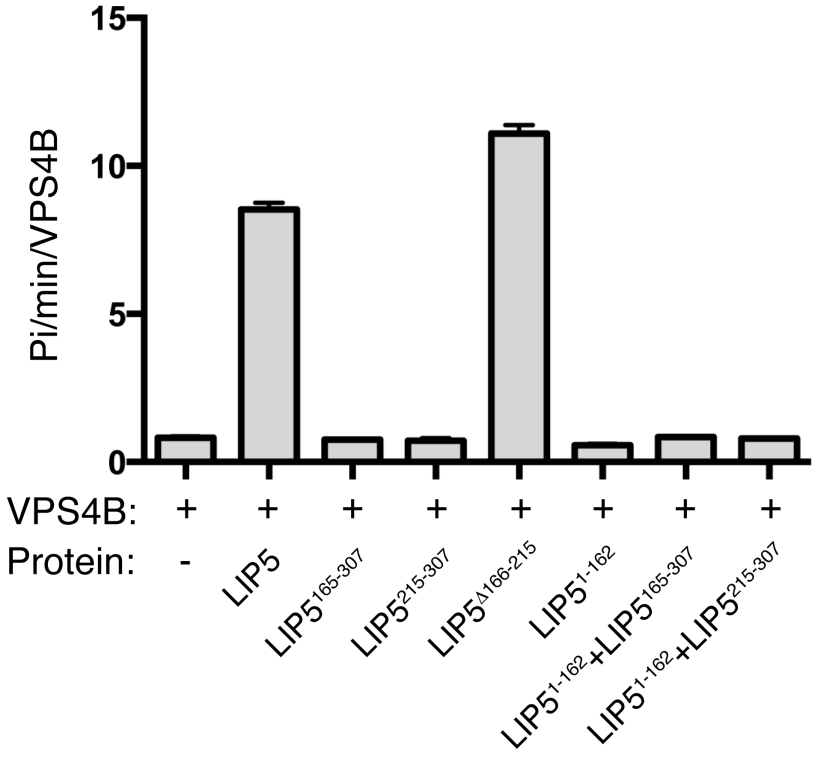

C

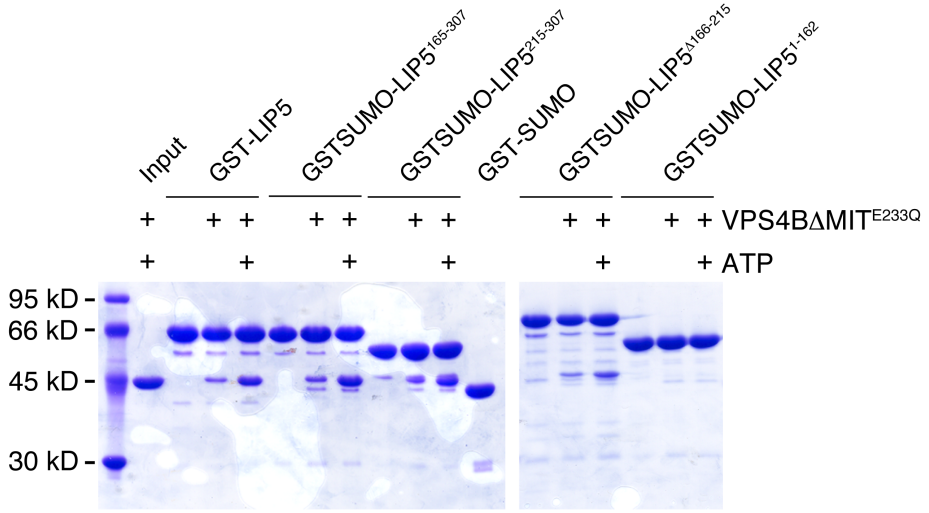

D

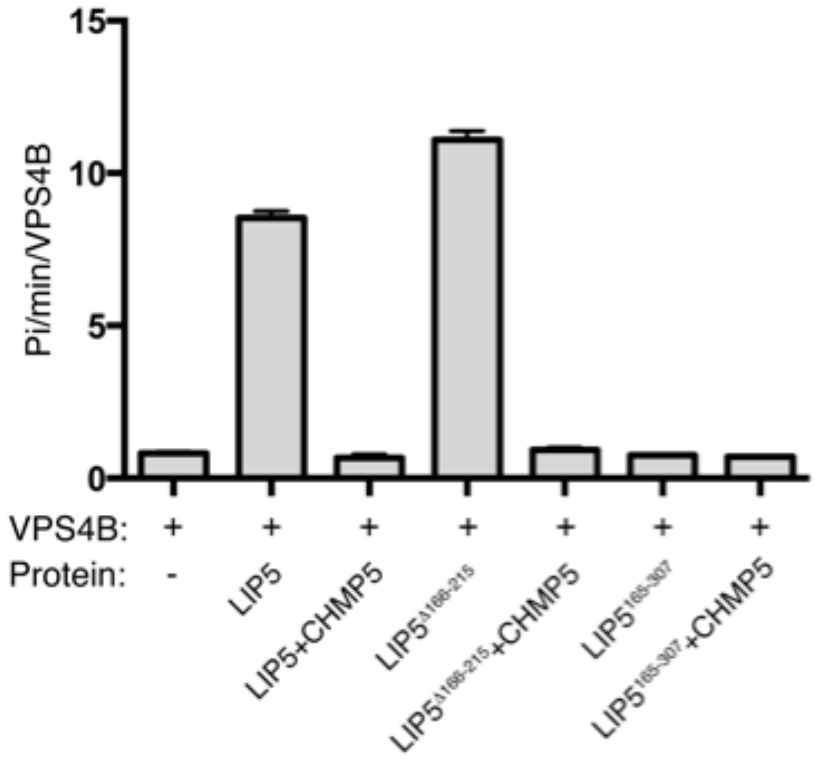

Figure 3.9 Both terminal domains of LIP5 are required for its VPS4 stimulatory activity.

(A) Schematic showing the LIP5 constructs used in the assay. (B) Various LIP5 truncation mutants or mutant combinations were assayed for their VPS4 stimulatory activity. Note that LIP5$^{\Delta 166\text{-}215}$ is equivalent to adding the two terminal domains in *cis*. (C) Various LIP5 truncation mutants were assayed for their binding affinity for VPS4B. GST-SUMO was used as a tag since some of the GST-LIP5 constructs run at a position similar to that of VPS4BΔMIT^{E233Q}. Binding analyses were performed in the presence or absence of ATP. (D) The inhibitory activity of CHMP5 does not depend on the linker region of LIP5. LIP5, LIP5$^{\Delta 166\text{-}215}$ and LIP5$^{165\text{-}307}$ were assayed for their abilities to stimulate VPS4B activity in the absence or presence of CHMP5.

This observation suggested that residues beyond the C-terminal region of LIP5 are required for LIP5 activity. To further map the location of these residues, we examined the activity of the following truncation mutants of LIP5 towards VPS4B: LIP5$^{165\text{-}307}$, LIP5$^{D166\text{-}215}$ and LIP5$^{1\text{-}162}$ (Figure 3.9A). The results showed that deletion of LIP5NTD (LIP5$^{165\text{-}307}$) led to a loss of stimulation, but deletion of the linker region (LIP5$^{D166\text{-}215}$) had no negative effect on the activity of LIP5 (Figure 3.9B). In fact, deletion of the linker region produced a mutant that was even more active (11.10 Pi/min/VPS4B) than the wild-type protein (8.54 Pi/min/VPS4B), suggesting an inhibitory role for this portion of the linker. Furthermore, LIP5NTD (LIP5$^{1\text{-}162}$) alone was not sufficient in stimulating VPS4. Hence, the two terminal domains of LIP5 are both required for the high stimulatory activity towards VPS4B while the linker region sequence is dispensable. Interestingly, only when the two terminal domains of LIP5 were added *in cis* but not *in trans* would the stimulatory activity be reproduced (Figure 3.9B). These results suggested that although the C-terminal domain is responsible for high affinity VPS4B binding, the stimulatory activity of LIP5 is likely the work of the N-terminal domain. Binding of the C-terminal domain to

VPS4B recruits the N-terminal domain to the site of action due to the physical linker between the two parts of LIP5.

Given that the activity of LIP5 does not depend on the LIP5 linker sequence, we explored whether CHMP5 still displayed the same inhibitory effect on LIP5 activity in the absence of the linker sequence. We observed a similar degree of inhibitory effect towards LIP5 activity for $LIP5^{D166-244}$ (Figure 3.9D). As a control, there was no reduction in the moderate ATPase activity generated by $LIP5^{165-307}$ when CHMP5 was added. Therefore, regulation of VPS4B activity by CHMP5 binding to LIP5NTD is unlikely mediated through the linker region, as has been suggested in the yeast (42). Instead, CHMP5 binding is more likely to modulate the interaction between LIP5NTD and VPS4B through a mechanism that involves the conformational change in LIP5NTD as seen in the ternary complex structure.

3.4 Discussion

Given the structural and functional complexity of the ESCRT machinery, it is not surprising that ESCRT assembly is under tight spatial and temporal control at multiple steps. Vps4 is the only energy-consuming enzyme within the ESCRT machinery and has long been viewed as the master regulator of the system. Vps4 engages in three types of protein-protein interactions: with itself, with ESCRT-III, and with Vta1. These interactions represent three general mechanisms that are used to control the activity of Vps4 in the cell: (a) ATP-dependent switching between “inactive” (unassembled) and “active” (assembled)

states, (b) recruitment to the site of action through specific protein-protein interactions, and (c) protein cofactors that promote or inhibit its activity.

Vps4 is a member of the AAA-ATPase family and it cycles between two different quaternary structures depending on the status of its bound nucleotide (35). In the absence of ATP, it exists as an inactive monomeric or dimeric species. Upon ATP binding, it forms a high molecular weight ring-shaped oligomeric structure, which recent evidence suggests is likely a hexamer (36). This cycle, however, appears to be highly inefficient if the ATPase has to undergo the assembly-disassembly process each time it binds and hydrolyzes ATP. In yeast, the cofactor Vta1 has been shown to bind Vps4 in an ATP-dependent manner and activate its ATPase activity (23,39). The action of Vta1 has been attributed to the structural features near the C-terminus as the N-terminal truncation mutant of Vta1 can recapitulate the full activity of Vta1 (42).

3.4.1 Stimulation of VPS4 by LIP5 requires both terminal domains connected in cis

While we demonstrated that human LIP5 stimulates the ATPase activity of VPS4, the mechanism of action appears to be different in the two systems. Although the C-terminal domain of LIP5 is both necessary and sufficient for binding VPS4, the C-terminal domain alone is not sufficient to reproduce the stimulatory activity of LIP5. Instead, the full-scale activity requires the presence of both terminal domains. Furthermore, a physical connection between the two domains is necessary as the two domains added *in trans* are not active. The

length as well as the sequence of the linker appears to be less critical. This is consistent with the fact that the sequence conservation at the linker region appears to be very low (Figure 3.7). We hypothesize that the C-terminal domain of LIP5 makes an initial binding to VPS4, likely to the conserved β-domain (Figure 3.10). This interaction brings the N-terminal domain close to the ATPase as it is connected to the C-terminal domain through the linker. This enables an additional interaction between the N-terminal domain and VPS4, which otherwise would not occur due to its weak inherent binding affinity. The activity of the full-length LIP5 to VPS4 is likely the result of the combined actions of the two domains. At this point, it is not clear how it exactly occurs but we suspect that LIP5 could promote the oligomerization of the ATPase as well as increase its catalytic efficiency.

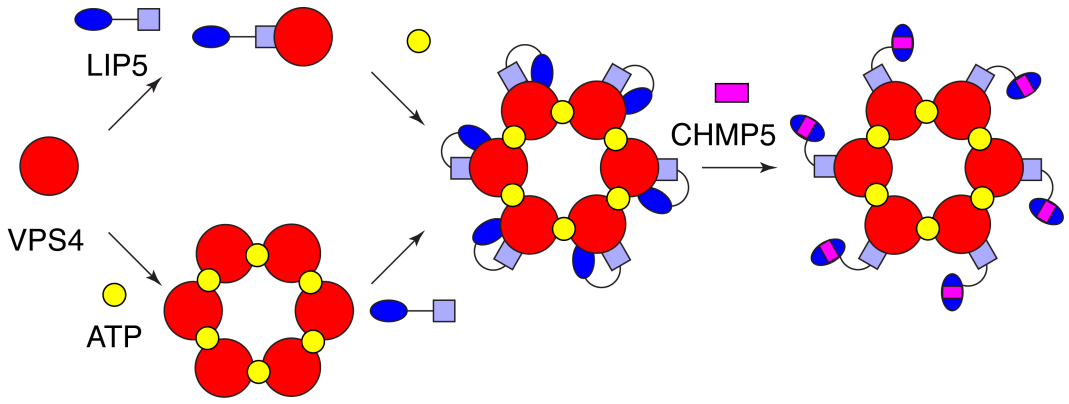

Figure 3.10 A model of VPS4 regulation by LIP5-CHMP5 complex.
The C-terminal domain of LIP5 makes an initial binding to VPS4. This interaction brings its N-terminal domain close to VPS4, which enables an additional interaction between the N-terminal domain and VPS4. The combined actions of the two domains lead to full activity of VPS4. Binding of CHMP5 to LIP5 weakens the interaction between the N-terminal domain and VPS4 and leads to an inhibition of LIP5 activity.

3.4.2 CHMP5 is potent inhibitor of LIP5 stimulation of VPS4

In contrast to CHMP1B, binding of CHMP5 to LIP5 potently inhibits the stimulatory activity LIP5 displays towards the VPS4 ATPase. This suggests that binding of CHMP5 could potentially serve as an allosteric power switch to spatially and temporally control the activity of VPS4. Sequence comparison has shown that the LIP5 MIT2 has diverged significantly from other known MIT domain sequences, suggesting that it might function as a specific CHMP5-binding domain (data not shown). Although most of the CHMP5-binding occurs on the MIT2 domain, there is also significant binding to the MIT1 domain, particularly near the MIT1-MIT2 interface. The latter is significant because it leads to the movement of MIT2 relative to MIT1, likely due to the insertion of a highly conserved Tyr182 of CHMP5 at the domain interface. We suspect that these changes form the structural basis for the inhibitory effect of CHMP5 on LIP5 function. As we have seen, the interaction between the N-terminal domain of LIP5 and VPS4 is required for the full stimulatory activity of LIP5. Movement of MIT2, induced by CHMP5 binding, could conceivably alter the interaction between LIP5 and VPS4 and hence the inhibition (Figure 10).

While most ESCRT-III proteins promote the activity of Vps4, it is not unprecedented for one of them to exhibit an inhibitory function. Early work studying the role of ESCRT in HIV-1 release found that siRNA silencing of CHMP5 in co-transfected human cells caused an increase in the release of infectious virus-like particles, suggesting a possible negative regulatory role for

CHMP5 *in vivo* (48). Additionally, Ist1 inhibits Vps4 oligomerization and ATPase hydrolysis (45). While Ist1 utilizes its C-terminal MIM for initial targeting to the MIT domain of Vps4, the subsequent association between the N-terminal ESCRT-III domain of Ist1 with Vps4 is responsible for the inhibition. LIP5-CHMP5 inhibition of VPS4B mirrors this mechanism, with the LIP5 VSL domain acting like the Ist1 MIM and the LIP5 NTD-CHMP5 MIM complex acting like the Ist1 ESCRT-III domain.

In summary, we have performed structural and functional analyses of molecular interactions between VPS4B and its various associated regulators to gain mechanistic insights into the regulation of ESCRT machinery in higher eukaryotes. The results show interesting mechanistic difference in yeast versus metazoan. Although Vta1 and LIP5 can both stimulate their cognate Vps4 ATPase activity, the structural requirement appears to be different. The C-terminal domain of Vta1 is sufficient for full activity in yeast (42) , whereas both terminal domains of LIP5 are required in metazoan. Furthermore, the effect of the ESCRT-III proteins upon binding to the N-terminal domain of Vta1/LIP5 is also dramatically different in terms of their ability to up or down regulate the stimulatory activity of Vta1/LIP5 towards the ATPase. Structural results from the current study, together with previous NMR structures of human LIP5-CHMP5 and yeast Vta1-Vps60 complexes (47,49), suggest that they are likely the results of different binding interactions. Interestingly, residues at the interface of LIP5 and CHMP5 are highly conserved throughout the metazoan but much less so in yeast

(Figure 3.4, 3.7), suggesting that the allosteric regulatory mechanism of LIP5 by CHMP5 has diverged during evolution.

3.5 Methods

3.5.1 Cloning, Expression, and Purification

DNA sequences encoding for various proteins and protein fragments were amplified from cDNAs (ATCC®) and cloned into a modified pET28b vector to generate N-terminal His_6-SUMO tagged fusion proteins. Point mutations were generated using a standard PCR mutagenesis protocol (Stratagene). Proteins were expressed in *Escherichia coli* Rosetta(DE3), where cells were grown at 37°C to log phase in standard LB media and induced with 0.2 mM Isopropyl β-D-1-thiogalactopyranoside followed by an additional 16-20h growth at 16°C. Seleno-methionyl $LIP5^{1-162}$ derivative was expressed in *E. coli* B834(DE3) using a minimal medium where methionines were replaced with seleno-methionines.

All proteins were purified using a similar protocol with adjustment made when necessary. Cells were pelleted and lysed by sonication in buffer A (25 mM Tris pH 8.0, 300 mM NaCl, 5 mM 2-mercaptoethanol, and 10 µg/mL (w/v) phenylmethylsulfonyl fluoride). Cell lysate was cleared by centrifugation and supernatant was loaded onto a Ni^{2+}-nitrilotriacetic acid affinity column, washed with buffer A and eluted with buffer A supplemented with 250 mM imidazole. Eluate was collected, digested with ULP1 to cleave the His_6-SUMO tag while being dialyzed against 50 mM Tris pH 8.0, 25 mM NaCl overnight. A moderate precipitation formed for $LIP5^{1-162}$ and $LIP5^{\Delta 166-214}$ during dialysis, which was

determined to be nucleic acid and could be cleared by centrifugation. Dialyzed protein mixture was passed over a second Ni^{2+}-nitrilotriacetic acid column to remove the His_6-SUMO tag. Proteins that would be used for GST-pulldown analysis were stored directly in -80°C. Proteins that would be used in ATPase assay were first concentrated using a Macrosep® (Pall Corporation) centrifugal device, diluted in ATPase buffer (100 mM Tris-HCl (pH 7.4), 20 mM KCl, 6 mM $MgCl_2$) and then stored at -80°C.

Proteins used for crystallization were further purified. $LIP5^{1-162}$ was further purified on a Source-S (GE Healthcare) cation exchange column using buffer C (50 mM HEPES pH 7.0, 50 mM NaCl, 1mM EDTA, 1mM DTT) as a loading buffer, and eluted via a gradient with buffer C supplemented with 1M NaCl. Fractions containing the protein was pooled, concentrated and loaded onto a HiLoad™ Superdex™ 75 (GE Healthcare) column and eluted with buffer C. With regards to the two protein complexes, purified ESCRT-III peptides were mixed with $LIP5^{1-162}$ in a saturating amount. These mixtures were concentrated and loaded onto the Superdex™ 200 column, and eluted with buffer C. Complex formation was confirmed by elution position change from the gel filtration column. The two ESCRT-III peptides were not detectable by Coomassie blue staining.

3.5.2 Crystallization and Data Collection

Complex crystals of LIP5-CHMP1B were grown by sitting drop vapor diffusion method at 4°C. Protein complex at 12.7 mg/ml was mixed in a 1:1 ratio with a solution of 16% MPD, 0.1 M Tris pH 9.0 and equilibrated against 500 µl of

a reservoir solution of 8% MPD, 0.1 M Tris pH 9.0. Two crystals with different morphology appeared. Long needle-like crystals would appear instantly and dissolve over time. Stable diamond-like crystals would appear later and were ultimately used for data collection. Crystals were micro-dialyzed (Hampton Research) against 30% MPD, 0.1 M Tris pH 9.0 for 16-24h before flash-frozen under liquid nitrogen. Data were collected at Advanced Photon Source beamline 21-ID, and processed and scaled using HKL2000 (HKL Research Inc.). Complex crystals of LIP5-CHMP1B-CHMP5 were grown by sitting drop vapor diffusion method at 4°C. Protein complex at 13.7 mg/ml was mixed in a 1:1 ratio with a reservoir solution of 19% PEG4000, 25 mM sodium acetate pH 5.5 and equilibrated against 500 µl of the reservoir solution. Large diamond shaped crystals would appear after a few days, which were then micro-dialyzed against 25% PEG4000, 20% ethylene glycol, 25 mM sodium acetate pH 5.5 before flash-frozen under liquid nitrogen. Data were collected at Advanced Photon Source beamline 21-ID, and processed and scaled using HKL2000.

3.5.3 GST Pull-down Analysis

GST pull-down analysis was performed following standard procedures in phosphate-buffered saline (PBS) solution supplemented with 1 mM DTT and 0.1% (v/v) Tween 20(33). Specific samples were also supplemented with 2 mM ATP as indicated. Purified proteins were incubated with GST alone, GST-SUMO alone or GST-tagged proteins immobilized on glutathione-agarose beads for 1 h at 4 °C. The beads were then washed extensively with the buffer before

bound proteins were analyzed on SDS-PAGE and visualized by Coomassie blue staining.

3.5.4 Malachite Green ATPase Assay

Malachite Green assay was used to measure the stimulation of VPS4BΔMIT by various protein mixtures as previously described with modifications (39). LIP5-binding ESCRT-III fragments instead of full-length ESCRT-III proteins were used in the assay due to difficulties in purifying full-length proteins. Briefly, 0.5 μM VPS4BΔMIT was incubated with buffer or 0.5 μM LIP5 (or LIP5 truncation mutation), and with additional 2 μM ESCRT-III peptides (all final concentrations) where indicated, in a 15 μl protein mixture. The reaction was started with the addition of 2 mM ATP (final concentration) to a final reaction volume of 25 μl. The reaction was allowed to proceed for 1h, 80 μl of Malachite green reagent was then added and finally quenched with the addition of 10 μl of 32% sodium citrate. The samples were mixed and incubated at 37 °C for 10 min before A_{620} was measured on a SpectraMax M5 microplate reader (Molecular Devices, Sunnyvale, CA). To account for background ATP hydrolysis, the signal from identically treated sample lacking VPS4BΔMIT was subtracted. Likewise, the background activities of LIP5 proteins or ESCRT-III peptides were subtracted from samples with an identical composition but lacking VPS4ΔMIT. Each experiment was done three times in triplicate, where error bars represent standard error from the mean. Significances in the data were assessed using one-way ANOVA in Prism5 (GraphPad).

3.6 Acknowledgements

We thank the staff at the Advanced Photon Source LS-CAT Sector 21 (21-ID-D) for access and help with data collection. Use of the Advanced Photon Source, an Office of Science User Facility operated for the U.S. Department of Energy (DOE) Office of Science by Argonne National Laboratory, was supported by the U.S. DOE under Contract No. DE-AC02-06CH11357. Use of the LS-CAT Sector 21 was supported by the Michigan Economic Development Corporation and the Michigan Technology Tri-Corridor (Grant 085P1000817). This work was supported by a grant to Z. Xu (GM095769) from National Institutes of Health.

3.7 References

1. Hurley, J. H. (2010) The ESCRT complexes. *Crit Rev Biochem Mol Biol* **45**, 463-487

2. Henne, W. M., Buchkovich, N. J., and Emr, S. D. (2011) The ESCRT pathway. *Dev Cell* **21**, 77-91

3. McCullough, J., Colf, L. A., and Sundquist, W. I. (2013) Membrane fission reactions of the mammalian ESCRT pathway. *Annu Rev Biochem* **82**, 663-692

4. Hanson, P. I., and Cashikar, A. (2012) Multivesicular body morphogenesis. *Annu Rev Cell Dev Biol* **28**, 337-362

5. Katzmann, D. J., Babst, M., and Emr, S. D. (2001) Ubiquitin-dependent sorting into the multivesicular body pathway requires the function of a conserved endosomal protein sorting complex, ESCRT-I. *Cell* **106**, 145-155

6. Sundquist, W. I., and Krausslich, H. G. (2012) HIV-1 assembly, budding, and maturation. *Cold Spring Harb Perspect Med* **2**, a006924

7. Carlton, J. G., and Martin-Serrano, J. (2007) Parallels between cytokinesis and retroviral budding: a role for the ESCRT machinery. *Science* **316**, 1908-1912

8. Jimenez, A. J., Maiuri, P., Lafaurie-Janvore, J., Divoux, S., Piel, M., and Perez, F. (2014) ESCRT machinery is required for plasma membrane repair. *Science* **343**, 1247136

9. Henne, W. M., Stenmark, H., and Emr, S. D. (2013) Molecular mechanisms of the membrane sculpting ESCRT pathway. *Cold Spring Harb Perspect Biol* **5**

10. Nickerson, D. P., West, M., Henry, R., and Odorizzi, G. (2010) Regulators of Vps4 ATPase activity at endosomes differentially influence the size and rate of formation of intralumenal vesicles. *Mol Biol Cell* **21**, 1023-1032

11. Baumgartel, V., Ivanchenko, S., Dupont, A., Sergeev, M., Wiseman, P. W., Krausslich, H. G., Brauchle, C., Muller, B., and Lamb, D. C. (2011) Live-cell visualization of dynamics of HIV budding site interactions with an ESCRT component. *Nat Cell Biol* **13**, 469-474

12. Jouvenet, N., Zhadina, M., Bieniasz, P. D., and Simon, S. M. (2011) Dynamics of ESCRT protein recruitment during retroviral assembly. *Nat Cell Biol* **13**, 394-401

13. Schuh, A. L., and Audhya, A. (2014) The ESCRT machinery: From the plasma membrane to endosomes and back again. *Crit Rev Biochem Mol Biol*

14. Adell, M. A., and Teis, D. (2011) Assembly and disassembly of the ESCRT-III membrane scission complex. *FEBS Lett* **585**, 3191-3196

15. Bajorek, M., Schubert, H. L., McCullough, J., Langelier, C., Eckert, D. M., Stubblefield, W. M., Uter, N. T., Myszka, D. G., Hill, C. P., and Sundquist, W. I. (2009) Structural basis for ESCRT-III protein autoinhibition. *Nat Struct Mol Biol* **16**, 754-762

16. Muziol, T., Pineda-Molina, E., Ravelli, R. B., Zamborlini, A., Usami, Y., Gottlinger, H., and Weissenhorn, W. (2006) Structural basis for budding by the ESCRT-III factor CHMP3. *Dev Cell* **10**, 821-830

17. Lata, S., Schoehn, G., Solomons, J., Pires, R., Gottlinger, H. G., and Weissenhorn, W. (2009) Structure and function of ESCRT-III. *Biochem Soc Trans* **37**, 156-160

18. Fabrikant, G., Lata, S., Riches, J. D., Briggs, J. A., Weissenhorn, W., and Kozlov, M. M. (2009) Computational model of membrane fission catalyzed by ESCRT-III. *PLoS Comput Biol* **5**, e1000575

19. Elia, N., Fabrikant, G., Kozlov, M. M., and Lippincott-Schwartz, J. (2012) Computational model of cytokinetic abscission driven by ESCRT-III polymerization and remodeling. *Biophys J* **102**, 2309-2320

20. Hurley, J. H., and Yang, D. (2008) MIT domainia. *Dev Cell* **14**, 6-8

21. Shim, S., Kimpler, L. A., and Hanson, P. I. (2007) Structure/function analysis of four core ESCRT-III proteins reveals common regulatory role for extreme C-terminal domain. *Traffic* **8**, 1068-1079

22. Scott, A., Gaspar, J., Stuchell-Brereton, M. D., Alam, S. L., Skalicky, J. J., and Sundquist, W. I. (2005) Structure and ESCRT-III protein interactions of the MIT domain of human VPS4A. *Proc Natl Acad Sci U S A* **102**, 13813-13818

23. Xiao, J., Xia, H., Zhou, J., Azmi, I. F., Davies, B. A., Katzmann, D. J., and Xu, Z. (2008) Structural basis of Vta1 function in the multivesicular body sorting pathway. *Dev Cell* **14**, 37-49

24. Hanson, P. I., Roth, R., Lin, Y., and Heuser, J. E. (2008) Plasma membrane deformation by circular arrays of ESCRT-III protein filaments. *J Cell Biol* **180**, 389-402

25. Saksena, S., Wahlman, J., Teis, D., Johnson, A. E., and Emr, S. D. (2009) Functional reconstitution of ESCRT-III assembly and disassembly. *Cell* **136**, 97-109

26. Davies, B. A., Azmi, I. F., Payne, J., Shestakova, A., Horazdovsky, B. F., Babst, M., and Katzmann, D. J. (2010) Coordination of substrate binding and ATP hydrolysis in Vps4-mediated ESCRT-III disassembly. *Mol Biol Cell* **21**, 3396-3408

27. Wollert, T., and Hurley, J. H. (2010) Molecular mechanism of multivesicular body biogenesis by ESCRT complexes. *Nature* **464**, 864-869

28. Wollert, T., Wunder, C., Lippincott-Schwartz, J., and Hurley, J. H. (2009) Membrane scission by the ESCRT-III complex. *Nature* **458**, 172-177

29. Adell, M. A., Vogel, G. F., Pakdel, M., Muller, M., Lindner, H., Hess, M. W., and Teis, D. (2014) Coordinated binding of Vps4 to ESCRT-III drives membrane neck constriction during MVB vesicle formation. *J Cell Biol* **205**, 33-49

30. Morita, E., Colf, L. A., Karren, M. A., Sandrin, V., Rodesch, C. K., and Sundquist, W. I. (2010) Human ESCRT-III and VPS4 proteins are required for centrosome and spindle maintenance. *Proc Natl Acad Sci U S A* **107**, 12889-12894

31. Morita, E., Sandrin, V., McCullough, J., Katsuyama, A., Baci Hamilton, I., and Sundquist, W. I. (2011) ESCRT-III protein requirements for HIV-1 budding. *Cell Host Microbe* **9**, 235-242

32. Scott, A., Chung, H. Y., Gonciarz-Swiatek, M., Hill, G. C., Whitby, F. G., Gaspar, J., Holton, J. M., Viswanathan, R., Ghaffarian, S., Hill, C. P., and Sundquist, W. I. (2005) Structural and mechanistic studies of VPS4 proteins. *EMBO J* **24**, 3658-3669

33. Xiao, J., Xia, H., Yoshino-Koh, K., Zhou, J., and Xu, Z. (2007) Structural characterization of the ATPase reaction cycle of endosomal AAA protein Vps4. *J Mol Biol* **374**, 655-670

34. Gonciarz, M. D., Whitby, F. G., Eckert, D. M., Kieffer, C., Heroux, A., Sundquist, W. I., and Hill, C. P. (2008) Biochemical and structural studies of yeast Vps4 oligomerization. *J Mol Biol* **384**, 878-895

35. Babst, M., Wendland, B., Estepa, E. J., and Emr, S. D. (1998) The Vps4p AAA ATPase regulates membrane association of a Vps protein complex required for normal endosome function. *EMBO J* **17**, 2982-2993

36. Monroe, N., Han, H., Gonciarz, M. D., Eckert, D. M., Karren, M. A., Whitby, F. G., Sundquist, W. I., and Hill, C. P. (2014) The oligomeric state of the active Vps4 AAA ATPase. *J Mol Biol* **426**, 510-525

37. Lottridge, J. M., Flannery, A. R., Vincelli, J. L., and Stevens, T. H. (2006) Vta1p and Vps46p regulate the membrane association and ATPase activity of Vps4p at the yeast multivesicular body. *Proc Natl Acad Sci U S A* **103**, 6202-6207

38. Azmi, I. F., Davies, B. A., Xiao, J., Babst, M., Xu, Z., and Katzmann, D. J. (2008) ESCRT-III family members stimulate Vps4 ATPase activity directly or via Vta1. *Dev Cell* **14**, 50-61

39. Vild, C. J., and Xu, Z. (2014) Vfa1 binds to the N-terminal microtubule-interacting and trafficking (MIT) domain of Vps4 and stimulates its ATPase activity. *J Biol Chem* **289**, 10378-10386

40. Azmi, I., Davies, B., Dimaano, C., Payne, J., Eckert, D., Babst, M., and Katzmann, D. J. (2006) Recycling of ESCRTs by the AAA-ATPase Vps4 is regulated by a conserved VSL region in Vta1. *J Cell Biol* **172**, 705-717

41. Yang, D., and Hurley, J. H. (2010) Structural role of the Vps4-Vta1 interface in ESCRT-III recycling. *Structure* **18**, 976-984

42. Norgan, A. P., Davies, B. A., Azmi, I. F., Schroeder, A. S., Payne, J. A., Lynch, G. M., Xu, Z., and Katzmann, D. J. (2013) Relief of autoinhibition enhances Vta1 activation of Vps4 via the Vps4 stimulatory element. *J Biol Chem* **288**, 26147-26156

43. Merrill, S. A., and Hanson, P. I. (2010) Activation of human VPS4A by ESCRT-III proteins reveals ability of substrates to relieve enzyme autoinhibition. *J Biol Chem* **285**, 35428-35438

44. Nickerson, D. P., West, M., and Odorizzi, G. (2006) Did2 coordinates Vps4-mediated dissociation of ESCRT-III from endosomes. *J Cell Biol* **175**, 715-720

45. Dimaano, C., Jones, C. B., Hanono, A., Curtiss, M., and Babst, M. (2008) Ist1 regulates Vps4 localization and assembly. *Mol Biol Cell* **19**, 465-474

46. Bajorek, M., Morita, E., Skalicky, J. J., Morham, S. G., Babst, M., and Sundquist, W. I. (2009) Biochemical analyses of human IST1 and its function in cytokinesis. *Mol Biol Cell* **20**, 1360-1373

47. Skalicky, J. J., Arii, J., Wenzel, D. M., Stubblefield, W. M., Katsuyama, A., Uter, N. T., Bajorek, M., Myszka, D. G., and Sundquist, W. I. (2012) Interactions of the human LIP5 regulatory protein with endosomal sorting complexes required for transport. *J Biol Chem* **287**, 43910-43926

48. Ward, D. M., Vaughn, M. B., Shiflett, S. L., White, P. L., Pollock, A. L., Hill, J., Schnegelberger, R., Sundquist, W. I., and Kaplan, J. (2005) The role of LIP5 and CHMP5 in multivesicular body formation and HIV-1 budding in mammalian cells. *J Biol Chem* **280**, 10548-10555

49. Yang, Z., Vild, C., Ju, J., Zhang, X., Liu, J., Shen, J., Zhao, B., Lan, W., Gong, F., Liu, M., Cao, C., and Xu, Z. (2012) Structural basis of molecular recognition between ESCRT-III-like protein Vps60 and AAA-ATPase regulator Vta1 in the multivesicular body pathway. *J Biol Chem* **287**, 43899-43908

Chapter 4 Vfa1, a Novel Vps4 regulator, binds to the N-terminal MIT domain of the AAA-ATPase

4.1 Abstract

The endosomal sorting complexes required for transport (ESCRTs) are responsible for multivesicular body (MVB) biogenesis, membrane abscission during cytokinesis, and retroviral budding. They function as transiently-assembled molecular complexes on the membrane and their disassembly requires the action of the AAA-ATPase Vps4. Vps4 is regulated by a multitude of ESCRT and ESCRT-related proteins. Binding of these proteins to Vps4 is often mediated via the microtubule interacting and trafficking (MIT) domain of Vps4. Recently, a new Vps4-binding protein Vfa1 was identified in a yeast genetic screen, where overexpression of Vfa1 caused defects in vacuolar morphology. However, the function of Vfa1 and its role in vacuolar biology were largely unknown. Here, we provide a first detailed biochemical and biophysical study of Vps4-Vfa1 interaction. The MIT domain of Vps4 binds to the C-terminal seventeen residues of Vfa1. This interaction is of high affinity and greatly stimulates the ATPase activity of Vps4. The crystal structure of the Vps4-Vfa1 complex shows that Vfa1 adopts a canonical MIT-interacting Motif 2 (MIM2) structure that has been previously observed in other Vps4-ESCRT interactions. These findings suggest that Vfa1 is a novel positive regulator of Vps4 function.

4.2 Introduction

Controlling and remodeling membrane structure is a vital process for cellular homeostasis. Topologically related events such as multi-vesicular body (MVB) biogenesis, retroviral budding, and abscission between daughter cells during cytokinesis require the action of a class of proteins collectively known as the Endosomal Sorting Complexes Required for Transport (ESCRT)(1-9). The ESCRT proteins are unique in that they deform cellular membranes to generate curvature and bud away from the cytosol(7,10). The molecular mechanisms underlying the function of these proteins are similar but distinct in different cellular processes, and are best studied in the context of MVB biogenesis.

The ESCRT proteins can be grouped into five distinct multi-meric protein complexes, ESCRT-0, -I, -II, -III and Vps4(11). It is believed that they work in a sequential manner to target cell surface receptors into MVB for eventual vacuolar/lysosomal degradation(12). Cargo molecules are first ubiquitinated and endocytosed into early endosome where they are recognized by ESCRT-0(13). Next, ESCRT-I and -II target and concentrate cargo molecules to the site of endosomal membrane deformation and may also directly cause change in membrane curvature (14). To complete the process of budding and vesicle formation, ESCRT-III oligomerizes and forms a filament structure on the endosomal membrane, which ultimately leads to scission of a forming vesicle(15,16). Ubiquitin tags are removed before cargo molecules are included in the vesicle. Finally, the ATPase Vps4 is recruited to the site of vesicle

formation. Through ATP hydrolysis, Vps4 is likely to drive the completion of vesicle formation in an irreversible direction and ultimately provide energy for the entire process(17,18). Biochemically, Vps4 catalyzes the removal of ESCRT-III oligomers from the endosomal membrane(19). This serves two critical functions: first, to provide proper temporal and spatial control of the ESCRT-III oligomerization, thus generating appropriately sized vesicles(20), and second, to recycle components of ESCRT-III to allow for continuous cargo trafficking(21). The role of the ESCRT proteins in MVB biogenesis is evolutionarily conserved in eukaryotic cells(6).

Vps4 is a member of the AAA-ATPase (ATPase Associated with diverse cellular Activities) family. The crystal structure of Vps4 shows that it contains an N-terminal Microtubule Interaction and Trafficking (MIT) domain and a C-terminal AAA-ATPase domain connected by a flexible linker region(22-24). Vps4 exists in two quaternary structures, as a monomer in the absence of ATP binding and as a hexameric ring upon ATP binding(22,25). Oligomerization of Vps4 is mediated through the AAA-ATPase domain with ATP binding sites located at the subunit interface. The hexameric ring structure of Vps4 is a transient species in solution, only stable with ATP bound. Vps4 binds to many proteins in the cell, most of which are mediated through the MIT domain(26). The MIT domain adopts a three-helix bundle structure that serves as a binding partner for the MIT-interaction motifs (MIMs) of ESCRT-III and ESCRT-III related proteins. The MIM was initially defined as a small sequence motif (~15-20 residues) at or near the

C-terminal end of ESCRT-III and ESCRT-III-related proteins(27). There have been speculations that the MIM binds to the ESCRT-III protein core structure in the auto-inhibited state of ESCRT-III. In the active state, it is exposed to the solvent and can be recognized by the MIT domain(28,29). Hence, the MIM serves as a bi-functional switch of ESCRT-III function. Based on the structure and the mode of interaction with the MIT domain, several different types of MIM have been described(30-36). For example, a MIM1 forms a small helix that binds between the second and third helices of the Vps4 MIT domain(30,31). Alternatively, a MIM2 adopts an extended structure that binds between the first and third helices(32). Binding of ESCRT-III to Vps4 can enhance the ATP hydrolysis by Vps4 although the mechanism of action is not clear(37). In addition to ESCRT-III and ESCRT-III-related proteins, there are also other regulators of Vps4 function. Vta1, a positive regulator of Vps4 ATPase, binds to a unique β-domain within the AAA-ATPase domain and presumably activates Vps4 by stabilizing the hexameric ring structure required for ATP hydrolysis(38,39).

A novel Vps4-binding protein, called Vps4 associated-1 (Vfa1), was recently identified in an overexpression study of all putative genes in *Saccharomyces cerevisiae* to look for vacuole morphology defects(40). Overexpression of Vfa1 caused altered vacuole size, indicative of MVB dysfunction. Most interestingly, Vfa1 was found to interact with Vps4. Given the lack of knowledge about Vfa1 and how essential Vps4 regulation is, we used biochemical and biophysical methods to show that Vfa1 binds to the Vps4 MIT

domain. We determined a high-resolution crystal structure of the Vps4 MIT domain in complex with a C-terminal Vps4-binding fragment of Vfa1, and identified residues important for binding. Vfa1 binds to Vps4 with high-affinity (~0.47 μM) and can stimulate Vps4 ATPase activity by more than 10-fold. These results suggest that Vfa1 is a *bona fide* regulator of Vps4 ATPase activity with a possible role in MVB regulation.

4.3 Results

4.3.1 Vfa1 binds to Vps4 in an ATP-independent manner

We first sought to confirm the interaction between Vps4 and Vfa1 as reported by Arlt et al.(40) using Glutathione-S transferase (GST)-pull down analysis. Vps4 has been shown to exist in two oligomeric states, as a monomer and, upon binding ATP, as a hexameric ring(2,24). Many binding partners of Vps4, including ESCRT-III and ESCRT-III-related proteins, show an ATP dependence for Vps4 binding, suggesting that they only bind to the hexameric form of Vps4(22,39). To maintain Vps4 in a stable hexameric structure, we used an ATPase-deficient mutant (E233Q) of Vps4(44). We saw that Vfa1 could bind to Vps4 in both the absence and presence of ATP (Figure 4.1A). We further used size exclusion chromatography to validate the interaction between Vps4 and Vfa1. Different proteins or protein mixtures (Vfa1, Vfa1 with 2 mM ATP, Vps4, Vps4 with 2mM ATP, Vps4 plus Vfa1, and Vps4 plus Vfa1 with 2 mM ATP) were loaded onto a 120ml Superdex-200 column respectively. Compositions of elution peaks were examined by SDS-PAGE gel analysis. Regardless of the presence of ATP, Vfa1 co-eluted with Vps4 at a position that was distinct from Vfa1 alone,

suggesting that it formed a stable complex with Vps4 in solution (Figure 4.1B).

Therefore, Vfa1 can bind to either a monomeric or hexameric form of Vps4.

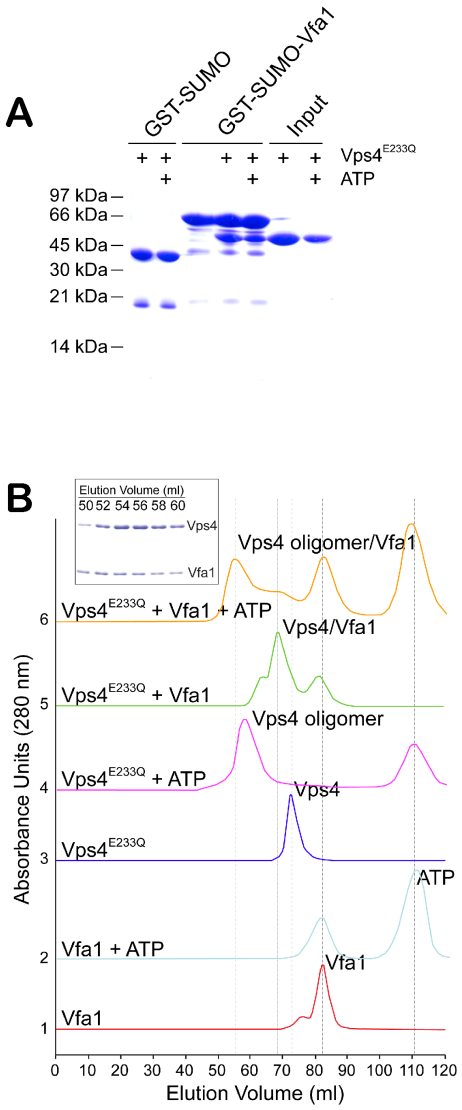

Figure 4.1 Vfa1 binds to Vps4 in an ATP-independent manner
(A) GST-SUMO or GST-SUMO-Vfa1 was used to pulldown Vps4^{E233Q}. GST-SUMO was used as a tag since GST-Vfa1 runs at a position similar to that of Vps4^{E233Q}. Vps4^{E233Q} oligomerizes in the presence of ATP. Binding analyses were performed in the presence or absence of ATP to determine whether Vfa1 binds to Vps4 monomer or oligomer. Proteins retained on the beads were analyzed by SDS-PAGE and visualized by Coomassie staining. (B) Size-Exclusion Chromatography (SEC) was used to compositions of molecular species in the following samples: Vfa1, Vfa1 + 2mM ATP, Vps4^{E233Q}, Vps4^{E233Q} + 2mM ATP, Vfa1 + Vps4^{E233Q}, and Vfa1 + Vps4^{E233Q} + 2mM ATP. Peak fractions were collected, analyzed by SDS-PAGE, and visualized by Coomassie stain.

The inset gel is a representation of the elution profile for the major peak in the Vfa1 + Vps4^{E233Q} + 2mM ATP sample run as described above.

4.3.2 Vps4-Vfa1 interaction is mediated through the N-terminal MIT domain of Vps4

We next identified the minimal binding domains between the two proteins. Vps4 contains an N-terminal Microtubule Interacting and Trafficking (MIT) domain and a C-terminal canonical AAA-ATPase domain. Since most of the ESCRT-III and ESCRT-III-related proteins bind to the MIT domain, we reasoned that it might also be the site of binding for Vfa1. Indeed, deletion of the MIT domain (Vps4-ΔMIT) abolished the interaction between Vps4 and Vfa1. This was reminiscent of the interaction between Vps4 and Ist1, an ESCRT-III-related Vps4 regulator that binds to Vps4 via the MIT domain in an ATP-independent manner(45), but different from another regulator Vta1 which binds to Vps4 in an ATP-dependent manner via the β-domain within the ATPase domain (Figure 4.2A). ESCRT-III proteins bind to the MIT domain via C-terminal sequence motifs, known as the MIT-interacting motifs (MIMs)(46). Secondary structure prediction showed that Vfa1 was largely an α-helical protein with a C-terminal helix suggestive of a potential site for MIT interaction (data not shown). We therefore made a truncation mutant of Vfa1 (Vfa1$^{1-186}$) with the C-terminal 17 residues deleted and tested whether it could still bind to Vps4. Removal of the C-terminal sequence abolished its interaction with Vps4 (Figure 4.2B). These results show that Vps4-Vfa1 binding is mediated through the N-terminal MIT domain of Vps4.

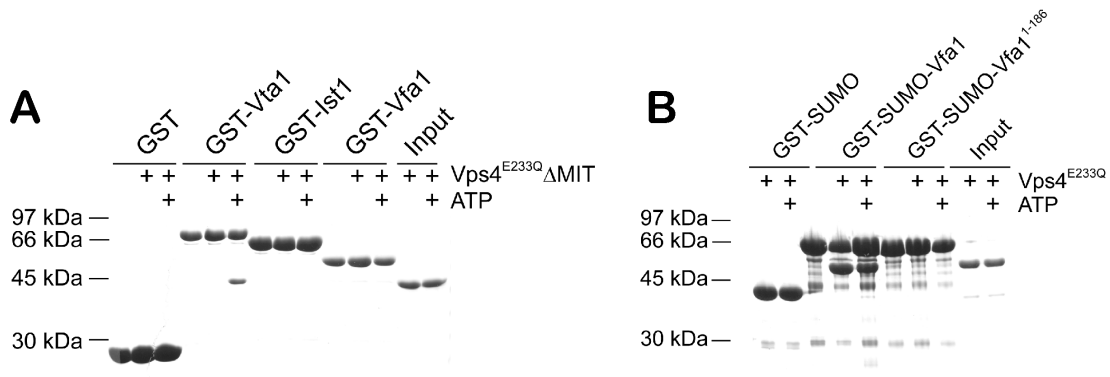

Figure 4.2 Mapping the binding interface between Vps4 and Vfa1
(A) The Vps4 MIT domain is necessary for Vfa1 binding. GST, GST-Vta1, GST-Ist1 and GST-Vfa1 were used to analyze their interactions with Vps4^{E233Q}ΔMIT (residues 83-437) in the presence or absence of ATP. Vta1 known to only bind to the oligomeric form of Vps4. Ist1 is an ESCRT-III related protein that binds to the Vps4 MIT domain. (B) The C-terminal sequence of Vfa1 is necessary for Vps4 binding. GST-SUMO, GST-SUMO-Vfa1, or GST-SUMO-Vfa1$^{1-186}$ was used to analyze their interactions with Vps4^{E233Q} in the presence or absence of ATP.

4.3.3 Binding of Vfa1 stimulates the ATPase activity of Vps4

When ESCRT-III and ESCRT-III-related proteins bind to Vps4, they often stimulate the ATPase activity of Vps4(37,47). To determine whether this was the case for Vfa1, we used the Malachite Green ATPase assay(41) to examine how Vfa1 might affect the ATPase activity of Vps4 (Figure 4.3). As a control, the addition of Bovine Serum Albumin (BSA) did not stimulate the ATPase activity of Vps4. Vta1, a known positive regulator of Vps4, was able to increase the rate of Vps4 ATP hydrolysis by three-fold when added in a 1:2 ratio. In comparison, addition of Vfa1 in a similar ratio increased the Vps4 ATPase activity by an approximate 10-fold as compared to the intrinsic activity of Vps4 even though Vfa1 itself had no ATPase activity. Vfa1 therefore appeared to be a much more potent activator of Vps4 than Vta1. To examine whether this stimulation was

dependent on the site of interaction we identified, we also included Vfa1$^{1-186}$ in the Vps4 ATPase assay. No stimulation was seen upon the addition of Vfa1$^{1-186}$ demonstrating that stimulation by Vfa1 requires the specific interaction between Vps4 and Vfa1.

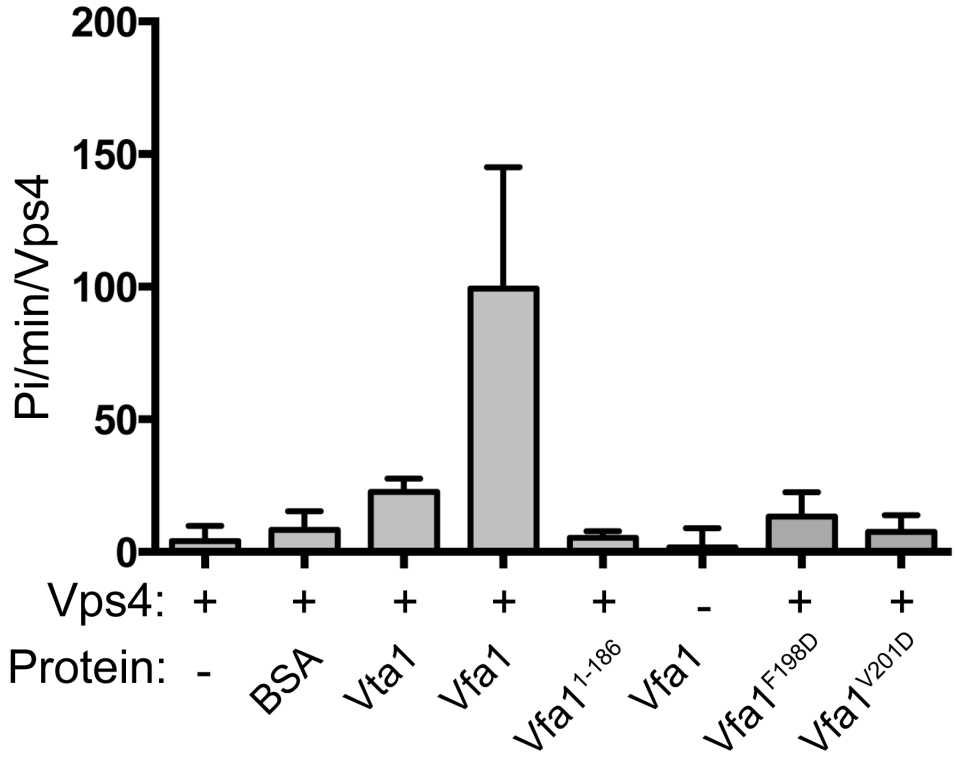

Figure 4.3 Vfa1 stimulates Vps4 activity.
ATP hydrolysis by 0.125 μM Vps4 (intrinsic, first column) was assayed under conditions of 1mM ATP at 37°C (see Experimental procedures). To observe stimulation of Vps4 activity, the following proteins (0.25 μM) were incubated with Vps4: Bovine Serum Albumin (second column), Vta1 (third column), Vfa1 (fourth column), Vfa1$^{1-186}$ (fifth column), Vfa1^{F198D} (seventh column), and Vfa1^{V201D} (eighth column). Each experiment was done in triplicate; all experiments were repeated a minimum of three times. Intrinsic ATPase activity for Vfa1 (0.25 μM) is shown in the sixth column.

4.3.4 Crystal structure of Vps4 MIT and Vfa1 MIM

To understand the structural nature of the Vps4-Vfa1 interaction, we determined the crystal structure of the Vps4-Vfa1 complex using the Vps4 MIT domain (residues 1-82) and a C-terminal fragment of Vfa1 that encompasses the

necessary Vps4-binding sequence (residues 183-203). The structure was determined by molecular replacement using the yeast Vps4 MIT domain structure as a search model(31) and refined to 2.3Å resolution (Table 4.1). The refined structure has an R-factor/R_{free} of 23.6%/25.7% with excellent parameters for stereochemistry. There are two molecular complexes of Vps4-Vfa1 in the asymmetric unit. The r.m.s deviations for Cα positions between the two complexes are 0.039 Å and 0.672 Å for Vps4 and Vfa1, respectively. The average buried surface area at the interface of Vps4 and Vfa1 is approximately 900 Å².

Table 4.1 Crystallographic data statstics

Data Collection	
Space group	$P2_12_12_1$
Unit cell parameters:	
a, b, c (Å)	38.5, 56.7, 84.2
Molecules per asymmetric unit	2
Wavelength (Å)	0.9998
Resolution (Å)	2.3
Unique reflections[1]	8662 (840)
Redundancy	7.1 (7.3)
Completeness (%)	99.9 (100.0)
Average I/σ (I)	34.6 (7.3)
R_{merge}	0.04 (0.34)
Refinement	
Resolution range (Å)	35.00-2.30
R_{work} (%)	23.6
R_{free} (%)	25.7
RMS deviations	
Bond lengths (Å)	0.011
Bond angles (°)	1.40
B-factor average (A^2)	43.1
Ramachandran Plot Regions	
Most favored (%)	95.9
Allowed (%)	4.1
Outliers (%)	0.0
PDB ID code	4NIQ

[1]Values in parentheses are for the specified high-resolution bin.

As shown in Figure 4.4A, the Vps4 MIT domain adopts a three-helix bundle fold (H1-H3). Binding of Vfa1 to Vps4 does not change the overall structure of the domain. The r.m.s deviations for Cα positions between the Vps4 MIT domain structure in the Vfa1 complex and other previously reported Vps4 MIT domain structures are in the range of 0.6-0.7 Å. The Vps4-binding sequence of Vfa1 can be divided into three regions: an N-terminal extended region (residues 183-188), a short 2-turn α-helix in the middle (residues 189-196) and a C-terminal extended region (residues 197-203). Interactions between Vps4 and Vfa1 are mediated through all three regions. The N-terminal extended region binds to the turn between the second and third helices of the MIT domain, while the middle helix and the C-terminal extended region binds predominantly between the first and third helices of the MIT domain.

4.3.5 Molecular interactions between the C-terminal extended region of Vfa1 fragment and Vps4

Vps4 presents a hydrophobic binding pocket between the first and third helices. As shown in Figure 4.4B, this hydrophobic pocket includes side chains from residues Leu7, Ile11, Val14, Ile18 (helix one) and Leu55, Ile56, and Tyr63 (helix three). In addition, the aliphatic portions of side chains from residues Lys59 and Arg66 also contribute to the pocket hydrophobicity, which allows for discrete interactions with the following Vfa1 residues: Leu192, Leu193, His196, Phe198, Pro199, Val201, and Pro202 (Figure 4.4B). A number of specific hydrogen bond interactions are also present at the interface. For example, the side chain of Vfa1 residue His196 forms a hydrogen bond with the main chain carbonyl oxygen of

Vps4 residue Gly4. A complete list of molecular interactions observed at the interface is tabulated in Table 4.2.

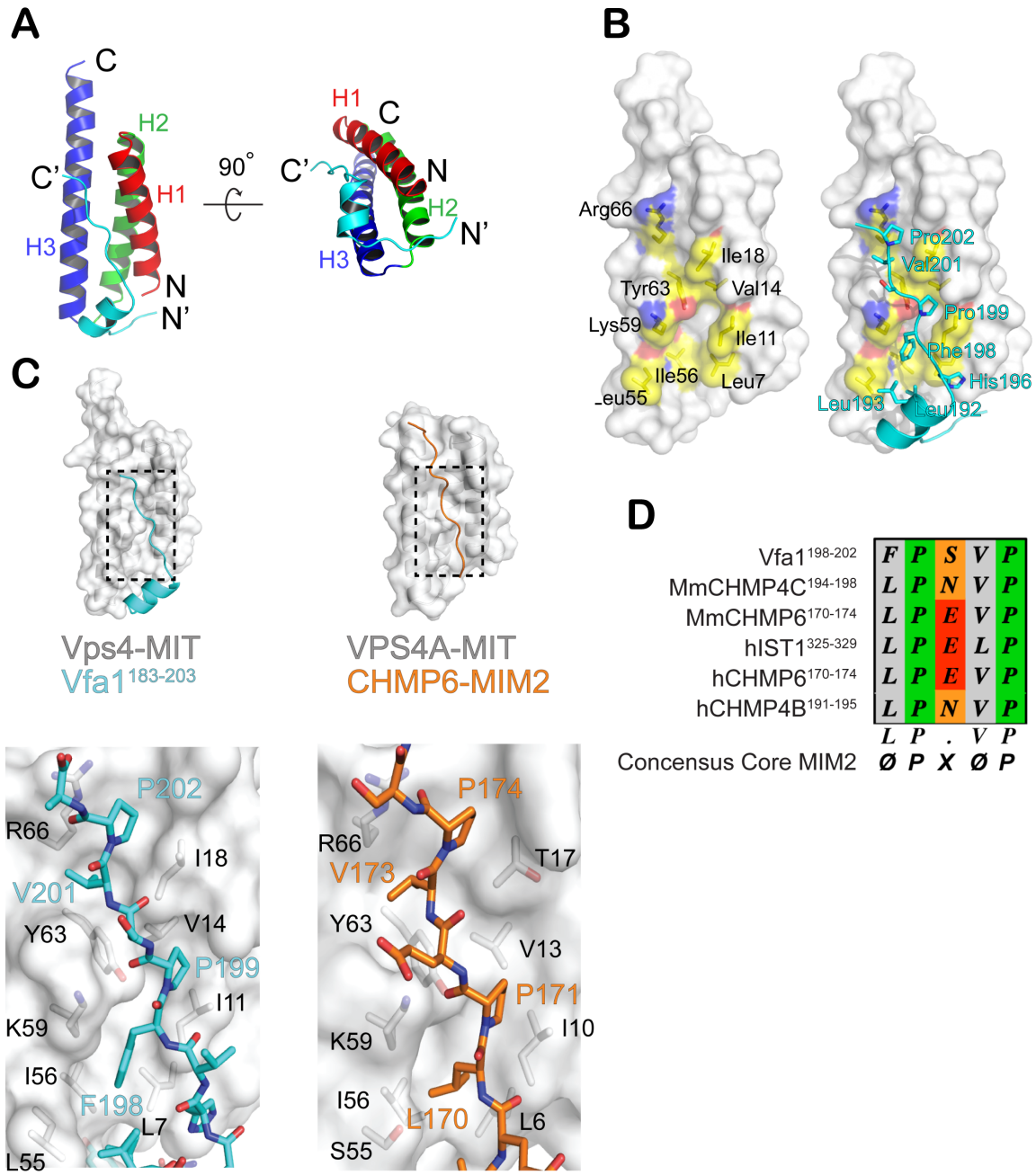

Figure 4.4 The crystal structure of the Vps4-Vfa1 complex.
(A) An overview of the Vps4-Vfa1 complex structure. Ribbon representation of Vfa1 (residues 183-203) in complex with Vps4 (1-82) in two orthogonal views. Vfa1 is colored in cyan, and the three helixes of the Vps4 MIT domain are colored red, green and blue, respectively. The N- and C- termini of the two proteins are labeled. (B) The C-terminal extended region of Vfa1 binds in a

hydrophobic pocket formed by helices 1 and 3 of the Vps4 MIT domain. Left panel is a surface representation of the Vps4 MIT domain and the Vfa1 binding pocket is selectively colored based on the underlying atoms: carbon, yellow; oxygen, red; and nitrogen, blue. Residues that contribute to binding are labeled in black. Right panel is the same surface representation with Vfa1 showing in cyan. Critical hydrophobic residues utilized by Vfa1 for binding Vps4 are labeled in cyan. (C) The C-terminal extended region of Vfa1 binds like a "MIM2". Top panels show ribbon and surface representations of the Vps4-Vfa1 complex and the hVPS4A-CHMP6 complex (PDB: 2K3W). Bottom panels show zoom-in views of the interactions within the two complex structures. Critical residues from the MITs are labeled in black. Residues that make close contacts from the MIM2s are in cyan for Vfa1 and orange for CHMP6. (D) Sequence alignment of various MIM2s.

Table 4.2 Detailed interactions between Vps4 and Vfa1

Vps4	Vfa1
Hydrogen bond interactions	
G4 O	H196 OE2
Y46 O	S185 N
E47 OE1	T187 OG1
E47 OE2	T187 N
K48 N	S185 O
N49 ND2	T187 O
N49 ND2	D188 OD1
S52 OG	T187 O
E62 OE2	V201 N
Y63 OH	P199 O
Van der Waals interactions	
L7	L192, H196, F198
I11	F198, P199
V14	P199
I18	P199, V201, P202
L40	F198
K51	P189
L55	P189, L192, L194, F199
I56	L192, F198
K59	F198
Y63	F198, P199, V201
R66	V201, P202

The interaction between Vps4 and the C-terminal extended region of the Vfa1 fragment is of particular interest. It is reminiscent of the MIT-MIM interaction as seen in the structure of human VPS4A and CHMP6, the human homolog of

Vps20 (a core ESCRT-III protein)(32). The MIM involved in this type of interaction has been termed as MIM2. In both the Vps4-Vfa1 and the VPS4A-CHMP6 complexes, the MIT domains adopt similar structures. When the conformations of the bound peptides in the two complexes are compared, it is clear that the C-terminal extended region of Vfa1 fragment adopts a conformation similar to that of the CHMP6 MIM2 (Figure 4.4C). Moreover, both peptides utilize hydrophobic residues including two signature prolines within their sequences to bind to Vps4. Specifically, CHMP6 MIM2 residues (Leu170, Pro171, Val173 and Pro174) fit into the hydrophobic pocket within the helical groove between helices one and three in a nearly identical fashion as the Vfa1 fragment.

Previous studies defined MIM2 as a MIT-binding motif that contains a conserved LP(E/D)VP sequence(32). In the Vps4-Vfa1 structure, Vfa1 utilizes a slight different $_{198}$FPSVP$_{202}$ sequence at the core of the binding interface. By aligning the MIT-binding motif of Vfa1 with other MIM2 sequences, we arrived at a more general ΦPXΦP motif (where Φ represents a hydrophobic residue) that is required for a peptide sequence to bind as a MIM2 (Figure 4.4D). Based on the structure shown here, the hydrophobic residues from the Vfa1 “MIM2” make contact with the hydrophobic pocket presented by the Vps4 MIT domain helices one and three. The variable residue X tends to be polar and always seems to point into solvent in different structures.

4.3.6 Additional interaction between Vfa1 MIM and Vps4

While the MIT-MIM2 interactions are similar in the two complex structures, CHMP6 does not contain sequence N-terminal to the MIM2 that makes additional contacts with VPS4A MIT. In Vfa1, these contacts include the N-terminal extended region and the middle helix. The middle helix is amphipathic and binds to the hydrophobic pocket formed by the first and third helices of the MIT domain via Pro189, Leu192 and Leu193 as described above (Figure 4.5). Interactions between the N-terminal extended region and Vps4 are largely polar. Vfa1 forms several hydrogen bond interactions with the backbone atoms from the turn between the second and third helices of the Vps4 MIT domain (Figure 4.5). Specifically, Vfa1 residues 185-186 and Vps4 residues 46-48 form parallel β-sheet like main chain hydrogen bonds. The side chain of Vps4 Glu47 forms bidentate hydrogen bonds with the side chain and the main chain atoms of Vfa1 Thr187. The amide nitrogen of Vps4 Asn49 side chain forms bifurcated hydrogen bonds with the main chain carbonyl oxygen atom of Vfa1 Thr187 and the side chain carboxyl oxygen atom of Vfa1 Asp188.

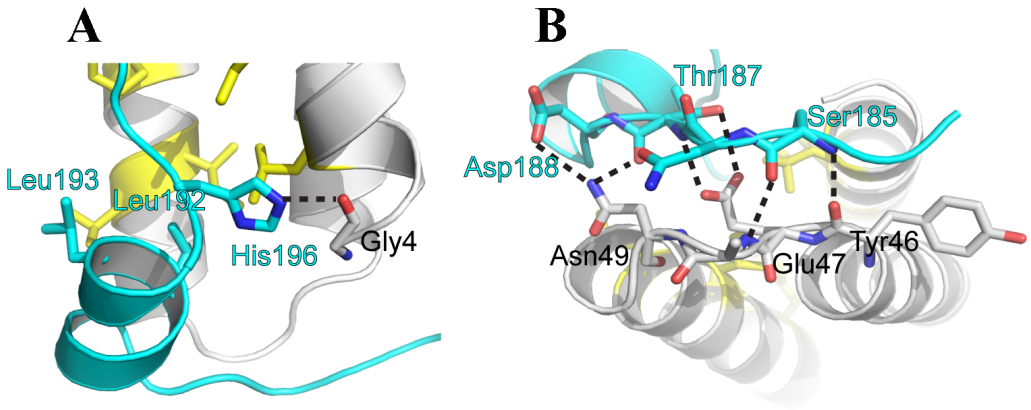

Figure 4.5 Additional interactions between Vps4 and Vfa1

Cartoon representation of Vfa1 (cyan) making contacts with Vps4 (grey) beyond the “MIM2” sequence. (A) Interactions involving the middle helix; (B) Interactions involving the N-terminal extended region. Residues that make distinct contacts are shown as stick models and labeled in cyan for Vfa1, black for Vps4. Hydrogen bonds are denoted as dashed lines.

4.3.7 Functional relevance of Vps4-Vfa1 interaction

We used site-directed mutagenesis and GST-pull down analysis to evaluate the contribution of interface residues to the overall stability of the complex. Interactions between Vps4 and MIM2-containing ESCRT-III proteins have been previously shown to be disrupted by mutation of Ile18, a residue located at the hydrophobic pocket formed by helices one and three of the Vps4 MIT domain(48). Since Ile18 is also located at the Vps4-Vfa1 interface, we reasoned that this mutant should also prevent Vfa1 from binding. Indeed, I18D failed to bind to GST-Vfa1 in our GST pull-down analysis, suggesting that Ile18 is essential for high-affinity binding interaction (Figure 4.6A). In contrast, mutation of Leu64 of Vps4, a residue important for interactions between Vps4 and MIM1-containing ESCRT-III proteins(30), had no effect on Vfa1 binding (Figure 4.6A). Moreover, Vfa1 mutants F198D and V201D also failed to bind to Vps4. As mentioned above, Phe198 and Val201 are part of the MIM2 sequence. Collectively, these results confirm the importance of Vfa1 MIM2 sequence to the overall stability of the complex.

Using Isothermal Titration Calorimetry (ITC), we measured the binding affinity between the Vps4 MIT domain and Vfa1. The MIM2-type MIT-MIM interaction has been previously characterized to have a low micromolarity dissociation constant (K_D ~5-10 μM)(32). Here, we saw that full-length Vfa1

bound to the Vps4 MIT domain with a significantly higher affinity (K_D = 0.47 μM ± 0.12) (Figure 4.6B). This is approximately 10-fold higher in affinity as compared to the CHMP6-hVPS4A interaction. This increase in affinity may have been due to the additional contacts between Vps4 and Vfa1 beyond the interaction that involves the C-terminal MIM2 sequence, which are not available in CHMP6. The contribution of Vfa1 sequence beyond MIM2 to the overall binding affinity of the complex was corroborated by the observation that Vps4 mutant E47A/N49A had a significantly decreased affinity for Vfa1 based on GST-pull down analysis (Figure 4.6C).

To further study the functional relevance of Vps4-Vfa1 interaction, we examined how point mutations within the Vps4-Vfa1 binding interface might affect the ability of Vfa1 to stimulate Vps4 ATPase activity. Two Vfa1 mutants F198D and V201D, which had drastically reduced affinities for Vps4 by both GST-pull down analysis and ITC, were unable to stimulate the ATPase activity of Vps4 (Figure 4.3). This again suggests that the specific interaction between Vfa1 and Vps4 is important for its role as a potential positive regulator of Vps4.

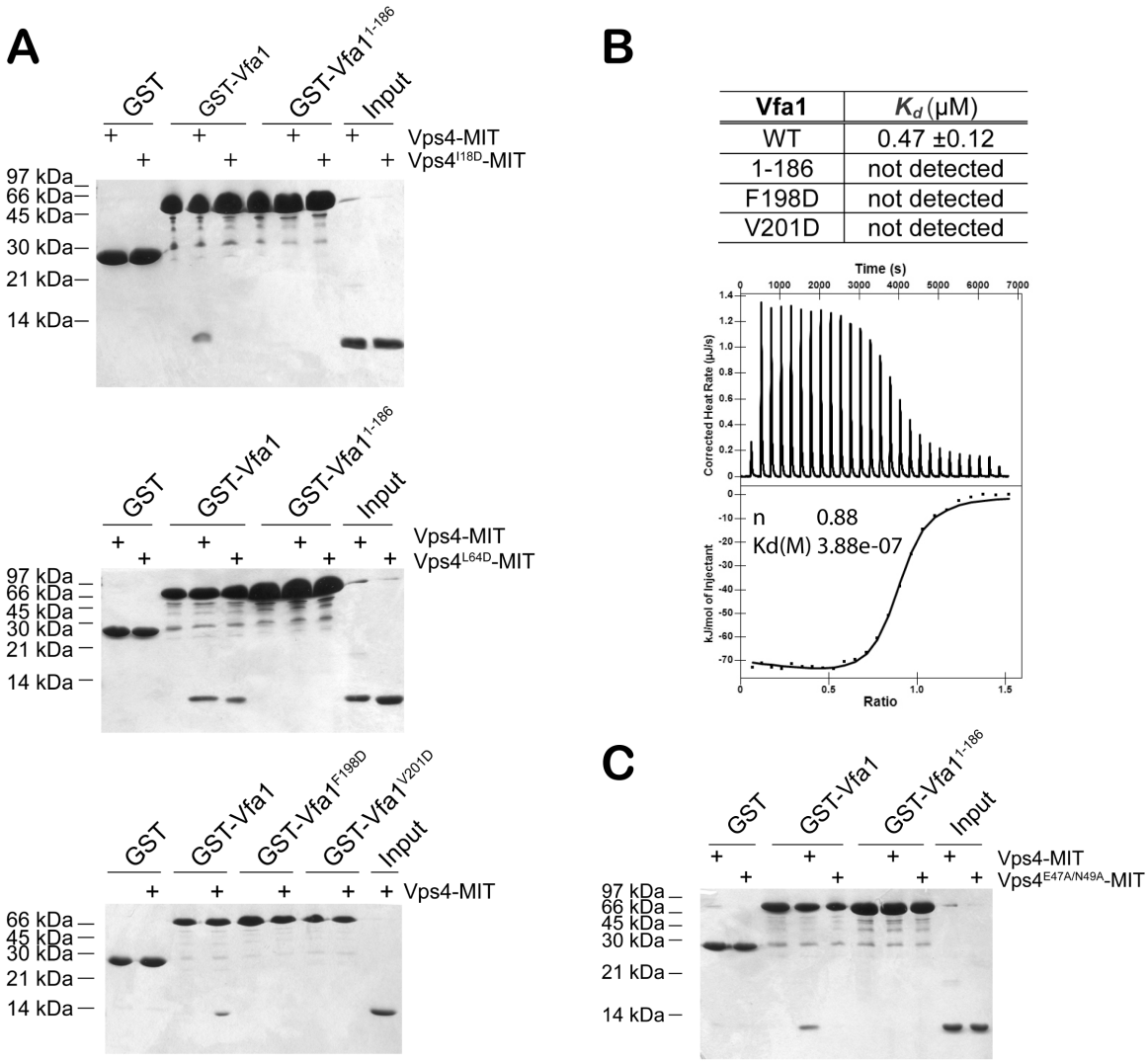

Figure 4.6 Critcal residues at the Vps4-Vfa1 binding interface
(A) Vfa1 binds in the first and third helical groove of Vps4 MIT as a "MIM2". Top panel, GST, GST-Vfa1, and GST-Vfa1$^{1-186}$ were used to analyze their respective interactions with Vps4-MIT and Vps4^{I18D}-MIT. Middle panel, GST, GST-Vfa1, and GST-Vfa1$^{1-186}$ were used to analyze their respective interactions with Vps4-MIT and Vps4^{L64D}-MIT. Bottom panel, GST, GST-Vfa1, GST-Vfa1^{F198D}, and GST-Vfa1^{V201D} were used to analyze their respective interactions with Vps4-MIT. (B) Binding affinities of Vps4-MIT to wild-type and mutant Vfa1 as determined by isothermal titration calorimetry (ITC) assay. A representative ITC enthalpy plot for the binding of Vps4-MIT to wild-type Vfa1 is also shown. (C) Region outside Vfa1 MIM2 contributes to Vps4 binding. GST, GST-Vfa1, and GST-Vfa1$^{1-186}$ were used to analyze their respective interactions with Vps4-MIT and Vps4$^{E47A/N49A}$-MIT.

4.4 Discussion

Oligomerization of ESCRT-III proteins on the endosomal membrane is a critical step in generating intra-luminal vesicles during MVB biogenesis. This step is terminated by the removal of ESCRT-III proteins from the membrane through the action of the AAA-ATPase Vps4. Activity of Vps4 is tightly regulated in the cell by a multitude of proteins that specifically bind to Vps4. A newly identified protein, Vfa1, which causes defects in vacuolar morphology upon overexpression in yeast, has been previously shown to bind to Vps4. In order to understand the molecular mechanism of Vfa1 function, we embarked on a detailed structural study of the interaction between Vps4 and Vfa1. We have confirmed that Vfa1 binds to Vps4 in an ATP-independent manner(40). In addition, the crystal structure of Vps4-Vfa1 complex reveals that Vfa1 binds to the N-terminal MIT domain of Vps4, utilizing a conserved ΦPXΦP binding motif (MIM2) that is shared among some ESCRT-III and ESCRT-III-related proteins. Moreover, binding of Vfa1 to Vps4 significantly stimulates the ATP hydrolysis activity of Vps4. These data strongly suggest that Vfa1 is a positive regulator of Vps4 in the MVB pathway.

4.4.1 Vfa1 binds to the Vps4 MIT domain using a canonical MIM2

The MIT domain is a protein-protein interaction domain mostly found in proteins involved in membrane trafficking (Vps4, AMSH, UBPY, Vta1, Spastin and Spartin)(26,49). Protein sequence motifs that specifically bind to the MIT domain are collectively termed as MIMs. They are often found at the C-terminal ends of ESCRT-III and ESCRT-III-related proteins and can bind to the MIT

domain in a variety of manners, utilizing different binding surfaces on the MIT domain. The MIT domain of Vps4 contains two MIM-binding surfaces. In the crystal structure of Vps4-Vps2 complex, the Vps2 C-terminal sequence forms a small helix that binds between helices two and three of the Vps4 MIT domain(31). In the solution structure of hVPS4A-CHMP6 complex, the C-terminal sequence of CHMP6 adopts an extended conformation and binds between helices one and three of the hVPS4A MIT(32). These two structures help define that any MIM that binds in a similar fashion (same orientation, with conserved binding interactions) would be a MIM1 (between helix 2/3) or a MIM2 (between helix 1/3). The complexity in binding illustrates the mechanism by which MIT domains discriminate specific binding partners. In the current work, we show that the C-terminal sequence of Vfa1 binds to the Vps4 MIT domain in a manner similar to that of CHMP6. Therefore, the structure should be classified as a MIM2. This finding strongly suggests that Vfa1 plays a role related to the function of Vps4 in the MVB pathway.

Beyond the MIM2 sequence, the molecular interfaces within the hVPS4A-CHMP6 complex and the Vps4-Vfa1 complex are significantly different. hVPS4A makes additional interactions with CHMP6 residues C-terminal to the MIM2. These interactions do not exist in Vfa1, as its MIM2 sequence is located at the very C-terminal end. For Vfa1, the sequence N-terminal to the ΦPXΦP motif makes additional contacts with Vps4 in the form of a short helix and an extended loop. As shown by mutagenesis and GST-pull down analysis, these interactions

do contribute to the overall stability of the complex. The CHMP6 fragment used in the structural study does not include additional sequence N-terminal to the MIM2. It is possible that the small helix seen in the Vfa1 structure may also exist in CHMP6 if more residues were included in the structural study. Indeed, secondary structure prediction of CHMP6 indicated the possibility of a small helix upstream of the MIM2 sequence. Nevertheless, the binding mechanism beyond the canonical MIT-MIM2 interface is likely to be distinct between the two complex structures. These differences suggest that interactions outside the consensus MIM2 sequence may provide a mechanism for MIT domains to distinguish among their various binding partners. Hence, regulation of Vps4 (and other ESCRT proteins) via MIT-MIM interaction can be more finely tuned than previously thought. More MIT-MIM complex structures will be needed to properly decipher the MIT-MIM 'binding code.'

4.4.2 Regulation of Vps4 by Vfa1

As previously noted, overexpression of Vfa1 in yeast cells leads to an alteration in vacuolar morphology(40). Since Vfa1 can bind to Vps4 in both *in vivo* and *in vitro* assays(40), these data seem to suggest that Vfa1 has an inhibitory role in Vps4 regulation. We have now shown that Vfa1 binds to the Vps4 MIT domain and contains a MIM2 sequence that has been previously identified in some ESCRT-III proteins. Binding of Vfa1 to Vps4 is ATP-independent and can greatly stimulate the ATPase activity of Vps4. Therefore, our biochemical and biophysical analysis instead suggest a positive regulatory role for Vfa1.

How does one reconcile the difference between the biochemical and biological data? The binding affinity of Vfa1 to Vps4 is about 10-20 fold higher than those of core ESCRT-III MIM2s to Vps4(32). While in cytosol, Vfa1 can form a complex with Vps4, which may stabilize the Vps4 oligomer, and is then recruited to the endosomal membrane. Due to an avidity effect of the ESCRT-III oligomer, while individually having a weaker affinity for Vps4 than Vfa1, the ESCRT-III oligomer can displace Vfa1 from Vps4 to allow for ESCRT-III disassembly. In a Vfa1 overexpression system, however, Vfa1 would outcompete the ESCRT-III proteins and block their binding to Vps4, thus preventing the proper function of Vps4.

Deletion of Vfa1 in yeast has no observable phenotype on vacuolar morphology. It is possible that other ESCRT-III-related proteins may have overlapping function with Vfa1. Vfa1 does not seem to be essential for ESCRT-III filament disassembly, but more likely plays a role in the temporal and spatial control of Vps4 function. Many known regulators of Vps4 have weak or no phenotype in their respective deletion strains (Vta1, Vps60, Did2, Ist1)(50). It is only when two or more of these genes are deleted do we see a synthetic phenotype of vacuolar morphology(47,51). Moreover, EM tomography has often revealed more subtle effects on MVB biogenesis in a single gene deletion strain of these proteins(20). Taken together, the lack of a distinct phenotype on vacuolar morphology suggests that Vfa1 acts at a similar level as other

regulators of Vps4. It will be interesting to see whether a synthetic phenotype exists when Vfa1 is deleted in conjunction with other ESCRT-III-related proteins. Yeast-two hybrid analysis showed that Vfa1 could bind to Vta1 and preliminary biochemical characterization suggested that other ESCRT-III and ESCRT-III-related proteins may also bind to Vfa1((52), data not shown). How Vfa1 works together with other ESCRT proteins to regulate Vps4 is a critical next step in understanding ESCRT function.

4.5 Methods

4.5.1 Cloning, Expression, and Purification

DNA fragments encoding Vfa1 and Vps4, and their various fragment constructs were amplified from the *S. cerevisiae* genomic DNA. These proteins were expressed in *E. coli* Rosetta(DE3) cells using a modified pET28b vector with a SUMO protein tag inserted between a His_6-tag and the respective protein coding region. The His_6-SUMO-tagged protein was purified by Ni^{+2}-NTA affinity chromatography following standard procedures. ULP1 protease was then added to remove the His_6-SUMO tag, and the digested protein mixture was passed over a second Ni^{+2}-NTA column. Proteins were further purified by ion exchange chromatography on a Source-S column (GE Healthcare) for Vfa1 proteins and a Source-Q column (GE Healthcare) for Vps4 proteins. The Vps4-Vfa1 complex was purified by mixing the two protein fragments in stoichiometric amounts followed by gel filtration chromatography using a HiLoad™ Superdex™ 200 (GE Healthcare) column.

4.5.2 GST pull-down Analysis

GST pull-down analysis was performed following standard procedures in Phosphate-buffered Saline (PBS) solution supplemented with 1mM DTT and 0.1% (v/v) Tween-20(22). Specific samples were also supplemented with 2mM ATP as indicated. Purified proteins were incubated with either GST alone or GST-tagged proteins immobilized on glutathione agarose beads for 1 hr at 4°C. The beads were then washed extensively with the buffer before bound proteins were analyzed on SDS-PAGE and visualized by Coomassie staining.

4.5.3 Isothermal Titration Calorimetry

To measure the binding affinity between Vfa1 and the Vps4 MIT domain (residues 1-82), Vfa1 or Vfa1 mutants were titrated against the Vps4 MIT domain using a Nano ITC^{TM} (TA instruments) or an ITC-200 microcalorimeter (GE Healthcare) at 25 °C. Data were processed using the NanoAnalyze software. All proteins were dialyzed against a buffer containing 50 mM HEPES (pH 7.5) and 50 mM NaCl, centrifuged to remove any particulates, and degassed before binding analysis. Vfa1 proteins were injected at 0.23 mM (or greater for mutants) against 0.06 mM Vps4 MIT domain. The concentrations of all proteins were determined using UV spectral analysis.

4.5.4 Malachite Green ATPase Assay

The procedure was adopted from previous studies with modifications as indicated(41). The reaction buffer used included 100 mM Tris–HCl (pH 7.4), 20mM KCl, 6mM $MgCl_2$. Malachite green reagent was prepared as follows: malachite green (0.081% w/v), polyvinyl alcohol (2.3% w/v), ammonium

heptamolybdate tetrahydrate (5.7% w/v in 6 M HCl) and double distilled water were mixed at a 2:1:1:2 ratio, then stored at 4°C for at least 30 min. For Vps4 stimulation experiments, a 15 µL protein mixture of 0.125 µM Vps4 and 0.25 uM of Vfa1, Vfa1 mutant, or Vta1 was incubated with 10 µL of 1.2 mM ATP (all final concentrations) at 37°C for 10 minutes in a 96-well plate. Protein concentrations were selected in order to see the stimulation of Vps4 hydrolysis and to avoid product inhibition. After the 10-minute incubation, 80 µL of malachite green reagent was added to each well. Immediately following this step, 10 µL 32% sodium citrate was used to inhibit the non-enzymatic hydrolysis of ATP. The samples were mixed thoroughly and incubated at 37 °C for 15 min before OD_{620} was measured on a SpectraMax M5 (Molecular Devices, Sunnyvale, CA). To account for intrinsic hydrolysis, the signal from ATP in identically treated buffer lacking Vps4 was subtracted.

4.5.5 Structural Study

Vps4-Vfa1 complex crystals were grown using the sitting drop vapor diffusion method at 25°C. The protein complex (17 mg/mL) was mixed in a 1:1 ratio with a reservoir solution of 26% (w/v) polyethylene glycol 4000, 10% (v/v) isopropanol and 0.1M HEPES, pH 6.5 in a final volume of 4 µL and equilibrated against 1 mL of reservoir solution. Clusters of sword-shaped crystals appeared after one day, and grew to full size after three days. Single crystals were isolated from the clusters and cryo-protected using the reservoir solution.

Diffraction data were collected at the Advanced Photon Source Beamline 21-ID-D. The Vps4-Vfa1 complex crystal diffracted to 2.3 Å. It belongs to the

space group of $P2_12_12_1$ and contains two molecular complexes in the asymmetric unit. Data were indexed, integrated and scaled using HKL2000 (HKL Research). PHENIX software suite was used for structure determination and refinement. The structure was solved by molecular replacement as implemented in the AutoMR module(42), using the Vps4 MIT domain (PDB accession code 2V6X) as an initial search model. Non-crystallographic symmetry restraint was applied throughout refinement. Model building was done with COOT(43).

4.6 Acknowledgements

We thank the staff at the Advanced Photon Source Sector 21 (21-ID-D) for access and help with data collection. Use of the Advanced Photon Source, an Office of Science User Facility operated for the U.S. Department of Energy (DOE) Office of Science by Argonne National Laboratory, was supported by the U.S. DOE under Contract No. DE-AC02-06CH11357. Use of the LS-CAT Sector 21 was supported by the Michigan Economic Development Corporation and the Michigan Technology Tri-Corridor (Grant 085P1000817). We thank J. Rauch and J. Gestwicki for assistance with Malachite Green ATP assays and K. Chinnaswamy and B. Wan for access and help for ITC experiments. We thank D. Gawron for help with data collection. This work was supported by an NIH grant (GM095769) to Z. Xu.

4.7 References

1. Hanson, P. I., and Cashikar, A. (2012) Multivesicular body morphogenesis. *Annu Rev Cell Dev Biol* **28**, 337-362

2. McCullough, J., Colf, L. A., and Sundquist, W. I. (2013) Membrane Fission Reactions of the Mammalian ESCRT Pathway. *Annu Rev Biochem* **82**, 663-692

3. Hurley, J. H., and Emr, S. D. (2006) The ESCRT complexes: structure and mechanism of a membrane-trafficking network. *Annu Rev Biophys Biomol Struct* **35**, 277-298

4. Henne, W. M., Buchkovich, N. J., and Emr, S. D. (2011) The ESCRT pathway. *Dev Cell* **21**, 77-91

5. Piper, R. C., and Katzmann, D. J. (2007) Biogenesis and function of multivesicular bodies. *Annu Rev Cell Dev Biol* **23**, 519-547

6. Winter, V., and Hauser, M. T. (2006) Exploring the ESCRTing machinery in eukaryotes. *Trends Plant Sci* **11**, 115-123

7. Gruenberg, J., and Stenmark, H. (2004) The biogenesis of multivesicular endosomes. *Nat Rev Mol Cell Biol* **5**, 317-323

8. Hurley, J. H., and Hanson, P. I. (2010) Membrane budding and scission by the ESCRT machinery: it's all in the neck. *Nat Rev Mol Cell Biol* **11**, 556-566

9. Hill, C. P., and Babst, M. (2012) Structure and function of the membrane deformation AAA ATPase Vps4. *Biochim Biophys Acta* **1823**, 172-181

10. Carlton, J. G., and Martin-Serrano, J. (2007) Parallels between cytokinesis and retroviral budding: a role for the ESCRT machinery. *Science* **316**, 1908-1912

11. Williams, R. L., and Urbe, S. (2007) The emerging shape of the ESCRT machinery. *Nat Rev Mol Cell Biol* **8**, 355-368

12. Teis, D., Saksena, S., and Emr, S. D. (2008) Ordered assembly of the ESCRT-III complex on endosomes is required to sequester cargo during MVB formation. *Dev Cell* **15**, 578-589

13. Bilodeau, P. S., Urbanowski, J. L., Winistorfer, S. C., and Piper, R. C. (2002) The Vps27p Hse1p complex binds ubiquitin and mediates endosomal protein sorting. *Nat Cell Biol* **4**, 534-539

14. Wollert, T., and Hurley, J. H. (2010) Molecular mechanism of multivesicular body biogenesis by ESCRT complexes. *Nature* **464**, 864-869

15. Elia, N., Fabrikant, G., Kozlov, M. M., and Lippincott-Schwartz, J. (2012) Computational model of cytokinetic abscission driven by ESCRT-III polymerization and remodeling. *Biophys J* **102**, 2309-2320

16. Rozycki, B., Boura, E., Hurley, J. H., and Hummer, G. (2012) Membrane-elasticity model of Coatless vesicle budding induced by ESCRT complexes. *PLoS Comput Biol* **8**, e1002736

17. Elia, N., Sougrat, R., Spurlin, T. A., Hurley, J. H., and Lippincott-Schwartz, J. (2011) Dynamics of endosomal sorting complex required for transport (ESCRT) machinery during cytokinesis and its role in abscission. *Proc Natl Acad Sci U S A* **108**, 4846-4851

18. Baumgartel, V., Ivanchenko, S., Dupont, A., Sergeev, M., Wiseman, P. W., Krausslich, H. G., Brauchle, C., Muller, B., and Lamb, D. C. (2011) Live-cell visualization of dynamics of HIV budding site interactions with an ESCRT component. *Nat Cell Biol* **13**, 469-474

19. Lata, S., Roessle, M., Solomons, J., Jamin, M., Gottlinger, H. G., Svergun, D. I., and Weissenhorn, W. (2008) Structural basis for autoinhibition of ESCRT-III CHMP3. *J Mol Biol* **378**, 818-827

20. Nickerson, D. P., West, M., Henry, R., and Odorizzi, G. (2010) Regulators of Vps4 ATPase activity at endosomes differentially influence the size and rate of formation of intralumenal vesicles. *Mol Biol Cell* **21**, 1023-1032

21. Wollert, T., Wunder, C., Lippincott-Schwartz, J., and Hurley, J. H. (2009) Membrane scission by the ESCRT-III complex. *Nature* **458**, 172-177

22. Xiao, J., Xia, H., Yoshino-Koh, K., Zhou, J., and Xu, Z. (2007) Structural characterization of the ATPase reaction cycle of endosomal AAA protein Vps4. *J Mol Biol* **374**, 655-670

23. Gonciarz, M. D., Whitby, F. G., Eckert, D. M., Kieffer, C., Heroux, A., Sundquist, W. I., and Hill, C. P. (2008) Biochemical and structural studies of yeast Vps4 oligomerization. *J Mol Biol* **384**, 878-895

24. Landsberg, M. J., Vajjhala, P. R., Rothnagel, R., Munn, A. L., and Hankamer, B. (2009) Three-dimensional structure of AAA ATPase Vps4: advancing structural insights into the mechanisms of endosomal sorting and enveloped virus budding. *Structure* **17**, 427-437

25. Monroe, N., Han, H., Gonciarz, M. D., Eckert, D. M., Karren, M. A., Whitby, F. G., Sundquist, W. I., and Hill, C. P. (2014) The Oligomeric State of the Active Vps4 AAA ATPase. *J Mol Biol* **426**, 510-525

26. Hurley, J. H., and Yang, D. (2008) MIT domainia. *Dev Cell* **14**, 6-8

27. Muziol, T., Pineda-Molina, E., Ravelli, R. B., Zamborlini, A., Usami, Y., Gottlinger, H., and Weissenhorn, W. (2006) Structural basis for budding by the ESCRT-III factor CHMP3. *Dev Cell* **10**, 821-830

28. Shim, S., Kimpler, L. A., and Hanson, P. I. (2007) Structure/function analysis of four core ESCRT-III proteins reveals common regulatory role for extreme C-terminal domain. *Traffic* **8**, 1068-1079

29. Rozycki, B., Kim, Y. C., and Hummer, G. (2011) SAXS ensemble refinement of ESCRT-III CHMP3 conformational transitions. *Structure* **19**, 109-116

30. Stuchell-Brereton, M. D., Skalicky, J. J., Kieffer, C., Karren, M. A., Ghaffarian, S., and Sundquist, W. I. (2007) ESCRT-III recognition by VPS4 ATPases. *Nature* **449**, 740-744

31. Obita, T., Saksena, S., Ghazi-Tabatabai, S., Gill, D. J., Perisic, O., Emr, S. D., and Williams, R. L. (2007) Structural basis for selective recognition of ESCRT-III by the AAA ATPase Vps4. *Nature* **449**, 735-739

32. Kieffer, C., Skalicky, J. J., Morita, E., De Domenico, I., Ward, D. M., Kaplan, J., and Sundquist, W. I. (2008) Two distinct modes of ESCRT-III recognition are required for VPS4 functions in lysosomal protein targeting and HIV-1 budding. *Dev Cell* **15**, 62-73

33. Yang, D., Rismanchi, N., Renvoise, B., Lippincott-Schwartz, J., Blackstone, C., and Hurley, J. H. (2008) Structural basis for midbody targeting of spastin by the ESCRT-III protein CHMP1B. *Nat Struct Mol Biol* **15**, 1278-1286

34. Solomons, J., Sabin, C., Poudevigne, E., Usami, Y., Hulsik, D. L., Macheboeuf, P., Hartlieb, B., Gottlinger, H., and Weissenhorn, W. (2011) Structural basis for ESCRT-III CHMP3 recruitment of AMSH. *Structure* **19**, 1149-1159

35. Yang, Z., Vild, C., Ju, J., Zhang, X., Liu, J., Shen, J., Zhao, B., Lan, W., Gong, F., Liu, M., Cao, C., and Xu, Z. (2012) Structural basis of molecular recognition between ESCRT-III-like protein Vps60 and AAA-ATPase regulator Vta1 in the multivesicular body pathway. *J Biol Chem* **287**, 43899-43908

36. Skalicky, J. J., Arii, J., Wenzel, D. M., Stubblefield, W. M., Katsuyama, A., Uter, N. T., Bajorek, M., Myszka, D. G., and Sundquist, W. I. (2012) Interactions of the human LIP5 regulatory protein with endosomal sorting complexes required for transport. *J Biol Chem* **287**, 43910-43926

37. Merrill, S. A., and Hanson, P. I. (2010) Activation of human VPS4A by ESCRT-III proteins reveals ability of substrates to relieve enzyme autoinhibition. *J Biol Chem* **285**, 35428-35438

38. Azmi, I., Davies, B., Dimaano, C., Payne, J., Eckert, D., Babst, M., and Katzmann, D. J. (2006) Recycling of ESCRTs by the AAA-ATPase Vps4 is regulated by a conserved VSL region in Vta 1. *Journal of Cell Biology* **172**, 705-717

39. Xiao, J., Xia, H., Zhou, J., Azmi, I. F., Davies, B. A., Katzmann, D. J., and Xu, Z. (2008) Structural basis of Vta1 function in the multivesicular body sorting pathway. *Dev Cell* **14**, 37-49

40. Arlt, H., Perz, A., and Ungermann, C. (2011) An overexpression screen in Saccharomyces cerevisiae identifies novel genes that affect endocytic protein trafficking. *Traffic* **12**, 1592-1603

41. Chang, L., Bertelsen, E. B., Wisen, S., Larsen, E. M., Zuiderweg, E. R., and Gestwicki, J. E. (2008) High-throughput screen for small molecules that modulate the ATPase activity of the molecular chaperone DnaK. *Anal Biochem* **372**, 167-176

42. McCoy, A. J., Grosse-Kunstleve, R. W., Adams, P. D., Winn, M. D., Storoni, L. C., and Read, R. J. (2007) Phaser crystallographic software. *J Appl Crystallogr* **40**, 658-674

43. Emsley, P., and Cowtan, K. (2004) Coot: model-building tools for molecular graphics. *Acta Crystallogr D Biol Crystallogr* **60**, 2126-2132

44. Babst, M., Sato, T. K., Banta, L. M., and Emr, S. D. (1997) Endosomal transport function in yeast requires a novel AAA-type ATPase, Vps4p. *EMBO J* **16**, 1820-1831

45. Bajorek, M., Morita, E., Skalicky, J. J., Morham, S. G., Babst, M., and Sundquist, W. I. (2009) Biochemical analyses of human IST1 and its function in cytokinesis. *Mol Biol Cell* **20**, 1360-1373

46. Scott, A., Gaspar, J., Stuchell-Brereton, M. D., Alam, S. L., Skalicky, J. J., and Sundquist, W. I. (2005) Structure and ESCRT-III protein interactions of the MIT domain of human VPS4A. *Proc Natl Acad Sci U S A* **102**, 13813-13818

47. Azmi, I. F., Davies, B. A., Xiao, J., Babst, M., Xu, Z., and Katzmann, D. J. (2008) ESCRT-III family members stimulate Vps4 ATPase activity directly or via Vta1. *Dev Cell* **14**, 50-61

48. Shestakova, A., Hanono, A., Drosner, S., Curtiss, M., Davies, B. A., Katzmann, D. J., and Babst, M. (2010) Assembly of the AAA ATPase Vps4 on ESCRT-III. *Mol Biol Cell* **21**, 1059-1071

49. Renvoise, B., Parker, R. L., Yang, D., Bakowska, J. C., Hurley, J. H., and Blackstone, C. (2010) SPG20 protein spartin is recruited to midbodies by ESCRT-III protein Ist1 and participates in cytokinesis. *Mol Biol Cell* **21**, 3293-3303

50. Giaever, G., Chu, A. M., Ni, L., Connelly, C., Riles, L., Veronneau, S., Dow, S., Lucau-Danila, A., Anderson, K., Andre, B., Arkin, A. P., Astromoff, A., El-Bakkoury, M., Bangham, R., Benito, R., Brachat, S., Campanaro, S., Curtiss, M., Davis, K., Deutschbauer, A., Entian, K. D., Flaherty, P., Foury, F., Garfinkel, D. J., Gerstein, M., Gotte, D., Guldener, U., Hegemann, J. H., Hempel, S., Herman, Z., Jaramillo, D. F., Kelly, D. E., Kelly, S. L., Kotter, P., LaBonte, D., Lamb, D. C., Lan, N., Liang, H., Liao, H., Liu, L., Luo, C., Lussier, M., Mao, R., Menard, P., Ooi, S. L., Revuelta, J. L., Roberts, C. J., Rose, M., Ross-Macdonald, P., Scherens, B., Schimmack, G., Shafer, B., Shoemaker, D. D., Sookhai-Mahadeo, S., Storms, R. K., Strathern, J. N., Valle, G., Voet, M., Volckaert, G., Wang, C. Y., Ward, T. R., Wilhelmy, J., Winzeler, E. A., Yang, Y., Yen, G., Youngman, E., Yu, K., Bussey, H., Boeke, J. D., Snyder, M., Philippsen, P., Davis, R. W., and Johnston, M. (2002) Functional profiling of the Saccharomyces cerevisiae genome. *Nature* **418**, 387-391

51. Rue, S. M., Mattei, S., Saksena, S., and Emr, S. D. (2008) Novel Ist1-Did2 complex functions at a late step in multivesicular body sorting. *Mol Biol Cell* **19**, 475-484

52. Yu, H., Braun, P., Yildirim, M. A., Lemmens, I., Venkatesan, K., Sahalie, J., Hirozane-Kishikawa, T., Gebreab, F., Li, N., Simonis, N., Hao, T., Rual, J. F., Dricot, A., Vazquez, A., Murray, R. R., Simon, C., Tardivo, L., Tam, S., Svrzikapa, N., Fan, C., de Smet, A. S., Motyl, A., Hudson, M. E., Park, J., Xin, X., Cusick, M. E., Moore, T., Boone, C., Snyder, M., Roth, F. P., Barabasi, A. L., Tavernier, J., Hill, D. E., and Vidal, M. (2008) High-quality binary protein interaction map of the yeast interactome network. *Science* **322**, 104-110

Chapter 5 Conclusions and Perspectives

Understanding the molecular mechanism of membrane vesiculation by the ESCRT machinery has long been a goal for those in the protein trafficking, virology, and cancer biology fields. While recent work has shown that restructuring of membrane by the ESCRT-III complex coupled with the hydrolysis of ATP by the AAA-ATPase Vps4 constitutes the final critical steps of vesiculation, there is a great gap in our knowledge about how Vps4 and ESCRT-III work together in this process. In particular, my thesis work has attempted to answer these questions by investigating how ESCRT-III proteins indirectly control Vps4 (in human: VPS4) activity by binding to its co-factor Vta1 (LIP5), namely Did2 (CHMP1B) and Vps60 (CHMP5). Furthermore, I looked to answer how a novel ESCRT-III protein, Vfa1, directly controls Vps4 function. While my thesis work has made gains in lessening this gap, there are still a significant amount of work that is needed to help us better understand this complicated mechanism.

One clear deficiency in the ESCRT field is that much of our current knowledge with regard to ESCRT function has come from studies in yeast. While I cannot stress enough how extremely fruitful and incredible insightful this work has been, until we test whether mechanisms in yeast are conserved within higher organisms it will be difficult directly to apply our knowledge about the ESCRT proteins to achieve therapeutic results. In Chapter 2, I examined whether the

Vps4 co-factor, Vta1 and LIP5 – two homologs that have low sequence identity to each other - maintained structural similarity over the course of evolution. I determined the crystal structure of the LIP5 N-terminal domain (NTD), and compared it to a previously determined crystal structure of Vta1NTD. Like its yeast counterpart, LIP5NTD is comprised of two microtubule-interacting and trafficking (MIT) domains. Overall, LIP5 and Vta1 adopt a similar fold, however the LIP5 MIT2 undergoes a 4 Å rotation relative to MIT1 when compared with the Vta1 MIT2. I also investigated how the two ESCRT-III proteins, Did2 (CHMP1B) and Vps60 (CHMP5), bind to Vta1/LIP5. It had been shown previously that the yeast ESCRT-III proteins bind to the second MIT domain. However, I discovered that Did2 binds to the MIT1 and confirmed that the Vps60 binds to the MIT2. When testing how their human orthologs bind LIP5, CHMP1B, like Did2, was found to bind to the MIT1. Interestingly, residues critical for Vps60 binding in Vta1 - while located at structurally analogous positions - are not essential for CHMP5 in human. This strongly suggested that Vps60/CHMP5 binding to Vta1/LIP5 has diverged during evolution. The fact that CHMP1B bound to the LIP5 MIT1 prompted me to determine the crystal structure of the minimal LIP5 binding sequence, the CHMP1B MIT-interacting motif (MIM), with the LIP5NTD. As suspected, CHMP1B binds via a canonical MIT-MIM1 binding motif as seen in other MIT-ESCRT-III structures. This indicates that all other ESCRT-III proteins that contain a MIM1 would bind LIP5 by a similar mechanism.

CHMP5 regulation of LIP5 has seem to have diverged from yeast, which made me question not only the mechanism of CHMP5 regulation of LIP5, but also whether LIP5 itself functions differentially in its direct role in VPS4 regulation, as described in Chapter 3. Using ATP hydrolysis as a functional readout, I saw that LIP5 does stimulate VPS4, as has been shown with yeast proteins, but CHMP1B MIM had no effect on LIP5 mediated stimulation of VPS4 while CHMP5 actually inhibited LIP5 stimulation. This was wholly unexpected, since both yeast proteins Vps60 and Did2 greatly stimulate Vps4 via Vta1. By determining the crystal structure of the LIP5NTD-CHMP1B MIM-CHMP5 MIM complex, I proposed a model that explains the likely mechanism for CHMP5 inhibition. A previously determined solution structure of LIP5NTD and the CHMP5 MIM, showed that one residue of CHMP5, Tyr182, exists in a dynamic equilibrium. Interestingly, I found that in the ternary complex crystal structure, this Tyr182 disrupts a conserved salt bridge between the MIT1-MIT2 interface, and causes a 2 Å shift in the MIT2 domain. Although Tyr182 does not affect the affinity between LIP5 and CHMP5, it does relieve the inhibitory effects of CHMP5 towards LIP5. I reasoned that if regulation by ESCRT-III proteins is different for the human protein, it is then possible that LIP5 itself may utilize a different regulatory mechanism towards VPS4. Indeed, unlike Vta1, which only requires a C-terminal VSL domain, LIP5 requires both its VSL and its NTD connected *in cis* for full activity. While the physical connection is essential, the actual LIP5 linker sequence is dispensable for LIP5 stimulation. Surprisingly, CHMP5 could also inhibit the LIP5 linker deletion mutant. Together, this suggests a model of

regulation where the LIP5 VSL initially binds to VPS4 and through the physical linkage to NTD, brings it in close proximity to VPS4 for full activity. When CHMP5 binds, the insertion of Tyr182 causes a conformational change in the LIP5NTD that precludes the stimulatory binding of LIP5NTD to VPS4.

Chapter 4 is devoted to the regulatory property of a newly identified Vps4 regulatory protein, Vfa1. Initially, Vfa1 was only known to interact with Vps4, and upon its over-expression, could cause slight morphological defects in the yeast vacuole (presumed to be caused by dysfunction in endosomal pathway). I found that Vfa1 not only binds Vps4, but this interaction dramatically potentiates Vps4 ATPase activity. I was able to map the binding interface between the two proteins and found that the Vps4 MIT domain interacted with the C-terminal portion of Vfa1. The crystal structure of the complex showed that Vfa1 binds Vps4 using a canonical MIT-MIM2 interaction, as described from previous structural work with the ESCRT-III proteins and Vps4. Perturbation to the binding interface ablates this high affinity MIT-MIM2 interaction, as well as prevented Vfa1 stimulation of Vps4 ATPase activity. This structure showed that Vfa1 is a *bona fide* ESCRT protein, and has greatly expanded our understanding of ESCRT function by adding a new family member.

While these results help us better appreciate the ESCRT-III/Vps4 interaction, more effort is needed to achieve a comprehensive understanding. The number of distinct MIT-MIM interactions has continued to expand, with a

total of 5 different types of interactions being classified to date [appendix]. So far, three of these MIT-MIM interactions have been shown to be utilized by the Vps4/Vta1 complex. The MIMs of the ESCRT-III proteins can also bind to other MIT domain containing proteins, thus encompassing the other two known MIT-MIM interactions. Yet, there are many other MIT containing proteins whose molecular interactions with the ESCRT-III proteins have not been classified. In human, 13 proteins have been predicted to contain MIT domains, but only 7 of them have been analyzed for ESCRT-III binding properties (1). The MIT-MIM interaction seems to be essential for the recruitment MIT containing proteins to the site of action. If we were to fully comprehend all of the various MIT-MIM interactions, would it be possible for us to 'decode' MIT-MIM interactome? This would allow us to selectively target certain MIT-MIM interactions to prevent a specific MIT containing protein from being recruited by the ESCRT-III proteins. In the context of therapeutic application, we could envision to essentially 'turn off' a single aspect of ESCRT function that has become deleterious, while allowing other ESCRT functions to continue normally.

Although the interactions between the ESCRT-III proteins, Vta1 and Vps4 have been studied in detail, the atomic resolution structure of a fully active Vps4 oligomer has remained elusive. Hence, we cannot fully apprehend the mechanism by which Vps4 converts the ESCRT-III proteins from a membrane bound conformation to a cytosolic one. It is presumed that the dynamic nature of Vps4 structure, between a monomeric species and an ATP-bound oligomer,

makes the protein challenging to crystallize. Other structural efforts using electron microscopy (EM), while thought to be initially successful, actually generated structures of Vps4 that were later proved to be non-physiological (2). However, improvements in cyro-EM technology and data collection may make it more feasible than ever to approach atomic level resolution for the Vps4 oligomer (3). Furthermore, recent work using the Vps4 homolog from thermophillic yeast (*Sulfolobus solfataricus*) proved useful in resolving oligomeric complexes by size-exclusion chromatography (2). Combining these two experimental approaches may be the trick necessary for us to finally obtain a high-resolution structure of the Vps4 complex. Another route may be using the lessons learned from obtaining the structure of another AAA protein, ClpX, where linkers were added to create one polypeptide encompassing all six subunits to force a stable oligomeric structure (4). By linking Vps4 together, it may be possible to generate a high-resolution structure by preventing the dissociation of the oligomer.

The prevailing model of Vps4 regulation is that the faster the enzyme can hydrolyze ATP, the better for its function *in vivo*. It will be interesting to actually correlate the rate of ATP hydrolysis with its physiological function. It has become quite successful in recent years to try to recapitulate ESCRT function using *in vitro* reconstitution (5), and I believe it is feasible to extend this further using a method developed by Saksena et al. (6). In brief, they recapitulate ESCRT-III assembly on a liposome, where one of the ESCRT-III proteins is conjugated to a dye that has different spectroscopic characteristics depending whether it is in

solution or in a lipid environment. Therefore, when Vps4 removes the ESCRT-III complex from the lipid membrane, the change in the spectroscopic property of the dye can followed kinetically. Unfortunately, the researchers only use the core ESCRT-III proteins (Vps20, Snf7, Vps24, and Vps2) and Vps4 for their analysis, and it will be interesting to see how the inclusion of the other ESCRT-III proteins (Did2, Vps60, Ist1, and Vfa1) in conjunction with Vta1 or by themselves, can influence this process. Did2, Vps60 and Vfa1 have all been shown to directly or indirectly stimulate Vps4 ATPase activity, and in contrast, Ist1 has been shown to inhibit Vps4 (7-9). It will be fascinating to see what interplay exists between these proteins, and whether an increase of ATPase activity directly contributes to the expedition of ESCRT-III disassembly.

One theme of this thesis work has been that some of our knowledge of the ESCRT system in yeast is not easily translatable to the human system. Unfortunately, study of ESCRT dysfunction in the metazoan MVB pathway in is challenging by conventional methods. In metazoan, our current understanding of ESCRT function predominantly comes from observing the efficiency of viral release or cytokinesis. While useful in their own right, ESCRT function is not ubiquitous for all processes. The early ESCRT complex, ESCRT-I, seems to be dispensable for viral release and cytokinesis, and therefore studies in these systems cannot recapitulate what we currently understand about MVB biogenesis (10). Furthermore, the yeast system is genetically tractable, while the metazoan experiments rely on siRNA to probe the function of a particular ESCRT

proteins. There is a great need for developing new methods for the study of metazoan MVB biogenesis system in a more native context. Recent work has begun to show the promise for *C. elegans* to be used as a model system for this exact purpose. During embryogenesis, there is a large and systematic flux of materials that goes through the MVB pathway, and as such this allows for the live organism imaging for protein factors, like individual ESCRT components, or movement of cellular receptors into MVBs (11). Taking advantage of the clustered, regularly interspersed, short palindromic repeats (CRISPR) RNA-guided Cas9 nuclease for genetic manipulations has the potential to exponentially increase the ease and tractability of the *C. elegan* system (12). Observing MVB biogenesis *in vivo* and, most importantly, in a metazoan system has the potential to dramatically increase our understanding of ESCRT function.

Until we can define mechanistic roles for all the ESCRT-III proteins and how they work together, it will be extremely challenging to fully comprehend the scission event carried out by this interplay. In MVB biogenesis, the vesicle formation is uniform and precise, suggesting a tightly controlled process that is not spontaneous. Even slight disruptions to ESCRT-III function can lead to improper development of MVBs. Hopefully, the work presented in this thesis has helped resolve some of the ambiguity surrounding Vps4/Vta1 regulation by the ESCRT-III proteins, and provided useful clues to help address the next critical question in the field.

5.1 References

1. Row, P. E., Liu, H., Hayes, S., Welchman, R., Charalabous, P., Hofmann, K., Clague, M. J., Sanderson, C. M., and Urbe, S. (2007) The MIT domain of UBPY constitutes a CHMP binding and endosomal localization signal required for efficient epidermal growth factor receptor degradation. *J Biol Chem* **282**, 30929-30937

2. Monroe, N., Han, H., Gonciarz, M. D., Eckert, D. M., Karren, M. A., Whitby, F. G., Sundquist, W. I., and Hill, C. P. (2014) The oligomeric state of the active Vps4 AAA ATPase. *J Mol Biol* **426**, 510-525

3. Li, X., Zheng, S. Q., Egami, K., Agard, D. A., and Cheng, Y. (2013) Influence of electron dose rate on electron counting images recorded with the K2 camera. *J Struct Biol* **184**, 251-260

4. Martin, A., Baker, T. A., and Sauer, R. T. (2005) Rebuilt AAA + motors reveal operating principles for ATP-fuelled machines. *Nature* **437**, 1115-1120

5. Wollert, T., and Hurley, J. H. (2010) Molecular mechanism of multivesicular body biogenesis by ESCRT complexes. *Nature* **464**, 864-869

6. Saksena, S., Wahlman, J., Teis, D., Johnson, A. E., and Emr, S. D. (2009) Functional reconstitution of ESCRT-III assembly and disassembly. *Cell* **136**, 97-109

7. Azmi, I. F., Davies, B. A., Xiao, J., Babst, M., Xu, Z., and Katzmann, D. J. (2008) ESCRT-III family members stimulate Vps4 ATPase activity directly or via Vta1. *Dev Cell* **14**, 50-61

8. Dimaano, C., Jones, C. B., Hanono, A., Curtiss, M., and Babst, M. (2008) Ist1 regulates Vps4 localization and assembly. *Mol Biol Cell* **19**, 465-474

9. Vild, C. J., and Xu, Z. (2014) Vfa1 binds to the N-terminal microtubule-interacting and trafficking (MIT) domain of Vps4 and stimulates its ATPase activity. *J Biol Chem* **289**, 10378-10386

10. McCullough, J., Colf, L. A., and Sundquist, W. I. (2013) Membrane fission reactions of the mammalian ESCRT pathway. *Annu Rev Biochem* **82**, 663-692

11. Wang, L., and Audhya, A. (2014) In vivo imaging of C. elegans endocytosis. *Methods*

12. Frokjaer-Jensen, C. (2013) Exciting prospects for precise engineering of Caenorhabditis elegans genomes with CRISPR/Cas9. *Genetics* **195**, 635-642

Appendix Structural basis of molecular recognition between ESCRT-III-like protein Vps60 and AAA-ATPase regulator Vta1 in the multivesicular body pathway

A.1 Abstract

The AAA-ATPase Vps4 is critical for function of the multivesicular body sorting pathway, which impacts cellular phenomena ranging from receptor down-regulation to viral budding to cytokinesis. Vps4 activity is stimulated by the interaction between Vta1 and Vps60, but the structural basis for this interaction is unclear. The fragment Vps60(128–186) was reported to display the full activity of Vps60. Vta1 interacts with Vps60 using its N-terminal domain (Vta1NTD). In this work, the structure of Vps60(128–186) in complex with Vta1NTD was determined using NMR techniques, demonstrating a novel recognition mode of the microtubule-interacting and transport (MIT) domain in which Vps60(128–186) interacts with Vta1NTD through helices α4′ and α5′, extending over Vta1NTD MIT2 domain helices 1–3. The Vps60 binding does not result in Vta1 conformational changes, further revealing the fact that Vps4 ATPase is enhanced by the interaction between Vta1 and Vps60 in an unanticipated manner

A.2 Introduction

Membrane budding away from the cytosol controls a number of biological processes important to cellular homeostasis and defenses against aging (1-3). The machinery responsible for executing this function consists of several distinct multimeric complexes known as the endosomal sorting complexes required for transport (ESCRTs) (4-6), which were originally identified in yeast and have been

implicated in multivesicular body (MVB) biogenesis in plants, fungi, and animals (6,7). MVBs are formed when the late endosomal membrane invaginates and forms vesicles in the lumen, carrying selected transmembrane protein cargoes in the budding process (2,3). MVB biogenesis and fusion of an MVB with the lysosome in a later step represent a mechanism in which eukaryotic cells down-regulate cell surface signaling via the endolysosomal degradation pathway (8). Components of the ESCRT machinery have been identified as potential tumor suppressors (9), mainly attributed to the involvement of the ESCRT machinery in mediating signal attenuation for activated receptors of growth factors, peptide hormones, and cytokines. The ESCRT machinery protects against age-related neurodegenerative diseases through either the canonical MVB pathway or autophagy (9,10). In addition, the ESCRT machinery also plays a pathological role in viral infection (2,11,12).

At least five distinctive multimeric complexes are involved in MVB biogenesis: ESCRT-0, ESCRT-I, ESCRT-II, ESCRT-III, and Vps4 (13,14). Their structure and function are highly conserved in all eukaryotes (9,10). ESCRT-0 is responsible for clustering of ubiquitylated cargoes to the site of MVB formation. ESCRT-I and ESCRT-II together generate membrane curvature and budding, whereas assembly of ESCRT-III at the bud neck catalyzes scission of the membrane. Completion of the process requires the AAA-ATPase Vps4, which disassembles ESCRT-III polymers upon ATP binding and hydrolysis (15,16). This ATP-consuming reaction is the only step in MVB biogenesis that inputs

energy into the system, therefore providing the thermodynamic driving force for processing. Importantly, the role of Vps4 is conserved in all biological processes that depend on the action of the ESCRTs. Similar to other AAA-ATPases, Vps4 functions as an oligomer whose structure likely contains two conformationally distinctive hexameric rings (17). The rings contain a central pore where ESCRT-III subunits may physically interact and pass through during the disassembly process. Initial binding of Vps4 to ESCRT-III subunits requires its N-terminal microtubule-interacting and transport (MIT) domain (18). The MIT domain appears to specifically recognize short peptide sequence MIT-interacting motifs (MIMs) at or near the C-terminal end of ESCRT-III subunits (19-24).

The *in vivo* activity of Vps4 is tightly regulated (25). To date, at least four proteins have been identified to bind to Vps4 and have roles in regulating its oligomerization and activity (26-29). Did2, Ist1, and Vps60 are ESCRT-III-related proteins whose mechanisms of action on Vps4 remain to be clarified. Vta1 is a positive regulator of Vps4 by promoting Vps4 oligomerization (26,30). Structural study of Vta1 has shown that it is a molecular dimer, with each subunit folded into two terminal domains linked by a flexible linker (29). Its C-terminal domain mediates dimerization and binds to a unique β-domain in the Vps4 AAA domain (31,32). Its N-terminal domain (residues 1–167; Vta1NTD) (Figure A.1) contains two tandem MIT domains, which specifically recognize Vps60 and Did2 but not other ESCRT-III subunits (27,29). The fragment Vps60(128-186) was reported to

display the full activity of Vps60, which stimulates Vps4 ATPase in a Vta1-dependent manner (27).

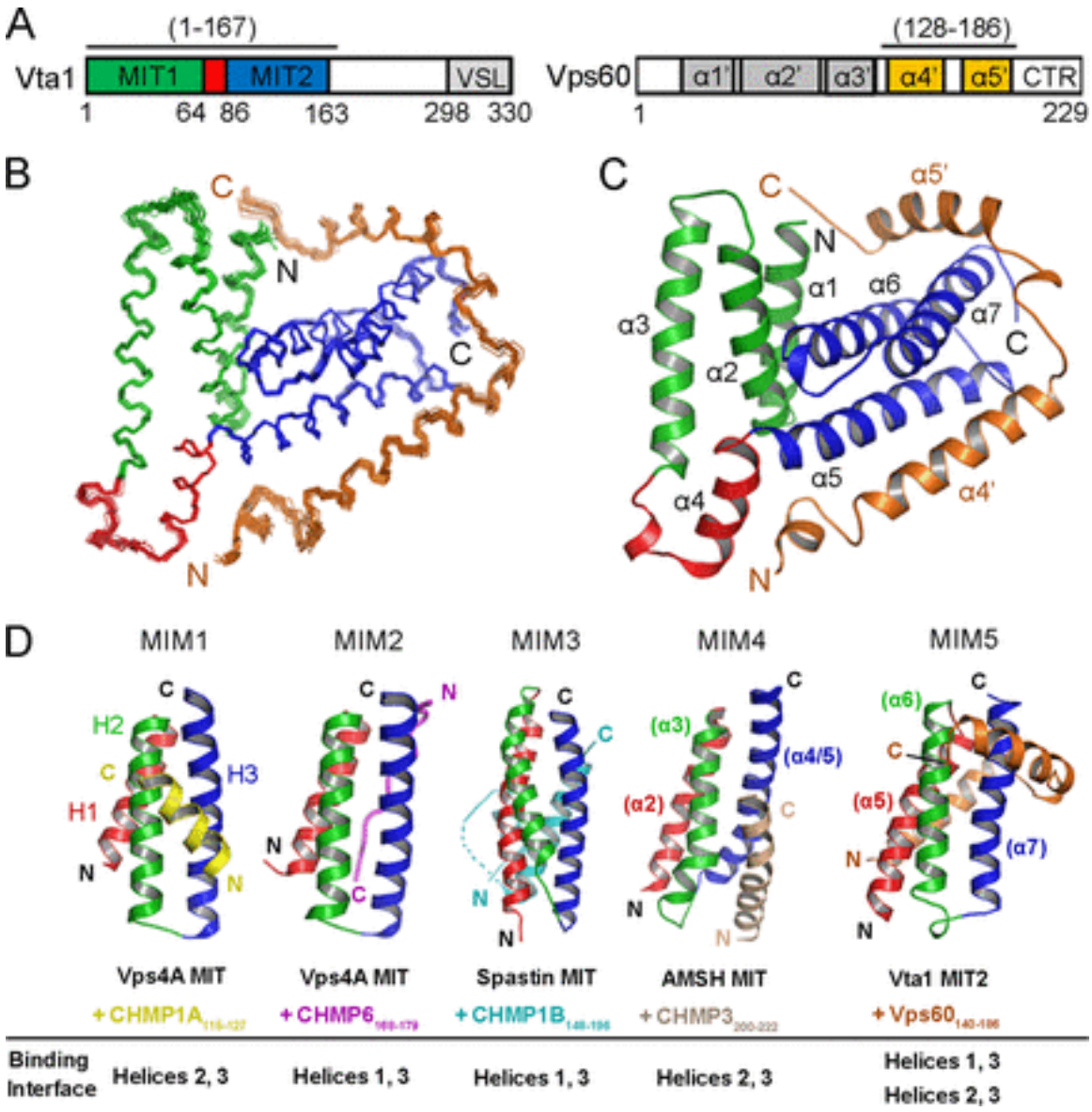

Figure A.1 Structural features of the Vta1NTD-Vps60(128–186) complex
(A) schematic representation of Vta1 and Vps60, highlighting regions critical for interactions that contribute to increased Vps4 ATPase activity. VSL, Vta1/SBP1/LIP5; CTR, C-terminal region. (B) backbone view of the ensemble of the 20 lowest energy Vta1NTD-Vps60(128–186) NMR structures, where Vps60(128–186) is displayed in orange. (C) three-dimensional representative structure of Vta1NTD-Vps60(128–186). The helices are numbered. (D) structural comparison of five different recognition modes of the MIT domain with MIM. Vps60 interacts with the first, second, and third helices of the Vta1NTD MIT2

domain together, which is different from a previously reported MIT ligand recognition mode.

In this work, to investigate how Vps60 interacts with Vta1NTD, we first measured the binding affinity of Vta1NTD for Vps60(128–186) (K_d ~ 0.7 μM) using isothermal titration calorimetry assay and then determined the solution structure of Vta1NTD in complex with Vps60(128–186). To confirm the residues involved in the interaction between Vta1NTD and Vps60(128–186), site-directed mutations and GST pulldown experiments were performed. The structure reveals that Vps60(128–186) interacts with Vta1NTD through a novel MIT domain recognition mode distinct from any reported mechanism.

A.3 Results

A.3.1 NMR Structural Determination

Initially, two basic sets of NMR mixed samples were made: 1) ^{13}C and ^{15}N isotope-labeled Vta1NTD with unlabeled Vps60(128–186) at a stoichiometric ratio of 1:1.2 and 2) ^{13}C and ^{15}N isotope-labeled Vps60(128–186) with unlabeled Vta1NTD at a stoichiometric ratio of 1:1.2, each of them for assignment of NMR signals belonging to the corresponding ^{13}C- and ^{15}N-labeled component and its structural determination. The intermolecular NOEs could be correctly assigned by confirming signals observed in three-dimensional ^{13}C-F1-edited, $^{13}C/^{15}N$-F3-filtered NOESY spectra acquired on both complex samples. In total, assignments of >96% of the main chain and 95% of the side chain atoms of the residues in the complex were completed. The NMR chemical shift changes of Vta1NTD backbone atoms ^{1}H and ^{15}N in the absence and presence of Vps60(128–186)

reveal that Vps60(128–186) addition mainly induced Vta1NTD MIT2 domain amide ^{15}N and ^{1}H chemical shift variations in residues of the Vta1NTD MIT2 domain (Figure A.2A), suggesting that Vps60-binding sites localize in these regions. This observation accords with the analysis of the electrostatic surface of Vta1NTD in its free state, which shows that the Vta1NTD MIT2 domain is more positively charged than the MIT1 domain (Figure A.2B and Figure A.2C), suitable for negatively charged Vps60 binding.

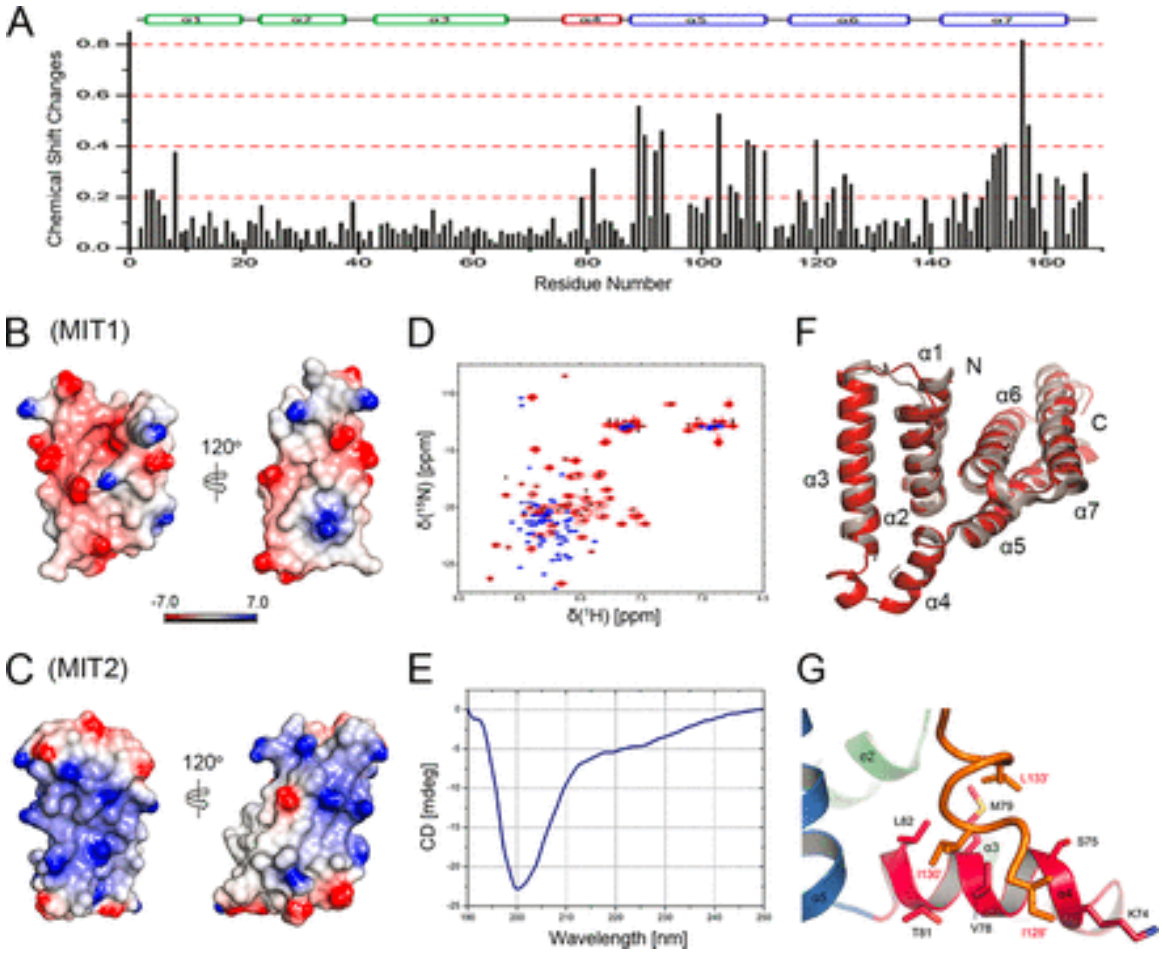

Figure A.2 Vps60 interacts with the Vta1NTD MIT2 domain motif, resulting in conformation stabilization of Vps60 and Vta1 NTD helix α4
(A) chemical shift changes in Vta1NTD backbone amide atoms ^{1}H and ^{15}N upon Vps60(128–186) binding, calculated using the following equation: $\Delta\delta_{av} = (0.5 \times (\Delta\delta(NH)^2 + 0.2 \times \Delta\delta(^{15}N)^2))^{1/2}$. The secondary structures are indicated at the top based on the crystal structure of free Vta1NTD (Protein Data Bank code 2RKK).

(B and C) electrostatic potential surfaces between helices 1 and 3 (left), helices 2 and 3 (right) of the MIT1 domain and between helices 1 and 3 (left) and helices 2 and 3 (right) of the MIT2 domain, respectively. The electrostatic potential surface was generated based on the crystal structure of free Vta1NTD using DelPhi software and visualized by PyMOL. (D) superimposition of two-dimensional ^{1}H-^{15}N HSQC spectra of Vps60(128–186) in the absence (blue) and presence (red) of Vta1NTD. (E) CD spectroscopy of free Vps60(128–186). (F) structural overlay of Vta1NTD in the free state (gray) and in complex with Vps60(128–186) (red). The N and C termini and the secondary structures are indicated. (G) interactions between the short N-terminal α-helix of Vps60(128–186) and helix α4 of Vta1NTD. The ribbon representation of Vta1NTD is colored in green for α2 and α3, red for α4, and blue for α5, with the N-terminal α-helix of Vps60(128–186) shown in orange.

The solution structure of the Vta1NTD-Vps60(128–186) complex was determined by a conventional heteronuclear NMR method using ^{15}N- or $^{13}C/^{15}N$-labeled protein. In total, 4469 distance restraints from NOE (286 intermolecular NOEs), 260 hydrogen bonds, and 390 dihedral angle restraints for backbone ϕ and ψ angles were used to calculate the solution structure. A best fit superposition of the ensemble of the 20 lowest energy structures represented in Figure A.1B is displayed, with root mean square deviations of 0.59 ± 0.13 Å for global backbone atoms and 1.07 ± 0.15 Å for global heavy atoms. The root mean square deviations were 0.46 ± 0.10 Å for the backbone atoms (N, Cα, and CO) and 0.87 ± 0.12 Å for all heavy atoms in the well-ordered secondary structure regions. The Ramachandran plot displays 94.1% of the residues in the most favored regions and 4.8% residues in additionally allowed regions (Table A.1), indicating that the structures are reasonable.

Table A.1 Experimental restraints and structural statistics for the Vta1NTD-Vps60(128-186) complex

NMR distance and dihedral constraints	
Distance restraints from NOEs	
Intramolecular	

Total	4183
Intraresidue ($i - j = 0$)	1215
Sequential ($\|i - j\| = 1$)	971
Medium-range ($1 < \|i - j\| \leq 5$)	1340
Long-range ($\|i - j\| > 5$)	657
Intermolecular	286
Hydrogen bonds	260
Dihedral restraints	390
ϕ	195
ψ	195
Structural statistics[a]	
r.m.s.d.[b] *versus* mean structure (Å)	
All backbone atoms	0.59 ± 0.13
All heavy atoms	1.07 ± 0.15
Backbone atoms (secondary structure)	0.46 ± 0.10
Heavy atoms (secondary structure)	0.87 ± 0.12
r.m.s.d. from experimental restraints	
NOE distances (Å)	0.023 ± 0.0003
Dihedral angles	0.685 ± 0.0136°
r.m.s.d. deviations from idealized geometry	
Bonds (Å)	0.0018 ± 0.000021
Angles	0.280 ± 0.0038°
Impropers	0.289 ± 0.0039°
Ramachandran analysis (%)	
Residues in most favored regions	94.1
Residues in additionally allowed regions	4.8
Residues in generously allowed regions	1.1
Residues in disallowed regions	0.0

↵[a] Structural statistics were calculated from the 20 lowest energy XPLOR-NIH structures.

↵[b] r.m.s.d., root mean square deviations.

A.3.2 Vta1 Binding Stabilizes Vps60(128–186) Helix Conformation

The two-dimensional NMR ^{1}H-^{15}N HSQC experiment with Vps60(128–186) in its free state (Figure A.2D) suggests that Vps60(128–186) in its free state is disordered because the cross-peaks are not dispersed, localizing mainly in the region between 8.0 and 8.5 ppm. To confirm this observation, we preformed CD spectroscopy on free Vps60(128–186), where negative absorption at ~200 nm shows a random coil conformation (Figure A.2E). Upon binding to Vta1NTD, the cross-peaks in two-dimensional NMR ^{1}H-^{15}N HSQC of Vps60(128–186) became dispersed (Figure A.2D), suggesting that Vps60(128–186) folds into an ordered structure, coinciding with the structure determined below. This demonstrates that Vta1NTD binding stabilizes Vps60 helix conformation.

A.3.3 Overall Complex Structure

The Vta1NTD-Vps60(128–186) structure shows that the bound Vta1NTD still has two MIT domains, each of them composed of three α-helices (MIT1: helices α1, α2 and α3; and MIT2: helices α5, α6, and α7) (Figure A.1C), almost similar to those observed in its free state (29). Helix α4 was much longer in Vta1NTD bound to Vps60(128–186) than in free Vta1NTD, which might have resulted from the conformational stabilization upon its binding to Vps60 (as demonstrated below), consistent with the secondary structure prediction based on the assignments of backbone atoms $^{13}C\alpha$, $^{13}C\beta$, ^{13}CO, ^{1}H, and ^{15}N (Figure A.3). The backbone atoms of bound Vta1NTD had a root mean square deviation of 1.07 Å from those of free Vta1NTD (Figure A.2F), indicating that Vps60(128–

186) binding does not induce overall major conformational changes in Vta1NTD. The secondary structure prediction and perceived structural homology to ESCRT-III protein Vps24/CHMP3 suggest that Vps60(128–186) corresponds to the fourth and the fifth helices within the Vps60 structure (42). In the current complex structure, Vps60(128–186) indeed folds into two α-helices (denoted as α4′ and α5′), and both helices are involved in the interaction with the MIT2 domain of Vta1NTD (Figure A.1). The two α-helices of bound Vps60(128–186) adopt an overall V-shaped helix-turn-helix structure and straddle on the third helix (α7) of the Vta1NTD MIT2 domain. The longer helix α4′ consists of residues 140′–157′ and interacts with α5 and α7, corresponding to the first and third helices of the Vta1NTD MIT2 domain. It runs diagonally from the N-terminal end of α5 to the C-terminal end of α7, maintaining a general direction parallel to both helices. The polypeptide chain crosses over to the other side of α7 near the C-terminal end of α7 and continues as α5′ (residues 168′–182′), running nearly vertical to helices α6 and α7. The Vta1-Vps60 complex buries a total of ~3600-Å2 surface area at the interface. In contrast to the MIT domains in Vps4, spastin, or AMSH (19-24), Vps60(128–186) interacts with Vta1NTD through helices α4′ and α5′, extending over Vta1NTD MIT2 domain helices 1–3. Thus, the Vta1NTD MIT2 domain displays a fifth and novel ligand recognition mode to bind to Vps60(128–186) (Figure A.1D and shown under “Discussion”).

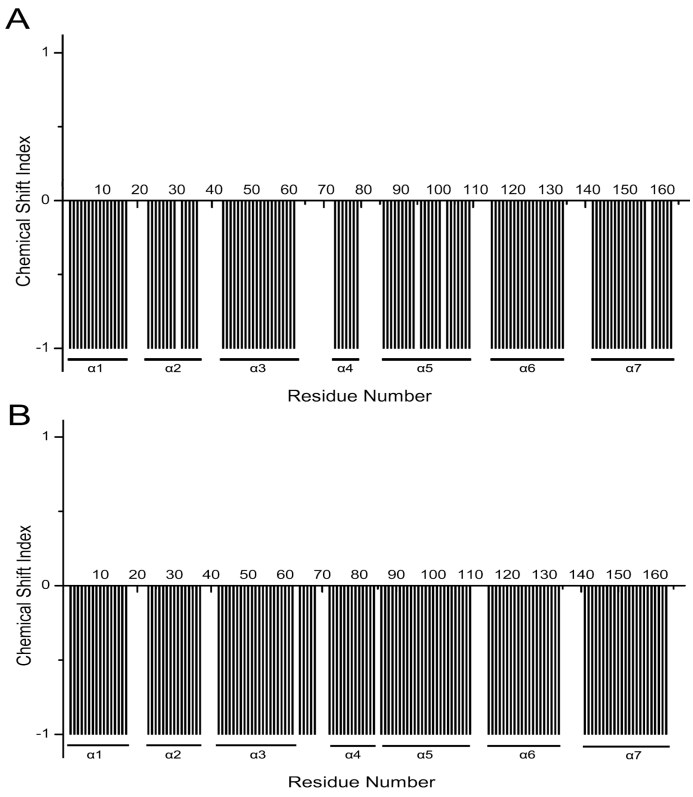

Figure A.3 Chemical Shift Index between Vta1NTD free and Vta1NTD in complex with Vps60
Graphs of the consensus plots of chemical shift index (CSI) based on the ^{1}Hα, ^{13}Cα, ^{13}Cβ and ^{13}CO chemical shifts of Vta1NTD in free (A, upper) and bound (B, down) with Vps60128-186

A.3.4 Vta1NTD Helix 4 Is Stabilized upon Vps60 Binding

In our complex structure, there are no significant structural changes in Vta1NTD except in the region that connects the two MIT domains. In the free Vta1NTD structure (29), the linker adopts largely a random coil structure, with only a one-turn α-helix occurring at residues 80–84. In particular, residues 65–75 appear to be disordered in the structure. Upon Vps60 binding, the linker becomes ordered. Residues 68–71 become a one-turn α-helix, and residues 73–84 adopt a longer helical structure (Figure A2.F). This conformational change might be caused by the interactions between helix α4 (positions 73–84) of

Vta1NTD and a short N-terminal α-helix (positions 128–134) of Vps60(128–186) (Figure A.2G). The interaction is predominantly hydrophobic, involving Ile-128′, Ile-130′, and Leu-133′ of Vps60, as well as Lys-74, Ser-75, Val-78, Met-79, Thr-81, and Leu-82 of Vta1NTD helix α4.

To confirm that the changes in helix α4 of Vta1NTD are generated due to Vps60(128–186) binding rather than crystallization, we assigned the chemical shifts of backbone atoms ^{13}Cα, ^{13}Cβ, ^{13}CO, ^{1}H, and ^{15}N of free Vta1NTD. The secondary structure prediction based on these assignments using the programs CSI (43) and TALOS (36-38) suggests that there are seven helices formed in free Vta1NTD, including α1 (Ala-2–Lys-17), α2 (Ile-23–Leu-36), α3, (Gln-43–Glu-62), α4 (Asp-73–Met-79), α5 (Gln-86–Lys-109), α6 (Val-115–Leu-134), and α7 (Thr-142–Lys-163), which are much similar to these observed in Vta1NTD bound to Vps60(128–186), except helix α4 (Figure A.3).

A.3.5 Interface in the Vta1-Vps60 Complex Structure

There are three major sites of interaction between the Vta1NTD MIT2 domain and Vps60(128–186) (Figure A.4). The first binding site (Figure A.4A and Figure A.4B) on Vta1NTD is predominantly hydrophobic and is lined by Ile-91, Tyr-92, Leu-94, Phe-96, Met-98, Tyr-101, Leu-105, Leu-108, Tyr-153, and Tyr-157 and the aliphatic chain of Lys-88, Lys-106, and Lys-109. The side chains of the residues located at Vps60(128–186) helix α4′, including Met-140′, Leu-141′, Leu-143′, Ile-144′, Leu-150′, Val-153′, and Leu-154′, are inserted into the groove of Vta1NTD helices 5 and 7. The Vps60(128–186) Ile-144′ side chain has a

hydrophobic interaction with the Vta1NTD Ile-91, Leu-94, and Met-98 side chains, as Pro-171 functions in the complex Vps4A-CHMP6(168–179) (21). Besides the hydrophobic interactions, complementary salt bridges are also formed by two of the adjacent conserved Vps60(128–186) residues (Glu-149′ and Glu-152′) (Figure A.4B). Moreover, the side chains of Vta1NTD Asn-95 and Asn-102 may form hydrogen bond interactions with the main chains of Met-140′ and Gln-146′, respectively. The second site on Vta1NTD binds mainly to the linker between α4′ and α5′ of Vps60(128–186) (Figure A.4*C*), most prominently to the side chains of Leu-163′ and Ile-166′. This site is also mainly hydrophobic and is lined by Tyr-153, Ile-156, and Tyr-157 and the aliphatic chains of Lys-149, Lys-152, and Lys-160, except that the side chain of Glu-162′ forms a complementary salt bridge with Lys-149. A previous alanine-scanning mutagenesis study showed that residues 139′–143′, 144′–148′, 154′–158′, and 164′–168′ of Vps60 are important for its interaction with Vta1 (27), which is consistent with our current structural observation. The third binding site on Vta1 contacts Vps60(128–186) helix α5′ (Figure A.4D), including previously identified Vta1 residues important for Vps60 interaction, Trp-122 and Lys-152 (27-29). In addition, the side chains of polar residues Lys-118, Arg-119, Lys-155, Lys-160, and Lys-163, as well as residues Ile-125, Ile-156, Leu-158, and Ala-162, largely hydrophobic in nature, form salt bridges with those of Asp-168′, Glu-170′, Asp-172′, Glu-174′, Asp-176′, Glu-181′, and Asp-182′ or have hydrophobic or stacking interactions with those of Leu-171′, Leu-175′, Leu-178′, Ala-179′, and F183′. A hydrogen bond interaction was observed between the side chain of Ser-159 and the main chain of Leu-171′.

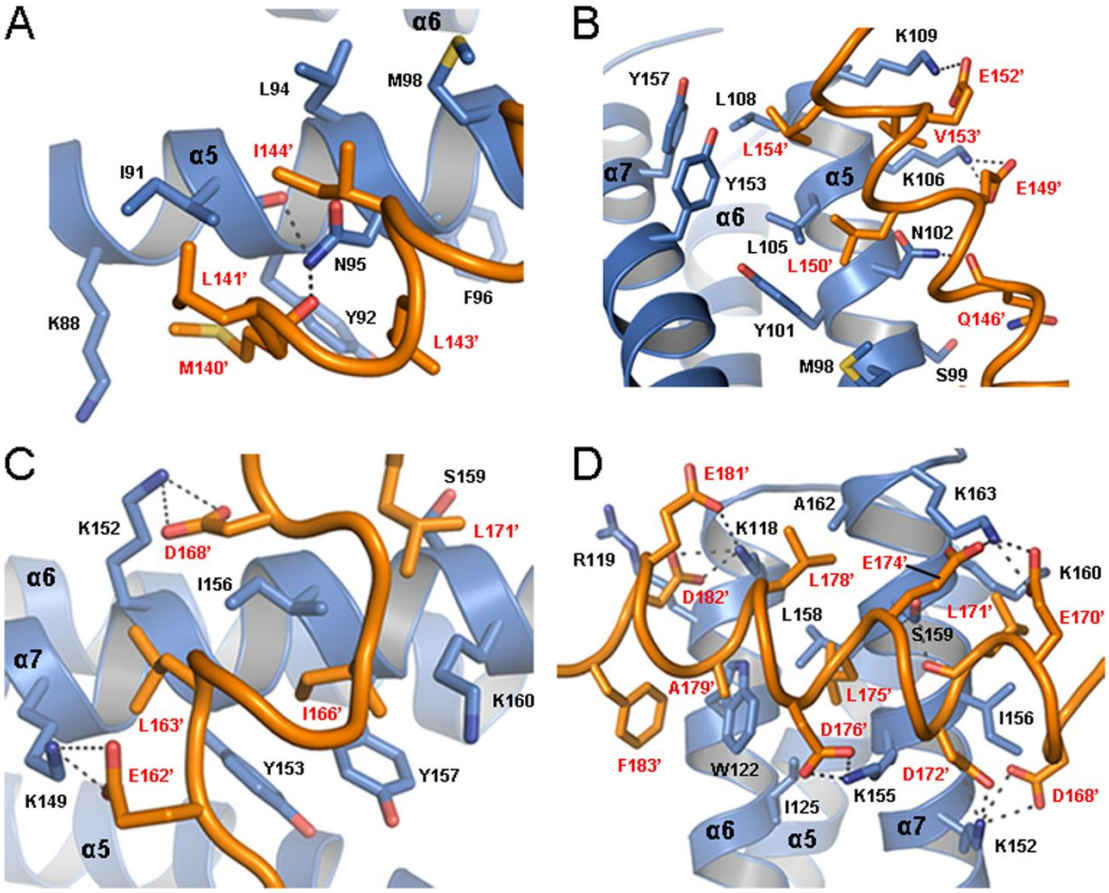

Figure A.4 Detailed interactions between Vps60(128–186) and the Vta1NTD MIT2 domain
*(*A and B*)*, ribbon representation of Vta1NTD shown in *blue*, with Vps60(128–186) helix α4′ shown in *orange.* (C) ribbon representation of Vta1NTD shown in *blue*, with the linker between Vps60(128–186) helices α4′ and α5′ shown in *orange.* (D) ribbon representation of Vta1NTD shown in *blue*, with Vps60(128–186) helix α5′ shown in *orange*.

A.3.6 Mutational Analyses of the Vta1-Vps60 Interaction

Mutations were introduced into these observed binding sites to test the importance of the residues to the overall stability of the complex. As shown in Figure A.5 and Table A.2, our *in vitro* GST pulldown experiments and isothermal titration calorimetry assay demonstrated that of all the single alanine or aspartic acid substitutions of Vta1NTD Lys-88, Ile-91, Met-98, Leu-105, Lys-106, Leu-108, Lys-109, Lys-118, Arg-119, Trp-122, Lys-149, Lys-152, Lys-155,

Ile-156, Leu-158, and Lys-163 have effects on Vps60(128–186) binding, confirming the energetic importance of all of these residues. Consistent with the large buried interface area of the Vta1-Vps60 complex, no single-site mutations could eliminate all detectable Vps60(128–186) binding.

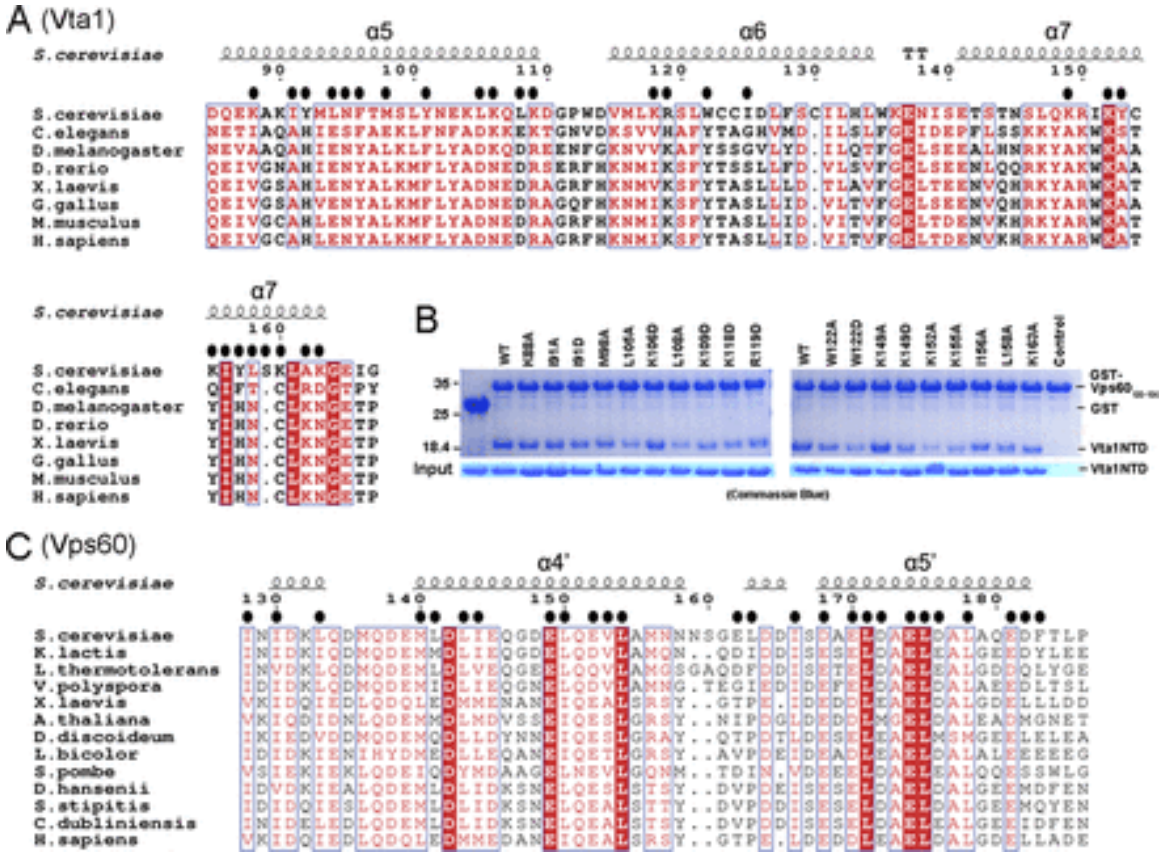

Figure A.5 Sequential and mutational analyses of the Vta1NTD-Vps60(128–186) complex.
(A) structure-based sequence alignments of the Vta1NTD MIT2 domain from various organisms. The residues involved in the interactions are indicated (black ovals). (B) GST pulldown assay of the Vta1NTD-Vps60(128–186) complex. GST or GST-tagged Vps60(128–186) was used to pull down wild-type or mutant ta1NTD as indicated. Proteins retained on the beads were analyzed by SDS-PAGE and visualized by Coomassie Blue staining. (C) sequence alignment of Vps60(128–186) helices α4′ and α5′ from various organisms. The residues involved in the interaction are indicated (black ovals).

Table A.2 Binding affinities of Vps60(128-186) for wild-type and muntant Vta1NTD determined by isothermal titration calorimetry assay.

Vta1NTD	K_d
	μ*M*
WT	0.7 ± 0.1
K88A	1.2 ± 0.3
I91A	0.9 ± 0.2
M98A	0.9 ± 0.2
L105A	3.1 ± 0.5
K106D	1.1 ± 0.2
L108A	1.4 ± 0.1
K109D	0.8 ± 0.1
K118D	1.7 ± 0.1
R119D	1.05 ± 0.04
W122A	1.4 ± 0.3
W122D	4.7 ± 0.3
K149A	1.0 ± 0.2
K149D	1.9 ± 0.1
K152A	3.9 ± 0.4
K155A	2.3 ± 0.1
I156A	1.5 ± 0.2
L158A	1.5 ± 0.1
K163A	1.1 ± 0.3

Based on the sequence alignment (Figure A.5A and Figure A.5C), the Vta1NTD MIT2 domain derived from *S. cerevisiae* has low sequence similarity to the other organisms, whereas Vps60(128–186) is highly conserved. The highly conserved Vta1NTD MIT2 domain residues Trp-122, Lys-152, and Ile-156 play more important roles in the Vta1-Vps60 interactions. Compared with the wild type, the binding affinities of the W122A, W122D, K152A, and I156A mutants for

Vps60(128–186) are reduced by ~2.0-, 6.7-, 5.6-, and 2.1-fold, respectively. Most notably, the non-conserved hydrophobic residues Leu-105 and Leu-108 in helix α5 of Vta1NTD are important as well; the L105A and L108A variants display an ~4.4- to 2.0-fold reduction in the binding affinities for Vps60(128–186). This demonstrates that Vps60(128–186) helix α5′ binds in a more conserved surface groove of Vta1NTD compared with Vps60(128–186) helix α4′ (Figure A.5A), indicating that the interactions between Vps60(128–186) helix α5′ and Vta1NTD are more common in all organisms, whereas the interactions between Vps60(128–186) helix α4′ and Vta1NTD make the interactions between Vta1NTD and Vps60(128–186) in yeast unique from those in other organisms. Thus, the Vta1NTD-Vps60(128–186) complex structure provides a structural basis for a previous study that showed that LIP5 (Vta1 in yeast) bound efficiently to a fragment of CHMP5 (Vps60 in yeast) that contained α5 but not α4 (44).

A.4 Discussion

A.4.1 Novel Mode of MIT-MIM interaction

The MIT domain is a versatile protein-protein interaction domain identified in proteins that have a role in vesicle trafficking, including Vps4, Vta1, AMSH, and UBPY, where they mediate interaction within the ESCRT-III complex (45). The MIT domain recognizes sequence motifs called the MIMs primarily within the ESCRT-III subunits. It has been suggested that the interaction between the MIT domain and MIM acts in regulating the disassembly of ESCRT-III, as well as in targeting specific proteins to the site of ESCRT function. At least four types of

MIM (MIM1, MIM2, MIM3, and MIM4) were reported to bind to different sites on the MIT domain (Figure A.1) (19-24).

MIM1 contains a sequence-conserved amphipathic helix ((D/E)xxLxxRLxxL(K/R)) along the groove between MIT domain helices α2 and α3 observed in the Vps4-Vps2(183–232) (19) and Vps4-CHMP1A(180–196) (20) complexes. MIM2 is a proline-rich sequence ($L^{170}P(E/D)VP^{174}$ and $R^{183}xLxPxLPxPP^{193}$) along the groove between MIT domain helices α1 and α3 found in the Vps4-CHMP6(168–179) (21) and Saci1372-Saci1337(183–193) (22) complexes, respectively. MIM3 is a highly specific mode along the groove between MIT domain helices α1 and α3 found in the spastin MIT-CHMP1B(148–196) complex (23) but with an interface twice large as that of the MIT domain of the Vps4-CHMP complex. MIM4 is a mainly polar sequence ($E^{203}xxxExx\varphi xx\varphi xxRLxTLR^{221}$) along a groove made up of helices 3 (Vps4 MIT domain helix 2) and 4/5 (Vps4 MIT domain helix 3) indentified in the AMSHΔC-CHMP3ΔN complex (24). Although the MIM4-binding site resembles the MIM1-binding surface, the contacts between the AMSH MIT domain and MIM4 are mostly polar interactions, whereas hydrophobic interactions play an important role in the Vps4 MIT-MIM1 and Vps4 MIT-MIM2 complexes.

Vta1NTD contains two tandem MIT domains as identified in its crystal structure (29), which mediate the interaction between Vta1 and the ESCRT-III-related proteins Vps60 and Did2. Our NMR structure of Vta1NTD-Vps60(128–

186) shows that Vps60 MIM binds exclusively to the second MIT domain of Vta1. Unlike other MIMs, the Vps60 MIM sequence (residues 140–186, defined as MIM5) is much longer and forms two helices (α4′ and α5′). The significant difference from the other MIMs is that Vps60 MIM5 can bind both surfaces made up of helices 5 and 7 (Vps4 MIT domain helices 1 and 3) and helices 6 and 7 (Vps4 MIT domain helices 2 and 3) of the Vta1 MIT2 domain. The Vta1 MIT2-Vps60 MIM5 contacts are a mixture of polar and hydrophobic interactions, as is the case for spastin MIT-MIM3. Thus, the structure of the Vta1-Vps60 complex provides a novel recognition mode of the MIT domain with its ligand and extends the diversity of MIT domain interaction surfaces for peptide ligands.

A.4.2 Vps60 Enhances Vta1 Stimulation of Vps4 in a Complex Manner

The dynamic assembly and disassembly of the ESCRT-III polymer play a critical role in ESCRT-mediated membrane deformation events and alterations of Vps4 ATPase activity. To address how Vps60 and Did2 binding enhances Vta1 stimulation of Vps4 ATPase activity, two models were presented (27). One is that their binding to the MIT2 domain results in conformation changes in Vta1; the other is that the interaction between Vta1 and Did2 or Vps60 increases the local concentration of Vta1-Vps4 *in vitro*. It was reported that removal of the two Vta1 tandem MIT domains (Vta1(165–330)) does not enhance the basal activation of Vps4 by Vta1, implying that Vta1 MIT domains do not autoinhibit Vps4 activation (27). The current NMR structure of the Vta1NTD-Vps60(128–186) complex provides further evidence that Vps60 binding does not induce overall conformational changes in the N terminus of Vta1 (Figure A.2F) and thus might

not lead to further structural arrangement in the C-terminal domain of Vta1. These observations suggest that Vps60 may not allosterically regulate Vta1 and thus could not potentiate its ability to activate Vps4.

The residues within Vps60(128–186) helix α5′ in the interface are composed of the sequence $D^{168'}xx^{L171'}xx(E^{174'})L^{175'}xxL^{178'}(A^{179'})$ (Figure A.6A), nearly identical to CHMP1A(180–196) MIM1 ((D/E)*xx*L*xx*RL*xx*L(K/R)) (19-20), except for Glu-174′ and Ala-179′ in contrast to the positively charged residues Arg-190 and Arg-195 in CHMP1A(180–196). In the Vta1NTD-Vps60(128–186) structure, the Vta1NTD MIT2 domain recognizes a new residue sequence $(L^{143'}(I^{144'})xxxxE^{149'}L^{150'}xE^{152'}V^{153'}L^{154'})$ within Vps60(128–186) helix α4′, which has low sequence similarity to CHMP6 MIM2 (Figure A.6B) (21), although Leu-143′, Glu-145′, Glu-152′, and Leu-154′ are conserved. Therefore, the interactions between Vta1 and Vps60 implied by the current complex structure do not mimic the interactions between Vps4 and the ESCRT-III subunits CHMP1A(180–196) and CHMP6(168–179). Thus, it is plausible that the specific interaction between Vta1 and Vps60 increases the local concentration of Vta1-Vps4 *in vitro* to enhance Vta1-Vps4 binding and thereby stimulate Vps4 activity.

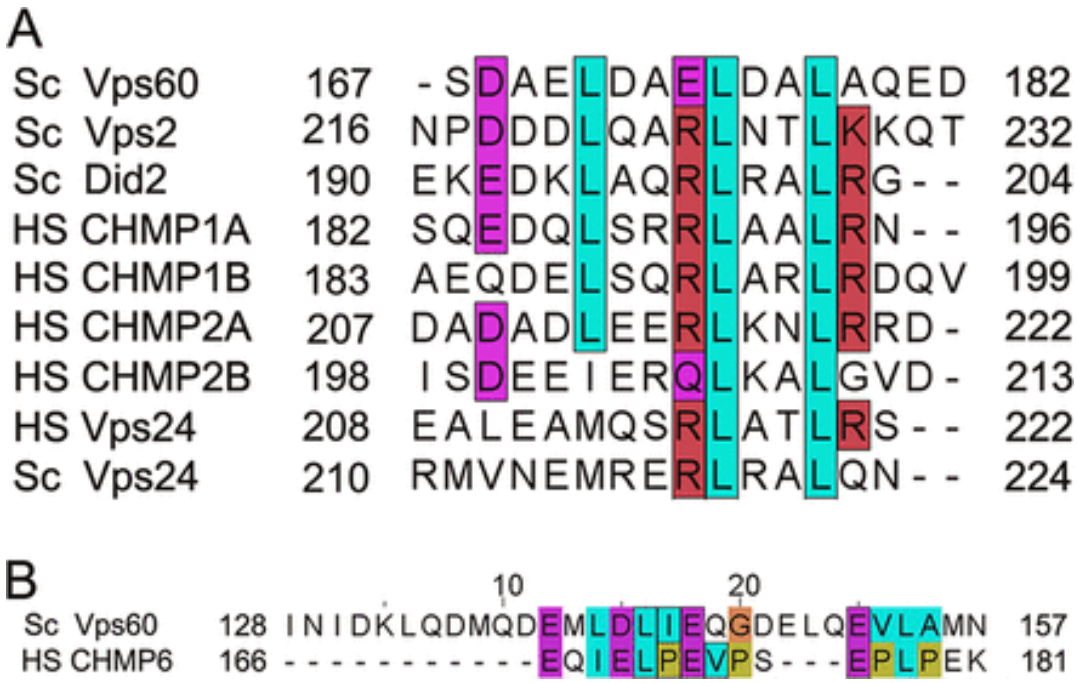

Figure A.6 Sequence alignments of Vps60(128–186) helices α4′ and α5′ with conserved MIM1 and MIM2.
A, Vps60(128–186) helix α5′ with MIM1 sequences. *B*, Vps60(128–186) helix α4′ with MIM2 sequences. *Sc*, *S. cerevisiae*; *HS*, *Homo sapiens*.

Taken together, the complex structure of Vta1NTD-Vps60(128–186) cannot account for all aspects of Vps4 activation, but it demonstrates a novel MIT recognition mode that has not been reported. Thus, to address how Vps4 ATPase is activated, further studies of the dynamics of ESCRT-III assembly and disassembly will be performed to better understand the precise function of Vta1 in the process of MVB sorting. The current structure further confirms that the interaction between Vps60 and Vta1 stimulates Vps4 ATPase in an unexpected manner.

A.5 Methods

A.5.1 Cloning, Expression, and Purification

DNA fragments encoding yeast Vta1 and Vps60 were amplified from *Saccharomyces cerevisiae* genomic DNA. Vta1NTD or Vps60(128–186) was expressed in *Escherichia coli* BL21(DE3) using a modified pET28b vector with a small ubiquitin-like modifier (SUMO) protein inserted between a His_6 tag and the Vta1NTD or Vps60(128–186) coding region, respectively. His_6-tagged SUMO-Vta1NTD or His_6-tagged SUMO-Vps60(128–186) was purified by nickel-nitrilotriacetic acid affinity chromatography following standard procedures. Ulp1 protease was then added to remove the His_6-SUMO tag, and the protein mixture was passed over a second nickel-nitrilotriacetic acid column and further purified by anion exchange chromatography on a Resource Q column (GE Healthcare). For isotope labeling, M9 minimal medium was supplemented with $^{15}NH_4Cl$ (Cambridge Isotope Laboratories) or $^{15}NH_4Cl$ and 2 g/liter [^{13}C]glucose (Cambridge Isotope Laboratories). Derivative proteins were purified in the same way as native proteins.

A.5.2 NMR Sample Preparation and Data Collection

Differentially labeled complex samples in 25 mM sodium phosphate (pH 7.0), 100 mM NaCl, 5 mM DTT-d_{10}, and 0.02% NaN_3 were prepared as follows: 1) 1.5 mMuniformly labeled $^{15}N/^{13}C$-labeled Vta1NTD plus 1.8 mM unlabeled Vps60(128–186) and 2) 1.5 mM uniformly labeled $^{15}N/^{13}C$-labeled Vps60(128–186) in complex with 1.8 mM unlabeled Vta1NTD. All NMR experiments were performed at 20 °C on a Varian Unity Inova 600 NMR spectrometer (with cryo-

probe) equipped with triple resonances and pulsed-field gradients or on a Bruker AVANCE III 800-MHz NMR spectrometer (with cryo-probe) equipped with four channels and *z* axis pulsed-field gradient. The standard suite of experiments for assigning the ^{1}H,^{13}C, and ^{15}N backbone and side chain chemical shifts of bound ^{13}C- and ^{15}N-double-labeled Vta1NTD in complex with unlabeled Vps60(128–186) or of bound^{13}C- and ^{15}N-double-labeled Vps60(128–186) in complex with unlabeled Vta1NTD and for the collection of NOE-based distance restraints were measured (33,34), including two-dimensional ^{13}C-edited heteronuclear single-quantum correlation (HSQC) in both aliphatic and aromatic regions and ^{15}N-edited HSQC; three-dimensional HNCA, HNCO, HN(CO)CA, HNCACB, CBCA(CO)NH, and ^{15}N-resolved HSQC- and HCCH-total correlation spectroscopy in both aliphatic and aromatic regions; ^{15}N-resolved and ^{13}C-resolved HSQC-NOESY for both aliphatic and aromatic resonances; and two-dimensional (Hβ)Cβ(CγCδ)Hδ and (Hβ)Cβ(CγCδCϵ)Hϵ spectra for correlation of Cβ and Hδ or Hϵ in aromatic rings used in aromatic proton assignment (35). The intermolecular NOEs between labeled Vta1NTD or the Vps60(128–186) peptide and the unlabeled Vps60(128–186) peptide or Vta1NTD were obtained by analyzing three-dimensional ^{13}C-F1-edited,^{13}C/^{15}N-F3-filtered NOESY spectra, respectively. All spectra were processed with the program NMRPipe (36) and analyzed with the SPARKY 3 software (37). The ^{1}H chemical shifts were referenced to 2,2-dimethylsilapentane-5-sulfonic acid, and the ^{13}C and ^{15}N resonances were indirectly referenced to 2,2-dimethylsilapentane-5-sulfonic acid.

A.5.3 NMR Structure Calculation

Calculations were carried out using a standard simulated annealing protocol implemented in the program XPLOR-NIH 2.19. Interproton distance restraints derived from NOE intensities were grouped into three distance ranges, 1.8–2.9, 1.8–3.5, and 1.8–6.0 Å, corresponding to strong, medium, and weak NOEs, respectively. The dihedral angles φ and ψ were derived from the backbone chemical shifts (HN, HA, CO, and CA) using the program TALOS (36-38). Slowly exchanging amide protons, identified in the two-dimensional ^{15}N HSQC spectra recorded after a H_2O buffer was exchanged with a D_2O buffer, were used in the structure calculated with the NOE distance restraints to generate hydrogen bonds for the final structure calculation, as done in the literature (39). A total of 10 iterations (50 structures in the initial eight iterations) were performed. 100 structures were computed in the last two iterations; 20 conformers with the lowest energy were used to represent the three-dimensional structures. In the ensemble of the simulated annealing 20 structures, there was no distance constraint violation of >0.3 Å and no torsion angle violation of >3°. The final 20 structures with the lowest energy were evaluated with the programs PROCHECK-NMR and PROCHECK (40) and are summarized in Table A.1. All figures were generated using the programs PyMOL and MOLMOL (41).

A.5.4 Isothermal Titration Calorimetry

To obtain a direct binding affinity between Vta1NTD (wild-type and mutants) and the Vps60(128–186) peptide, wild-type Vta1NTD and mutants were titrated with the Vps60(128–186) peptide using an iTC-200 microcalorimeter (GE

Healthcare) at 25 °C. All proteins and peptides were exchanged with buffer containing 20 mM sodium phosphate (pH 7.0) and 0.1 M NaCl by gel filtration chromatography, centrifuged to remove any particulates, and degassed. To obtain a direct binding affinity between Vta1NTD variants and the Vps60(128–186) peptide, a solution of ~0.1 mM wild-type and mutant Vta1NTD was titrated with 1.0 mM Vps60(128–186) peptide, respectively. The accurate concentrations of Vta1NTD and its mutants were determined using their A_{280} constants.

A.5.5 Circular Dichroism Spectroscopy of Free Vps60(128–186)

To probe the folding of free Vps60(128–186), the CD experiment was performed at 25 °C on a JASCO-715 spectropolarimeter (Jasco International Co., Tokyo, Japan). Data were collected at 0.1-nm intervals at a scan speed of 20 nm/min, 1-nm bandwidth, and 0.25-s response time from 250 to 190 nm. Circular quartz cells of 1- and 0.1-cm path length were used for the far-UV regions. The CD intensities are expressed as molar residue ellipticities given in units of degrees cm2 mol−1. The concentration of Vps60(128–186) was ~10 μM. The buffer conditions used for running CD spectra were 20 mM sodium phosphate and 50 mM NaCl (pH 7.5).

A.5.6 GST Pulldown Experiments

The experiments were performed following standard procedures in buffer containing 25 mM Tris-HCl (pH 8.0), 150 mM NaCl, and 5 mM 2-mercaptoethanol. Purified wild-type Vta1NTD and mutants were incubated with GST alone or with GST-tagged Vps60(128–186) immobilized on glutathione-agarose beads for 3 h at 4 °C. The beads were then washed extensively three

times with the above buffer, and bound proteins were separated by SDS-PAGE and visualized by Coomassie Blue staining.

A.6 Acknowledgements

This work was supported by National Basic Research Program of China Grants 2009CB918600 and 2011CB966300, National Science Foundation of China Grants 30970595 and 20921091, International Cooperation Foundation Grant 09540703800 from the Science and Technology Commission of Shanghai Municipality, National New Drug Design Program Grant 2011ZX09506 from the Ministry of Health of China, and Grant T151102 from the State Key Laboratory of Magnetic Resonance and Atomic and Molecular Physics, Wuhan Center for Magnetic Resonance, Wuhan Institute of Physics and Mathematics, Chinese Academy of Sciences

A.7 References

1. Gruenberg, J., and Stenmark, H. (2004) The biogenesis of multivesicular endosomes. Nat. Rev. Mol. Cell Biol. **5**, 317–323

2. Morita, E., and Sundquist, W. I. (2004) Retrovirus budding. Annu. Rev. Cell Dev. Biol. **20**, 395– 425

3. Carlton, J. G., and Martin-Serrano, J. (2007) Parallels between cytokinesis and retroviral budding: a role for the ESCRT machinery. Science **316**, 1908 –1912

4. Babst, M. (2005) A protein's final ESCRT. Traffic **6**, 2–9

5. Hurley, J. H., and Emr, S. D. (2006) The ESCRT complexes: structure and mechanism of a membrane-trafficking network. Annu. Rev. Biophys.Biomol. Struct. **35**, 277–298

6. Piper, R. C., and Katzmann, D. J. (2007) Biogenesis and function of multivesicular bodies. Annu. Rev. Cell Dev. Biol. **23**, 519 –547

7. Winter, V., and Hauser, M. T. (2006) Exploring the ESCRTing machinery in eukaryotes. Trends Plant Sci. **11**, 115–123

8. Katzmann, D. J., Odorizzi, G., and Emr, S. D. (2002) Receptor down-regulation and multivesicular-body sorting. Nat. Rev. Mol. Cell Biol. **3**, 893–905

9. Saksena, S., and Emr, S. D. (2009) ESCRTs and human disease. Biochem. Soc. Trans. **37**, 167–172

10. Raiborg, C., and Stenmark, H. (2009) The ESCRT machinery in endosomal sorting of ubiquitylated membrane proteins. Nature **458**, 445–452

11. Bieniasz, P. D. (2009) The cell biology of HIV-1 virion genesis. Cell Host Microbe **5**, 550 –558

12. Fujii, K., Hurley, J. H., and Freed, E. O. (2007) Beyond Tsg101: the role of Alix in 'ESCRTing' HIV-1. Nat. Rev. Microbiol. **5**, 912–916

13. Williams, R. L., and Urbé, S. (2007) The emerging shape of the ESCRT machinery. Nat. Rev. Mol. Cell Biol. **8**, 355–368

14. Hurley, J. H. (2008) ESCRT complexes and the biogenesis of multivesicular bodies. Curr. Opin. Cell Biol. **20**, 4 –11

15. Babst, M., Wendland, B., Estepa, E. J., and Emr, S. D. (1998) The Vps4p AAA ATPase regulates membrane association of a Vps protein complex required for normal endosome function. EMBO J. **17**, 2982–2993

16. Xiao, J., Xia, H., Yoshino-Koh, K., Zhou, J., and Xu, Z. (2007) Structural characterization of the ATPase reaction cycle of endosomal AAA protein Vps4. J. Mol. Biol. **374**, 655– 670

17. Yu, Z., Gonciarz, M. D., Sundquist, W. I., Hill, C. P., and Jensen, G. J. (2008) Cryo-EM structure of dodecameric Vps4p and its 2:1 complex with Vta1p. J. Mol. Biol. **377**, 364 –377

18. Shestakova,A.,Hanono,A.,Drosner,S.,Curtiss,M.,Davies,B.A.,Katz- mann, D. J., and Babst, M. (2010) Assembly of the AAA ATPase Vps4 on ESCRT-III. Mol. Biol. Cell **21**, 1059 –1071

19. Obita, T., Saksena, S., Ghazi-Tabatabai, S., Gill, D. J., Perisic, O., Emr, S. D., and Williams, R. L. (2007) Structural basis for selective recognition of ESCRT-III by the AAA ATPase Vps4. Nature **449**, 735–739

20. Stuchell-Brereton, M. D., Skalicky, J. J., Kieffer, C., Karren, M. A., Ghaffarian, S., and Sundquist, W. I. (2007) ESCRT-III recognition by VPS4 ATPases. Nature **449**, 740 –744

21. Kieffer,C.,Skalicky,J.J.,Morita,E.,DeDomenico,I.,Ward,D.M.,Kaplan, J., and Sundquist, W. I. (2008) Two distinct modes of ESCRT-III recogni- tion are required for VPS4 functions in lysosomal protein targeting and HIV-1 budding. Dev. Cell **15**, 62–73

22. Samson, R. Y., Obita, T., Freund, S. M., Williams, R. L., and Bell, S. D. (2008) A role for the ESCRT system in cell division in archaea. Science **322**, 1710 –1713

23. Yang,D.,Rismanchi,N.,Renvoisé,B.,Lippincott-Schwartz,J.,Blackstone, C., and Hurley, J. H. (2008) Structural basis for midbody targeting of spas- tin by the ESCRT-III protein CHMP1B. Nat. Struct. Mol. Biol. **15**, 1278 –1286

24. Solomons, J., Sabin, C., Poudevigne, E., Usami, Y., Hulsik, D. L., Macheboeuf, P., Hartlieb, B., Göttlinger, H., and Weissenhorn, W. (2011) Structural basis for ESCRT-III CHMP3 recruitment of AMSH. Structure **19**, 1149 –1159

25. Babst, M., Davies, B. A., and Katzmann, D. J. (2011) Regulation of Vps4 during MVB sorting and cytokinesis. Traffic **12**, 1298 –1305

26. Azmi, I., Davies, B., Dimaano, C., Payne, J., Eckert, D., Babst, M., and Katzmann, D. J. (2006) Recycling of ESCRTs by the AAA-ATPase Vps4 is regulated by a conserved VSL region in Vta1. J. Cell Biol. **172**, 705–717

27. Azmi, I. F., Davies, B. A., Xiao, J., Babst, M., Xu, Z., and Katzmann, D. J. (2008) ESCRT-III family members stimulate Vps4 ATPase activity directly or via Vta1. Dev. Cell **14**, 50 – 61

28. Dimaano, C., Jones, C. B., Hanono, A., Curtiss, M., and Babst, M. (2008) Ist1 regulates Vps4 localization and assembly. Mol. Biol. Cell **19**, 465–474

29. Xiao, J., Xia, H., Zhou, J., Azmi, I. F., Davies, B. A., Katzmann, D. J., and Xu, Z. (2008) Structural basis of Vta1 function in the multivesicular body sorting pathway. Dev. Cell **14**, 37– 49

30. Lottridge, J. M., Flannery, A. R., Vincelli, J. L., and Stevens, T. H. (2006) Vta1p and Vps46p regulate the membrane association and ATPase activity of Vps4p at the yeast multivesicular body. Proc. Natl. Acad. Sci. U.S.A. **103**, 6202– 6207

31. Scott, A., Chung, H. Y., Gonciarz-Swiatek, M., Hill, G. C., Whitby, F. G., Gaspar, J., Holton, J. M., Viswanathan, R., Ghaffarian, S., Hill, C. P., and

Sundquist, W. I. (2005) Structural and mechanistic studies of VPS4 proteins. EMBO J. **24**, 3658 –3669

32. Yang, D., and Hurley, J. H. (2010) Structural role of the Vps4-Vta1 interface in ESCRT-III recycling. Structure **18**, 976 –984

33. Bax, A., and Grzesiek, S. (1993) Methodological advances in protein NMR. Acc. Chem. Res. **26**, 131–138

34. Clore, G. M., and Gronenborn, A. M. (1998) Determining the structures of large proteins and protein complexes by NMR. Trends Biotechnol. **16**, 22–34

35. Yamazaki, T., Formankay, J. D., and Kay, L. E. (1993) Two-dimensional NMR experiments for correlating C-13-beta and proton-delta/epsilon chemical shifts of aromatic residues in 13C-labeled proteins via scalar cou- plings. J. Am. Chem. Soc. **115**, 11054 –11055

36. Delaglio, F., Grzesiek, S., Vuister, G. W., Zhu, G., Pfeifer, J., and Bax, A. (1995) NMRPipe: a multidimensional spectral processing system based on UNIX pipes. J. Biomol. NMR **6**, 277–293

37. Goddard, T. D., and Kneller, D. G. (2001) SPARKY 3, University of California, San Francisco

38. Cornilescu, G., Delaglio, F., and Bax, A. (1999) Protein backbone angle restraints from searching a database for chemical shift and sequence homology. J. Biomol. NMR **13**, 289 –302

39. Wang, C., Shen, J., Yang, Z., Chen, P., Zhao, B., Hu, W., Lan, W., Tong, X., Wu, H., Li, G., and Cao, C. (2011) Structural basis for site-specific reading of unmodified R2 of histone H3 tail by UHRF1 PHD finger. Cell Res. **21**,1379 –1382

40. Laskowski, R. A., Rullmannn, J. A., MacArthur, M. W., Kaptein, R., andThornton, J. M. (1996) AQUA and PROCHECK-NMR: programs for checking the quality of protein structures solved by NMR. J. Biomol. NMR **8**, 477– 486

41. Koradi, R., Billeter, M., and Wüthrich, K. (1996) MOLMOL: a program for display and analysis of macromolecular structures. J. Mol. Graph **14**, 51–55

42. Muzioł, T., Pineda-Molina, E., Ravelli, R. B., Zamborlini, A., Usami, Y., Göttlinger, H., and Weissenhorn, W. (2006) Structural basis for budding by the ESCRT-III factor CHMP3. Dev. Cell **10**, 821– 830

43. Wishart, D. S., and Sykes, B. D. (1994) The ^{13}C chemical-shift index: a simple method for the identification of protein secondary structure using 13C chemical-shift data. J. Biomol. NMR **4**, 171–180

44. Shim, S., Merrill, S. A., and Hanson, P. I. (2008) Novel interactions of ESCRT-III with LIP5 and VPS4 and their implications for ESCRT-III disassembly. Mol. Biol. Cell **19**, 2661–2672

45. Hurley, J. H., and Yang, D. (2008) MIT domainia. Dev. Cell **14**, 6 – 8